Max Planck Graduate Center
mit der Johannes Gutenberg-Universität Mainz

Towards Antibody-mediated Targeting of Dendritic Cells for Cancer Immunotherapy with Multivalent Polymer-Antigen Conjugates

Dissertation

zur Erlangung des akademischen Grades eines
„Doctor rerum naturalium“ (Dr. rer. nat.) der Fachbereiche:

Physik, Mathematik und Informatik,
Chemie, Pharmazie und Geowissenschaften,
Biologie, Universitätsmedizin

vorgelegt von

Anika Reuter

Mainz, August 2013

Tag der mündlichen Prüfung: 26. September 2013

Dekan:

1. Berichterstatter:

2. Berichterstatter:

Die vorliegende Arbeit wurde in der Zeit von September 2010 bis August 2013 am Institut für Physikalische Chemie der Johannes Gutenberg-Universität in Mainz unter der Betreuung von [redacted] und an der Hautklinik der Universitätsmedizin der Johannes Gutenberg-Universität Mainz unter der Betreuung von [redacted], sowie während eines Aufenthalts an der University of Melbourne, Australien, in der Gruppe von [redacted] angefertigt.

Ich versichere, dass ich meine Dissertation selbstständig verfasst und ausschließlich die angegebenen Quellen und Hilfsmittel verwendet habe. Alles, was ich aus fremden Quellen übernommen habe, habe ich deutlich gemacht.

Mainz, 12. August 2013

I hereby declare that I wrote the dissertation submitted without any unauthorized external assistance and used only sources acknowledged in the work. All textual passages which are appropriated verbatim or paraphrased from published and unpublished texts as well as all information obtained from oral sources are duly indicated and listed in accordance with bibliographical rules. In carrying out this research, I complied with the rules of standard scientific practice as formulated in the statutes of Johannes Gutenberg-University Mainz to insure standard scientific practice.

Mainz, 12. August 2013

Meiner Familie

Wichtig ist, dass man nie aufhört zu fragen...

Albert Einstein

Abstract

The aim of this thesis was to study polymeric bioconjugates and their application in cancer immunotherapy. Two different polymeric carriers were investigated, linear poly-*L*-lysine (PLL) and a polylysine brush (PLL brush). The PLL brush was expected to exhibit better body distribution than the linear polymer and prolonged circulation time in the blood stream due to its anisotropic shape. To impart biological function, three bioactive components were conjugated to these polymers: an antiDEC205 (aDEC205) antibody for specific targeting of CD8+ dendritic cells, an ovalbumin (OVA)-specific model antigen with the core peptide sequence SIINFEKL which initiates a specific immune response against cancer cells presenting this antigen, and an oligonucleotide adjuvant (CpG1826) which targets the toll like receptor 9. The ability of the polymer-drug conjugate to activate DC to induce an immune response against OVA-expressing cancer cells was expected to be significantly enhanced by attaching the three components onto one polymeric carrier molecule.

Linear PLL was investigated as a model system to establish the conjugation chemistry and to transfer it to the polylysine brush, which is a cylindrical brush polymer with poly-*L*-lysine side chains. With these two polymeric carriers two different topologies (coil and brush-like) were distinguished. The influence of the structural differences on conjugation reactions as well as on the final *in situ* and *in vitro* behavior was studied.

PLL labeled with AlexaFluor488 was modified with thiol reactive maleimide groups using the bifunctional crosslinker sulfo-SMCC. Thiol modified CpG and thiol modified antigen-AlexaFluor546 were coupled to PLL through a Michael addition of the thiol to the maleimide groups. Subsequently, aDEC205-AlexaFluor647 was conjugated to PLL either via Schiff Base reaction of the oxidized antibody with PLL and following reduction to a stable secondary amine or via click reaction of PEG-azide modified antibody with a dicyclobenzyl cyclooctylene (DIBO)-functionalized PLL.

Conjugation of the bioactive components to the polymer was confirmed using UV/Vis spectroscopy, flow cytometry and confocal laser scanning microscopy. While the PLL brush alone showed very high cytotoxicity on HeLa and JAWS II cells, PLL and PLL-conjugates as well as PLL brush-conjugates exhibited no distinct cytotoxicity. The polymer conjugates revealed no aggregation in human blood serum which was detected by multi-angle light scattering. Confocal laser scanning microscopy (CLSM) images demonstrated colocalization of all fluores-

cent dyes inside the cells which indicated successful conjugation and internalization of the conjugate. Flow cytometry measurements exhibited slightly increased internalization into bmDC of the targeted PLL-Antigen-aDEC205 conjugate compared to the untargeted PLL-Antigen. Flow cytometry measurements performed with the Specific Hybridization Internalization Sensor (SHIP) revealed an internalization of PLL-antibody conjugates into immature splenic CD8+ DC, but not into mature CD8+ DC which implied that conjugation of aDEC205 did not induce receptor-mediated endocytosis.

T cell proliferation assays showed an activation of CD8+ T cells induced by all antigen-containing conjugates while conjugates without antigen served as negative controls and revealed no T cell activation. However, no difference was observed between targeted and untargeted conjugates due to the unspecific uptake of the polymer. SIINFEKL alone also induced T cell proliferation at lower antigen concentrations. These results suggest that PLL-conjugates exhibited unspecific uptake into cells due to the high cationic charge and no receptor-mediated endocytosis could be imparted by conjugation of the aDEC205 antibody.

In summary, it was possible to conjugate three biologically active components to one polymeric carrier and characterize composition, size and activity of these hybrid materials. The polymer-conjugates are unspecifically internalized into DC and can induce an immune response, however, the antibody does not promote receptor-mediated endocytosis of the conjugate. These studies offer a promising first step to developing new nanomaterials for application in cancer immunotherapy.

Zusammenfassung

Der Fokus dieser Arbeit lag auf der definierten Synthese multifunktioneller Polymer-Konjugate zur Anwendung in der Krebs-Immunotherapie. Durch gezielte Variation der Konjugationsbedingungen wurde Zusammensetzung, Größe und Aggregationsverhalten in Zellmedium sowie in humanem Serum untersucht. Nach definierter physikalisch-chemischer Charakterisierung wurde dann die induzierte Antigen-Präsentation zur Aktivierung der T-Zellproliferation analysiert.

Dafür wurden zwei verschiedene polymere Carrier-Systeme gewählt, lineares Poly-*L*-lysin und eine Polylysinbürste (PLL-Bürste). Es wird vermutet, dass die PLL-Bürste aufgrund der anisotropen Form eine bessere Verteilung im Körper und eine verlängerte Zirkulationsdauer zeigen wird. Die zu konjugierenden biologisch aktiven Komponenten waren der antiDEC205-Antikörper (aDEC205) für die gezielte Adressierung CD8-positiver dendritischer Zellen (DC), ein Ovalbumin (OVA)-spezifisches Antigen mit der Kernsequenz SIINFEKL für die Spezifität der Immunantwort gegen Krebszellen, die dieses Antigen tragen, und ein immunaktivierender TLR9-Ligand, CpG1826. Die Effizienz dieses Konjugates dendritische Zellen zu aktivieren, welche wiederum eine Immunantwort gegen OVA-exprimierende Krebszellen induzieren, wurde durch die Konjugation aller Komponenten am identischen Trägermolekül deutlich höher erwartet.

Lineares Poly-*L*-lysin diente als Modellsystem um die Konjugationschemie zu etablieren und dann auf die zylindrische Polylysinbürste zu übertragen. Anhand dieser polymeren Träger wurde das Verhalten der verschiedenen Topologien des Knäuels und der Bürste im Hinblick auf den Einfluss struktureller Unterschiede sowohl auf Konjugationsreaktionen als auch auf das *in situ* und *in vitro* Verhalten untersucht.

Fluoreszenzmarkiertes Antigen und der CpG Aktivator konnten jeweils aufgrund einer Thiol-Modifizierung an die Thiol-reaktive Maleimidgruppe des heterobifunktionellen Linkers Sulfo-SMCC an PLL-AlexaFluor48 konjugiert werden. Anschließend wurde aDEC205-AlexaFluor647 an PLL gekoppelt, entweder durch Schiff Base-Reaktion des oxidierten Antikörpers mit PLL und anschließender Reduzierung oder durch Click-Reaktion des PEG-Azids modifizierten Antikörpers mit Dicyclobenzylcyclooctin (DIBO)-funktionalisiertem PLL. Die Konjugation der biologisch aktiven Komponenten wurde mit Durchflusszytometrie (FACS) und konfokaler Laser Scanning Mikroskopie (CLSM) untersucht und die Zusammensetzung des Konjugates

mittels UV/Vis-Spektroskopie bestimmt. Die PLL-Bürste alleine zeigte eine hohe Zytotoxizität bei HeLa und JAWS II Zelllinien, wohingegen lineares PLL und PLL-Konjugate sowie die PLL Bürsten-Konjugate keine ausgeprägte Zytotoxizität aufwiesen. Die Polymer-Konjugate wiesen keine Aggregation in Zellmedium oder humanem Serum auf, was mittels winkelabhängiger dynamischer Lichtstreuung bestimmt wurde. CLSM Aufnahmen zeigten Kolokalisation der an die einzelnen Komponenten gebundenen Fluoreszenzfarbstoffe in dendritischen Zellen, was die erfolgreiche Konjugation und Internalisierung der Konjugate in die Zellen belegen konnte. FACS Messungen ergaben eine geringfügig erhöhte Aufnahme des adressierten PLL-Antigen-Antikörper-Konjugates verglichen mit dem PLL-Antigen-Konjugat. Experimente mit dem „Specific Hybridization Internalization Sensor“ (SHIP) zeigten jedoch nur Aufnahme der PLL-Konjugate in CD8+ unreife DC, nicht in reife DC, die nicht mehr unspezifisch, sondern nur noch über Rezeptoren internalisieren. Dies bewies die unspezifische Aufnahme des Konjugates, da Antikörper-Konjugation keine Rezeptor-vermittelte Endozytose in reife DC induzieren konnte. T-Zell-Proliferationsassays ergaben eine Aktivierung von CD8+ T-Zellen induziert durch Antigen-tragende Konjugate, wohingegen Konjugate ohne Antigen als Negativkontrollen dienten und keine T-Zell-Proliferation erzielten. Es konnte jedoch kein Unterschied zwischen adressierten und nicht adressierten Konjugaten aufgrund der unspezifischen Aufnahme durch das Polymer beobachtet werden. Lösliches SIINFEKL alleine bewirkte schon bei geringeren Konzentrationen eine T-Zell-Proliferation.

Es war somit möglich, drei biologischen Komponenten an einen polymeren Träger zu konjugieren und diese Konjugate im Hinblick auf Zusammensetzung, Größe, Internalisierung in dendritische Zellen und Aktivierung der T-Zell-Proliferation zu untersuchen. Außerdem wurde die Konjugationschemie erfolgreich von dem Modellsystem des linearen PLL auf die PLL-Bürste übertragen. Die Polymer-Konjugate werde unspezifisch in DC aufgenommen und induzieren T-Zellproliferation, die mit Antigen-Präsentationsassays nachgewiesen wird. Es konnte jedoch durch Konjugation des Antikörpers keine Rezeptor-vermittelte Aufnahme in CD8+ DC erzielt werden.

Diese Studien stellen einen erfolgsversprechenden ersten Schritt zur Entwicklung neuer Nanomaterialien für die Anwendung in Krebs-Immuntherapie dar.

Table of contents

1. Introduction

Cancer is still one of the most common causes of death in industrial countries.

In order for cells to become malignant, several mutations in their genes of proto oncogenes and tumor suppressor genes have to occur to enable cells to proliferate uncontrollably. During the development of a tumor, affected cells alter and express tumor antigens. Tumor antigens are proteins that are predominantly produced and presented by tumor cells[1]. Oftentimes, the immune system does not recognize these cellular alterations as tumor cells are only weak antigen presenting cells and tumor antigens are mostly endogenous[2].

Immunoediting is the process by which the body is protected from tumor growth and the development of tumor immunogenicity by the immune system. Immunoediting describes how the immune system deals with transformed cells and arising tumors and consists of three phases: elimination, equilibrium and escape[3]. Elimination, i.e. immunosurveillance, protects the body from transformed cells and malignancies by continuously recognizing and eliminating those cells before they can form a tumor. During the equilibrium stage, lymphocytes and interferons exert selection pressure onto malignant cells that avoided elimination. Transformed cells that obtained resistance against the immune system can now escape elimination and grow uncontrollably to form a malignant tumor[4]. Thus, the tumor protects itself against infiltrating effector cells by recruiting and inducing regulatory leukocytes such as myeloid-derived suppressor cells[184] (MDSC) and/or regulatory T cells (T_{reg})[5]. These T_{reg} can now inhibit effector T cells, natural killer cells (NK cells) or dendritic cells (DC)[6]. With these mechanisms tumors avoid detection by the immune system and enable them to grow and manifest. Instantaneously, the question is raised, how the immunological behavior of cancer cells can be altered to end up in an efficient immunotherapy, instead of operation, radiation and chemotherapy, which are until now the most common cancer treatments.

The oldest treatment of cancer is surgical removal of the tumor. This is a challenge if vital inner organs are beset with tumors or small, nearly invisible metastases. Furthermore, operation is only successful as long as the primary tumor has not metastasized or if metastases are detected and able to be surgically removed. In later stages with multiple metastases even radical surgery does not prohibit relapse of cancer.

During chemotherapy the patient is treated with cytotoxic drugs, so called cytostatica, that induce death of rapidly dividing cells. These chemicals do not exclusively kill tumor cells but all other cells with a high dividing frequency, like hair follicle or mucosa for example in the gastrointestinal tract. Although chemotherapeutic agents kill most cells in a tumor, it is believed that they spare tumor stem cells, which may be an important mechanism of drug resistance[7].

Radiation is oftentimes combined with chemotherapy or operation. Tumors are treated with ionizing radiation which promotes death of the tumor cells. Radiation is a local treatment and size and location of the tumor has to be determined in order to minimize damage of adjacent tissue. Due to the localization of this treatment, metastases are not affected.

These therapies are known for many years and no real alternatives or new therapeutic methods evolved in the last 50 years. The crux about these therapies are the strong side effects like nausea, loss of hair, the multi-drug resistance tumors build up and many more.

Therefore, new strategies have to be created. New therapeutic opportunities arise from the cancer stem cell model[7], an increasing understanding of the tumor-promoting signaling cascades and the development of targeted therapies against intracellular signaling molecules, and also from immunological approaches.

1.1. Immunotherapy for Cancer Treatment

Cancer immunotherapy and thereby especially cancer vaccines aim to stimulate a patient's immune system to attack and destroy tumors, thereby providing active immunization against cancer cells[8].

Cancer cells can escape the immune response due to various reasons. Cancer cells carry tumor-associated antigens additionally to normal self antigens. But cancer cells can undergo genetic changes that can lead to the loss of tumor antigens and thus are not detected by immune cells anymore. Additionally to avoiding detection, cancer cells can also suppress an anticancer immune response by killer T cells by the production of inhibitory molecules and regulatory immune cells.

Therefore, cancer vaccines for tumor immunotherapy need to provide a strong stimulation of a specific immune response against the correct target. Moreover, this specific immune

response needs to be sufficient enough to overcome the protective mechanisms of cancer cells against the body's immune response so that no immunotolerance is induced.
With cancer immunotherapy immunosurveillance is enabled. The immune system is activated to specifically recognize and attack tumor cells. There are different types of immunotherapy for cancer treatment. These treatments either work by stimulation of the immune system to fight the disease or by the use of immune system components like monoclonal antibodies[9]. These monoclonal antibodies can either boost the immune system or they can specifically bind to cancer cells and inhibit growth signals or induce apoptosis. Treatments to stimulate the body's own immune response are cancer vaccines that can induce a very specific response or non-specific immunotherapies that enhance the immune response in a more general way.

1.1.1. Monoclonal Antibodies

Monoclonal antibodies (mAb) are prepared in the lab and can be administered to bind specifically to antigens within the body, e.g. tumor antigens on tumor cells, which provides specific targeting of the tumor. After binding they can recruit other immune cells to destroy the targeted cell or they can block the receptor and inhibit growth signals. mAb are not only used for cancer treatment but are applied for many other diseases, e.g. rheumatoid arthritis. Identification of the targeted antigen is important for the design of mAb. Over the past decade the US Food and Drug Administration (FDA) has approved twelve of these mAb for cancer treatment and more clinical trials are currently performed[10].
There are two types of mAb treatments, naked mAbs and mAb conjugates. Naked mAb usually bind to cancer cells or other immune cells and enhance an immune response, block receptors and/or induce cell death. For example, the monoclonal antibody Trastuzumab (Herzeptin®) binds to human epidermal growth factor receptor number 2 (HER-2) that is augmentedly expressed on rapidly dividing breast cancer cells[11]. If the therapeutic antibody binds to this receptor the signaling cascade is interrupted, cell proliferation and therefore tumor growth are inhibited. This antibody is oftentimes used as an adjuvant therapy[12] and in addition to operation or chemotherapy. But only 25-30% of all breast cancer patients show overexpression of HER-2 and therefore therapy is limited to this group of patients[13],

[14]. Further therapeutic antibodies approved are e.g. Rituximab (MabThera®), an antiCD20 antibody that is used for the treatment of non-Hodgkin's lymphoma. The monoclonal antibody binds to B cell lymphoma cells which leads to their destruction by the immune system[15]. Other antibodies like Sorafenib (Nevaxar®)[16], [17] or Bevacizumab (Avastin®)[18], [19] inhibit angiogenesis which prevents development of new blood vessels that supply the tumor with oxygen and nutrition for tumor growth.

Conjugated mAb carry a chemotherapeutic drug (chemolabeled Ab), a toxin (immunotoxin) or a radioactive particle (radioimmunotherapy). The antibody provides delivery of its cargo specifically to the site of action, the cancer cell.

Currently, two chemolabeld Ab are approved by the FDA for the treatment of cancer. Brentuximab vedotin (Adcetris®) is a monoclonal Ab targeting CD30 antigen on B and T cells that is conjugated to the antineoplastic agent Monomethyl auristratin E (MMAE)[20], [21]. MMAE is an antimitotic agent that blocks polymerization of tubulin and thus inhibits cell division. Brentuximab vedotin is used for the treatment of non-Hodgkin's lymphoma. Adotrastuzumab (Kadcyla™) is a combination of the trastuzumab mAb and the chemotherapeutic agent mertansine (DM1) which is used for treating breast cancer patients that are positive for HER-2[22].

For radioimmunotherapy, Ibritumomab tiuxetan (Zevalin®), a combination of a monoclonal antibody with Yttrium-90 radioactive particles used for non-Hodgkin's lymphoma, is approved by the FDA[23]. The monoclonal antibody binds to the CD20 receptors on cancerous B cells and delivers the radiation which then destroys cells[24].

Immunotoxins are currently being investigated, but no agent is approved for cancer treatment so far.

Therapy with monoclonal antibodies is highly specific and therefore shows only minimal side effects compared to the side effects of chemotherapy[25]. The side effects often depend on the target of the mAb.

1.1.2. Cancer Vaccines

Vaccination is usually administered to healthy people in order to prevent infection with diseases. These conventional vaccines use dead or small parts of bacteria or viruses in order to

induce an immune response. Some cancer vaccines help preventing diseases (prophylactic vaccines), but most cancer vaccines induce an immune response in an already infected body (therapeutic vaccines).

Cancer can be caused by viruses, e.g. the human papilloma virus (HPV) that leads to cervical cancer, or chronical infections with the hepatitis B virus (HBV)[26] that might cause liver cancer. These types of cancer can be impeded by prophylactic vaccination (Gardasil® and Cervarix® against HPV[27]) against the virus, but these vaccines do not target cancer directly. Most cancers are not caused by viruses and therefore other vaccinations directly against cancer are needed.

Other cancer vaccines do not prevent infection but try to activate the body's immune system to attack already existing tumors. These vaccines use parts of cancer cells or tumor antigens to teach the immune cells which structures to attack within the body. By using tumor antigens to boost the immune system, this therapy is highly specific against those cells that present this antigen. Vaccines are mostly used in combination with adjuvants to enhance the immune response. Adjuvants are molecules that resemble conserved molecular motifs characteristic of pathogens, such as unmethylated cytosine-guanidine (C-G) oligonucleotide sequences (characteristic for bacterial DNA), single-stranded RNA sequences (characteristic for viral genomes) or lipopolysaccharides (signature of Gram negative bacteria)[8]. Therefore, it is hoped that cancer vaccines activate the immune system to attack specifically tumor cells and form a long lasting memory to prevent the tumor to relapse.

Types of specific cancer vaccines being investigated are dendritic cell vaccines, antigen vaccines, tumor cell vaccines, DNA vaccines and vector-based vaccines.

An example for a **dendritic cell vaccine** is Sipuleucel T (Provenge®) against metastatic prostate cancer [28], the first therapeutic cancer vaccine approved by the FDA in 2010. This dendritic cell-based vaccine induces an immune response to prostatic acid phosphatase (PAP), a tumor-associated antigen presented by most prostate cancer cells. Dendritic cells (DC) are generated *ex vivo* from the patient's blood through leukapheresis and then cultured with a conjugate of PAP and granulocyte-macrophage colony-stimulating factor (GM-CSF). The glycoprotein GM-CSF stimulates the immune system and increases antigen presentation. After co-culturing of DC with PAP-GM-CSF, activated DC are reinfused into the patient and the highest antigen presentation is achieved after three injections every two weeks. So far this

vaccination does not cure cancer but prolongates survival of men with a certain type of metastatic prostate cancer by 4 months[28]. Studies to apply this vaccine in early stages of prostate cancer are in preparation. Other cancer vaccines are currently in clinical trials, but have not been approved by the FDA yet.

These dendritic cell-based vaccines are autologous, which means they are made from the patient who will be treated with ("personalized medicine"). Dendritic cells, that are antigen-presenting cell (APC), are incubated with cancer cells or antigens, which they process and present to other immune cells on their cell surface to stimulate an immune response by T cells specifically against these cancer cells. But the process of autologous DC-based vaccines is complex and expensive.

Tumor cell vaccines are made from cancer cells that have been removed during surgery and manipulated e.g. with radiation so that they are not tumorigenic anymore. Reinjected into the patient these cells are recognized by the immune system, an immune response against cells with these features is induced and all of these cells are searched and destroyed[29]. Mostly, these types of vaccines are autologous, but some vaccines are allogeneic, which means the tumor cells originate from another patient. Autologous vaccines are more complex and difficult to make than allogeneic vaccines and so far it is not known which approach exhibits more effective results.

Antigen vaccines activate the immune system to specifically recognize antigens on tumor cells within the body. These vaccines in contrast to tumor cell vaccines use only one antigen, usually a protein or a peptide, rather than whole tumor cells. The immune response induced is specific, although these vaccines are not autologous.

Tumor cell or antigen vaccines are recognized as foreign and are quickly destroyed by the immune system if an additional immunostimulatory signal is provided, e.g. by a potent immunologic adjuvant. This may cause the desired immune response at first, but lead to a decrease in efficiency over time. **DNA vaccines** are thought to provide a continuous supply of antigens to keep the immune response going[30]. DNA can be introduced into the cell via vectors and lead to expression of the protein the DNA encodes for. Vectors can be viruses, bacteria or other structures that can include DNA and transport it into the body. Vectors have the advantages of being able to deliver more than one antigen simultaneously and they can trigger their own immune response which overall boosts the antigen-specific immune re-

sponse even more. Additionally, vector-based vaccines are oftentimes cheaper and easier to make than for instance autologous vaccine strategies.

1.1.3. Non-specific Immunotherapies and Adjuvants

Non-specific immunotherapies do not target a cancer cell or a tumor antigen specifically, but they stimulate the immune system in a general way. This general stimulation may still result in immune responses against cancer cells. They can either be administered by themselves as cancer treatments or as adjuvants to another therapy to improve the outcome of other treatments like specific cancer vaccines.

The most commonly used non-specific immunotherapeutic adjuvants are and cytokines. Cytokines are chemicals made by the immune system that play a crucial role in controlling growth and activity of immune cells and blood cells. There are different classes of cytokines. Interleukins are one class of cytokines that act as chemical signals for communication between immune cells. Synthetic interleukin-2 (IL-2) has been approved by the FDA in 1992 for the treatment of advanced kidney cancer as the first immunotherapy approved to be used alone in the treatment of cancer. Today it is also used to treat people with metastatic melanoma. IL-2 induces T cell proliferation and acts on B cells as a growth factor and stimulant of antibody production[31]. Other interleukins (e.g. IL-7, IL-12 and IL-21) are investigated for their use in cancer treatment either as adjuvants or alone.

Interferons (IFN), another class of cytokines, have antiviral, antiproliferative and immunomodulatory effects in the body. IFN-α enhances the ability of immune cells to attack cancer cells and can help to decelerate tumor growth and angiogenesis. It is approved to treat hematological malignancies like hairy cell leukemia, chronic myelogenous leukemia and multiple myeloma, as well as solid tumors like malignant melanoma, renal cell carcinoma and AIDS-related Kaposi's sarcoma.

Granulocyte-macrophage colony-stimulating factor (GM-CSF) is a cytokine that causes production of immune cells and blood cells in the bone marrow. The synthetic reagent Sagramostim (Leukine®) is often used after chemotherapy to induce the production of white blood cells[32].

Synthetic drugs that enhance the immune system in a similar way to cytokines are also used in the treatment of cancer. The most common drugs are Imiquimod (Aldara®), a cream that is applied locally to treat early stages of skin cancer, as well as Thalidomide (Thalomid®) and Lenalidomide (Revlimid®), which are used for multiple myelomas.

So far, not many specific immunotherapeutic agents in the treatment of cancer have been approved. For preventive cancer vaccination the Hepatitis B vaccination[26] and the HPV vaccination are the most significant reagents. But even though the HPV vaccination decreased the incidence of pre-cancerous cervical disease and vaccine type specific HPV infection, there is no evidence of a reduction of cervical cancer incidence and mortality. The only therapeutic cancer vaccine approved is Sipuleucel T that shows a survival benefit of 4 months compared to patients treated with a placebo against asymptomatic, metastatic hormone refractory prostate cancer[28].

1.2. Polymers in Cancer Immunotherapy

Polymers are an attractive platform as carriers for drug delivery and cancer immunotherapy. Polymer systems can encapsulate high amounts of bioactive components and thereby reduce their toxicity and protect them from premature interaction or degradation in order to release them either spontaneously or controlled over a certain time at the site of action[33]. Conjugation of small biomolecules to polymers increases their bioavailability due to an extended circulation half life in the blood stream[34] and polymers control the pharmacokinetic and drug distribution profile *in vivo*[35]. The main benefits for their use in immunotherapy are the ability to overcome mechanisms of drug resistance and to elicit immunostimulatory effects[36]. Due to their high variability in synthesis and composition, polymers can be extensively modified to improve conjugation chemistry, biocompatibility or transport abilities. Polymers are well characterized and can easily be functionalized to achieve a high load with one bioactive component or various components. Simultaneous delivery of antigen and activator to dendritic cells greatly enhances the efficiency of the immune response[37].

Polymers have to comply with several requirements to be eligible as drug carriers. The most important properties for *in vivo* applications are low toxicity and immunogenicity. The poly-

mers must not be toxic or immunogenic, which means they must not induce an immune response themselves. Furthermore, polymers should be soluble or colloidal under aqueous conditions for increased effectiveness and exhibit a huge difference in the uptake efficiency into targeted cells over other cells. Other important parameters of nanoparticles are size, surface properties and conjugation with targeting ligands. After delivering its cargo the polymer ideally is removed from the body via renal clearance in order to minimize side effects from the polymer itself. The threshold for renal filtration is a molar mass between 30 and 50 kDa or a hydrodynamic radius of 5nm to be filtered by the kidneys which is especially important for non-biodegradable polymers. Other parameters that can be tuned to eliminate the polymer from the body are flexibility, molecular conformation and incorporation of linkages that are cleavable by hydrolysis or enzymes. This enables the use of larger polymers that have a longer circulation time within the body and an enhanced tumor penetration[38]. The size of a polymeric therapeutic nanoparticle optimally lies between 10 and 100-150nm in diameter. The lower limit is defined by the pore size of the glomerular basement membrane for elimination via renal clearance and the upper limit by the size of the leakages in tumor blood vessels for tumor penetration[34]. For cancer immunotherapy the lower size limit applies as it avoids fast elimination from the blood stream, but the upper size limit is not so important as the efficiency does not relate to tumor penetration but to targeting of and internalization by dendritic cells and DC can internalize particles much larger than 100 nanometer.

The fate of the particle depends on the interaction with its environment which is determined by size and surface properties. As nanoparticles have a high surface to volume ratio, the surface properties of these nanomaterials are of great significance. Particles with only slightly positive or negative charges and additional sterical stabilization, e.g. via PEGylation, exhibit only minimal interaction of particles with serum proteins[8]. Higher surface charge leads to elimination of the particles by macrophages. In general, cationically charged materials have a higher potential to induce an inflammatory reaction of the immune system via complement activation and secretion of cytokines such as TNFα, IL-12 and IFNγ or overexpression of surface markers on dendritic cells[39]. For targeted nanomaterials a high positive charge is disadvantageous as this leads to unspecific uptake by all cell types, before the targeting ligand reaches its destination.

Conjugates of polymers with targeting ligands, such as antibodies or proteins, can specifically address certain cell populations that express the associated receptor. Binding of the antibody-polymer conjugate to the cell surface receptor leads to receptor mediated endocytosis. For example, dendritic cells carry the DEC205 receptor (CD205) and can be targeted with antiDEC205 antibodies.

Polymers currently used in clinical practice as drug carriers are polyglutamic acid (polyglutamic acid-paclitaxel in phase III against lung cancer)[40], polyethylene glycol with various components like anticancer agents or IFNα[41], N-(2-Hydroxypropyl)methylacrylamid (HPMA e.g. conjugated to Doxorubicin)[42] and polysaccharides. Examples for nanocarrier-based drugs on the market are the polymer-protein conjugates styrene maleic anhydride-neocarzinostatin (SMANCS) (Zinostatin/Stimalmer®) against hepatocellular carcinoma[43] and PEG-*L*-asparaginase (Oncaspar®) against acute lymphoblastic leukemia and the albumin-bound paclitaxel nanoparticle Paclitaxel (Abraxane®) against metastatic breast cancer[35].

Furthermore, many basic studies are performed with polymers for cancer vaccines[44], [45]. For example, van Broekhoven *et al.* encapsulated antigen within liposomes consisting of phosphatidylethanolamine-polyethylene glycol-2000 (PE-PEG_{2000}) and α-palmitoyl-β-oleoyl-phosphatidylcholine (POPC) and simultaneously loaded these liposomes with the danger signals lipopolysaccharides (LPS) or IFNγ to achieve sufficient anti-tumor immunity[46]. Kwon *et al.* used pH-responsive microparticles to target DC with the aDEC205 antibody and showed a nearly three times more efficient uptake of targeted microparticles into DC than control particles *in vivo*[47]. Hubbell et al. invented poly(propylene sulfide) (PPS) nanoparticles as drug carriers[48]. Especially poly(ethylene glycol) (PEG)-stabilized PPS nanoparticles, that consist of a rubbery hydrophobic PPS core surrounded by a hydrophilic PEG corona and have diameter of 20-45 nm, can be used for the specific targeting of lymph node DC without the use of a targeting ligand. The hydrophobic PPS domain can carry hydrophobic drugs and release them due to hydrophilization and degradation within mildly oxidative environments[49].

Fahmy *et al*. used poly(lactic-co-glycolic acid) (PLGA) nanoparticles for targeting DC with the aDEC205 antibody[50], e.g. to deliver mycophenolic acid (MPA), a common immunosuppressant[51], or for the delivery of different cytokines to CD4+ T cells[52]. Figdor *et al.* generated nanovaccine carriers made of biodegradable poly(*D,L*-lactide-co-glycolide) harboring super-

paramagnetic iron oxide particles (SPIO) and fluorescently labeled antigen. They targeted these carriers with the DC-specific receptor DC-SIGN to human dendritic cells[53].

Nonetheless, it is difficult to achieve FDA approval of new polymers. Polymeric carriers have to be reproducibly synthesized by good manufacturing practice (GMP) and extensively characterized and tested especially for their toxicity, immunogenicity and metabolic fate within the body.

1.3. Motivation

Solid tumors form by manifestation of tumor cells that avoided detection by the immune system. Tumors use immunoregulatory mechanisms to grow despite an intact immune system. For vaccination strategies to overcome these mechanisms high amounts of antigen and a strong activator are needed to induce a specific milieu for activation of DC. The activator boosts the immune response to sufficiently stimulate T cells without inducing immunotolerance or autoimmune reactions.

Rosenberg et al proposed 2004 three criteria for immunologic destruction of established tumors[54]. First, *in vivo* generation of sufficient numbers of immune cells that exhibit highly avid recognition of tumor antigens is needed. Second criteria is that these immune cells must be able to migrate to and infiltrate the tumor stroma. Last, the immune cells must be activated at the tumor site to feature appropriate effector mechanisms like cytokine secretion or direct tumor lysis which results in tumor destruction.

Cancer vaccines are supposed to meet these criteria by inducing an immune response specifically against tumor antigens by *in vivo* targeting dendritic cells with tumor antigens. Dendritic cells are a promising target for cancer vaccines as they are potent antigen presenting cells and link the innate and the adaptive immune system by controlling and coordinating immunological processes. These cells internalize antigen, process it and present it on major histocompatibility (MHC) complexes to T cells. Together with costimulatory molecules such as interferons and interleukins a potent immune activation takes place and cytotoxic T lymphocytes can now destroy the tumor that expresses the tumor antigens on its cell surfaces.

So far, *ex vivo* loading of dendritic cells with tumor antigens (Figure 1b) is examined in clinical trials[55], but only little success can be achieved by inducing an anti-tumor immune response. Therefore, current studies concentrate on *in vivo* vaccination strategies of DC (Figure 1d).

Targeting of dendritic cells *in vivo* can be achieved with monoclonal antibodies directed against specific surface receptors. CD8+ dendritic cells express the DEC205 receptor (CD205) on their cell surface and can be addressed with the antiDEC205 antibody[56]. CD8+ DC are able to present exogenous antigen on MHC class II complexes to CD4+ T cells and additionally on MHC class I complexes to CD8+ T cells via cross-presentation.

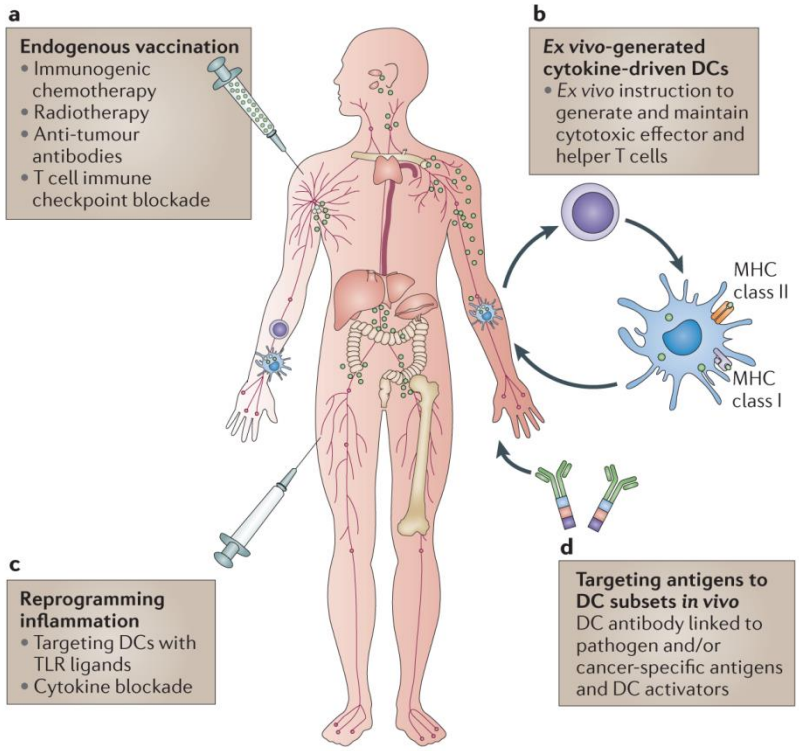

Figure 1: Dendritic cells and cancer immunotherapy (figure from Palucka *et al.*)[56]; a: random targeting of DC by in vivo antigen release by immunogenic death cells after chemotherapy, radiation and immunomodulation approaches targeting T cells; b: Ex vivo loading of DC with tumor-antigen and reinjection into the patient; c: reprogramming pro-tumor inflammation by targeting DC in the tumor microenvironment; d: Specific targeting of DC in vivo with DC antibodies fused with antigens and DC activators.

This leads to more efficient T cell activation and immune stimulation and therefore the research focus for particle vaccines lies on targeting with the aDEC205 antibody. The first vaccine particles targeting DC with aDEC205 resulted in an increase in DC uptake of particles as well as in the magnitude of T cell responses *in vivo*[47]. Poly(lactic-co-glycolic acid) (PLGA)-Nanoparticles targeting DC induced secretion of IL-10 and IL-5, Th2-associated cytokines, by

DC and T cells and evoked IgG1 antibodies depending on the density of a DEC205 on the NP surface[50]. PLGA NPs that encapsulate tumor antigens and a TLR4 antagonist are able to activate DCs in lymph nodes and induce anti-tumor immune responses that reduced melanoma tumors *in vivo*[8].

Particle size and linker chemistry between polymer and antibody appear to be important factors in the targeting efficacy of DC[8]. Ideally, cancer vaccination induces a specific immune response against a tumor associated antigen (TAA) that is efficient and long lasting. Thus, activation of DC is essential. This can be achieved with a system consisting of a targeting moiety, which is the aDEC205 antibody, a tumor associated antigen for specificity of the immune response and an activator, e.g. CpG oligonucleotides, lipopolysaccharides (LPS) or polyinosinic:polycytidylic acid (poly I:C).

Kreutz *et al.* investigated the antibody-mediated co-delivery of antigen and adjuvant[37]. They conjugated antigen and adjuvant directly to the antibody, either by biochemical conjugation of antigen and adjuvant or by genetic fusion of antibody and antigen and subsequent biochemical conjugation of adjuvant. They showed that these conjugates are more potent at inducing a cytotoxic T lymphocyte (CTL) response than antibody-antigen conjugates administered with soluble adjuvant. Although antigen and adjuvant altered binding and uptake of the conjugate by mediating binding to DC independently of aDEC205, the conjugate with aDEC205 as targeting antibody exhibited better induction of CTL responses and efficiently induced anti-tumor immunity in a murine B16 pseudo-metastasis model than the control conjugate without antibody.

Polymers can serve as carriers for conjugation of a targeting moiety, an antigen and an activator to specifically deliver antigens and an activator simultaneously to DC. Macromolecules are very convenient as they can be loaded with a high amount of antigen and activator without the load influencing the pharmacokinetic properties of the particle. Additionally, several targeting ligands can be conjugated to one polymer that enables multivalent binding to surface receptors. Targeting ligands can be proteins, such as antibodies or antibody fragments, nucleic acids (aptamers) or receptor ligands such as peptides, vitamins or carbohydrates. More than 200 delivery systems based on targeting via antibodies or antibody fragment are currently in pre-clinical and early clinical studies. Antibodies can be used native or as fragments, whereas whole antibodies provide the advantage of two binding sites in one mole-

cule and therefore achieve a higher binding affinity. One major disadvantage of native antibodies is that they can unspecifically bind to other immune cells with their Fc-region which leads to higher immunogenicity and uptake of nanoparticles into liver and spleen[35].

Targeted nanoparticles are internalized into the cell via receptor-mediated endocytosis and therefore avoid multidrug resistance that relies on protein pumps in the cell membrane. For this type of immunotherapy methods have to be established to specifically load DC with antigen and activate them with a strong stimulus.

Palucka and Banchereau state that for therapeutic vaccination via DC and an efficient immune response at least four components of the immune response are necessary: "the presence of appropriate DC, the quality of induced CD4+ T helper cells, the elimination and/or non-activation of T_{reg} cells and the breakdown of the immunosuppressive tumor microenvironment"[56]. Thus, polymeric carriers loaded with a targeting ligand, tumor-associated antigens and adjuvants are a promising approach for the treatment of cancer via immune stimulation.

1.4. Scope of Work

In this thesis, dendritic cells will be targeted and activated with a polymer conjugate to load DC with tumor-associated antigen (TAA) and induce a T cell immune response specifically against tumors that carry this antigen.

First, the optimal targeting ligand for dendritic cells shall be identified and characterized. Former studies explain that it is advantageous for the induction of an immune response to target CD8+ dendritic cells with the aDEC205 antibody as this DC subpopulation is able to cross present exogenous antigen to CD8+ T cells[57]. Therefore, aDEC205 is compared to other antibodies that target dendritic cells with regard to binding specificity, internalization kinetics and localization within the cell. Other antibodies investigated are CD11c, an integrin which is expressed in high levels on CD8- and CD8+ DC, and Clec9a[58], [59] and Clec12a[60] that were recently discovered as targeting ligands for CD8+ dendritic cells.

The polymer serves as a carrier to which the bioactive components are attached. Linear poly-L-lysine (PLL) is investigated as a model system and the conjugation chemistry is transferred

to the polylysine brush (PLL brush). Linear PLL is chosen as it is already used a drug carrier and for DNA transfection [61], [62] and it is commercially available. The quantity of amine groups of the lysine is a good target for covalent attachment of biomolecules through a variety of linkers. On the other hand the high number of free amines can lead to aggregation with serum components and positively charged particles exhibit problems regarding solubility of conjugates due to aggregation and precipitation[63]. These problems are further enhanced by the application of linkers like Sulfo-SMCC and DIBO that are typically hydrophobic. In order to detect and avoid these problems, PLL and the PLL brush shall be characterized prior to their use as polymeric carriers regarding their hydrodynamic radius, their internalization into splenic and bone marrow-derived DC and their toxicity. Furthermore, functionalization is considered to reduce the amount cationic charges, both by chemical transfer and sterical shielding.

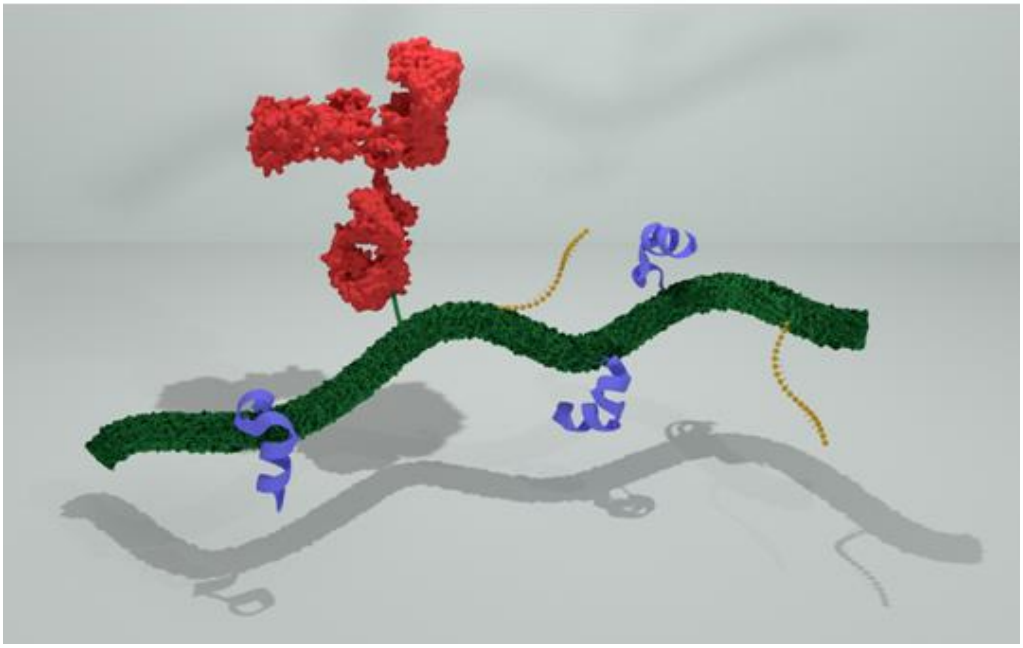

Figure 2: Scheme of the PLL brush-Antigen-CpG-aDEC205 conjugate; green: PLL brush, blue: OVA-specific antigen, yellow: oligonucleotide CpG1826, red: aDEC205 antibody

The tumor-associated antigen conjugated to the polymeric carrier is an ovalbumin (OVA)-specific antigen, a short peptide consisting of 16 amino acids with the core peptide sequence SIINFEKL. This antigen resembles structures presented on the surface of tumor cells and thus induces specificity of the immune response against the tumor. Additionally, an immunoactivating component is needed for secretion of costimulatory molecules. Therefore, an im-

muno-activating Toll-like receptor (TLR) 9 ligand, the oligonucleotide CpG1826, is introduced into the system. This oligonucleotide binds to TLR 9 within the endosome and induces a milieu (e.g. with Interleukin-12) that provokes maturation of DC and development of T cells to T_{H1}-cells that mediate a cytotoxic CD8 T cell immune response and therefore a sufficient activation of the immune system.

A conjugation strategy for the antibody, antigen and activator must be established and the conjugates will be characterized with respect to the conjugation efficiency, size and their behavior in buffer and blood serum, internalization into CD8+ dendritic cells and T cell activation ability. The antibody is conjugated to the polymer via two strategies; site specific conjugation is performed via oxidation of its glycosidyl residues and subsequent reductive amination with the amine groups of PLL. Another method of conjugating the antibody is copper free click chemistry via the heterobifunctional crosslinker DIBO linked to PLL and PEG-azide modified antibody. Antigen and activator are conjugated via their free-thiol groups to maleimide-functionalized PLL. Conjugation efficiencies will be tested with UV/Vis spectroscopy, internalization of the conjugates into dendritic cells with flow cytometry and confocal laser scanning microscopy and the ability to induce an immune response with T cell proliferation assays.

The efficiency of the polymer-drug-conjugate and the capacity of dendritic cells to induce an immune response against OVA-expressing cancer cells are expected to be significantly enhanced by attaching the three components, targeting antibody, TAA and activator onto a polymeric carrier (Figure 2). Co-administration of antigen and activator to the same place at the same time is needed to induce a powerful and lasting immune reaction[37].

To summarize, a conjugate consisting of PLL or PLL brush as polymeric carrier, aDEC205 as targeting antibody, SIINFEKL as a model tumor-associated antigen and CpG 1826 as an adjuvant have to be synthesized and characterized. These conjugates are expected to target CD8+ dendritic cells via the DEC205 receptor on the cell surface and the aDEC205 antibody at the conjugate and internalize into DC via receptor-mediated endocytosis. Within the DC the antigen will be cleaved or not from the conjugate, but processed. After processing, the antigen will be cross-presented on MHC class I complexes and activate CD8+ T cells. In order to induce a sufficient cytotoxic T lymphocyte response against cancer cells, the activator,

CpG 1826 binds to the TLR9 receptor in the endosome of DC and mediates the release of costimulatory molecules such as interferons and interleukins (Figure 3). Due to the memory function of memory T cells this approach is thought to exhibit a specific, efficient and long-lasting immune response against tumor cells.

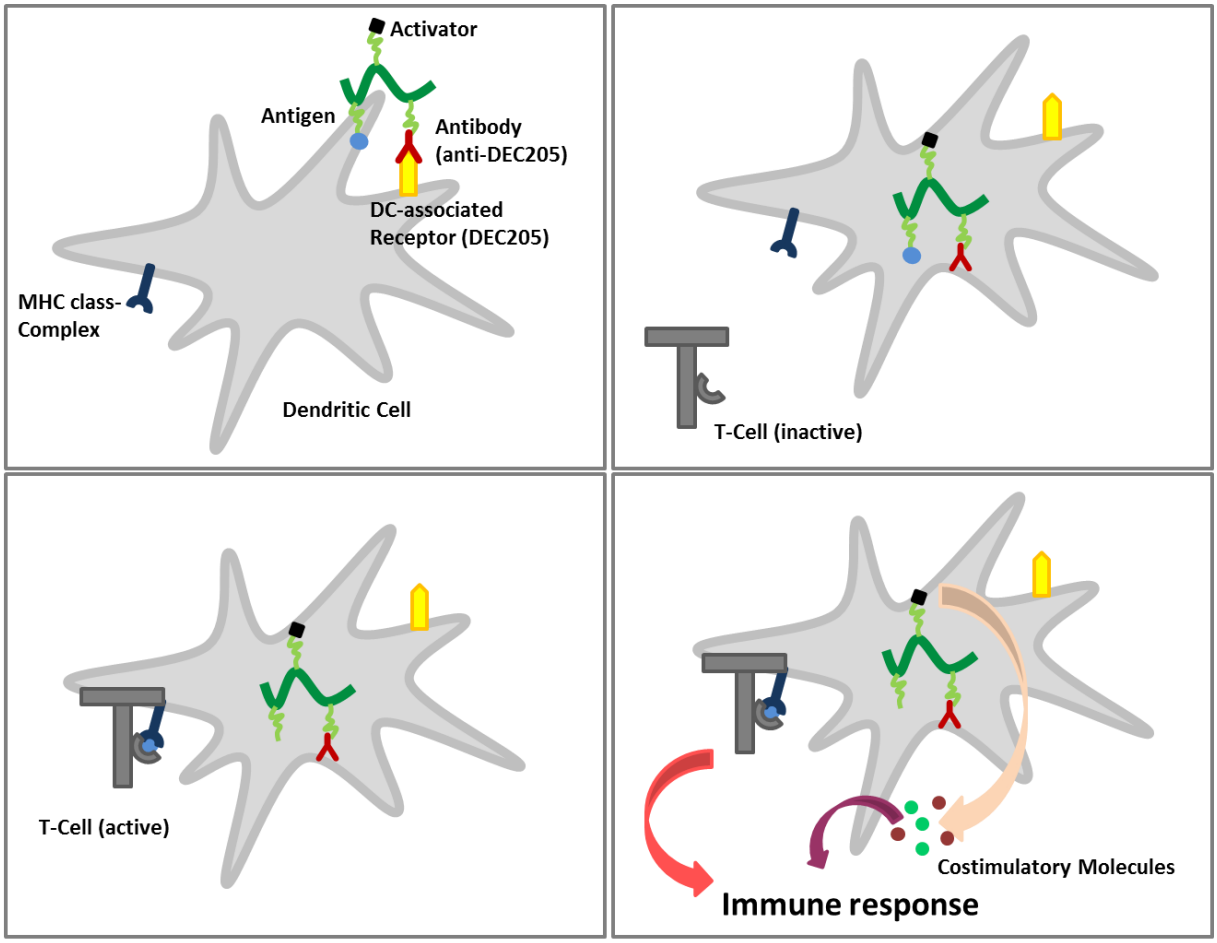

Figure 3: Scheme of internalization into DC and mechanism of action for the PLL-Antigen-ODN-aDEC205 conjugate. The conjugate reaches its site of action, the dendritic cell, via the aDEC205 antibody and is internalized via receptor-mediated endocytosis of the DEC205 receptor on the DC surface. The dendritic cell processes the antigen and presents it on MHC class I complexes to naïve T cells which leads to T cell activation. The activator, a CpG TLR9 antagonist, binds to TLR9 in the endosome of DC which initiates secretion of costimulatory molecules that enhance T cell proliferation and an efficient anti-tumor immune response.

2. Theory

2.1. Immune System

The immune system protects the body from foreign microorganisms, toxins and malignant cells. Thus, an important function is the differentiation between “self” and “non-self” antigens. “Self” antigens have to be recognized and tolerated in order to avoid destructive autoimmune responses. “Non-self” antigens have to be destroyed upon detection in order to avoid infections and to stay healthy.

2.1.1. Innate and Adaptive Immune System

The immune system is divided into the innate (antigen-nonspecific) and the adaptive (antigen-specific) immune system.

The innate immune system is the defense mechanism against infection caused by pathogens invading the body. It unspecifically attacks any pathogen independent on the type. The first barriers that should prevent pathogens to infiltrate the body are the natural protective acid mantle of the skin, the intact epidermis, the complement system, antimicrobial enzymes and unspecific mediators such as interferons and interleukins. Cells of innate immunity are granulocytes, mast cells, macrophages, natural killer (NK) cells and dendritic cells (Figure 4). When a conserved microbial pathogen that represents a pathogen associated molecular pattern (PAMP) infiltrates the body it usually is detected by pattern recognition receptor (PRR) such as Toll-like receptors (TLR). These receptors are selected by phylogenesis and therefore represent a genetically conserved memory of PAMP. PRR play an important role in inducing a primary immune response and activating cells of the adaptive immune system[64], [65].

But there are also other recognition mechanisms like the complement system, specialized receptors that enable NK cells to sense non-self, “missing-self” and “induced-self”, and certain intracellular sensors[66]. Inflammation is a crucial defense process that recruits all defense forces to the infection site via a complex network of humoral and cellular components.

Pathogens are loaded with proteins of the complement system and thus marked for phagocytosis by macrophages. Secretion of mediators induces vasodilation and enhanced permeability of the capillary barriers which enables granulocytes and macrophages to migrate to the infection site and to abolish and phagocytose marked pathogens. Innate immunity acts within a few hours after infection.

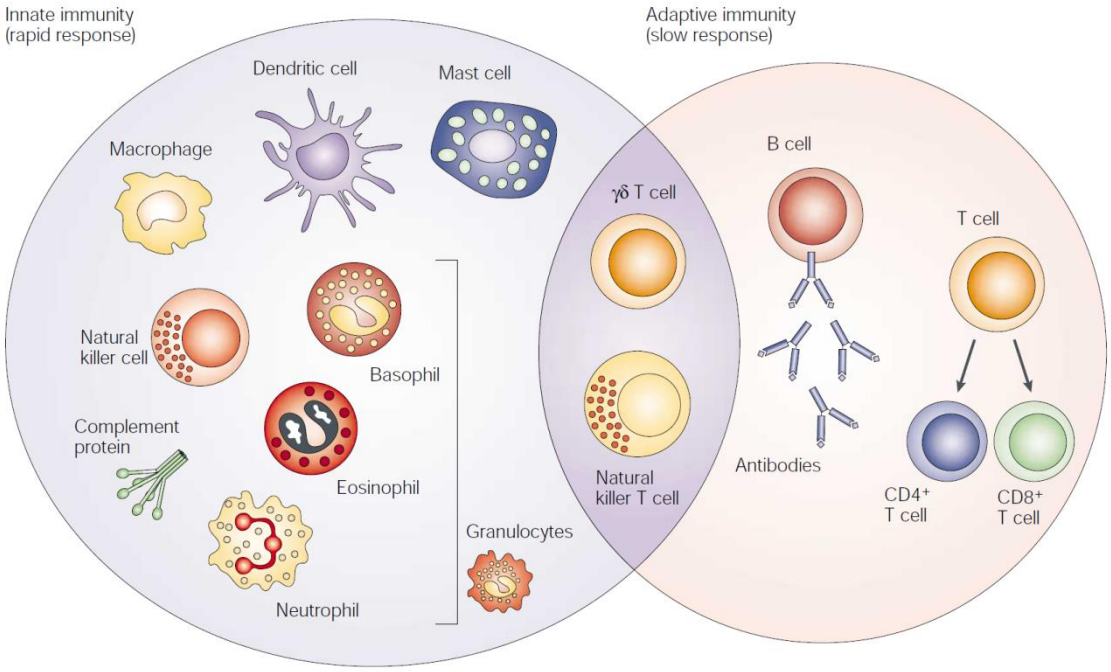

Figure 4: The innate and adaptive immune response(figure from Dranoff *et al.*)[67]

These systems ensure the development of a subsequent adaptive immune response. The adaptive immune response develops humoral immunity by neutralization and eradication of extracellular microbes and toxins via antibodies secreted by B (bursal or bone marrow-derived) lymphocytes and cell-mediated immunity via T (thymus-derived) lymphocytes (Figure 4). The cells of the adaptive immune system act highly specific to the invading antigen and the antigen-specific cells proliferate via clonal expansion which induces a very efficient specific immune response and memory function against this antigen via memory T cells.

B cells hold several immunological functions in the adaptive immune response. They are mainly considered to be positive regulators of immune responses and to contribute to the pathogenesis of immune related diseases due to their ability of antibody production[68].

Binding of an antigen presented on MHC complexes of DC enables differentiation of B cells into plasma cells that express antigen-specific antibodies and secrete them into the blood[69]. T lymphocytes have two main functions in the adaptive immune system, the regulation of the complex adaptive immune response and destruction of infected cells due to their cytotoxicity. Every T cell subset expresses a unique T cell receptor (TCR) that enables binding to dendritic cells that present antigen either on MHC class I or class II complexes. Upon binding to an antigen, activation occurs which is mediated by the assembly of receptors and mediating factors secreted at the interface between T cell and antigen presenting cell[8]. Depending on their surface molecules and the induced immune response T lymphocytes can be subdivided into CD8+ T cells and CD4+ T cells (Figure 4). CD4+ T cells are responsible for differentiation of T helper cells while CD8+ T cells induce a CTL immune response that is important for destruction of anti-tumor immunity. Upon encountering of tumor-derived antigen presented by MHC class I complexes, naïve CD8+ T cells initiate differentiation of cytotoxic T lymphocytes (CTL). The quality of the CTL response is regulated by CD4+ T cells, as they influence the differentiation and expansion of TAA-specific CTL and induce differentiation of memory CD8+ T cells [56]. Furthermore, CD4+ T cells destroy tumors by activation of macrophages at the tumor site and by actively killing tumor cells. On the other hand, regulatory CD4+ T cells (Treg) can also suppress CTL differentiation and therefore induce immune tolerance[56]. T helper cells (T_{H1} and T_{H2}) activate many other immune cells such as B cells, T_{reg} have a regulatory function, while CTL delete infected cells, e.g. cancer cells in an early stage before they escape immunosurveillance.

There are two different types of killer cells, CTL of the adaptive immune system and natural killer (NK) cells belonging to the innate immune system. Killer cells contain granula filled with mediators such as interferons and interleukins that they release onto the target cell after binding. CTL need a specific to MHC-self marker bound antigen for binding, while NK cells detect the target cell due to missing of MHC-self markers. Therefore, NK cells acts more unspecific and can detect many foreign cells.

2.1.2. Dendritic Cells in Cancer Immunotherapy

Dendritic cells (DC) are bone marrow-derived cells that function as professional antigen-presenting cells (APC) and hold a regulatory function in the adaptive immune system[70], [71]. DC are able to distinguish between self antigens and foreign antigens using receptors of the innate immune system, e.g. Toll-like receptors (TLR). DC can also interact with cells of the innate immune system, such as macrophages, phagocytes and natural killer cells and therefore forming a link between innate and adaptive immune response[72].

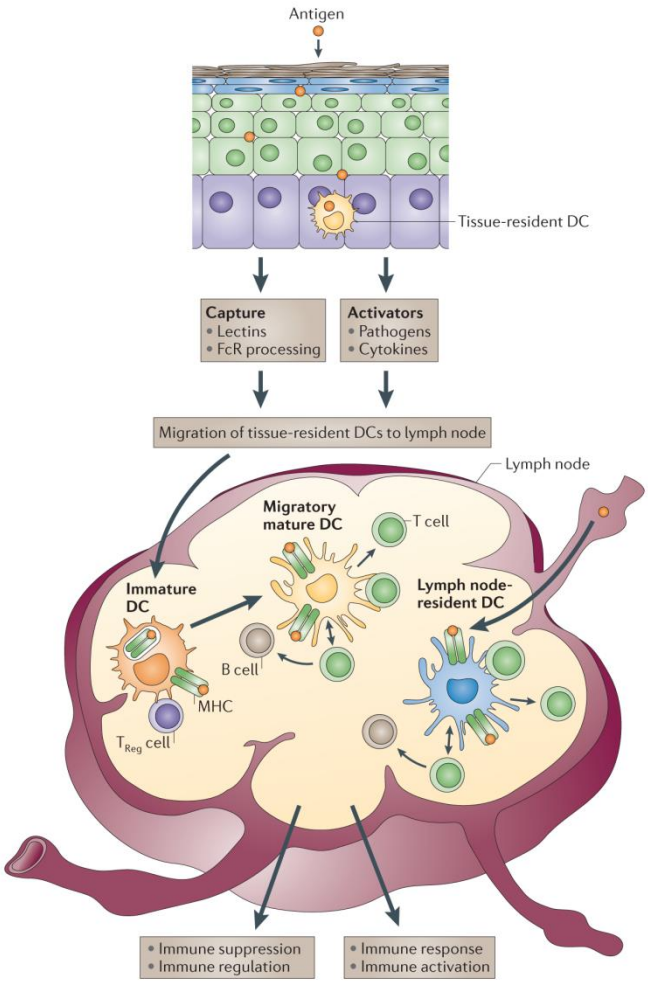

Figure 5: Induction of an immune response by dendritic cells (figure from Palucka *et al.*)[56]. Antigens are delivered to the lymph nodes via two pathways: via lymphatics, where the antigen is captured by lymph node-resident DC or via DC that reside in the tissue. Immature DC capture antigen and upon activation DC migrate towards secondary lymphoid organs and mature. Antigen-presentation occurs via MHC class I or class II complexes that recruit antigen-specific T lymphocytes. Activated T cells push DC to their terminal maturation which induces further expansion and differentiation of T lymphocytes into effector T cells. Without a maturation signal, DC remain immature and antigen-presentation leads to immunity against the presented antigen.

When antigen is captured in the presence of inflammatory stimuli or microbial products, immunity is provoked, while without these danger signals tolerance is elicited[73]. DC are sampling antigens and present them on MHC complexes to naïve T cells in lymphoid tissue. DC residing in the lymph node and capturing antigen in the lymph activate CD4+ T cells which leads to priming of T cells and IL-2 production which then results in T cell proliferation and clonal expansion. If tissue-resident DC capture antigen in peripheral tissues, they migrate into the lymph node and present antigen to the already activated CD4+ T cells(Figure 5). This leads to the generation of antigen-specific T effector cells. CD4+ T cells can differentiate into T helper cells (Th1, Th2 and Th17) or T follicular helper cells (TFH) that induce differentiation of B cells into antibody-secreting cells or regulatory T cells (T_{reg}) that downregulate the function of other lymphocytes and induce tolerance mechanisms. Upon interaction with DC naïve CD8+ T cells induce proliferation of cytotoxic T lymphocytes (CTL). The type of T cell response depends on the subset of DC presenting the antigen[58].

CD8+ DC and cross-presentation

DCs can be subdivided into two major subsets; myeloid (conventional) DC and plasmacytoid DC that differ in their Toll-like receptor expression[74]. Murine blood-borne precursors reside in the spleen and the lymph nodes and differentiate into immature conventional DC (cDC) which sample the blood for pathogens. These lymphoid tissue-resident cDC can be subdivided into subsets regarding their expression of CD8α and CD4 (Figure 6). CD8+ DC express CD8α but no CD4, CD4+ DC carry CD4 but no CD8α and the double negative (DN) DC express none of these surface molecules[75]. CD4+ and DN DC are usually referred to as CD8- DC. The lymph nodes additionally contain migratory DC subsets that do not differentiate from precursors within the lymph node but migrate to the lymph node via the afferent lymphatics in mature state (Figure 6). All cDC subsets have the ability to internalize, process and present antigen which then activates naïve T cells. But these subsets exhibit specific functions regarding their presentation mechanisms and type of T cell response they induce. The important feature of CD8+ DC is their superior ability to present exogenous antigens on MHC class I molecules to CD8+ T cells[76]. This mechanism is called cross-presentation and is crucial for the induction of cytotoxic T lymphocytes and thus an efficient anti-tumor immunity[58].

The reason for CD8+ DC to be superior at cross-presenting lies in the selective expression of phagocytotic receptors and the specialization of their endocytotic pathway[77]. In the endocytotic pathway of CD8+ DC proteolysis is limited which avoids degradation of potential epitopes. Different mechanisms inhibit proteolysis, including the inhibition of acidification in endosomes and phagosomes through the production of reactive oxygen species[76]. Additionally, an exogenous antigen has to be transferred into the cytosol for efficient cross-presentation through the proteasome-dependent pathway which is more efficient in CD8+ than CD8- DC[78].

Therefore, CD8+ DC are more efficient at inducing antigen-specific CD8+ T cell responses, while CD8- targeted antigen more potently facilitates CD4+ T cell responses (Figure 6). This implies that CD8- DC are inherently predominant at MHC class II presentation of antigen while CD8+ DC cross-present antigen on MHC class I complexes.

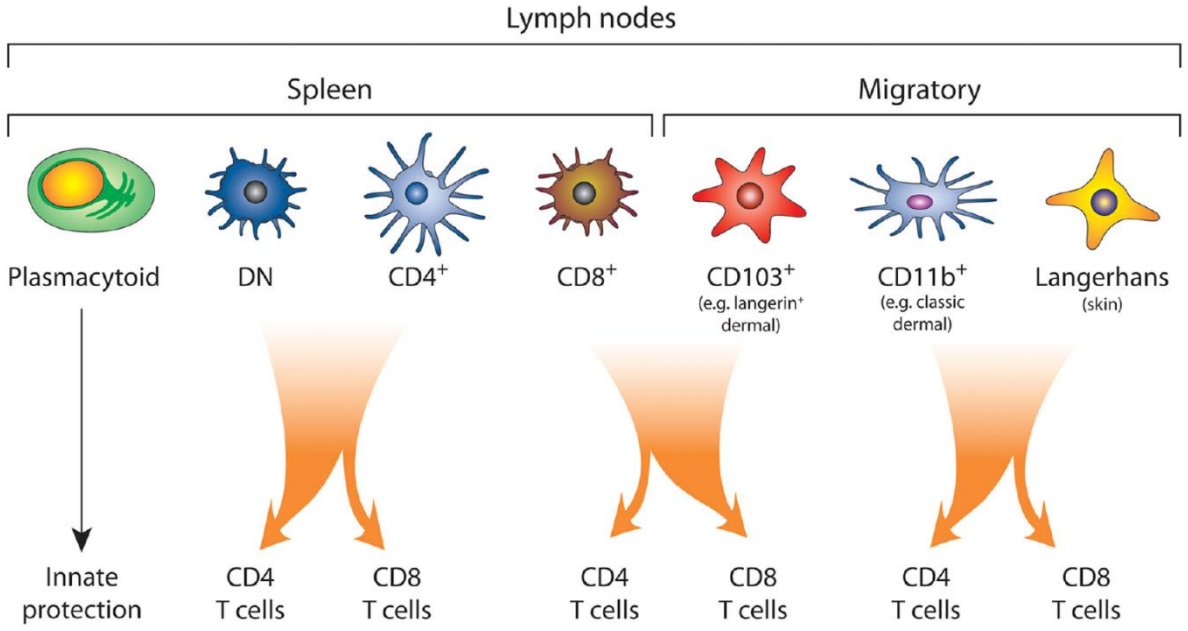

Figure 6: Dendritic cell subsets and their T cell activation (figure from Caminschi *et al.*)[74]. Plasmacytoid DC secure innate protection against pathogens by efficient production of type I IFN. Conventional DC include lymphoid tissue-resident and migratory DC and provide adaptive immunity. Splenic DC are segregated into CD4+, CD8+ and double negative DC. Migratory DC are divided into CD103+, CD11b+ (dermal) and Langerhans' cell of the skin. DC subsets exhibit functional specialization. Splenic DN and CD4+ cells and lymphoid CD11b+ and Langerhans' cells are more efficient to induce CD4+ T cell responses via antigen presentation on MHC class II molecules. CD8+ and CD103+ DC are superior in cross-presenting antigen on MHC class II molecules and thus inducing a CD8+ T cell response.

For *in vivo* delivery of antigens to DC it is important to target the antigen exclusively to DC without simultaneously loading other cell types as e.g. antigen presentation by B cells is

known to induce tolerance rather than immunity. So, for efficient cancer immunotherapies based on antigen cross-presentation by antigen delivery to DC highly specific targeting is a stringent condition of an interference-free immune system processing. Only very few surface molecules are exclusively expressed on DC. An example is Clec 9A that is selectively expressed by CD8+ DC and to a small amount on plasmacytoid DC but not on other cell types[58]. Nonetheless, CD11c, DEC205, mannose receptor and Clec12A have been shown to induce efficient immune responses, despite their expression by non-DC such as macrophages and natural killer cells [74]. Supposably, targeting of different DC subsets may lead to different types of immune response.

The molecule that is most extensively studied for delivering antigen to DC is the aDEC205 antibody that binds to the DEC205 receptor on DC. DEC205 is a multi-lectin endocytic receptor that is highly expressed on DC8+ DC[79], but also found on other DC subsets to a lower amount. The primary function of DEC205 still remains unknown, but it has been reported to bind bacterial components and dead cells and targeting this receptor with antigen and adjuvant results in a strong cellular and humoral response. Without maturation signal, targeting antigen to DEC205 may lead to T cell tolerance by deletion of T cells and generation of T_{reg}[46].

Immature versus mature DC

The paradigm of dendritic cells is that immature DC are potent at sampling antigen, but cannot efficiently interact with T cells while mature DC are ineffective antigen sampler but strong immune stimulators for T cells specific for antigen captured in the immature state[72]. DC need to achieve a certain level of maturation to effectively stimulate and expand antigen-specific T cells or to induce tolerance.

DCs in peripheral tissues are usually immature. The main ability of immature DC is efficient capture of antigens via endocytosis through a variety of mechanisms, including nonspecific uptake via macropinocytosis and specific uptake via receptor-mediated endocytosis and phagocytosis[73]. Additionally, immature DC accumulate MHC class II molecules in the late endosomal-lysosomal compartment and exhibit low level-expression of costimulatory molecules and low secretion of cytokines [80]. If the antigen is presented by non-activated (imma-

ture) DC to T cells, immune tolerance is induced either through deletion of T cells or through differentiation of regulatory or suppressor T cells.

Environmental signals, such as inflammatory stimuli or bacteria, can mediate differentiation of DCs into mature DC that can efficiently induce immune responses. Upon maturation DC undergo dramatic functional and morphological changes that maximize antigen presentation to T cells. In the course of maturation, DC downregulate their antigen-capture activity, acidify the lysosomal compartments for effective antigen processing and increase the expression of surface MHC class I and class II molecules by reorganizing them from the late endocytic compartment to the plasma membrane[73]. Expression of costimulatory molecules is upregulated, as well as the ability to secrete cytokines and expression of chemokine receptors CCR7 that enables migration into the draining lymph nodes[80]. Thus, mature DC exhibit an increased capability of antigen presentation which is important for activation of T cells in the draining lymph nodes.

It is recently discovered that although mature DC downregulate unspecific uptake, they maintain the ability to specifically internalize via receptor-mediated endocytosis and phagocytosis via clathrin-dependent pathways. Antigens taken up by mature DC are processed normally within late endosomes and lysosomes and efficiently presented on MHC class II or cross-presented on MHC class I molecules. This indicates that mature DC are able to initiate immune responses to newly encountered antigens during the process of an infection[73].

The ligation of the costimulatory receptor CD40 is a crucial signal for complete DC maturation and adaptive T cell-mediated immunity. Additionally, activated DC can facilitate maturation of activated B cells into plasma cells via cytokines and surface signaling. If activated (mature) DC present antigens, antigen-specific T cell differentiate into effector T cells with unique functions and cytokine profiles and an immune response is launched.

For DC vaccination strategies the maturation state of the DC plays an important role. When addressing immature DC it is crucial to simultaneously deliver a maturation stimulus as otherwise immune tolerance is induced upon antigen presentation. An adjuvant is required to induce cellular immunity by cytotoxic T lymphocytes[74],[81]. Mahnke et al showed that expression of regulatory T cells is induced when targeting antigen to immature DC[82] while

efficient protection against melanoma due to melanoma-specific CD4 and CD8 responses could be achieved when targeting antigen to activated DC[83].

This may even indicate that targeting immature DC for vaccination purposes shall be avoided as immature DC are poor immunogens and can induce T_{reg} cells and thus fatal tolerance[84]. Furthermore, mature DC are clearly superior at inducing T effector cell proliferation and immunity and therefore should be considered as a target for vaccination[85].

bmDC vs. splenic DC

For *in vitro* experiments, murine DC either have to be cultured from bone marrow progenytor cells, or isolated from non-lymphatic organs such as the skin, lung or gut, or from lymphatic organs such as the spleen or lymph nodes. These two ways of isolation result in slightly different DC regarding their type and maturation state. Bone marrow-derived DC (bmDC) are derived from pluripotent precursors that have to be cultured *in vitro* in granulocyte macrophage-colony stimulating factor (GM-CSF) and interleukin-4 for 6 days to differentiate into immature DC and mature *in vitro* for additional one to four days to become fully mature[86]. This generation of DC from GM-CSF-driven bone marrow cultures yielded important insights, but these cells reflect extreme simplified conditions of the *in vivo* counterpart[87]. It is currently believed that DC generated from murine bone marrow (or human peripheral blood) resemble inflammatory DC as their *in vivo* counterpart.

Splenic DC originate from precursors in the bone marrow or in the blood that differentiate in the spleen *in vivo* and are isolated as immature DC[88]. Splenic DC cannot be cultured *in vitro* for prolonged periods of time as they immediately mature and lose ability to process native protein antigen. Moreover, they are a heterologous cell population, consisting of at least two functionally different DC subtypes, CD4-expressing DC that are most effective in stimulating T helper cell responses, and CD8+ DC, which are potently able to cross present antigen and activate cytotoxic T cells. Freshly isolated splenic DC show similar processing ability to bmDC and are therefore considered to be the *in vivo* counterpart of bmDC. BmDC and splenic DC show comparable ability to induce T cell proliferation[86]. Therefore, it has to be carefully considered which type of DC at which maturation state is used for *in vitro* experiments and how to interpret the results with respect to the type of DC that is used.

2.2. Components of the Immuno-Activating Conjugate

As described in the scope of work in Chapter 1.4. an immune-activating conjugate, consisting of PLL as polymeric carrier, aDEC205 as DC-targeting antibody, an OVA-specific antigen and an activator, will be synthesized. These components are described in detail in the following section.

2.2.1. aDEC205 Antibody

Specific targeting of components like drugs or drug-conjugates to certain cells is important for the specificity of action, e.g. infected cells can be destroyed while healthy cells are spared.

In this thesis, the monoclonal antibody aDEC205 is used to specifically target the DEC205 receptor on the surface of dendritic cells which leads to receptor-mediated endocytosis.

DEC205 (CD205) is a 205kDa molecule which belongs to the C-type multilectin receptor family, which also includes the macrophage mannose receptor (MMR) and the phospholipase A2 receptor. This family of receptors is characterized structurally by a cysteine-rich N-terminal domain, an adjacent fibronectin type II domain and an internalization sequence in its cytoplasmic domain. In case of aDEC205 ten C-type lectinlike domains, which are carbohydrate recognition domains, subsequently follow, whereas the other receptors only contain only eight carbohydrate recognition domains. In contrast to MMR, DEC205 uptake is an effective pathway for antigen presentation [79].

The domain structure of the DEC205 receptor indicates the potential for recognition of multiple ligands[89]. The ligand specificity has not been described yet, but there is some evidence that DEC205 recognizes protein modifications other than glycosylation patterns identified by MMR[90]. Recently, Lahoud *et al.* described that the DEC205 receptor is also involved in binding and internalization of CpG ODN *in vivo* and therefore is important for the adjuvancy effects of B ODN[89]. This aspect will be further discussed in the theory about CpG and the results part of this thesis.

DEC205 is mostly expressed on CD8+ DC, but also to a small amount on B cells, macrophages and CD8+ T cells[74, 89]. The DEC205 receptor recycles from the late endosomes to the cell

surface and enhances antigen presentation[79]. Thus, the receptor targets late endosomes or lysosomes rich in MHC class II products and therefore enhances antigen presentation on the surface of DC. This late endosomal targeting is caused by two functional regions of the DEC205 receptor. A membrane-proximal region is responsible for uptake, while a distal region mediates the unusual deeper targeting. The membrane proximal region includes the amino acid sequence FSSVRY that equals the sequence for coated pit localization described for many other receptors[91]. The distal region of the DEC205 receptor contains the EDE triad, a cluster of acidic amino acids, that mediates the unusual deeper targeting. Thus, the cytosolic domain of the receptor conveys receptor-mediated endocytosis that causes efficient recycling through late endosomes and an enhanced efficiency of antigen presentation to CD4+ T cells and cross-presentation to CD8+ T cells.

The aDEC205 antibody targets this receptor on DC and therefore induces receptor-mediated endocytosis of antibody-bound components[57]. aDEC205 belongs to the class of immunoglobulin 2a (IgG2a) antibodies and consists of 2 heavy chain fragments and two light chain fragments linked via disulfide bonds, three bonds in the hinge region between the two heavy chains and one between each heavy and light chain, respectively (Figure 7).

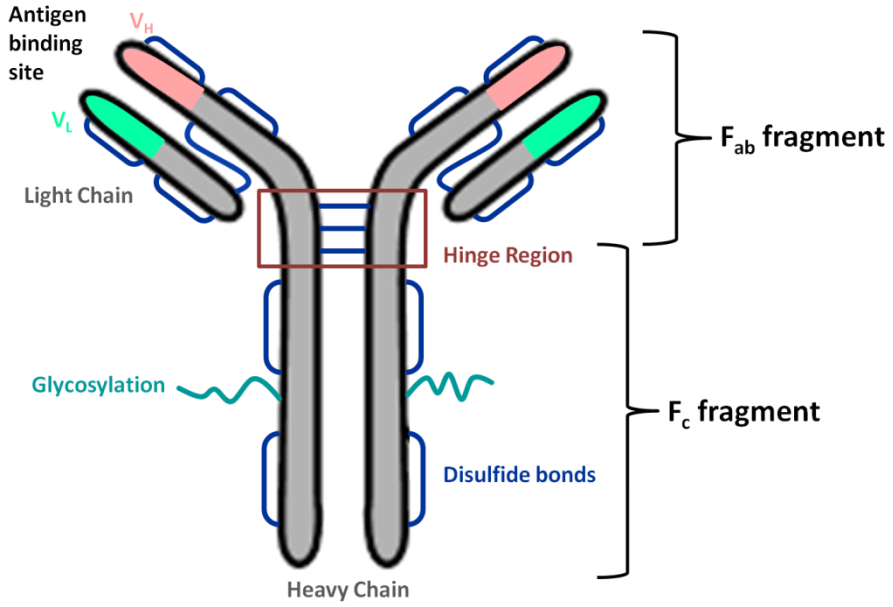

Figure 7: Primary structure of an IgG2a monoclonal antibody

The heavy γ chain has a molecular weight of 50kDa and is conserved for all IgG molecules. The light chains have a molecular weight of 25 kDa each which results in ~150kDa for the

whole IgG molecule. Immunoglobulins consist of 82-96% polypeptides and 4-18% carbohydrates which are N- and O- bound oligosaccharides[92]. The heavy chain is glycosylated mostly in the C_H^2 domain of the Fc fragment ("fragment crystallizable") which can serve for site-specific conjugation via the carbohydrates. Every IgG molecule has two antigen binding sites located at the interface of heavy and light chain (variable domain pair V_L:V_H) close to the N terminus in the hypervariable region formed by six hypervariable loops at the tips of the "Y" structure (Figure 7)[93]. This tertiary structure provides the conformation that is needed to bind to antigens/receptors. The binding site exhibits a high binding specificity for one special antigen molecule due to high structural complementary and a combination of van der Waals forces as well as ionic and hydrophobic interactions[94].

Several strategies can be used for conjugation of antibodies. A popular target for chemical ligation are the amine and carboxyl groups of lysine and the acidic amino acids glutamic acid and aspartic acid which are in large quantity widely distributed over the antibody molecule. These groups can be reacted with heterobifunctional crosslinkers to introduce reactive moieties. The most popular crosslinker to conjugate antibodies is Sulfosuccinimidyl-4-(N-maleimidomethyl)cyclohexane-1-carboxylate (Sulfo-SMCC)[95], [83], [96], [94] that introduces a maleimide functionality to the ε-amino groups of lysine which then can react with sulfhydryl groups. The disadvantage of this method is that conjugation can occur at the antigen binding site as these groups are equally distributed over the whole molecule. This may lead to sterical shielding or chemical modification of the binding site and thus to reduced binding affinity and immunological activity, which of course has to be judged with respect to Kato[90].

Site-specific conjugation can be achieved by conjugating to free thiols after reducing disulfide bonds or modification of the glycosidyl residues. The disulfide bonds in the hinge region can be reduced with the reducing agents mercaptoethylamine (MEA), dithiothreitol (DTT) or tris(2-carboxyethyl)phosphin (TCEP) to obtain two antibody fragments with one binding site each[97]. These fragments containing free thiol groups can be functionalized with thiol-reactive crosslinkers, e.g. N-succinimidyl-3-(2-pyridyldithio)propionate (SPDP). The problem with reduction of disulfide bonds is the low selectivity and the possible reduction of the disulfide bonds between heavy and light chain which leads to destruction of the antigen binding site.

Another approach for site-specific conjugation is modification of oligosaccharides in the Fc region of the IgG. Carbohydrates are not involved in antigen binding and therefore their modification retains full activity of the antibody[92]. Periodate oxidatively cleaves adjacent hydroxyls located in the carbohydrate chains affording a ring-opened residue containing reactive aldehyde groups[98]. These reactive aldehydes can react with primary amines under Schiff base formation or with hydrazides. The labile Schiff base bonds have to be reduced with sodium cyanoborohydride to obtain stabile secondary amines[94]. The disadvantages of this approach are the low reaction efficiencies. Furthermore, for conjugation with heterobifunctional linkers every modification of charges in the antibody molecule results in dramatic charge alteration effects[99]. Conjugation through lysine residues diminishes the net positive charge of the antibody by one for each attached linker if the linker is uncharged which leads to a dramatic heterogeneity of the conjugates. For conjugation through carbohydrates the charge of the antibody is not affected[100].
In general, the aDEC205 antibody is widely used for targeting dendritic cells to deliver antigens or drugs[101], [95], [57].

2.2.2. OVA-specific Antigen

Adaptive immunity needs T cell activation through antigen presentation on MHC molecules by DC. Intracellularly synthesized (endogenous) antigens are loaded onto MHC class I molecules and presented to cytotoxic CD8+ T cells. Extracellular (exogenous) antigens are presented on MHC class II molecules and activate CD4+ T helper cells. Cross-presentation enables the presentation of exogenous antigens also on MHC class I complexes and thus results in CD8+ T cell activation which is essential for anti-tumor immunity[102]. Antigen-based cancer vaccines are intensively studied with respect to enhancing anti-tumor immunity due to the increased T cell activation. Ovalbumin (OVA) is one of the most intensively investigated model antigens in cross-presentation so far. Soluble OVA is thought to be internalized via the mannose receptor (MR) into specialized stable early endosomal compartments from where it is exported into the cytosol and there processed by proteasomal degradation. Subsequently, it is transported into the early endosome again via transporter associated with antigen processing (TAP) in order to be modified by the insulin-regulated aminopeptidase (IRAP),

loaded onto MHC class I molecules and finally transported to the cell surface of dendritic cells to be presented to T cells. Though this is investigated for OVA, different types of antigen may be cross-presented via different routes[95], [103].

Short peptide sequences that exactly resemble the short sequence of the MHC class I binding CD8+ T cell epitope are used in most preclinical and clinical studies[104], [105]. Although these studies show high numbers of activated T cells, no long term tumor immunity can be observed[54].

Elongation of the peptide leads to longer duration of antigen presentation and enhanced immunogenicity of these epitopes[106]. The reason might be that longer peptides have to be internalized, processed and loaded onto MHC class I complexes on the surface of dendritic cells in order to specifically address CD8+ T cells[107], [106]. Minimal CTL epitopes like SIINFEKL alone can charge antigen presenting cells (APC) directly by being exogenously loaded onto MHC class I molecules without being internalized and processed and presented by both professional APC like DC and non-professional APC like T cells and B cells If antigen is presented for example on B cells, this is reported to lead to a transient CTL response and subsequent deletion of CD8+ T cells or to a tumor-protective CTL response and thus to immunotolerance[106]. Therefore, presentation of TAA on DC is crucial for induction of anti-tumor immunity.

Additionally, longer 30mer peptides have been reported to be internalized by DC and to be processed by MHC class II and class I pathways[108], while shorter exogenous peptides are restricted to the MHC class II pathway, and cross-presentation is also crucial for an effective immune response.

In this thesis, an ovalbumin (OVA)-specific antigen with the peptide sequence H-Cys-Ser-Gly-Leu-Glu-Gln-Leu-Glu-Ser-Ile-Ile-Asn-Phe-Glu-Lys-Leu-OH as a trifluoroacetate salt is attached to the conjugate. The core peptide sequence SIINFEKL is a K^b-presented immunodominant CD8+ T cell epitope which is processed from OVA[109]. The additional amino acids introduce a predetermined break zone for the release of SIINFEKL. For conjugation to the polymer a cystein residue at the N-Terminus is introduced that can react with a maleimide-functionalized polymer through formation of stable thioether bonds.

With this model antigen it will be investigated, if the conjugate is able to transport antigen to DC and induce T cell proliferation *in vitro*.

2.2.3. Immuno-activating TLR9 ligand CpG1826

Deoxycytidyl-deoxyguanosin oligodeoxynucleotides (CpG ODNs) are known to be potent immunostimulators and induce maturation of dendritic cells via inducing secretion of costimulatory molecules. CpG ODN, a dinucleotide sequence cytosine-guanidine (CG) within a certain conserved sequence motif, is more common in prokaryotic cells, e.g. bacteria, than in eukaryotic cells and is unmethylated in bacteria, while cytosine is methylated in eukaryotes. Therefore, the unmethylated CpG motif serves as a pathogen-associated molecular pattern (PAMP) and is recognized by PRRs within eukaryotic cells.

CpG is an immunostimulating Toll-like receptor 9 ligand that binds to the PRR TLR9 in the late endosome of DC and activates the TLR/IL-1 signal pathway, thus triggering defense mechanism[110]. Subsequently, expression of costimulatory molecules and proinflammatory cytokines like TFN-α, IL-6 and IL-12[109] is induced in immature DC as antigen-reactive CD4 T helper cells do via CD40 signaling[111] which leads to DC maturation and activation.

But how CpG ODN gets to the TLR9 receptor located in the endosomal compartment remains unclear. Recently, Lahoud *et al*. demonstrated that DEC205 is a cell surface receptor for CpG oligonucleotides[89]. DEC205 can bind CpG motifs on the cell surface and traffic to late endosomes and lysosomes where CpG can bind to TLR9. But CpG can also be internalized unspecifically in the absence of DEC205 expression, but this internalization is less effective and dose-dependent[89].

TLR9 does not only recognize bacterial CpG motifs, but also short synthetic ODNs[65]. TLR9 recognition needs a partial double-stranded ODN region with a CpG and a single-stranded free 5’ end of the ODN without end modification as this free end is thought to play a crucial role in interaction with the receptor[65].

Synthetic ODN with a phosphodiester backbone are inefficient due to degradation by extra- and intracellular nucleases. Therefore, ODNs are modified with a thioate-deoxyribose backbone that enhances stability and efficiency. There are two major types of immunostimulatory CpG DNAs[112]. ODNs can consist of an entire phosphorothioate backbone with central CpG dinucleotides. These CpG induces B cell proliferation and production of IL-6 and IL-12[113]. Other ODNs have a phosphorothioate G rich sequences at the ends and a phos-

phodiester palindromic sequence with a CpG dinucleotide in the middle which induces IFN-g production by NK cells[112].

In this thesis, CpG1826 with an entire phosphorothioate backbone and the DNA sequence 5'-tcc atg a**cg** ttc ctg a**cg** tt-3' with a thiol modification at the 3' end is used as an activator.

This CpG1826 ODN is optimized for activation of B cells and dendritic cells and Th1-like cytokine expression[114]. CpG1826 was investigated by Beloeil *et al*. regarding its impact on CD8+ T cell primary response and survival[115]. They reported that CpG1826 is able to induce antigen-specific T cell responses where CD8+ T cells can undergo multiple divisions *in vivo* and express IFN-g and up-regulate memory associated cell surface markers. Thus, a long-term survival of antigen-specific CD8+ T cells after immunization is achieved. Additionally, CpG is found to increase the cytotoxic activity of CD8+ T cells and promote differentiation to CTL. Hence, CpG1826 is an efficient adjuvant that increases CD8+ T cell effector responses and promotes long-term survival of antigen-specific T cells *in vivo*[115].

Therefore, CpG ODNs find various therapeutic applications and is used as an adjuvant in prophylactic as well as therapeutic cancer vaccines. In various studies it is applied in combination with or antigen-based vaccines to enhance the antigen-specific antibody-dependent cellular cytotoxicity[116], [110], [117]. Furthermore, activation of the immune system with CpG induces recession of lymphoma, neuroblastoma and glioblastoma[114].

2.2.4. Polymeric Carriers

In this study, linear poly-L-lysine (PLL) and the PLL brush are investigated as polymeric carriers for cancer vaccines (Figure 8).

The conjugation chemistry for attaching bioactive components is established for linear PLL as a model system and afterwards transferred to the PLL brush. The advantages of poly-*L*-lysine as a polymeric carrier are that it is already used as a drug carrier and for DNA transfection [61], [62] and in antigen peptide based tumor-vaccines[118]. PLL is commercially available and the ε-amine groups are a good target for covalent attachment of linkers or biomolecules.

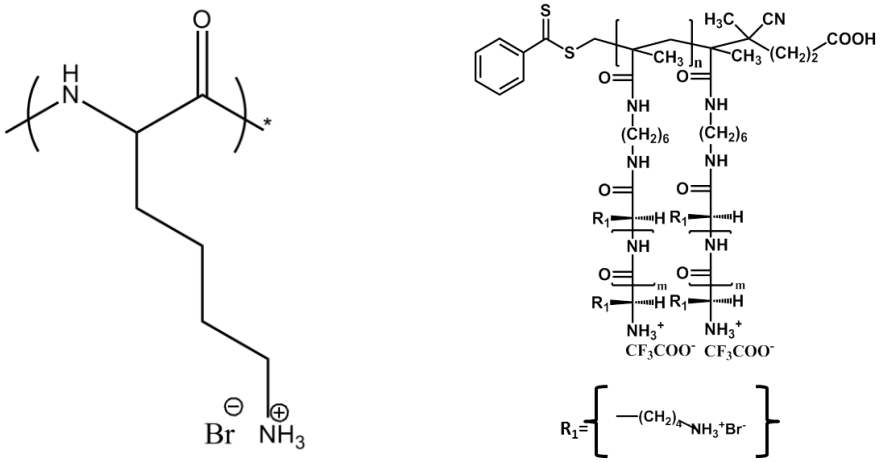

Figure 8: Scheme PLL and PLL brush

Additionally, PLL is not proteolytically stable and can be completely degraded via trypsin cleavage[119] which is important for renal clearance after delivering its cargo. As PLL is not inert it can influence a variety of cellular processes. PLL can exert selective toxicity on some tumor cells[120], activate phospholipases and thus affect permeability of the membrane[121].

Proteins and larger molecules are usually conjugated to a polymeric carrier at a molar ratio of 1 to 1 to the polymer while with smaller molecules higher conjugation efficiencies can be achieved[122]. Degols *et al.* reported that 15-17mer oligonucleotides conjugated to poly-*L*-lysine provide 50fold better protection against infection by vesicular stomatitis virus in cell culture compared to unconjugated oligonucleotides[123]. The conjugates are proposed to enter the cell via absorptive endocytosis[124]. Trubetskoy *et al.* describe the specific coupling of an antibody to PLL through modification of Poly(ε-benzyloxycarbonyl (CBZ)-*L*-lysine) with SPDP, deprotection with a solution of HBr in glacial acetic acid and subsequent addition of an iminothiolane-modified antibody[125].

The disadvantages of PLL as a carrier are its highly cationic charge and its relatively broad molecular weight distribution. Hydrophobicity, size and surface charge have an important influence on the biocompatibility of nanoparticles[126]. Highly cationically charged polymers are usually more cytotoxic than neutral or slightly negatively charged particles. Positive charges induce hemolysis and aggregation of serum components. Low molecular weight cations induce an osmotic shock which highly contributes to immediate cell death. The important mechanism of cytoxicity for higher molecular weight analogous is direct cell membrane disruption[119]. Furthermore, positively charged particles exhibit problems regarding solubility of the components and conjugates due to aggregation and precipitation[63]. These

problems are enhanced by using linkers that are typically hydrophobic. Zhou et al. report a method to decrease the high cationic charge of PLL for in vivo application. The primary amines are modified to obtain acid-labile carboxylamides which results in a pH-dependent charger-inverting carrier. The negatively charged PLL-amide exhibits only low cytotoxicity and little interaction with cells and is suitable for in vivo application. When the particle entered the lysosomes within the cell, the acid-labile amide is cleaved to obtain the primary amine and PLL can escape the lysosome and get into the nucleus[127].

It is still under discussion if PLL is immunogenic. Some groups report no or little immunogenic potential for PLL, while other groups show the production of antibodies after injection of poly-*D*-lysine with Freund's adjuvant[122]. Due to the cationic charge, PLL and positively charged PLL complexes can activate the complement system.

For uptake into cells PLL binds to the negatively charged cell surface molecules such as heparin sulfate, proteoglycans and integrins and is subsequently internalized via absorptive endocytosis[128], [129], [130], [131]. The pathways of endocytosis of cationic molecules are very diverse, but generally PLL and PEI complexes are thought to be internalized via clathrin-mediated endocytosis although there is evidence that caveolae are also involved[132], [133], [134]. The uptake of cationic polymers is receptor-independent and therefore unspecific.

PLL is synthesized via ring-opening polymerization of N-ε-(ter-butoxycarbonyl)-*L*-lysine-N-carboxyanhydride using benzylamine as the initiator and subsequent side-chain deprotection. In conventional N-carboxyanhydride (NCA) polymerization there is no control over the reactivity of the growing polymer chain-end during the course of the polymerization[135]. Thus, a variety of side and determination reactions can occur which then lead to a broadened molecular weight distribution[136], [135]. A broad distribution is disadvantageous as it makes characterization difficult and it enhances the heterogeneity of the conjugates obtained.

The PLL brush is synthesized by [redacted] during his PhD thesis in the group of [redacted] and consists of a polymethacrylamide backbone with polylysine side chains. The brush has a more persistent structure than PLL which has a coiled coil formation. Therefore, the brush is thought to exhibit a different behavior in the body, for example longer circulation times and thus better bioavailability[137], [8]. Additionally, the anisotropic shape

of the cylindrical brushes (worm like chains) is known to induce an enhanced uptake compared to spherical analogous[138], [139] and show less detection by macrophages[137]. A disadvantage of the high molecular weight brush is its higher cytoxicity as the cytotoxicity of synthetic polycations generally increases with molecular weight and charge density[119].

In this thesis, PLL is modified with Sulfo-SMCC to introduce maleimide-functionalities that can subsequently react with free thiol-groups of the antigen or CpG or PLL is used unmodified for a Schiff base reaction with the aldehyde moieties of the oxidized antibody.

2.3. Characterization Methods

2.3.1. UV/Vis Spectroscopy

In UV/Vis absorption measurements the sample is exposed to light of wavelengths between 200nm and 740nm (UV/Vis range)[140]. Light can excite valence electrons to transit from a lower energy occupied orbital into a higher energy orbital, if the energy of the incident photon equals the energy gap between the ground and the excited state. Therefore, absorption is dependent on the wavelength of the incident light and the absorbed energy is dependent on the type of electronical transition occurring. In the UV/Vis range n-π* und π-π* transitions are observed.

The measurements are performed using a spectral photometer. The light of a Deuterium or Tungsten lamp is fractionized by a monochromator into its single wavelengths and then focused on the sample. In a reference cuvette the absorption of the solvent is measured and the difference in absorption of the reference and the sample is detected with a photomultiplier. Thereby, the absorption of the solvent is eliminated and the corrected absorption of the sample can be obtained.

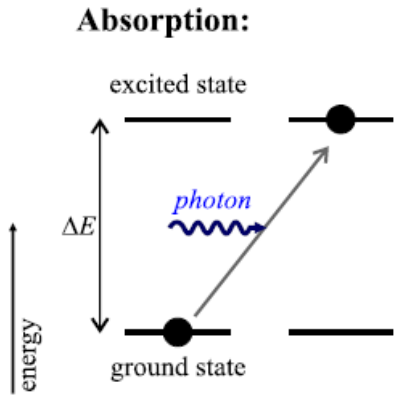

Figure 9: Absorption of an incident photon in a simplified fluorophore electronic state system (figure from Krieger *et al.*)[141]

The Lambert Beer law describes the linear relationship between absorbance and concentration of a sample. The attenuation of the intensity of light irradiated through a sample, thus the absorption A through a homogeneous isotropic medium, is proportional to the concentration c and the path length d.

$$A = \log\frac{I_0}{I} = \varepsilon * c * d \quad (1)$$

I_0 and I correspond to the intensities before and after the sample at the given wavelength λ. The molar extinction coefficient ε is an intrinsic property of the sample.

The law is only valid for monochromatic light under disregard of reflection and stray light loss for diluted solutions. Measuring the absorption A of a sample at every wavelength λ in the UV/Vis range and plotting A(λ) versus λ provides the absorption spectra of the sample.

Absorption bands in general are relatively broad due to the overlap of electronical transitions and rotational oscillation transitions. Thus, a quantity of energetically close transitions account for the broadening of the bands. So called impact broadening of the band occurs due to collision of the sample molecule with molecules of the solvent.

The concentration of peptides can be determined on the basis of their characteristic absorption at 190 and 280 nm. Non-aromatic peptides are detected at 190 nm due to the π-π* transition of the peptide bonds. The n-π* transition at 220 nm is too weak and overlayed with the absorption of some amino acid residues (e.g. aspartic acid) to be consulted for peptide analysis. Peptides containing aromatic amino acids, for example tyrosine and tryptophan, show an absorption maxima at 280 nm which relates to the π-π* transitions of the aromatic residues. The detection of peptides is influenced by strong variation of the absorption due to the amount of aromatic amino acids and the absorption of buffers and other components in this wavelength range[140].

In this thesis UV/Vis spectroscopy is mainly used to determine the ratio of the dye-labeled components in the conjugate. The dyes attached to the components are AlexaFluor 488 (ε = 73 000 L*mole^{-1}*cm^{-1}), AlexaFluor 546 (ε = 112 000 L*mole^{-1}*cm^{-1}) and AlexaFluor 647 (ε = 270 000 L*mole^{-1}*cm^{-1}). With the linear relation between absorption and concentration and the known extinction coefficients the concentration can be calculated from the absorption values at the absorption maxima.

Table 1: Fluorescent dyes used in UV/Vis Spectroscopy

Dye	Structure	Molar extinction coefficient ε / L * mole^{-1} * cm^{-1}
AlexaFluor 488 (Alexa Fluor® 488 carboxylic acid, 2,3,5,6-tetrafluorophenyl ester)	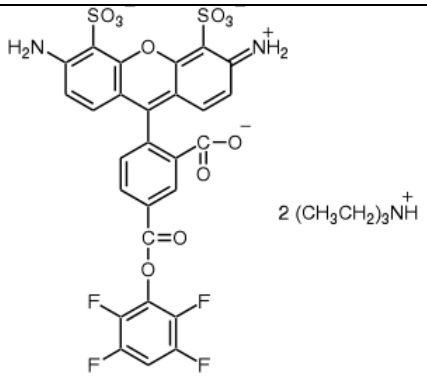	73 000
AlexaFluor 546 (Alexa Fluor® 546 carboxylic acid, succinimidyl ester)	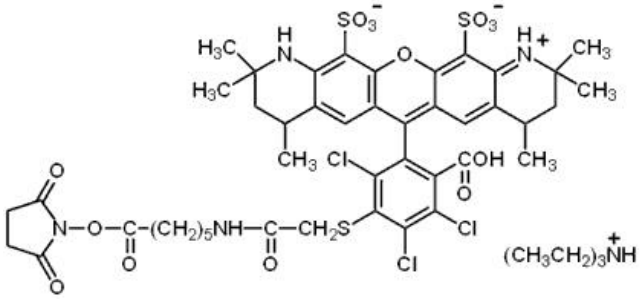	112 000
AlexaFluor 647	N/A	270 000

2.3.2. Fluorescence Spectroscopy

If an excited dye molecule returns to its ground state a photon with the energy difference between excited and ground state is emitted. Fluorescence is the result of a three-stage process in the electron shell of fluorophores[142], [141], [140].

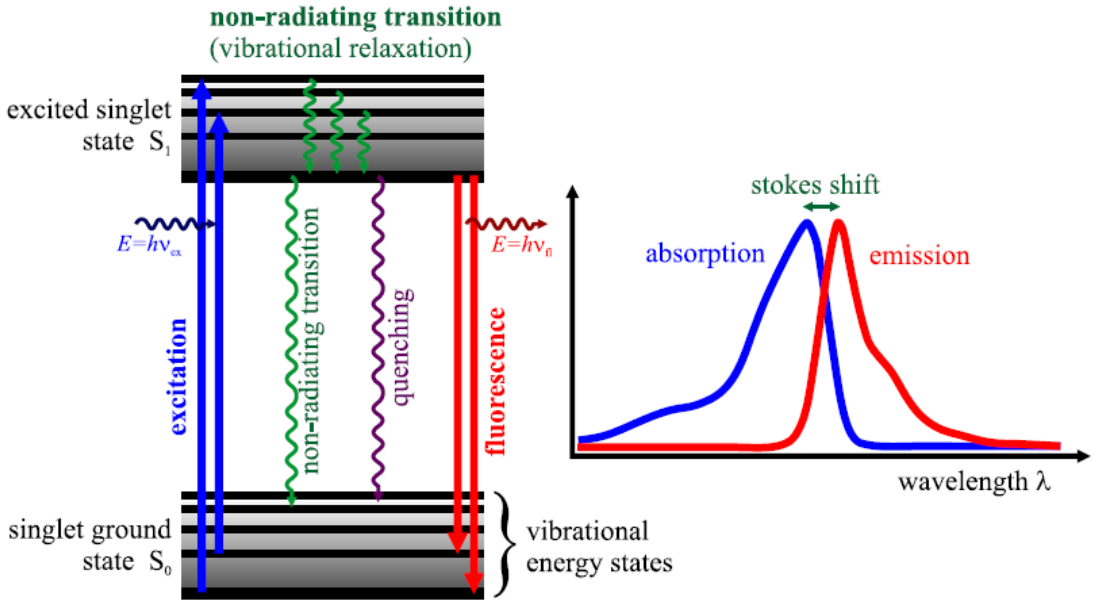

Figure 10: Jablonski diagram and spectra, illustrating the processes involved in the creation of an excited state by optical absorption and subsequent emission of fluorescence (figure from Krieger *et al.*)[141]

The three processes involved are excitation, non-radiating transition and emission.

Excitation is the process when a photon supplied by a light source is absorbed by the fluorophore. The absorbed energy excites the electrons of the fluorophore to transit from the ground state to an excited state (t = 1 fs = 10^{-15} s).

During the time the electron spends in the excited state (typically 1-10 ns) some fluorophores are able to undergo conformational changes and can interact with its molecular environment. Thus, the energy of the excited state partially dissipates and the electron falls to a relaxed singlet excited state. This is typically the vibrational ground state of the singlet's state from which fluorescence occurs. Next to fluorescence emission there are other ways for molecules to return to the ground state. These processes can be collisional quenching, fluorescence energy transfer (FRET), intersystem crossing and photochemical reactions.

For fluorescence emission the energy of the emitted photon is lower than the energy gap between ground and excited state due to energy dissipation during the excited state lifetime. Therefore, the energy of the emitted photon is of a longer wavelength which results in a Stokes shift, the energy difference between absorption and emission maxima.

$$\Delta\lambda_{Stokes} = \lambda_{max,em} - \lambda_{max,abs} \quad (2)$$

Fluorescence is a cyclic process and can be repeated until the fluorophore photochemically reacts in the in the excited state which is called photobleaching. Polyaromatic molecules

show a broad fluorescence excitation and emission spectrum. The fluorescence excitation spectrum of a fluorophore is usually laterally reversed to its absorption spectrum. The shape of the fluorescence emission spectrum ideally is independent of the excitation wavelength and the emission intensity is proportional to the amplitude of the fluorescence excitation spectrum at the excitation wavelength.

Fluorescence spectra measurements are performed using a fluorescence spectrometer. This consists of a monochromatized excitation light source and a detection channel also with a monochromator, which is aligned perpendicular to the light source in order to minimize detection of excitation both from scattering and reflection.

An emission spectrum is obtained at constant excitation wavelength while the detection wavelength is scanned over a given range. When the excitation wavelength is scanned while the detection wavelength is fixed, an excitation spectrum is received.

Fluorescence intensity is proportional to the concentration of the sample:

$$F = I_0 * \phi * (3.303 * \varepsilon * c * d) \quad (3)$$

With F = fluorescence intensity, I_0 = intensity of irradiated light, ϕ = fluorescence quantum yield (ratio of emitted to absorbed photons), ε = molar extinction coefficient, c = concentration and d = path length.

Additionally, a red shift of the spectra towards longer wavelengths can occur with increasing concentration. This shift to wavelengths of lower energy is due to partial reabsorption (concentration quenching) due to partial overlap of absorption and emission spectra. Energy is transmitted from an excited molecule to another molecule, so that probability of emission decreases and the excited state can non-radiatingly transform to the ground state. Due to decreasing overlap of absorption and emission spectra with increasing wavelength, probability of a red shift emission is higher.

Fluorescence spectra are highly influenced by environmental factors like solvent polarity, pH of the aqueous medium, temperature and also proximity and concentration of quenching species.

AlexaFluor dyes, sulfonated dyes used in this thesis, are designed to be more independent of the pH, but binding of a fluorophore to a target can dramatically affect its quantum yield.

In order to determine the fluorescence quantum yield ϕ_{fl} (λ) a relation between radiating and non-radiating decays of the excited state is needed.

$$\emptyset_{fl}(\lambda) = \frac{N_{em}}{N_{abs}(\lambda)} \quad (4)$$

with N_{em} = number of emitted photons and N_{abs} = number of absorbed photons.

With certain fluorophores as standards the quantum yield can be calculated as:

$$\frac{\emptyset_{sample}}{\emptyset_{reference}} = \frac{\frac{N_{em,sample}}{N_{abs,sample}}}{\frac{N_{em,ref}}{N_{abs,ref}}} = \frac{N_{em,sample}}{N_{em,ref}} * \frac{N_{abs,ref}}{N_{abs,sample}} = \frac{I_{em,sample}}{I_{em,ref}} * \frac{A_{abs,ref}}{A_{abs,sample}} \quad (5)$$

With I = measured intensity and A = measured absorbance. The last equality is only correct if all intensities and absorbances are measured at the same excitation/ detection wavelength and optical density OD ≤ 0.1. Furthermore measurements should be performed in dilute solutions to avoid concentration quenching[141].

2.3.3. Fluorescence Correlation Spectroscopy

Fluorescence Correlation Spectroscopy (FCS) is a very sensitive optical technique that uses a confocal microscope to measure dynamical properties of particles such as the diffusion coefficient D (in $\mu m^2/s$) and thereby the hydrodynamic radius of a species or the formation of bonds or interaction between two fluorescently labeled particles[142]. Its advantages are the high resolution which enables single molecule detection, the small sample volume ($1\mu m^3$ = 1 fL) and the short measurement times[141], [143], [144].

The principle of a spectrometer is that, by focusing the laser in a solution and directing the beam through a pinhole, a very small sample volume can be observed. Fluorescent photons in this sample volume are counted over time and the fluctuations in intensity are detected. These intensity fluctuations are based on fluctuations of fluorescent molecules which occur due to diffusion of particles in and out of the detection volume and can be described by Poisson statistics.

Diffusion is due to the Brownian motion of particles and can be described as a random walk in solution. The larger the diffusion coefficient the faster a particle moves.

$$D = \frac{k_B T}{6\pi\eta R_h} \quad (6)$$

With k_B = $1.3806504*10^{-23}$ J/K the Boltzman's constant, T = absolute temperature, η = viscosity of the solution and R_h = hydrodynamic radius of the particle

The mean squared displacement in three-dimensional space

$$\Delta x^2 = 6D\Delta t \tag{7}$$

describes the volume that a particle perambulates during a random walk and can be experimentally determined with FCS.

The analysis of FCS measurements is based on autocorrelation functions G(τ). This function describes the correlation of the fluorescence signal at different times t and t+τ. Thus, fluctuations

$$\delta F(t) = F(t) - \langle F(t) \rangle \tag{8}$$

(deviation of the fluorescence from the mean fluorescence) of a certain time t are multiplied with the fluctuations at time t+τ and normalized to give the autocorrelation function:

$$G(\tau) = \frac{\langle \delta F(t) * \delta F(t+\tau) \rangle}{\langle F(t) \rangle^2} \tag{9}$$

The time course of G(τ) contains information about characteristic times of the involved dynamic processes.

The basic equation of FCS is derived by applying Poisson statistics to calculate entrance probability of different particles and allows to evaluate the diffusion times τ_D from intensity autocorrelation function.

$$G(t) = \frac{1}{N} * \left(1 + \frac{\tau}{\tau_D}\right)^{-1} * \left(1 + \frac{\tau}{s^2 * \tau_D}\right)^{-\frac{1}{2}} \tag{10}$$

Where s is the axis ratio of the ellipsoidal detection volume, τ is the correlation time and τ_D is the diffusion time.

The mean retention time of a molecule in the detection volume (=”diffusion time”) τ_D depends on the short axis radius of the ellipsoidal detection volume r_0 and the diffusion coefficient D, which means that the diffusion coefficient is not determined on an absolute scale, as for example in DLS measurements, but on a relative scale. Calibration of the detection volume typically is prenormed with labels of similar brilliance and know diffusion coefficient.

$$\tau_D = \frac{r_0^2}{4D} \tag{11}$$

With the Stokes Einstein equation the diffusion coefficient is inversely proportional to the hydrodynamic radius of the particle (equation 6).

Change in the molecular mass, for example due to complexation or conjugation, changes the diffusion time and can be used to analyze thermodynamic or kinetic interaction parameters.

Mobility coefficients and characteristic velocity constants for inter- and intramolecular reactions at nanomolar concentrations can be obtained. Hence, FCS is an important tool in biomolecular analysis for example for the determination of DNA- and RNA-protein interaction[145].

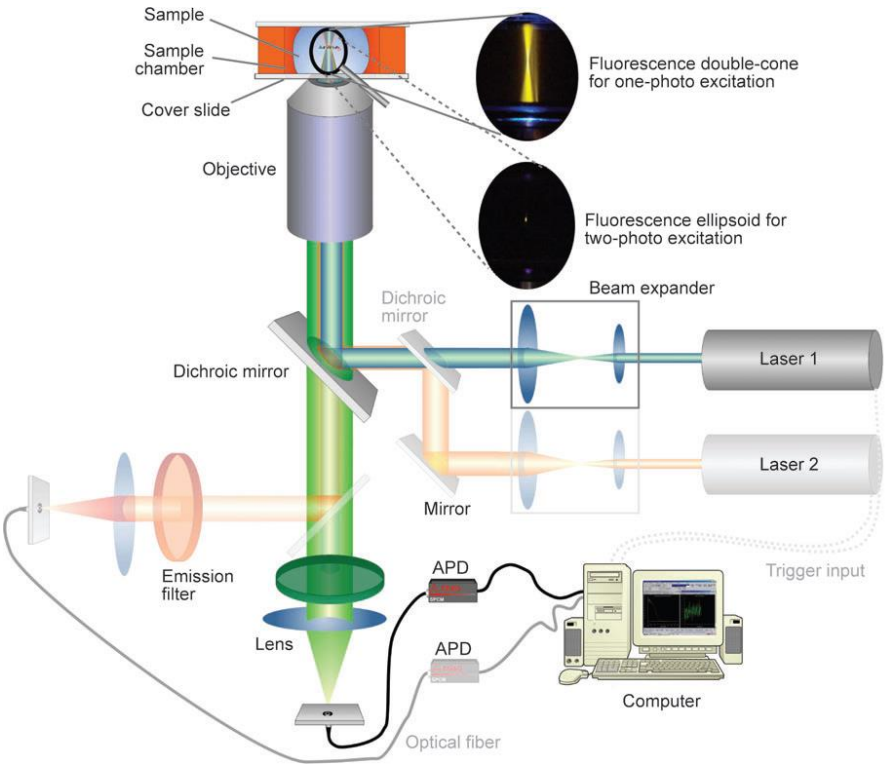

Figure 11: Schematic setup of a confocal microscope for fluorescence correlation spectroscopy for single channel measurements (blue-green emission and green detection channel) or dual-color cross-correlation (green and red beam path) (figure from Haustein *et al.*)[146]

2.3.4. Confocal Laser Scanning Microscopy

The development of fluorescence microscopy enables the analysis of localization, dynamics and interaction of molecules within living cells. With Confocal Laser Scanning Microscopy (CLSM) light emitted from a sample out of the layer of focus is collected. Laser light is focused on a point of the layer of focus. The emitted light is focused to a pinhole and collected by a detector behind that pinhole. As the level of focus and the pinhole are confocal (aligned parallely), only light emitted from the point of focus can be detected. Scattered light that comes from levels other than the level of focus is not detected[140], [147].

Analogous to a conventional fluorescence microscope, the LSM also contains a dichroic mirror that leads exciting light from the light source to the sample and directs emitted light of the sample towards the detector. Newer systems can come with an AOTF (acousto-optical beam-splitter) instead of the dichroic mirror, which has the advantage of higher throughput of light to the sample and larger flexibility for detection due to the fast switching. In contrast to conventional microscopy where the whole field of view is excited and detected, excitation and detection with LSM occur grid-like (point by point and line by line). Laser light is directed with galvanometric scanner mirrors sequentially through the sample, which provides a sharp optical section with high resolution. By sequentially moving the layer of focus in z-direction, z-stacks of optical sections can be assembled to achieve a three-dimensional image.

Therefore LSM is an important tool to analyze physiological and pathological parameters in cells and cellular uptake of material into cells.

In this work CLSM is mainly used to analyze uptake of polymer conjugates into dendritic cells and for colocalization studies of the fluorophores attached to the components of the conjugates or of components with different cell compartment stains.

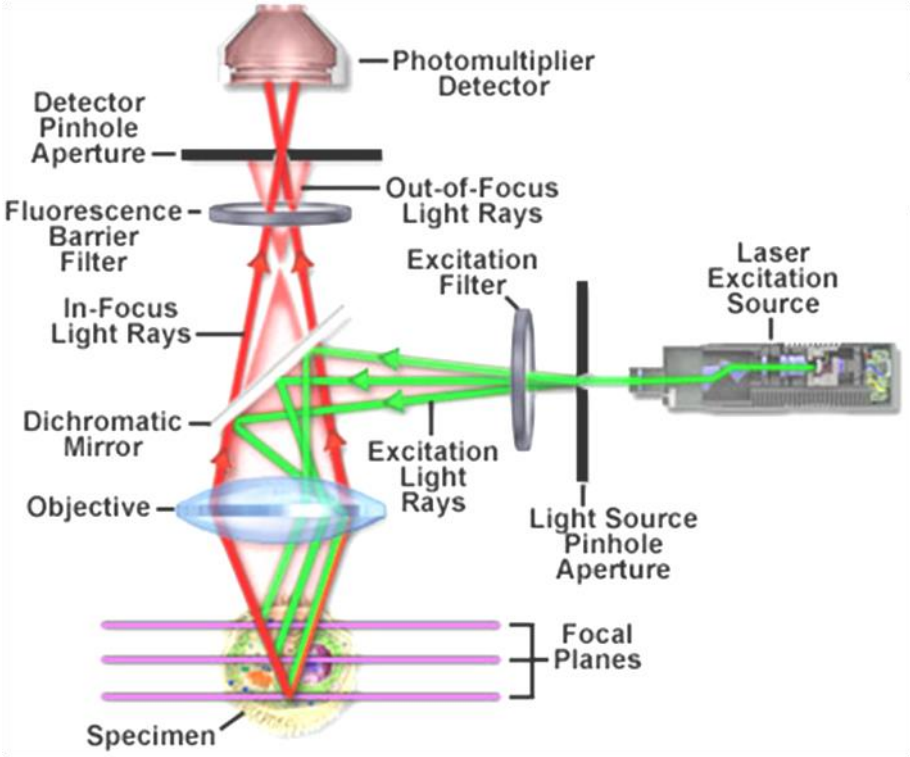

Figure 12: Setup of a confocal laser scanning microscope[147]

2.3.5. Flow Cytometry

Flow cytometry, also called Fluorescence activated cell sorting (FACS), is a technique for counting cells by suspending them in a stream of fluid to form a single cell suspension and passing them by a laser and an electronic detection apparatus. This provides simultaneous analysis of multiple parameters of the physical and molecular properties of thousands of cells per second[148].

A laser of a single wavelength is directed onto a hydrodynamically focused stream of the single cell suspension to analyze each cell individually. Multiple detectors are aligned to the point where the stream passes through the laser beam. The detector in line with the laser beam is called forward scatter (FSC) and its magnitude is roughly proportional to volume and size of the cell. The side scatter (SSC) detector is perpendicular to the beam and side scatter is caused by granularity and complexity inside the cell. Furthermore there are several fluorescent detectors in line with the SSC detector. When a cell (with a size between 0.2 and 150 µm) passes through the beam it scatters light and fluorescent probes in or attached to the cell are excited to emit light at a longer wavelength than the light source. The intensity of the emitted fluorescence is proportional to the number of the fluorochromes in or attached to the cell.

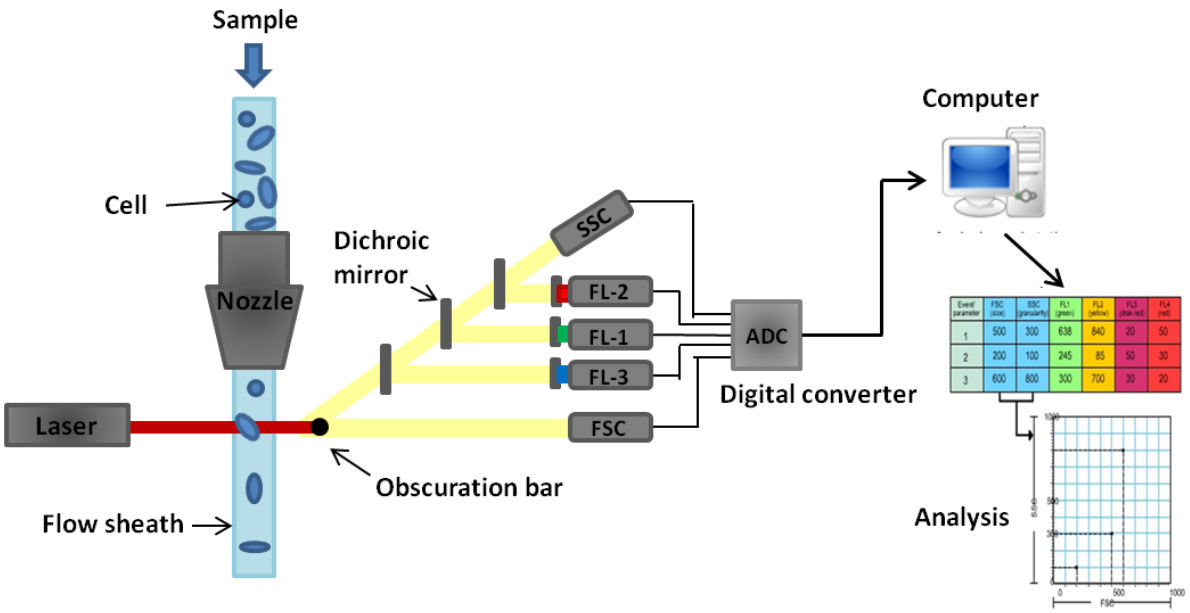

Figure 13: Setting of a flow cytometer (adapted from [149] and [150])

A simultaneous analysis of multiple different fluorescent dyes (Table 2) is possible, if the dyes (e.g. FITC, PE, PerCP) are excited by the same laser (Argon laser, 488nm) but have different dye-specific emission spectra. More dyes can be excited with a second laser (e.g. Helium-Neon, 633nm) due to spatial separation. Spatial separation limits the bleeding through into the other channels for the different dyes and therefore less compensation is needed.
The scattered and emitted light is detected by the detectors and fluctuations in brightness can be analyzed at each detector individually to give data about the physical and chemical structure of the cell.

Table 2: Used Fluorochromes and their Absorption and Excitation maxima

Laser	**Fluorochrome**	**Abbreviation**	**Abs_{max} [nm]**	**Em_{max} [nm]**	**Extinction coefficient [M^{-1} cm^{-1}]**
Blue Argon Laser 488 nm	Fluoresceinisothiocyanate	FITC	495	519	70 000
	R-Phycoerythrin	PE	480; 565	578	1 960 000
	AlexaFluor488	AF488	495	519	73 000
	AlexaFluor 555	AF555	555	565	155 000
	Propidiumiodide	PI	550	650	5900
Yellow green Laser 561 nm	AlexaFluor 546	AF546	556	573	112 000
Red diode Laser 635 nm	Allophycocyanin	APC	650	660	700 000
	Cyanine 5	Cy5	649	670	250 000
	AlexaFluor647	AF647	647	660	270 000
Violet Laser 405 nm	Brilliant Violet 421	BV421	407	421 (448)	2 500 000
	Brilliant Violet 605	BV605	405	603	2 400 000

If the emission spectra of the dyes overlap (e.g. FITC and PE) the signals from the individual detectors have to be compensated to avoid wrong negative or positive results. In order to

compensate the fluorescent signal of a sample, a single color control for each fluorescent dye is needed. The compensation can be done either before the measurement electronically at the instrument or afterwards computationally with the analyzing software. For electronical compensation of unwanted emission of a fluorochrome in the adjacent channel an appropriate voltage value can be subtracted proportionately (e.g. FL2-%FL1 for FITC emission into the PE/FL2 channel or FL1-%FL2 for PE emission into the FITC/FL1 channel)[151].

The obtained data can be plotted in histograms (single dimension, one parameter in relation to the signal intensity) or in dot plots (two dimensions, diagram of two parameters/detectors). In order to compare two different samples, overlay histograms are presented. Special regions of these plots can be sequentially separated based on fluorescence intensity. The series of subsets extractions are called “gates” and is used for example to differentiate between dead or live cells or separate cells carrying a fluorochrome from unlabeled cells. The determination of viability is performed with propidium iodide, which emits in channel FL3. The dye can only enter dead cells and intercalates in the DNA. Therefore this dye labels dead cells and the live/dead ratio can be determined.

The main application is to use fluorescently labeled samples to determine specific properties of cells and cell populations on a single cell level. The differentiation of different cell populations is achieved by labeling cells due to their differing cell surface markers. The basic principle is the antigen-antibody interaction with a fluorescently labeled antibody which is highly specific. Through a combination of different monoclonal antibodies cell, surface markers and proteins on the cell surface can be analyzed quantitatively which is called phenotyping.

In this thesis flow cytometry is used to determine the internalization of different antibodies and polymer conjugates into dendritic cells. For antibody internalization studies the cells are phenotyped (PT) with CD11c-FITC as universal DC marker (detected in the green FL1 channel) and CD8-PE in order to determine CD8 positive DC (detected in the orange FL2 channel). The internalization sensor is labeled with Cy5 (and detected in the APC channel).

For polymer-antibody internalization studies with the SHIP sensor different phenotyping stains have to be used because of the number of fluorochromes attached to the components of the conjugate. The cells are stained with CD11c-brilliant violet 421 and CD8-brilliant violet

605. The fluorochromes on the components are AlexaFluor488 for PLL and PLL brush, AlexaFluor555 for aDEC205, CD11c and cIgG.

The polymer conjugate is labeled with the following fluorochromes: PLL-AF488, Antigen-AF546 and aDEC205-AF647 and therefore phenotyping has to be performed with brilliant violet dyes.

2.3.6. Specific Hybridization Internalization Probe

Specific Hybridization Internalization Probe (SHIP) is a method to determine the cellular uptake of a variety of materials in a simple way with high throughput. This technique was recently invented by Haiyin Liu and Angus Johnston at the University of Melbourne[152]. It is advantageous over conventional internalization techniques as it is compatible with conventional cell phenotyping and independent of the cellular fate of the material.

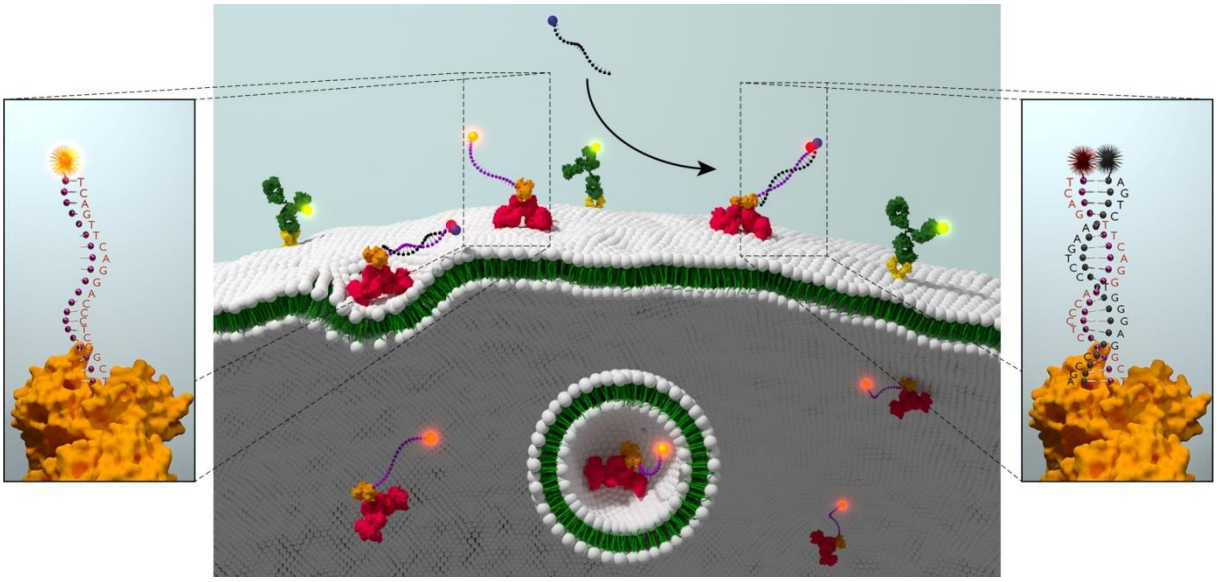

Figure 14: Specific Hybridization Internalization Probe (SHIP) (figure from Liu *et al.*)[152]

The internalization of different materials can be analyzed, for example of proteins or nanoparticles. The material of interest is labeled with a fluorescent DNA sequence (the Fluorescent Internalization Probe – FIP, in this thesis called SHIP) by click reaction of the DIBO-functionalized material and azide-modified DNA. The labeled material is incubated with the

cells for a certain period of time before a quenching probe (QP_C, in this thesis called Quencher) is added. The Quencher is incubated with cells at 4°C. At this temperature no internalization of the Quencher occurs. Therefore, it specifically quenches the fluorescence of the SHIP-conjugate on the cell surface, but it cannot access the fluorescence of internalized SHIP within the cell, or affect other surface markers.

The samples are analyzed by flow cytometry. By calculating the ratio of quenched to unquenched fluorescence of a sample at a certain time point the percent of internalization after certain incubation times can be determined.

$$Internalization\ /\ \% = \frac{I\ (quenched, t=i)}{I\ (unquenched, t=i)} * 100 \qquad (12)$$

If loss in fluorescence over time occurs the sample is affected by capping, which means that the whole sample-receptor complex is pulled from the surface rather than being internalized. Capping is not well understood so far and no references can be found in literature. But capping has to be considered for calculation to not overestimate the amount of material internalized.

With this technique, capping can be taken into account by normalizing not to the unquenched fluorescence at a specific time point but by dividing by the unquenched fluorescence at zero time point where no capping has occurred. Thus, the SHIP internalization technique is quantitative and not affected by capping.

2.3.7. Size Exclusion Chromatography

Size Exclusion Chromatography (SEC), oftentimes called Gel Permeation Chromatography (GPC), is an important relative method to determine the molecular weight and the molecular weight distribution of polymers[153]. The separation of polymers with different molecular weights is achieved by the different hydrodynamic radii R_h of macromolecules. The sample is pumped though a set of columns which are filled with a porous gel. The gel material is mostly highly cross-linked polystyrol beads with a defined pore size.

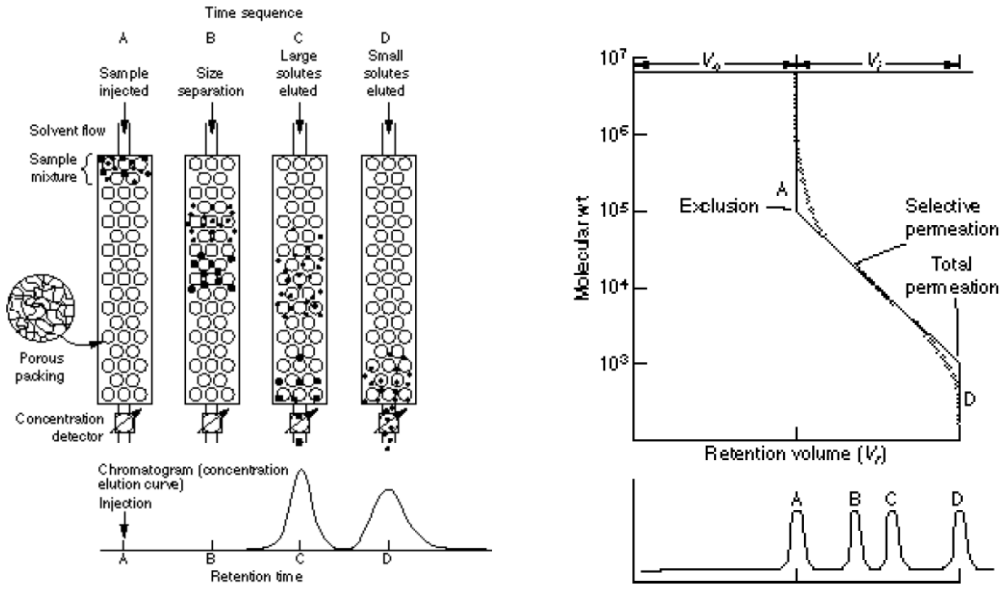

Figure 15: SEC scheme and exclusion limits (figure from Meunier)[154]

The concentration gradient between inner volume (pore volume) and outer volume (interstitial volume) drives the diffusion of macromolecules into the pores of the stationary phase. First, there is only solvent in the pores, which enhances diffusion of the polymers into the pores. As soon as the concentration gradient inverts, which means that there are more polymers inside the pores than in the interstitial volume, the polymer starts diffusing back to the interstitial volume and can be transported with the eluent and finally be eluted. Molecules with a small hydrodynamic volume have a longer retention time as they can enter more pores. Larger molecules have a smaller retention time because they can only interact with fewer pores and therefore, they elute first. The elution of molecules is commonly detected with refractive index- (RI) and UV/Vis-detector simultaneously. As GPC is a relative method a calibration curve with polymers of a known molecular mass has to be measured in order to determine the molecular weight of a polymer[153].

The elution volume increases with the logarithm of the molar mass:

$$V_e = C_1 - C_2 * \log(M) \tag{13}$$

The constants C_1 and C_2 can be obtained from the linear segment of the plot log(M) versus V_e. The linear segment (Figure 15 b) depicts the area between upper and lower exclusion limit. The exclusion limit is not sharply defined, but a broad transition area. An approximation is described with the following polynomial function:

$$log(M) = A + B * V_e + C * V_{e2} + D * V_{e3} + \dots \tag{14}$$

With two data points of the linear segment constant C_2 can be calculated with the following equation:

$$C_2 = \frac{Ve,II - Ve,I}{log(\frac{MI}{Mu})} \equiv S \quad (15)$$

Constant C_2 is also called selectivity factor which is characteristic for the column that is used. Figure 15 explains that all molecules with a molar mass larger than M_u and the corresponding exclusion volume $V = V_0$ elute at the same time. No separation takes place for these molecules above the upper exclusion limit as the molecules are too big to interact with the pores. All molecules with $M > M_u$ elute with the eluent. Below the lower exclusion limit all molecules with $M < M_l$ and the corresponding elution volume $V = V_0 + V_i$ elute at the same time as the molecules are too small and they all interact with all pores. The exclusion limits of this column are $M = M_u$ and $M = M_l$. All molecules with $M_l < M < M_u$ remain in the column for a different period of time and can therefore be separated due to size differences.

2.3.8. Gel Electrophoresis

Gel electrophoresis is an important tool for the characterization of biomolecules like peptides or DNA[155], [156], [157].

The basic principle of electrophoresis is migration of charged particles in an electric field. In this external electric field two forces act on the charged particle; the accelerating force F_e is proportional o the effective charge q of the particle and the electric field E.

$$F_e = q * E \quad (17)$$

The friction force F_f decelerates the migration of the particle proportional to its velocity v and the friction coefficient f.

$$F_f = f * v \quad (18)$$

A steady state velocity is achieved when the accelerating and the frictional force are equal and the velocity of the particle can be described as

$$v = \frac{q}{f} * E = \mu * E \quad (19)$$

The proportionality factor of velocity and electrical field is the electrophoretic mobility μ. This substance specific factor determines the migration velocity and thus is crucial for separation of different substances in a gel.

The friction coefficient can be estimated for spherical particles by Stoke's law to be

$$f = 6\pi\eta R_h \tag{20}$$

The inverse proportionality between the electrophoretic mobility and the friction factor shows that with larger R_h the electrophoretic mobility becomes smaller. Furthermore, the frictional forces depend on the pore size of the gel matrix and the viscosity of the medium.

For non-spherical particles like peptides and proteins an empirical relation between mobility and molecular mass is declared

$$\mu \sim \frac{q}{M^{2/3}} \tag{21}$$

Theoretical studies from Muthukumar[158] with poylelectrolytes show that this relation has to be adapted. He proposes that the electrophoretic mobility is not directly proportional to the molecular weight, but also depends on electrostatic interactions. Therefore this concept has to be extended with the function $M(\kappa R_g)$. This provides the following equation for μ

$$\mu = \frac{Q}{6\pi\eta_0 R_g} M\,(\kappa R_g) \tag{22}$$

where Q: total charge

η_0: viscosity of the solvent

R_g: radius of gyration at a certain salt concentration

κ: salt concentration

This function reaches its limits $(\kappa R_g)^{1-df}$ and $(lnN-1)$ for very high and very low salt concentration. Therefore for very high salt concentrations ($\kappa R_g >> 1$) μ can be described as

$$\mu \sim \frac{Q}{\eta_0 R_g^{d_f}} * \frac{1}{\kappa^{d_f-1}} \tag{23}$$

with d_f: fractal dimension

For very low salt concentrations ($\kappa R_g << 1$) μ can be expressed as

$$\mu = \frac{Q}{6\pi\eta_0 R_g}(\ln N - 1) \tag{24}$$

with N: molecular weight of the polyelectrolyte

and $R_g = \frac{Nl}{\sqrt{12}}$

As the electrophoretic mobility μ does not depend on the molecular weight, this theory shows that additionally to the electrophoretic mobility of a particle a gel matrix is necessary to separate particles with different molecular weight. Thus, the pore size of the gel correlates with the particle size to achieve good separation.

Two main types of gels are commonly used today, polyacrylamide gels for protein characterization[159] and agarose gels for DNA separation[156].
In this thesis, sodium dodecyl sulfate-polyacrylamide gel electrophoresis (SDS-PAGE) is used to analyze the molecular weight of proteins, peptides and polymer-protein conjugates.
Polyacrylamide gels are chemically inert and very stable. These gels are formed by polymerization of acrylamide with a crosslinker N,N'-methylenbisacrylamide. Pore sizes of 10 to 100 nm can be obtained depending on the degree of crosslinking and the total concentration of acrylamide. These gels are optically clear and electrically neutral, which prevents the electroendosmotic effect[140].
During sample preparation for SDS-PAGE the anionic detergent SDS is added to the sample and to the running buffer in excess. The detergent shields the peptide charge and forms micelles with a constant negative charge per mass unit: 1.4g SDS per 1g protein. Due to the constant mass to charge ratio a separation depending only on the molecular weight of the sample is achieved.
Sample preparation was performed under reducing and non-reducing conditions. By addition of a reducing agent like DTT disulfide bonds can be cleaved which destroys the tertiary structure of a protein. If the whole IgG protein needs to be detected no reduction is performed to not disintegrate the protein into its subunits. But if the polypeptide is unfolded incompletely this might lead to a faster migration through the gel and apparently smaller molecular weights. Therefore, only the molecular mass of subunits can be determined exactly. Glycoproteins are not loaded with SDS to the same amount as non-glycosylated proteins are. This leads to a slower migration of glycoproteins and therefore an apparently higher molecular weight of the glycoprotein.

2.3.9. Light Scattering

Light Scattering is an important technique to determine shape, size, molecular weight and behavior of macromolecules in solution[160], [161]. Its advantages are that no calibration is needed as it is an absolute method and the analyzed molecule is not affected.

If laser light in its characteristic as an electromagnetic wave hits a molecule, its electrons are excited to oscillate. An oscillating dipole is induced that sends electromagnetic waves, so called elastic scattering waves, isotropically in every direction. Angular dependent detection of this scattered light is the basis of analysis of the sample.

Generally, there are two different ways to measure light scattering, static and dynamic light scattering. Static light scattering (SLS) uses scattering intensity averaged over time for determination of the weight average of the molar mass M_w, the second virial coefficient A_2 and the z-average of the squared radius of gyration $\langle R_g^2 \rangle_z$. Dynamic light scattering (DLS) measures intensity fluctuations over time and provides information about the mobility of the macromolecule, which is the diffusion coefficient D and the hydrodynamic radius R_h.

Static Light Scattering

Static light scattering exclusively regards elastic scattering, where the wavelength of the scattered light wave is identical to that of the incident light wave. The scattered intensity is measured depending on the scattering angle and averaged over a certain period of time.

Particles smaller than λ/20 can be considered to be point scatterer where the scattering centers within the molecule lie so close together that no interference occurs.

Thus, scattering intensity is independent of the scattering angle and can be expressed by fluctuation theory to be

$$I \propto KkT \frac{c}{\left(\frac{\partial \pi}{\partial c}\right)_{T,N}} \tag{25}$$

where K = contrast factor that describes the scattering power of single particles, k = Boltzman constant and T = temperature.

Van't Hoff describes the osmotic pressure of real solutions as

$$\frac{\partial \pi}{\partial c} = RT\left(\frac{1}{M} + 2A_2 + \cdots\right) \tag{26}$$

where M = molar mass of the dissolved particle and A_2 = 2nd virial coefficient.

The scattering power of particles depends on the polarizability of the particles and thus on the difference in the refractive index between dissolved particle and solvent.

Therefore, the contrast factor K can be put as

$$K = \frac{4\pi^2 n_D^2}{\lambda_0^4 N_L}\left(\frac{\partial n}{\partial c}\right)^2 \quad (27)$$

Where n_D = refractive index of the dissolved particle, λ_0 = wavelength of incident light, N_L = Avodagro's number and $\frac{\partial n}{\partial c}$ = refractive index increment.

As the absolute value of the intensity also depends on extrinsic factors such as laser power, distance of detector to sample r_D and the size of the scattering volume, the sample should always be calibrated with a standard (most commonly toluene) to obtain the Rayleigh ratio

$$R = (I_{solution} - I_{solvent})\frac{r_D^2}{V} = \frac{I_{solution} - I_{solvent}}{I_{standard}} * RR_{standard} \quad (28)$$

Combining equations 25, 26 and 27 yields the **Zimm equation** for small particles

$$\frac{Kc}{R} = \frac{1}{M} + 2A_2 c \quad (29)$$

Particles larger than λ/20 obtain more than one scattering center in one molecule, thus constructive and destructive interference occurs. Scattering intensity is no longer independent of the angle as interference changes with the observation angle. Therefore, the scattering vector $\vec{q}$ is introduced as the difference between the scattering beam and the incident beam.

$$|q| = \frac{4\pi n}{\lambda}\sin\left(\frac{\theta}{2}\right) \quad (30)$$

In very dilute solutions only the interactions between scattering centers within one molecule, not the interference of scattering light from different molecules, has to be considered. Hence, the scattering intensity can be calculated by summarizing pairwise over all interactions.

$$I(q) = NK\sum_{i=0}^{Z}\sum_{j=0}^{Z}\exp(-i\vec{q}\vec{r}_{ij}) \quad (31)$$

Where N = number of identical particles within the scattering volume, Z = number of scattering centers per particle and $\vec{r}_{ij}$ = distance vector between two scattering centers within one particle.

The particle form factor, which is the normed scattering of a single isotropic particle, can be derived by series expansion:

$$P(q) = \frac{1}{NZ^2K}\, I(q) = \frac{1}{Z^2}\sum_{i=0}^{Z}\sum_{j=0}^{Z}\exp(-i\vec{q}\vec{r}_{ij}) = \frac{1}{Z^2}\sum_{i=0}^{Z}\sum_{j=0}^{Z}(1-\frac{1}{6}\,q^2\,\vec{q}\vec{r}_{ij}+\cdots) \quad (32)$$

With the definition of the squared radius of gyration R_g

$$\langle R_g^2\rangle = \frac{1}{2Z^2}\sum_{i=0}^{Z}\ \langle\overrightarrow{r_{ij}}^2\rangle \quad (33)$$

The particle form factor can be derived as

$$P(q) = 1 - \frac{1}{3}\langle R_g^2\rangle q^2 + \cdots \quad (34)$$

Where termination after the first term is appropriate for $q^2\langle R_g^2\rangle \ll 1$.

For consideration of the angular dependency of the scattering on larger particles the form factor is inserted into the **Zimm equation** (eqn. 29)

$$\frac{Kc}{R} = \frac{1}{MP(q)} + 2A_2c = \frac{1}{M_w}\left(1+\frac{1}{3}\langle R_g^2\rangle_z q^2\right) + 2A_2c \quad (35)$$

The weight average of the molar mass is defined as

$$M_w = \frac{\sum_i N_i M_i^2}{\sum_i N_i M_i} \quad (36)$$

and the z-average of the squared radius of gyration R_g as

$$\langle R_g^2\rangle_z = \frac{\sum_i N_i M_i^2 \langle R_g^2\rangle_i}{\sum_i N_i M_i^2}. \quad (37)$$

The squared radius of gyration $\langle R_g^2\rangle$ describes the sum over the square of the distances from the center of mass of the analyzed structure and is related to the geometric radius,

$$\langle R_g^2\rangle = \frac{\int_0^R n(r) r^2 dr}{\int_0^R n(r) dr} \quad (38)$$

where the integral n(r) is the distribution function of scattering centers (volume elements) that are located at the distance r from the center of mass und the assumption that all volume elements have the same mass.

With the **Zimm plot** (Figure 16) that is derived from the Zimm equation (eqn. 35) the weight average of the molar mass Mw, the z-average of the squared radius of gyration $\langle R_g^2\rangle_z$ and the second virial coefficient A_2 of the osmotic pressure can be determined through dual extrapolation to c = 0 and q = 0.

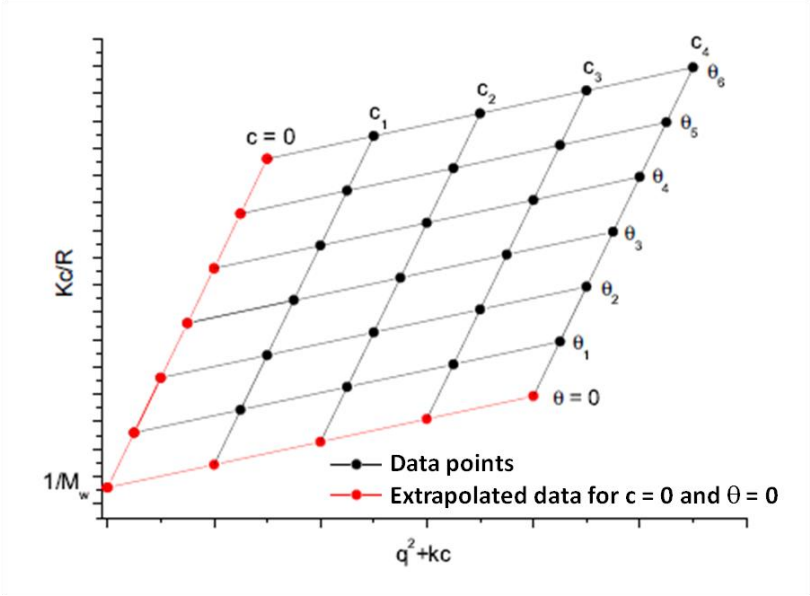

Figure 16: Zimm plot obtained from angular- and concentration-dependent static light scattering[162]

Dynamic Light Scattering

Dynamic light scattering measurements record the fluctuation of the scattering intensity with time in an angular-dependent manner using an intensity-time-correlator. These fluctuations are due to interparticle interference and induced by Brownian motion of the macromolecules in solution, changing the phase relations of the individual moving of scattering centers, which is described by the mean squared displacement (see equation 7) and therefore related to diffusion.

Photons reaching the detector are not averaged over time as it is done for static light scattering, but correlated, which gives the intensity-time-correlation function $g_2(t)$.

$$g_2(\tau) = \langle I(q, t) * I(q, t+\tau) \rangle \tag{25}$$

This correlation function describes the interaction of two particles at the time t and $t+\tau$ with the correlation time τ. The correlator multiplies the detected scattering intensities at time t and $t+\tau$. The squared bracket describes the average over time. Figure 17 illustrates the principle of dynamic light scattering. The intensity-time correlation function $g_2(t)$ decays with time from $\langle I(t)^2 \rangle$ to $\langle I(t) \rangle^2$ because the particles diffuse away from each other and their correlation decreases. The dotted line is the averaged scattering intensity measured with SLS.

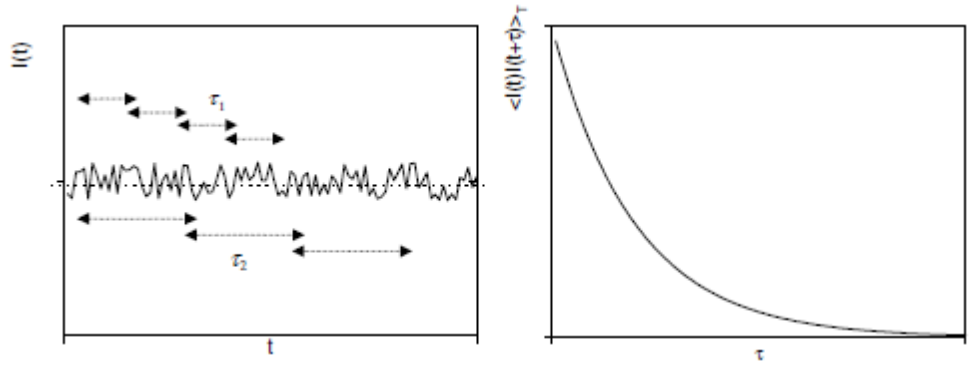

Figure 17: Correlation function[163]

The intensity autocorrelation function is related to the amplitude autocorrelation function $g_1(q,\tau)$ with the help of the Siegert relation[160].

$$g_1(q,\tau) = \sqrt{\frac{\langle I(q,t)*I(q,t+\tau)\rangle}{\langle I(q,t)\rangle^2} - 1} = \sqrt{g_2 - 1} \tag{26}$$

$g_1(q,\tau)$ is a Fourier transform function of the van Hove-self correlation function which provides a relation to the diffusion coefficient. For small monodisperse particles the correlation function decays like a simple exponential function.

$$g_1(t) = B * exp(-q_2 Dt) \tag{27}$$

where B: Signal-to-noise ratio (dependent on the experimental setup)

D: translational diffusion coefficient

For larger polydisperse samples $g_1(q,\tau)$ cannot be described as a simple exponential function but consists of an overlay of multiple weighted with the distribution function P(D)

$$g_1(q,t) = \int_0^\infty P(D)\exp(-q^2 D_i \tau) dD \tag{28}$$

The distribution function depends on the number of particles, their molar mass and the particle form factor.

With the initial gradient of the correlation function the z-average of the diffusion coefficient D_z for a certain angle can be calculated. As the diffusion factor depends on the form factor, it also shows an angular dependency. Therefore, the diffusion coefficient is only an apparent diffusion coefficient D_{app}.

$$D_{app} = \frac{\sum n_i M_i^2 P_i(q) D_i}{\sum n_i M_i^2 P_i(q)} \tag{29}$$

The z-average of the diffusion coefficient $\langle D \rangle_z$ is obtained by extrapolation of the apparent diffusion coefficient for q= 0, because for q= 0 all form factors are P(q)=1.

Using the Stokes-Einstein equation the hydrodynamic radius as the inverse z-average can be calculated from the z-average of the diffusion coefficient.

$$R_h \equiv \langle \frac{1}{\mathrm{R_h}} \rangle_z^{-1} = \frac{\mathrm{kT}}{6\pi\eta \mathrm{D_z}} \tag{30}$$

The ρ-ratio links characteristic parameters of dynamic and static light scattering and provides the shape of a polymer in solution. Its is defined as

$$\rho = \frac{R_g}{R_h} = \frac{\langle R_g^2 \rangle_z^{1/2}}{\langle \frac{1}{R_h} \rangle_z^{-1}} \tag{31}$$

The ρ-ratio for different shapes is summarized in Table 3.

Table 3: Theoretically calculated ρ-ratios for different particle shapes[164]

ρ-ratio	**Particle shape**
0.775	Monodisperse hard spheres
1	Monodisperse hollow spheres, vesicles
1.5	Monodisperse Gaussian coiled coils in θ solvent
1.78	Monodisperse Gaussian coiled coils in a good solvent
1.73	Polydisperse Gaussian coiled coils in θ solvent
>2	Rigid rods

Experimental Setup

The experimental setup for a light scattering measurement contains a laser as light source, different lenses and a pinhole to focus the laser beam. Scattering light is detected with a photomultiplier which is attached to a moveable goniometer and analysis is performed with a correlator, digital-analog-converter and a computer.

The setup for multi-angle light scattering additionally has multiple detectors with a fixed distance to each other attached to the goniometer which facilitate simultaneous measurement at multiple angles. Typical angles are between 30 and 150° and the cuvette with the

sample is tempered in a toluene bath usually at 20°C. Toluene is used because its refractive index is nearly the same as that of the fused silica glass of the cuvette which eliminates reflections.

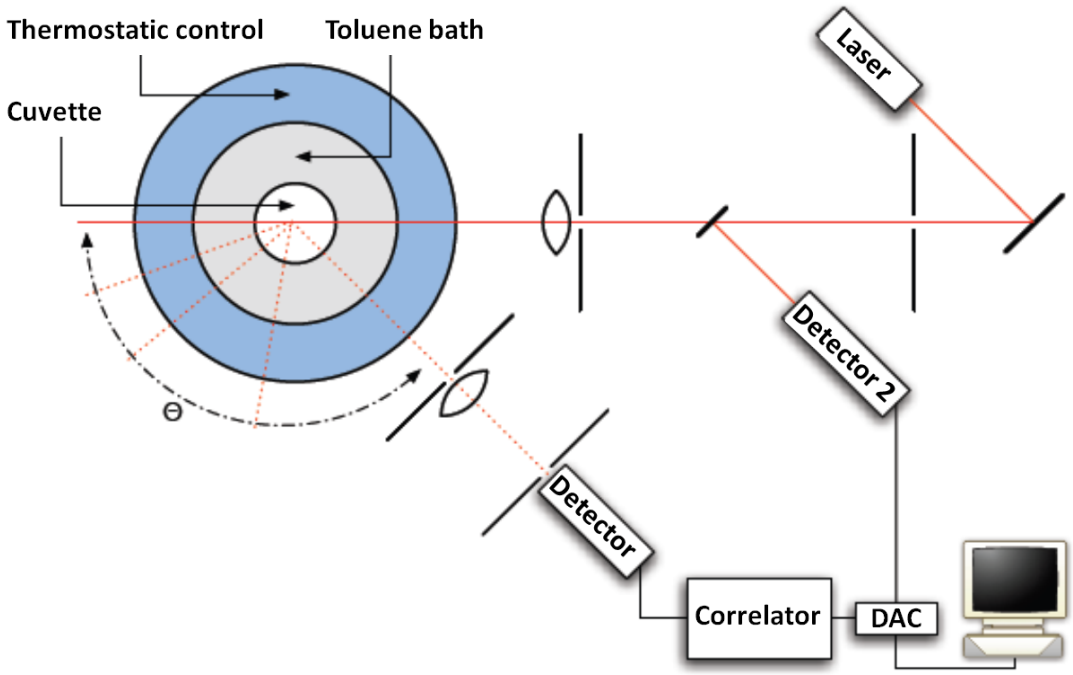

Figure 18: Light Scattering Setup[162]

3. Results and Discussion

3.1. Antibody Internalization and Characterization Studies

The aim of this section is to identify and characterize the best antibody for targeting CD8+ dendritic cells. Thus, first different antibodies are compared for their internalization kinetics and then the aDEC205 antibody is characterized.

3.1.1. Internalization Studies of Different Antibodies into Dendritic Cells

SHIP Internalization experiments[152] with different antibodies are performed to find the most suitable antibody to target dendritic cells. For these experiments the antibodies aDEC205 (NLDC-145), CD11c (N418), MHC class II (M5/114), Clec12a (5P1) and Clec9a (20/04-10B4-24-8 Facs 9-6) are used.

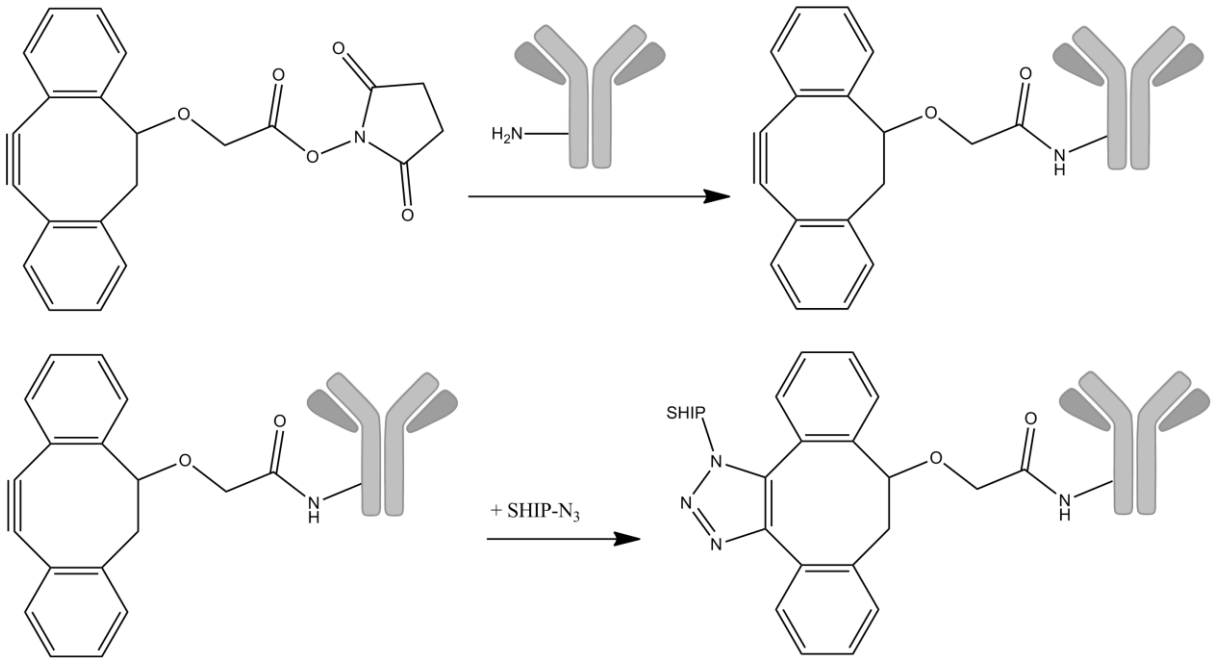

Figure 19: Scheme of antibody-SHIP conjugation

The antibody-SHIP conjugates are synthesized via copper-free click reaction. First, lysine residues of the antibody react with Click-IT® Succinimidyl Ester dicyclobenzyl cyclooctylene (DIBO) and in the second step the commercially available SHIP-Cy5-azide reacts with the alkyne group under triazole formation. Click chemistry is used because this reaction between alkyne and azide is bioorthogonal, efficient and no extreme temperatures or solvents are required. With the elimination of copper, no detectable damage to cells or proteins occurs which is of great advantage for sensitive biological systems. Furthermore the reaction product is stable and the components of the reaction are bioinert. The most important advantage is the specificity of the reaction as no side reactions occur which makes it an attractive reaction for complex biological samples.

The ratio of SHIP to antibody was determined with UV measurements as the ratio of the absorbance of protein at 280 nm and the absorbance of SHIP-AlexaFluor 647 at 650 nm to be ~ 1 for each antibody-SHIP sample.

With these antibody-SHIP conjugates the internalization of the antibody can be determined as described in Chapter 2.3.6. First, spleen dendritic cells are isolated from murine spleen and then immediately incubated with the samples. With incubation at 4°C binding of the samples to the cell surface is achieved, cells are washed to remove excess of sample and then incubated for certain time points at 37°C and 10% CO_2 to obtain internalization kinetics. In order to differentiate between binding and internalization half of the cells are incubated after phenotyping with the Quencher at 4°C. This enables quenching of remaining SHIP sample on the cell surface, but at 4°C the quencher cannot internalize into the cell and therefore not affect fluorescence inside the cell. Internalization experiments of SHIP show that there is no binding of SHIP to dendritic cells at 4°C and therefore no internalization occurs at 37°C.

The ratio of the fluorescence intensity of the quenched and unquenched sample gives the amount of sample internalized.

The binding specificity is determined as the percentage of binding to spleen DC by incubating 30 min at 4°C. In order to analyze different subpopulations with flow cytometry, cells have to be phenotyped for the cell surface markers. For these experiments cells are phenotyped with the fluorescently labeled antibodies CD11c-FITC and CD8-PE that bind to surface molecules of specific DC subpopulations. This way, dendritic cells can be identified with the uni-

versal DC marker CD11c-FITC and the subpopulation of CD8 positive DC can be determined with CD8-PE.

This graph (Figure 20) confirms the specificity of binding for the different antibodies to spleen CD8– and CD8+ DC. CD11c receptor is expressed on both CD8 positive (99.8%) and negative DC (99.7%), as CD11c integrin is a universal marker for dendritic cells. DEC205 is present to an amount of 81.5% on CD8 positive DC, but only 5.3% of CD8 negative DC bind aDEC205. The same trend can be observed for Clec12a, which shows a high binding specificity of 80.2% to CD8 positive DC and only very low binding of 9.7% to CD8 negative. There is low level expression of M5/114 and Clec9a on both CD8 positive and negative DC, but still both show ~10% more binding to CD8+ DC than to CD8-. The binding specificity to mature CD8+ DC is 87.2% for aDEC205 and 100% for CD11c and to mature CD8- DC 18.9% for aDEC205 and 100% for CD11c. The high binding specificity of aDEC205 and CD11c to mature DC and the only marginal difference of binding regarding the maturation state of the DC is in accordance to the fact that mature DC do not downregulate receptor-mediated endocytosis[73].

SHIP shows only very low binding to immature dendritic cells and therefore is suitable for internalization experiments.

Table 4: Binding specificity of different antibodies to iDC and mDC

		Phenotyping	**SHIP**	**aDEC205**	**CD11c**	**M5/114**	**Clec12a**	**Clec9a**
iDC	**CD8+**	6.2±0	5.1±0.1	81.5±0.2	99.8±0.1	19.0±5.0	80.2±0.8	13.6±1.3
	CD8-	0.4±0	0.5±0.1	5.3±0.1	99.7±0	10.5±1.1	9.7±0.35	3.7±0.6
mDC	**CD8+**	0.8±0	16.0±1.4	87.2±0.6	100.0±0			
	CD8-	2.5±0	6.1±0.6	18.9±0.1	100.0±0			

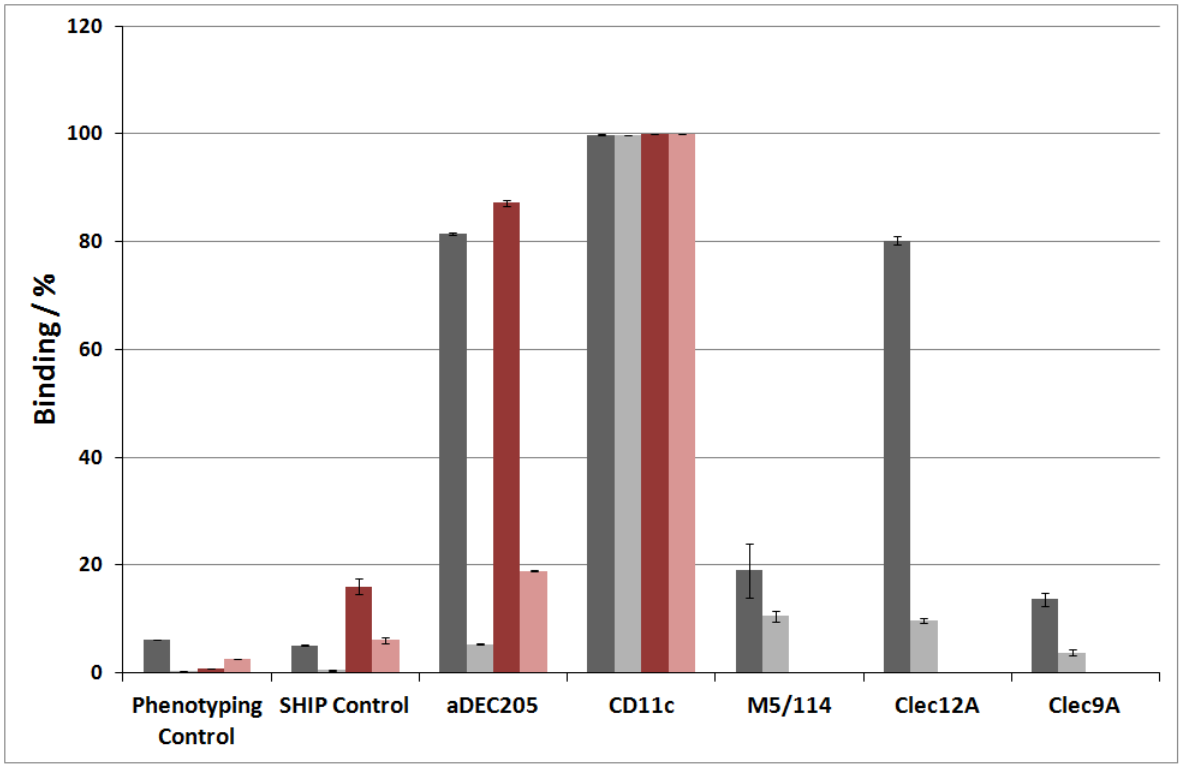

Figure 20: Binding specificity of different antibodies to CD8+ and CD8- immature and mature dendritic cells; CD8+ iDC, CD8- iDC, CD8+ mDC, CD8- mDC

We want to target CD8+ DC as this subpopulation has the ability to cross present exogenous antigens on MHC class I molecules to CD8+ T cells[165]. This difference between CD8+ and CD8- DC lies in the selective expression of phagocytotic receptors (e.g. for dead cells) and on the specialization of their endocytotic pathway. CD8+ DC have developed specific adaptions of their endocytotic pathway like high pH and low degradation in their endosomes and high export to the cytosol[77].

Proteolysis in CD8+ DC is limited which avoids destruction of potential epitopes on antigens. This is achieved by several mechanisms, e.g. acidification in endosomes is inhibited through the production of reactive oxygen species[76]. Exogenous protein is released into the cytosol more efficiently in CD8+ than in CD8- DC, which is important for cross presentation through the proteasome-dependent pathway[78].

As we want to achieve presentation of exogenous antigen to CD8+ T cells in order to induce a CD8+ cytotoxic T lymphocyte activation, only CD8+ DC are analyzed in the following experiments.

When the antibody binds to the receptor on the cell surface and the antibody-receptor complex is formed, not only receptor-mediated endocytosis of the antibody can occur, but also capping. Capping is a phenomenon when the entire antibody-receptor complex is pulled from the cell surface rather than being internalized (see also Chapter 2.3.6.). Some antibodies show this effect more than other, but it is not known why.

The amount of capping can be determined by SHIP-internalization experiments (Figure 21). Normalized fluorescence intensity is plotted over time for the different antibodies in immature (left) and mature dendritic cells (right). If no capping occurs fluorescence intensity is expected to remain the same over time, while loss in intensity indicates capping.

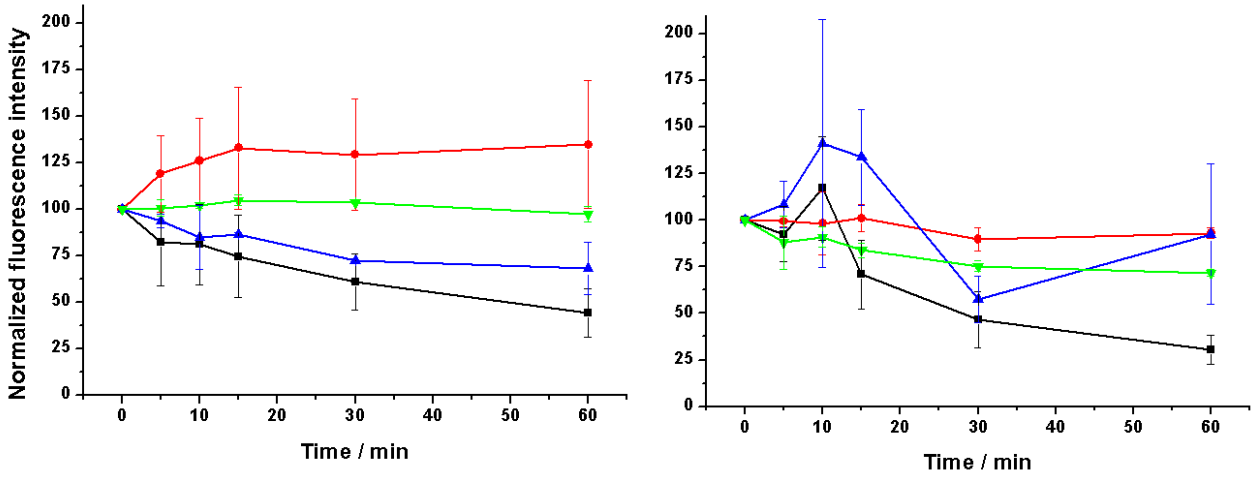

Figure 21: Normalized fluorescence intensity of DEC205, CD11, M5/114 and 5P1 in immature CD8+ DC (left) and mature CD8+ DC (right); ● aDEC205, ■ CD11c; ▲ M5/114; ▼ 5P1

The data shows that with immature dendritic cells capping is occurring and most pronounced with CD11c and a little bit with M5/114, while aDEC205 and Clec12a do not seem to be affected. Intensity for CD11c goes down to only 44.2% after 60 min incubation time and for M5/114 to 68.4% (Figure 21 a).

For activated DC there is no capping for aDEC205 and only a little bit for Clec9a (71.7% intensity). Capping does not appear for the MHC class II antibody but there is a lot of error in this particular data set. CD11c still shows most capping and loses 69.5% of its original fluorescence (30.5% intensity remain) (Figure 21 b).

To highlight the importance of capping the normalized fluorescence intensity for MHC II is compared in immature (black curve) and mature CD8+ DC (grey curve, Figure 22). In both iDC and mDC capping occurs to an amount of ~ 25%.

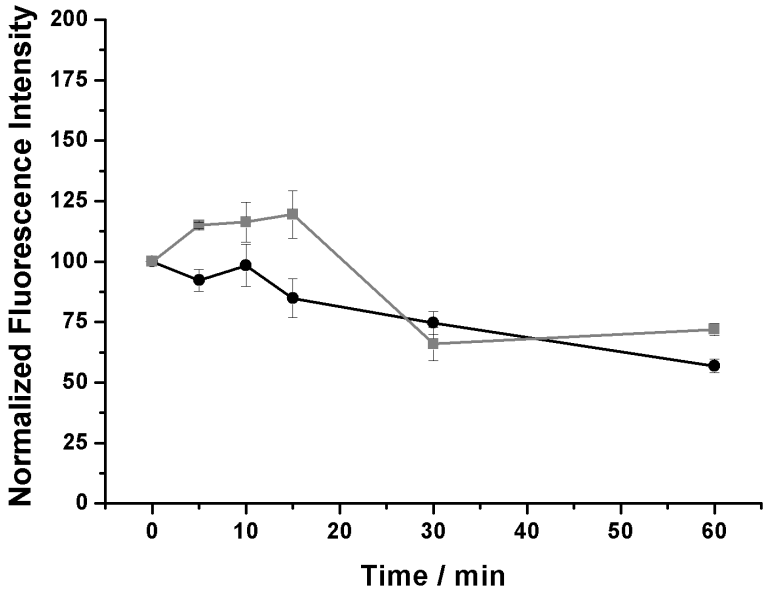

Figure 22: Normalized fluorescence intensity of M5/114 in CD8+ DC; ● immature CD8+ DC, ■ mature CD8+ DC

In Figure 22 internalization of MHC class II antibody is shown into CD11c+ dendritic cells (CD8 positive and CD8 negative DC). There is no huge difference between the MHC II expression on CD8+ and CD8- cells so there is no need to distinguish between them for the analysis of capping.

In Figure 23, for the particular data set in the left graph capping is neglected and for the one in the right graph capping is taken into account. In the data set not corrected for capping the internalization is calculated by the ratio of the quenched sample at a specific time point divided by the unquenched sample at the same time point times 100%. When correcting for capping the quenched fluorescence intensity has to be normalized to that of the unquenched sample at t=0.

Figure 23 shows that internalization is overestimated if capping is not taken into account internalization into iDC seems to be 33.8%, while the analysis corrected for capping yields 15.3% internalization. This is another advantage of the SHIP internalization techniques over pulse chase that capping can be calculated and accounted for. So for further internalization

studies and data evaluation capping has to be considered for CD11c and M5/114 while it can be neglected for aDEC205 and Clec12a.

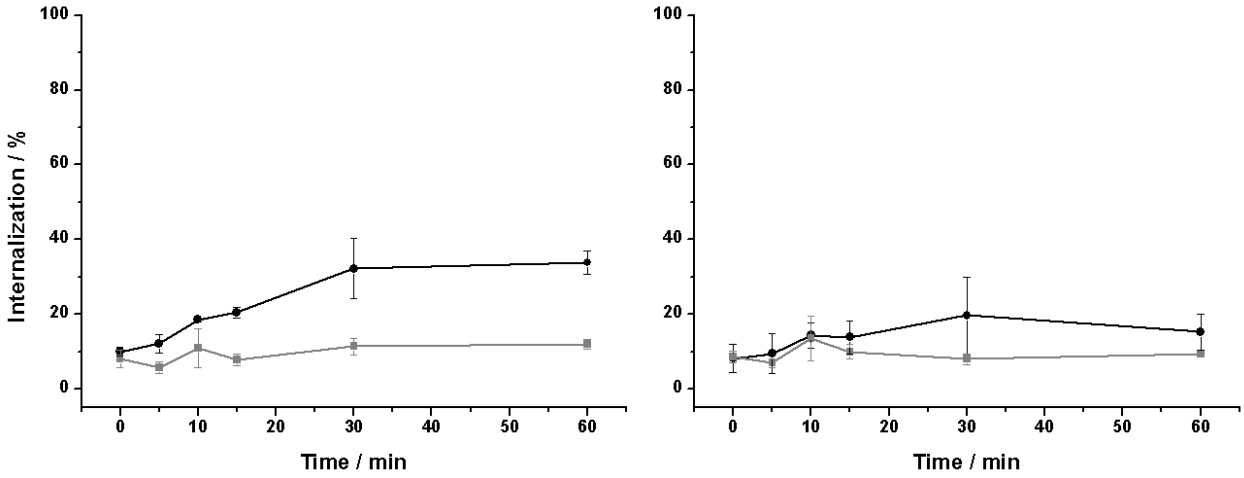

Figure 23: Internalization of M5/114 non-corrected (a) and corrected (b) for capping; ● immature CD8+ DC, ■ mature CD8+ DC

Figure 24 explains the gating strategy for CD8+ immature DC and the differentiation between living and dead mature DC.

In Figure 24 a, with the forward and side scatter plot living cells are determined, in this example to be 50.7%. Then, live cells are plotted with CD8 over CD11c. CD11c positive cells, which are dendritic cells, show high fluorescence intensity in the FITC channel. If cells are CD11c and CD8 positive they exhibit high fluorescence in both CD11c-FITC and CD8-PE channels. Therefore, in this example the CD11c positive and CD8 positive dendritic cells are determined to be 22.0% and the CD11c positive and CD8 negative DC 35.6%.

As during overnight maturation of DC some cells die, these cells have to be excluded for analysis. With propidium iodide dead cells can be identified (Figure 24 b) as it binds to the DNA by intercalating between the bases, but it is membrane impermeant and therefore excluded from viable cells. The cells are gated in the FSC-SSC plot and the populations seperately plotted in histograms for propidium iodide. The overlay of these histograms can be seen in Figure 24 b on the bottom. Of all events, the total percentage of cells is 75.4% (46.4+29%), the other 24.6% are debris. Of these cells, the population positive for propidium iodide gives the dead cell population (red, in this example 61.5% (46.4/75.4)) and the population negative for propidium iodide represents the viable cell population (blue, 38.5% (29/74.5)). The reason for so many dead cells is that splenic DC naturally die when they are

put in culture. For analysis of all experiments with mDC, the population of living cells is evaluated.

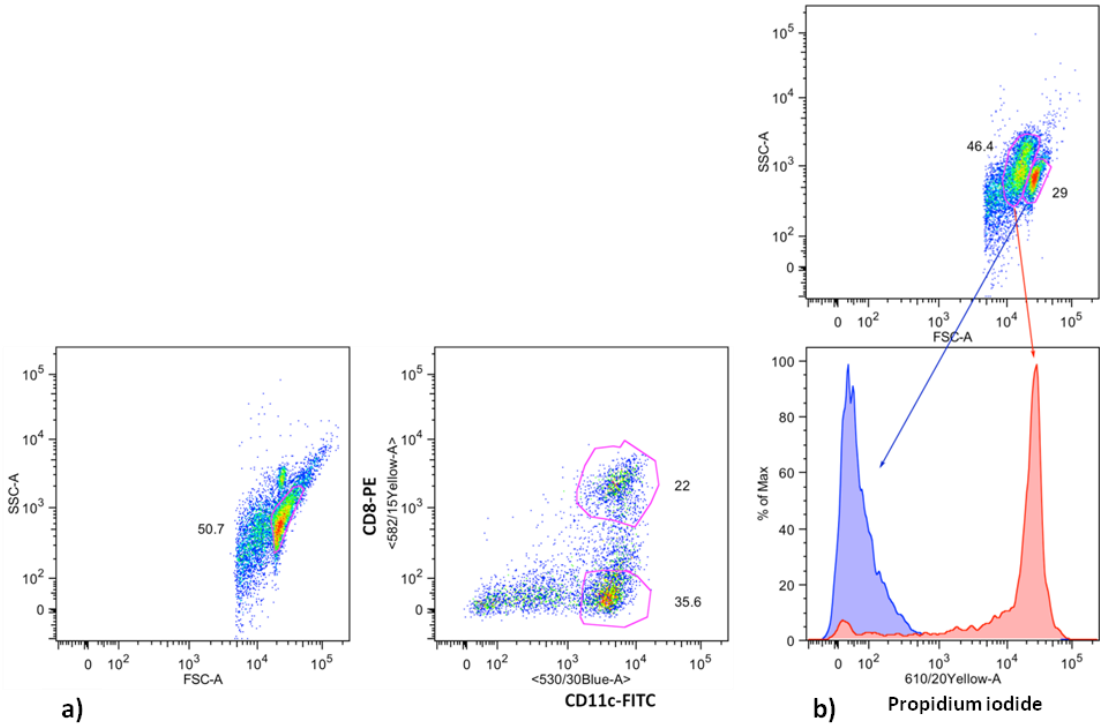

Figure 24: a) Gating strategy for CD8+ immature DC and b) Gating for dead and live mature DC; a) left: Forward scatter-side scatter plot; FSC-A: forward scatter, SSC-A: side scatter; right: Dot-plot CD8-PE against CD11c-FITC; <582/15Yellow-a> = CD8-PE; <530/30Blue-A> = CD11c-FITC; b) top: Forward scatter-side scatter plot; bottom: Histogram over <610/20Yellow-A> = Propidium iodide; ▬ viable cells, ▬ dead cells

For the SHIP internalization experiment the fluorescence of the SHIP sensor (Cy5) is compared in the unquenched and the quenched sample. In Figure 25 the histograms on the left show the CD8+ iDC populations after 30 min incubation of cells with aDEC205-SHIP at 4°C (t=0) which leads to binding of the sample to the cell surface. Low temperature is a general inhibitor of endocytosis due to energy depletion and if the temperature is below the T_g of the lipid membrane, the membrane is too rigid to allow internalization[166].

The histograms on the right hand side show cells incubated with aDEC205-SHIP for 60 min at 37°C (t=60) which leads to internalization of the aDEC205-SHIP sample.

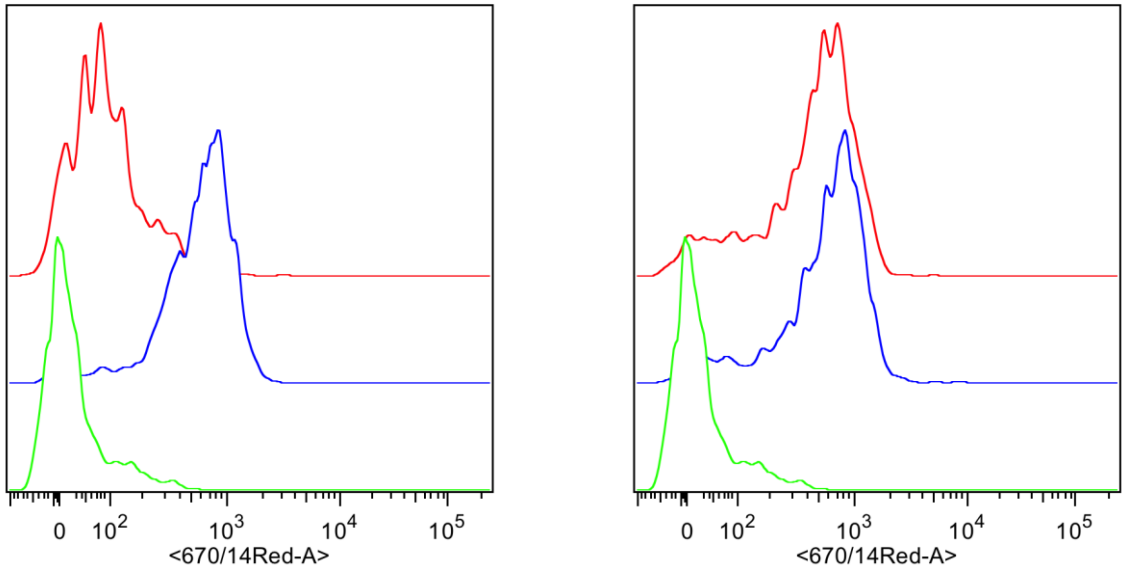

Figure 25: Histograms for cells (▬), aDEC-SHIP unquenched (▬) and aDEC-SHIP quenched (▬), left: binding for 30 min at 4°C, right: internalization for 60 min at 37°C;

The negative cell control shows negligible binding for SHIP to immature and mature DC (Figure 20) and no fluorescence signal after incubation which means no internalization (not shown). Cells incubated with aDEC205-SHIP show a shift of the population to higher fluorescence intensities to the same magnitude for both incubation times, 30 min at 4°C (left) and 60min at 37°C (right). This is expected as the cells are washed after 30 min incubation at 4°C before they are incubated at 37°C. The washing step removes all excess of sample in solution so that only sample that is bound to the cell surface is internalized during the following incubation at 37°C. Therefore, the fluorescence signal is expected to be the same for all incubation times.

In order to determine whether the signal is located on the cell surface or if the sample was internalized, cells are quenched with a black hole quencher, a single stranded DNA complementary to the SHIP sensor. After binding at 4°C (Figure 25, histogram on the left) the fluorescence signal can be quenched nearly completely which means that aDEC205-SHIP was mainly bound to the cell surface and only very little was internalized. Incubation for 60 min at 37°C results in nearly complete internalization of the sample as the fluorescence signal cannot be quenched any longer (Figure 25, histogram on the right).

By analyzing the ratio of the fluorescence of the quenched sample over the fluorescence of the unquenched sample the percent internalization can be determined.

The internalization experiments are performed with immature and mature dendritic cells isolated from spleen. Dendritic cells mature due to different stimuli[167]. One way is to culture splenic DC overnight. Another way for DC to mature is to respond to stimuli like CpG, LPS[168] and poly I:C.

The internalization of aDEC205 into splenic DC matured with different stimuli is studied in collaboration with Haiyin Liu at the University of Melbourne. Dendritic cells are cultured in DC media and CpG, LPS or poly I:C was given to the media at a final concentration of 10µg/mL. The cells are cultured overnight at 37°C and 10% CO_2. The next day the cells are washed once with DC media and then incubated with aDEC205-SHIP conjugate for internalization kinetic studies.

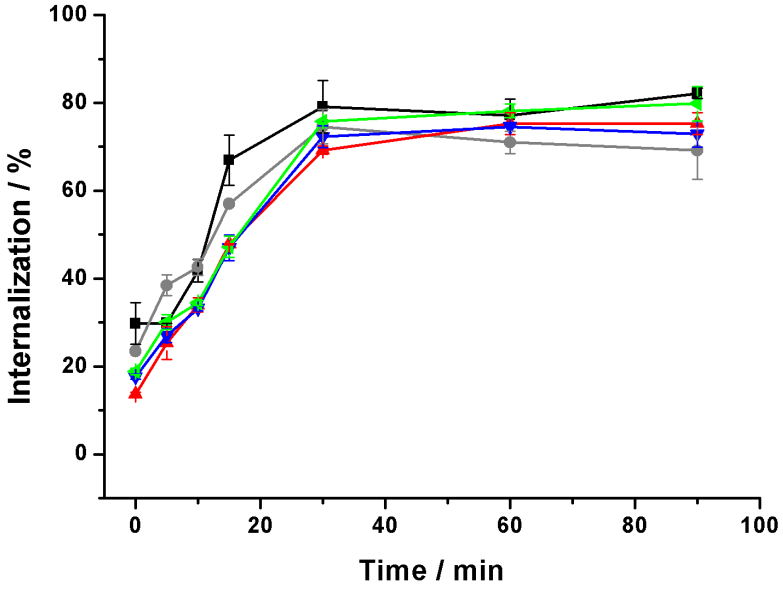

Figure 26: Internalization of aDEC205 into splenic DC matured with different stimuli; ■ immature DC, ● mature DC without stimuli, ▲ DC matured with CpG, ▼ DC matured with LPS, ◀ DC matured with poly I:C

Figure 26 shows that there is no significant difference in the internalizations into immature DC and mature DC. In general, uptake into mature DC is marginally decreased. Maturation by different stimuli does not alter the internalization kinetics of aDEC205. Therefore, cells are cultured overnight without additional maturation stimuli for all further mDC experiments.

Internalization experiments are performed with the antibodies aDEC205 (NLDC-145), CD11c (N418), MHC class II (M5/114) and Clec12a (5P1), and also with spleen dendritic cells in the immature and the mature state (Figure 27). The graph on the left side shows internalization

of the different antibodies into immature DC, the graph on the right hand side into mature DC which were cultured over night.

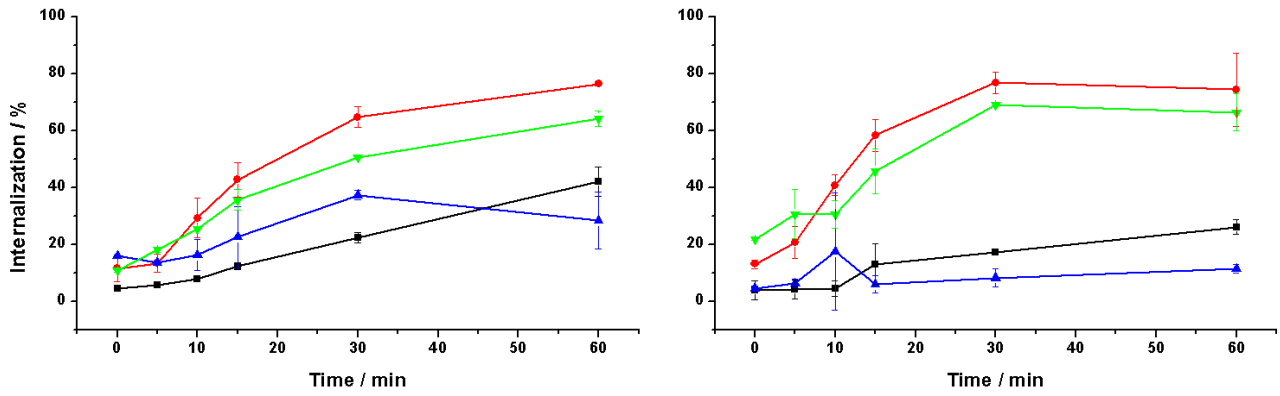

Figure 27: Internalization of aDEC205, CD11c, M5/114 and 5P1 into immature CD8+DC (left) and mature CD8+ DC (right); ● aDEC205, ■ CD11c, ▲ M5/114, ▼ Clec12a

When the internalization of aDEC205 and CD11c is compared, the data shows a higher and faster uptake of aDEC205 (red curve) into immature and activated DC than CD11c (black curve). After 60 minutes 76.5% of aDEC205 is internalized into CD8+ iDC and 74.5% in mDC, while only 42.1% of the immature and 26.2% of the mature DC take up CD11c. Clec12a internalization resembles that of aDEC205, 64.3% into CD8+ iDC and 66.5% into mDC after 60 minutes incubation at 37°C. aDEC205 and Clec12a are not affected by DC activation, while CD11c is internalized less into mDC. The data shows that the MHC class II antibody (M5/114) is internalized only to a small amount into immature DC (28.5%) and even less in activated DC (11.5%). Internalization is summarized in Table 5.

Table 5: Internalization of different antibodies into CD8+ iDC and mDC after incubation for 60min at 37°C and 10%CO_2

Internalization	**aDEC205**	**CD11c**	**M5/114**	**Clec12A**
CD8+ iDC	76.5%	42.1%	28.5%	64.3%
CD8+ mDC	74.5%	26.2%	11.5%	66.5%

In Figure 28 the internalization kinetics of aDEC205 and CD11c are compared for immature and mature CD8+ DC. The data for aDEC205 remains uncorrected for capping, as aDEC205 does not undergo this process. The data for CD11c is corrected for capping. This correction makes the difference of internalization between the two antibodies even more pronounced.

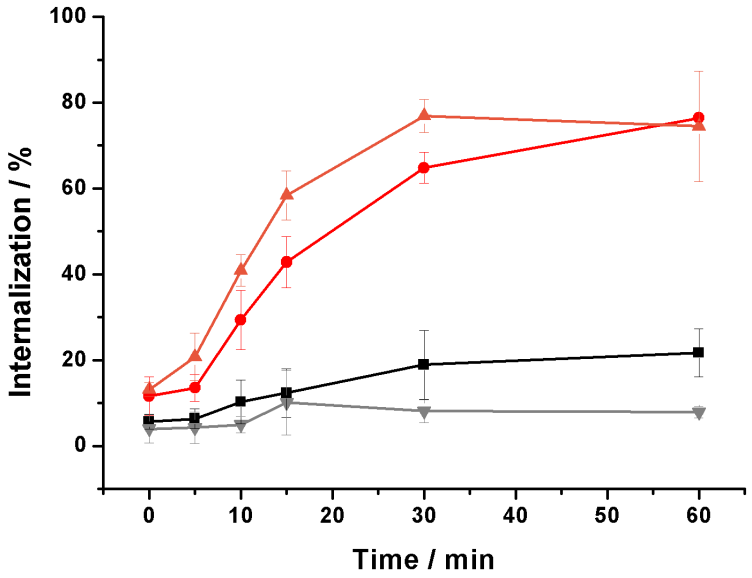

Figure 28: Internalization of DEC205 and CD11c into immature and mature CD8+ DC; ● aDEC205 in iDC, ▲ aDEC205 in mDC, ■ CD11c in iDC, ▼ CD11c in mDC

As aDEC205 is internalized faster and more efficiently into CD8 positive dendritic cells than CD11c, this strongly suggests that the mechanism of internalization is different for aDEC205 and CD11c.

Therefore colocalization studies of the antibody-SHIP conjugates with different cell compartment markers are performed.

Cells are incubated with aDEC205-AlexaFluor555 or CD11c-AlexaFluor555 first for 30min at 4°C for binding, washed twice with PBS and then incubated for 60 min at 37°C for internalization. Afterwards the cells are fixed and permeabilized and incubated with anti-lysosome associated membrane protein (Lamp 1, Rat Lamp, 1D4B), Clathrin (D3C6 XP™ Rabbit mAb) or Caveolin (D46G3 XP™ Rabbit mAb) primary antibodies. After 60 min incubation at RT the cells are washed and then incubated with a secondary antibody fluorescently labeled with AlexaFluor488. In the following microscopy images the antibody is visible in the green channel, while the cellular compartment stain is red.

In Figure 29 no colocalization of aDEC205 with lysosomes can be observed. For DC it is difficult to achieve a sufficiently bright lysosome staining with Lamp-1. Lysotracker cannot be used because the lysosomes of DC are not very acidic in comparison to other cell types[77]. This high pH is important for the efficient antigen presentation by DC. Lysosomes often combine with MIIC compartments where MHC class II complexes are loaded with antigen

and recycled to the cell surface where antigen is presented. Lamp-1 stain gives a high background signal und unspecific staining if used in higher concentrations. Therefore the specific signal for Lamp-1 is very low.

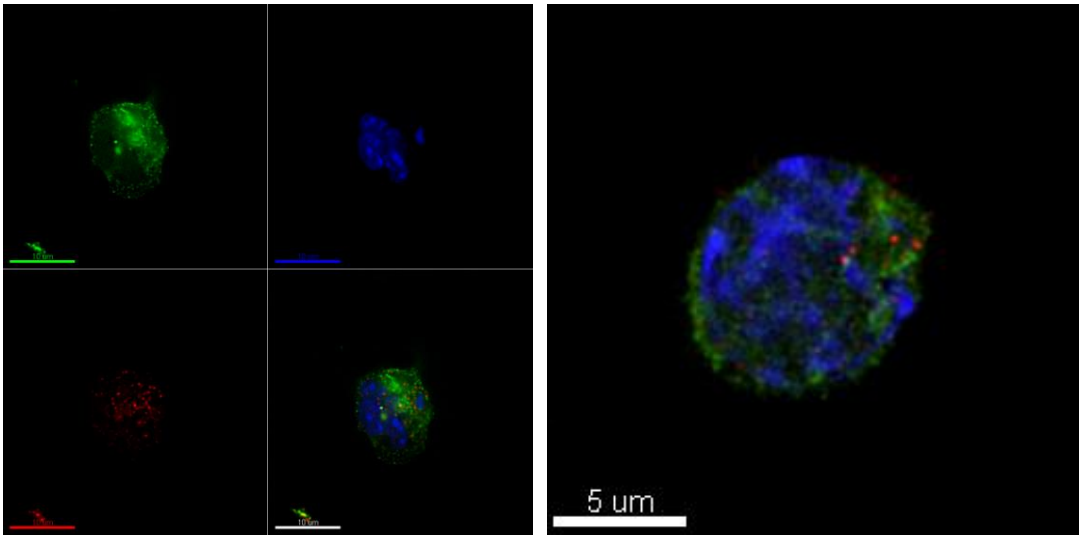

Figure 29: Colocalization of DEC205 and Lamp-1. Green: DEC205-AF647, red: Lamp-1 stain, blue: DAPI, scale bar: left: 10µm, right: 5µm

No colocalization of aDEC205 with Clathrin coated pits can be found in Figure 30.

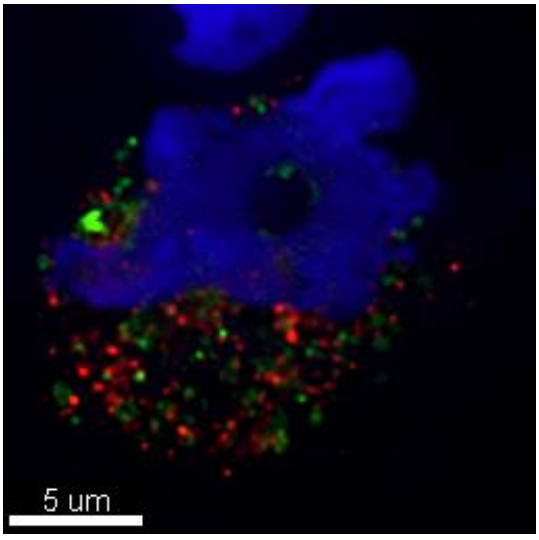

Figure 30: Colocalization of DEC205 and Clathrin. Green: DEC205-AF647, red: Clathrin stain, blue: DAPI, scale bar: 5µm

Relatively strong colocalization of aDEC205 with Caveolin can be observed in Figure 31. Caveolae in general are highly stable, small (50-60nm) vacuoles with a small fluid phase volume and they are only slowly internalized in contrast to rapid Clathrin-mediated uptake[169],

[170]. Caveolin-dependent endocytosis is a nonacidic and nondigestive route of internalization[132]. There is no drop in pH in caveolae and most pathogens internalized by caveolae are avoiding lysosomal degradation and are directly transported to the Golgi or endoplasmatic reticulum[171], [132]. Thus, this pathway seems to be of advantage for DNA delivery. Additionally this pathway is preferred for the uptake of large particles of ~500nm[172]. But there is no evidence in literature that antibody-receptor complexes are internalized Caveolin-dependent.

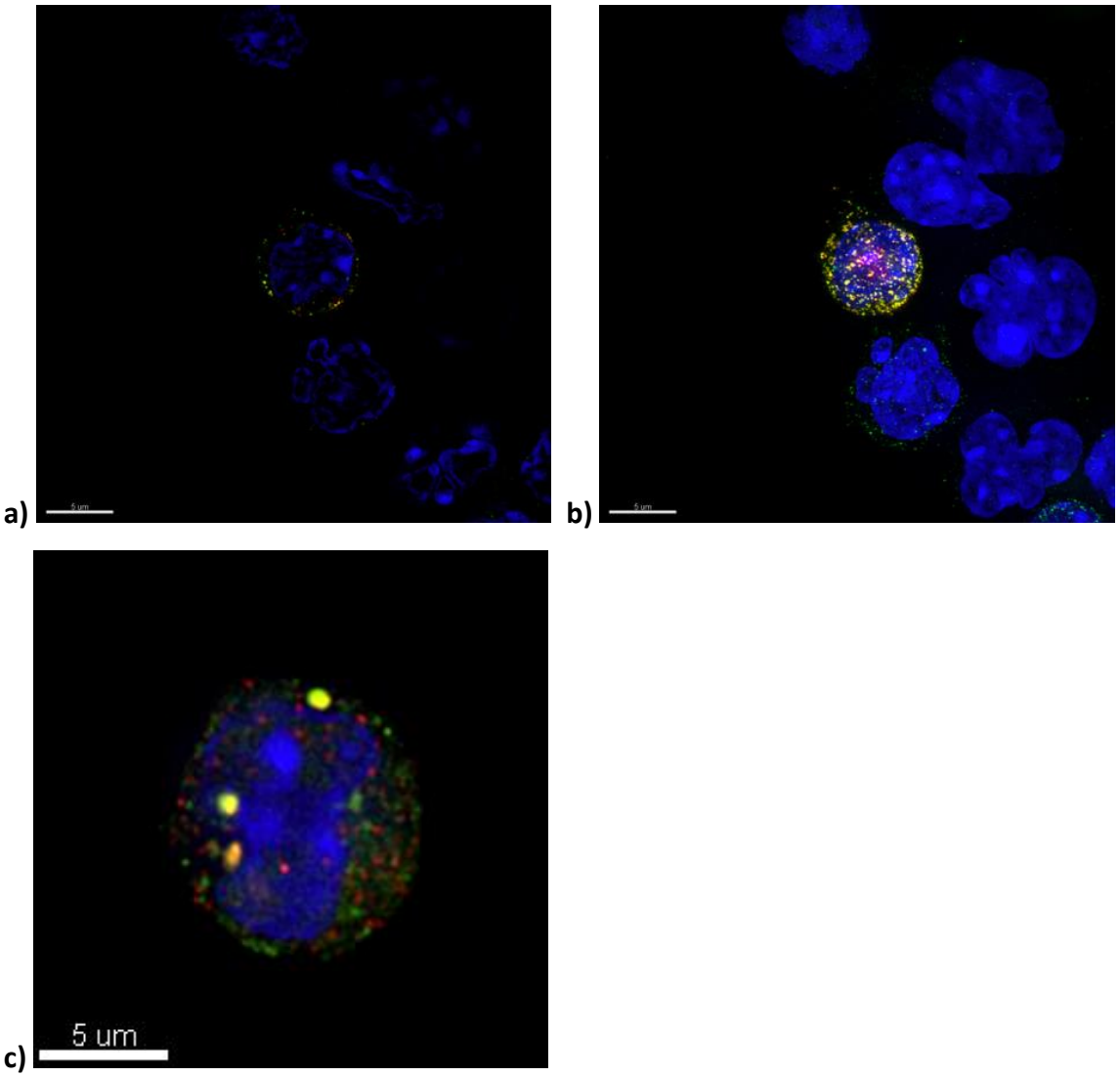

Figure 31: Colocalization of DEC205 and Caveolin. Green: DEC205-AF647, red: Caveolin stain, blue: DAPI; a: single focus plane, b and c) maximum intensity projection, scale bar: 5µm

Controversially, in literature Mahnke *et al.* propose colocalization of aDEC205 with anti-lysosome associated membrane protein (Lamp-1)[79]. These results indicate targeting of aDEC205 to late endosomes. This is surprising as endocytosis receptors like MMR typically

target to early endosomes and the DEC205 receptor is a homologue to the MMR, localizing to coated pits and enhancing ligand uptake[173].

This deep endosomal targeting has its origin in the two functional regions of the DEC205 receptor. The membrane-proximal region of the DEC205 receptor contains the amino acid sequence FSSVRY, which resembles the sequence for coated pit localization described in many other receptors[91]. Therefore colocalization with Clathrin based on the formation of Clathrin coated pits would be expected. The distal region of the DEC205 receptor contains a cluster of acidic amino acids, the EDE (Glu–Asp-Glu) triad which leads to distinct intracellular movements, the unusual deeper targeting.

This ability makes the DEC205 receptor a hybrid between two groups of receptors. Some receptors mediate ligand uptake via receptor-mediated endocytosis and subsequently discharge their cargo in early endosomes from where the intact receptor is recycled back to the cell surface. Other receptors are involved in signaling for cell activation and growth where ligand and receptor digestion takes place in the lysosome. For DEC205 the cytosolic domain enables receptor-mediated endocytosis that entails efficient uptake through late endosomes and following recycling of apparently intact receptors. Simultaneously there is a great improvement in the efficiency of antigen processing and presentation on MHC complexes which leads to improved antigen presentation to CD4+ T cells and cross-presentation to CD8+ T cells.

This difference in localization within the cell between Mahnke's results and ours might be due to the type of dendritic cell that is used. Mahnke *et al*. performed the experiment with bmDC on day 6 while we used freshly prepared spleen DC[79]. Another problem could be the Lamp-1 stain that we used as we never got a high fluorescence signal without unspecific background.

In general, there are more facts that indicate Clathrin-mediated endocytosis of DEC205 with trafficking to late endosomes. Caveolin-dependent endocytosis seems unlikely due to the cross-presentation of material delivered by the DEC205 receptor. For cross-presentation lysosomes have to combine with MIIC vacuoles. This presumes uptake into late endosomes and lysosomes and no trafficking via caveolae to Golgi or endoplasmatic reticulum. Therefore, further experiments to determine the pathway of DEC205 have to be performed.

As already mentioned in the theory, Lahoud *et al*. proposed that the DEC205 receptor, as a "promiscuous" antigen receptor, is also essential in binding and internalization of CpG ODN[89]. If CpG already promoted receptor-mediated endocytosis into DC via the DEC205 receptor, additional conjugation of aDEC205 for the specific targeting of CD8+ DC would be unnecessary. Therefore, we tested the binding specificity of aDEC205 in comparison to CpG ODN by incubating splenic DC with CpG-Cy5 and aDEC205-Cy5 for 30 min at 4°C, washed the cells and measured the binding with flow cytometry. Our results show that aDEC205 shows high binding to the DEC205 receptor, while we obtain no binding for CpG at the concentrations that match those of SHIP internalization experiments (Figure 32). In this paper, concentrations that are one to two orders of magnitude higher are used to perform the experiments. This result indicates that the aDEC205 antibody is still necessary to induce receptor-mediated endocytosis of nanomaterials into CD8+ DC.

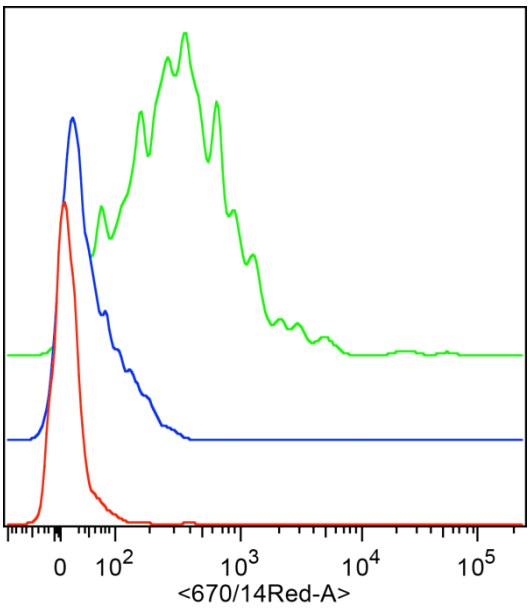

Figure 32: Histograms for cells (▬), CpG-Cy5 (▬) and aDEC-Cy5 (▬)

The internalization results of aDEC205 are compared with the internalization studies of CD11c. As shown above in Figure 28 the internalization into immature DC is 76.5% for aDEC205 and 42.1% for CD11c. Additionally the kinetics are different, aDEC205 is internalized much faster.

In Figure 33 the histograms of the internalization of CD11c into iDC are shown. Figure 33 a and b show the histograms of phenotyped cells (green), the fluorescence of CD11c-SHIP un-

quenched (red) and quenched (blue). On the left hand side the incubation was performed for 30 min at 4°C (Figure 33 a). It can be seen that only binding occurs as the fluorescence can be quenched completely. After 60 min incubation at 37°C (right, Figure 33 b) internalization took place. The fluorescence cannot be quenched completely anymore which proves uptake of CD11c into iDC. But there is still a shift in the population between the unquenched and the quenched sample. This ratio gives the lower internalization of CD11c with 42.1% in comparison to the histogram of aDEC205 where the shift is only marginal and the internalization accounts for 76.5%.

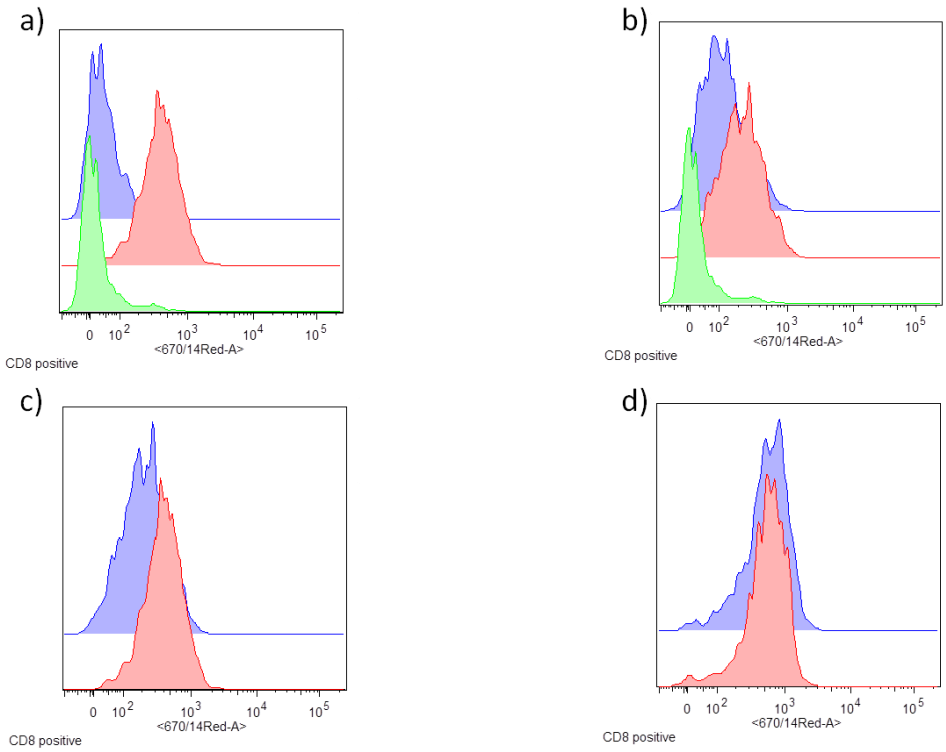

Figure 33: Gating strategy for CD11c, histograms with <670/14Red-a> = SHIP-Cy5; a) CD11c, incubation for 30 min at 4°C (t=0); cells, CD11c-SHIP unquenched, CD11c-SHIP quenched; b) CD11c, incubation for 60 min at 37°C (t=60); cells, CD11c-SHIP unquenched, CD11c-SHIP quenched; c) CD11c-SHIP unquenched, t=0, t= 60; d) aDEC205-SHIP unquenched, t=0, t= 60

In Figure 33 c and d the histograms of aDEC205 and CD11c are compared for the unquenched sample at t=0 (red) and t=60 minutes (blue). aDEC205 (d) shows no population shift, while there is a shift of population for CD11c (c). This is based on the capping phenomenon which was found to be a lot more pronounced for CD11c than for aDEC205. CD11c loses 55.8% of its fluorescence intensity after 60min incubation while no evidence of capping can be found for aDEC205.

Colocalization studies of CD11c show no colocalization of CD11c with Lamp-1 or Clathrin and only a little for CD11c with Caveolin (Figure 34).

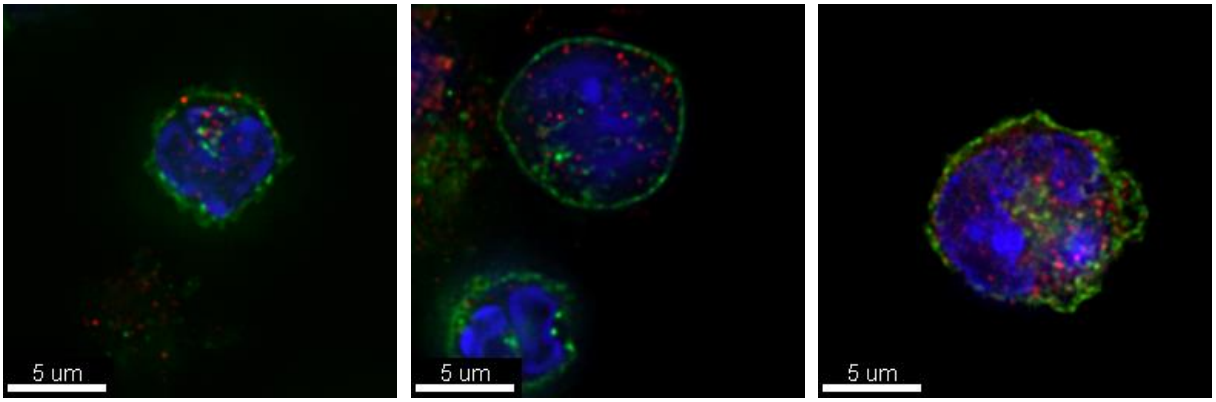

Figure 34: Colocalization of CD11c and Lamp1, Clathrin and Caveolin, scale bar: 5µm

Summary of internalization studies of different antibodies into splenic DC

The comparison of aDEC205 with other DC targeting antibodies like CD11c, MHC class II, Clec9a and Clec12a show the superiority of aDEC205. aDEC205 shows a high binding specificity for CD8+ DC with 81.5% and only very low binding of 5.3% to CD8- DC. The internalization of aDEC205 is fastest and to a high amount of 76.5% into iDC. Furthermore DEC205 does not undergo capping which enhances the internalization efficiency. CD11c and MHC class II show comparable low amount of internalization and capping is most pronounced with CD11c. Clec12a shows similar uptake like aDEC205 and also a high binding specificity and no capping. But Clec12a is not well studied so far and its internalization pathways are not well understood.

For maturation of splenic DC cells are cultured overnight at 37°C and 10% CO_2 without addition of maturation stimuli like CpG or LPS. The comparison of internalization into immature DC and mature DC shows that there is nearly no difference in the uptake of aDEC205 in iDC or mDC.

In literature, it was assumed for a long time that mature DC shut down all mechanisms of endocytosis. This idea suits the immunological explanation of the presentation of pathogens that are captured at the time of activation, while self-antigens that are acquired before or

after that event are not presented. Immature DC internalize antigens avidly through several mechanisms, e.g. non-specific uptake via macropinocytosis and specific uptake through receptor-mediated endocytosis[80]. Macropinocytosis is upregulated immediately after activation[174], which subsequently follows a radical downregulation[175]. But it is reported that mature DC continue to form clathrin-coated vesicles which indicates that surface molecules are still internalized in mDC[175]. Platt et al. report that mature DC continue to internalize antigens via receptor-mediated endocytosis and that these antigens are normally localized within the late endosome, loaded onto MHC class I and II molecules and presented to CD4+ and CD8+ T cells in the cell surface of mature DC. Thus, despite downregulation of macropinocytosis, mature DC still capture, process and present antigens via endocytic receptors. This indicates that mature DC can still induce immune responses to newly encountered antigens during the course of an infection[73] and thus appear to be an interesting target for cancer immunotherapy.

Our results also suggest that DC do not shut down receptor-mediated endocytosis upon maturation as the aDEC205 and CD11c targeting surface receptors are still internalized by mature DC.

Colocalization experiments in DC show colocalization of aDEC205 with Caveolin which contradicts literature that proposes Clathrin-mediated uptake[173]. Therefore, further experiments have to be performed.

In summary, aDEC205 is the most suitable antibody to target nanomaterial to immature and mature CD8+ dendritic cells and therefore it is characterized in detail in the next chapter and used for the vaccine conjugate.

3.1.2. Characterization of aDEC205

Having identified aDEC205 as the most promising candidate to target CD8+ DC, we have characterized its hydrodynamic radius, its binding affinity to bone marrow dendritic cells and aggregation behavior of aDEC205 in presence of poly-*L*-lysine.

The aDEC205 monoclonal antibody (NLDC-145) was purchased from BioXCell and is characterized with different techniques. First, the hydrodynamic radius is determined with dynamic light scattering to be 5nm. Experiments during my diploma thesis with aDEC205 of a different charge showed aggregate formation of aDEC205 when the antibody was filtered with GHP200nm. With the new charge of antibody, repeated freeze-thaw cycles were avoided by aliquoting the antibody, storing it at -20°C and not re-freezing it after thawing. DLS measurements show that no aggregate formation occurs and that there is no difference in the correlation functions at 30° for GHP200nm and Anotop 20nm filtered aDE205 (Figure 35). Both correlation functions can be fitted with a biexponential fit and R_{h1} is 5nm for both filters. R_{h2} is with 11.2nm a little larger for the GHP 0.2µm filter than for the Anotop 0.02µm filter with 8.9nm (summarized in Table 6). This difference cannot be really explained with the filter size as the larger R_h of ~11nm which equals a diameter of 22nm is still in the range of the 20nm pore size of the Anotop filter. As the R_h describes a distribution of particles with different sizes, it may be possible, that larger particles are filtered out, while particles a little smaller than 20nm remain in solution, which then results in the smaller R_h of 8.9nm for the Anotop filtrated sample. It can also be assumed that that the difference is within the error of analysis.

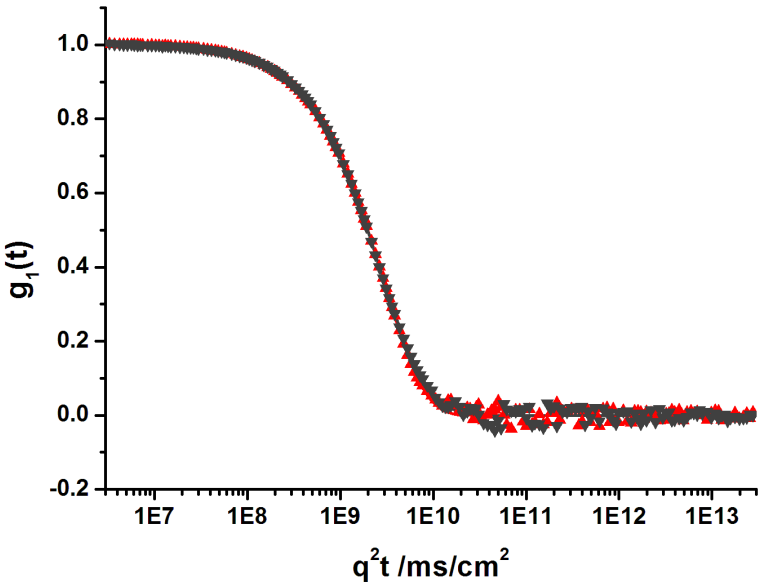

Figure 35: Correlation function of aDEC205 with different filters, 1x PBS, ϑ= 30°, T= 293.15K; ▲ GHP 0.2µm, — Fit GHP 0.2µm, ▼ Anotop 0.02µm, — Fit Anotop 0.02µm

Additionally, DLS measurements with the GHP 0.2µm filtrated aDEC205 at different temperatures are performed. Usually, DLS measurements are conducted at 20°C, but as the body temperature is 37°C and in experiments *in vitro* cells are always incubated at 37°C, DLS is also measured at this temperature. Figure 36 shows that there is no difference in the correlation function of aDEC205 at 20°C and 37°C. For higher temperature the hydrodynamic radius is marginally smaller as the apparent R_h is 5.7nm at 37°C instead of 5.9nm at 20°C (Table 6). So the hydrodynamic radius does not change with temperature and is still ~5nm at body temperature.

Table 6: R_h of the biexponential fit of aDEC205 with different filters and temperatures

	$R_{h,app}$ / nm	Rh_1 / nm	Rh_2 / nm
GHP	5.9	5.0	11.2
Anotop	6.1	5.0	8.9
GHP 37°C	5.7	4.8	10.5

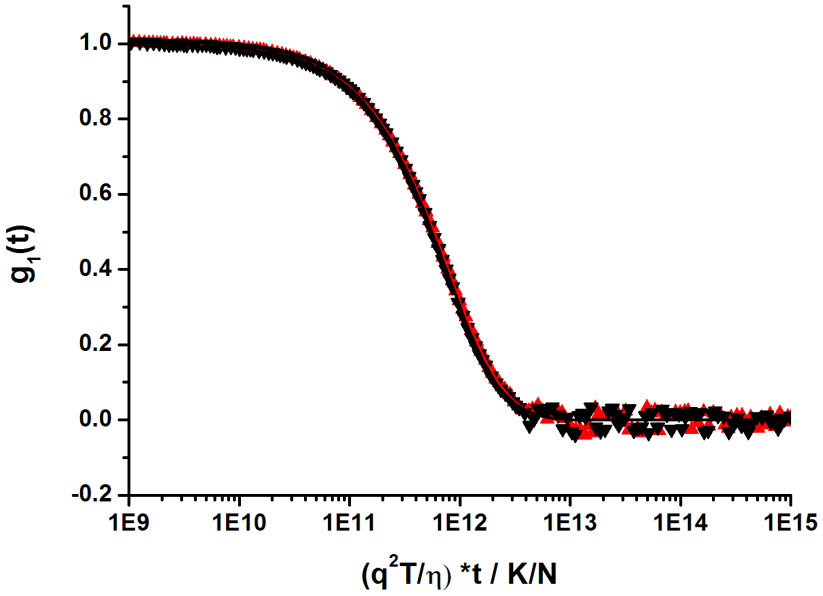

Figure 36: Correlation function of aDEC205 at different temperatures, 1x PBS, θ= 30°, $q^2(30°) = 4.684*10^9$ cm^{-2}, T= 293.15K and 310.15K; ▲ GHP 0.2µm, T = 293.15K, η = 0.9961 Ns/m^2, ▬ Fit GHP 0.2µm 293.15K, ▼ GHP 0.2µm 310.15K, η = 0.6941 Ns/m^2, ▬ Fit GHP 0.2µm 37°C

Furthermore, aDEC205 filtrated with different filters is analyzed with GPC measurements. aDEC205 is applied to Tosoh G2500PW+G3000PW columns and eluted with 1x PBS buffer. The elugram (Figure 37) shows that there is only little filtration loss as the peaks get only marginally smaller after filtration. The filtration loss with a GHP 0.2µm filter is determined with a Bradford-Assay of aDEC205 to be ~15%. Additionally to the main peak, a smaller peak at shorter elution times is observed. This peak is probably due to impurities that may be caused by dimerization of the antibody.

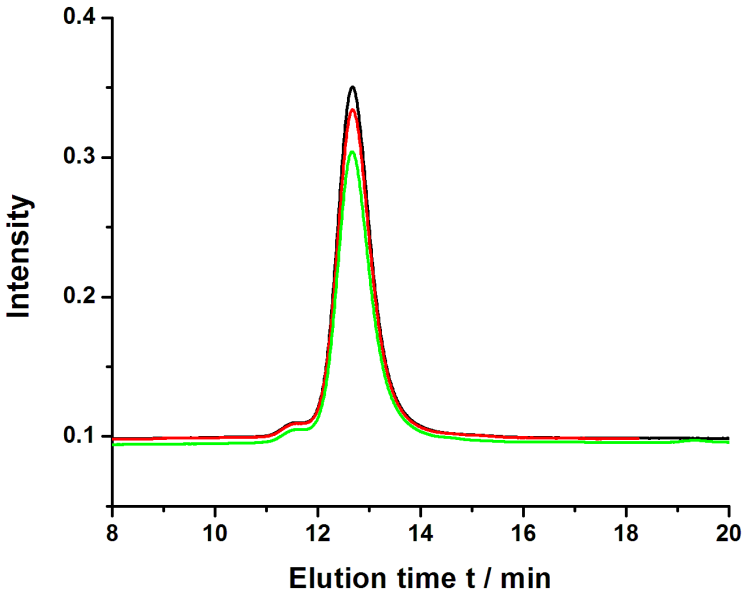

Figure 37: GPC Elugram of aDEC205 with different filters; columns: Tosoh G2500PW + G3000PW (HEMA), eluent: 1x PBS, pH 7.2; ▬ unfiltrated, ▬ VV 0.1µm, ▬ Anotop 0.02µm

Former experiments with another charge of aDEC205 exhibited aggregate formation between aDEC205 and linear poly-*L*-lysine. Aggregate formation leads to diminished reaction efficiency and therefore needs to be avoided. The new aDEC205 charge, where repeated freeze and thaw-cycles are avoided, is again checked for aggregate formation with PLL and no formation of aggregates is detected. Therefore, aDEC205 and PLL are used for conjugation experiments without filtration.

Different gels are run with aDEC205 to determine its molecular weight and to investigate reduction of the antibody (Figure 38).

On the left gel the antibody (30µg) is analyzed under non-reducing conditions. If the gel is conducted without addition of a reducing agent, the antibody shows two very light bands and one very intense and broad band at around 160kDa that relates to the aDEC205 antibody with a molecular weight of 150kDa. The light band below 40kDa may be due to the light chain (25kDa) and the other band below 500kDa may be due to dimer or trimer formation of the antibody (~300kDa or ~450kDa).

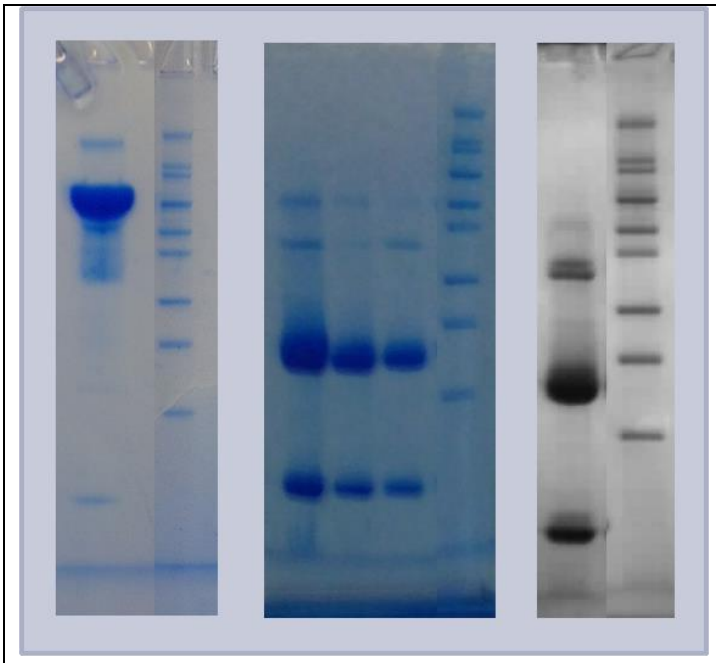

Lane	Sample
1	aDEC205 (30µg)
2	HiMark Protein Marker
3	aDEC205 red. (30µg)
4	aDEC205 red. (10µg)
5	aDEC205 red. (7.5µg)
6	HiMark Protein Marker
7	aDEC205 red. (10µg)
8	HiMark Protein Marker

Figure 38: NUPAGE Tris-Glycine Gel 4-12% of aDEC205; left gel: non-reducing, Lane 1: aDEC205 (30µg), Lane 2: HiMark Unstained HMW Protein Marker (40, 55, 66, 97, 116, 160, 240, 290, 500); middle gel: reducing, Lane 1-3: aDEC205 (30, 10 and 7.5µg), Lane 4: HiMark Unstained HMW Protein Marker; and right gel: reducing, Lane 1 aDEC205 (10µg), Lane 2: HiMark Unstained HMW Protein Marker

If the antibody gel is run under reducing conditions (middle and right gel) the five disulfide bonds within the aDEC205 molecule are partially reduced. Two intensive bands appear below 40kDa and between 40 and 55kDa. These bands depict the light chain (25kDa) and the heavy chain (50kDa) and show that all disulfide bonds in the hinge region between the two heavy chains and also between the heavy and the light chain are reduced. Neither the heavy nor the light chain alone are biofunctional as the antigen binding site is located at the interface of heavy and light chain. A light band between 66 and 97 kDa can be assigned to the heavy-light chain fragment (75kDa) which is still able to bind antigen. The very light band around 116kDa can be related to the heavy-heavy-light chain fragment (HHL, 125 kDa) where only one light chain is split off the whole antibody molecule.

If the gel is stained with silver staining, which is more sensitive to lower protein content than simply blue safe stain, another band appears just above the band related to the HL fragment. The origin of this band cannot be explained. In literature, selective reduction of the disulfide bonds in the hinge region is proposed[176], but no evidence, e.g. a gel image, is given. We are not able to selectively reduce the aDEC205 antibody, but always obtain separation into other fragments as well.

aDEC205 is labeled by reaction of its lysine residues with the fluorescent dye AlexaFluor647 Carboxylic Acid Succinimidyl Ester in accordance to the labeling protocol from Invitrogen. The degree of labeling can be obtained by UV/Vis and FCS measurements and both methods gave a congruent labeling efficiency of ~3 dyes per antibody. Fluorescence measurements showed that there is no drop in the quantum yield for this labeling reaction.

The fluorescently labeled aDEC205 antibody can be used with flow cytometry to determine the number of CD8+ DC of the bone marrow derived DC. aDEC205 specifically binds to CD8+ DC and therefore with a fluorescently labeled aDEC205 these cells can be marked and analyzed (Figure 39). Thus, bmDC are incubated with aDEC205-AF647 for 30 min on ice and at 37°C and for 4h at 37°C. The cells are not washed after addition or incubation with aDEC205.

After 30 min on ice 20.8% of the bmDC bound aDEC205 on the cell surface and after 30min at 37°C 27.4% of the cells have aDEC205 bound to the surface or internalized. Incubation of cells at 37°C for 4h exhibits 17.4% of positive cells. It is expected to see an increase in positive cells from the incubation on ice to the incubation at 37°C. At 4°C only binding to the cell surface and no internalization occurs, while at 37°C binding and internalization is possible so that DEC205 receptors can be endocytosed after binding of aDEC205 and afterwards be recycled back to the cell surface to bind new antibody. The decrease in positive cells after incubation for 4h at 37°C is unexpected. Instead of a further increase in signal due to uptake of more and more antibody the fluorescent intensity drops. This can have several reasons. First, the dye might be degraded within the lysosome or endosome of DC and therefore the fluorescence fades. This is not very likely though, as DC have not very acidic lysosomes and additionally the Alexa Fluor dyes are very stable over a wide pH range and not very susceptible to degradation. Another reason might be capping of the antibody-receptor complex. In Chapter 3.1 it is shown that aDEC205 shows no capping in splenic DC. We can make no assumption about capping in bmDC as nothing is known about the origin of and the reason for capping.

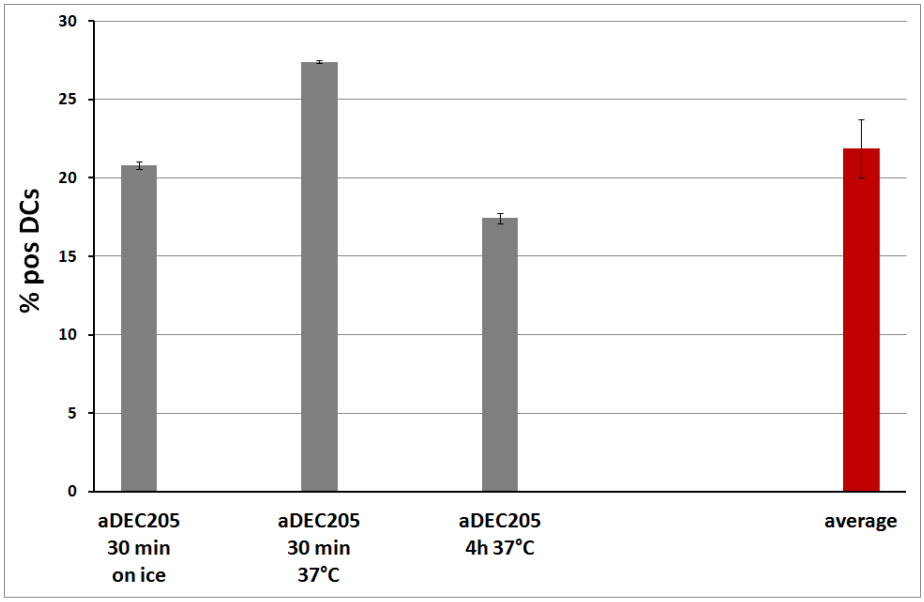

Figure 39: Labeling of CD8+ DC with aDEC205-AF647

Summary of the characterization of aDEC205

In this thesis the commercially available antibody is characterized and used for conjugation due to the very low yield of the antibody production and thus time reasons.

The aDEC205 antibody has a hydrodynamic radius of 5nm and can be reduced with DTT and TCEP to obtain the heavy and light chain fragments. There is only little filtration loss from GHP 0.2µm to Anotop 0.02µm filter. As GHP filtrated aDEC205 does not aggregate with PLL, no further purification is done before using the antibody for conjugation experiments. Fluorescence labeling of the lysine residues is possible for the antibody without losing biofunctionality and the degree of labeling is determined to be 3 dyes per antibody molecule. The labeled antibody binds to ~21% of the bone marrow DC which identifies those as CD8 positive.

3.2. Characterization of PLL and PLL brush and Internalization Studies into Dendritic Cells

In this chapter linear poly-*L*-lysine and the polylysine brush are characterized and their internalization bone marrow derived dendritic cells is studied.

3.2.1. Characterization of PLL and PLL brush

Linear poly-*L*-lysine is analyzed by static and dynamic light scattering to obtain the molecular weight and the hydrodynamic radius. The manufacturer specifies the molecular weight to be 15-30 kDa determined with viscosity (Sigma Aldrich, Cat #: P7890).

The Zimm Plot of PLL (Figure 40) gives an M_w of 14700 g/mole and $\langle R_g^2 \rangle_z^{1/2}$ is smaller than 10 nm. Dynamic light scattering exhibits a $\langle \frac{1}{R_h} \rangle_z^{-1}$ of 3.1nm.

With the mixed anionic mechanism of polymerization of protected PLL and a μ_2=0.1 obtained from DLS a PDI = 2 is reasonable. With PDI and M_w an approximate M_n of 7500 g/mole is assumed. This molecular weight is used to calculate all scales for conjugations.

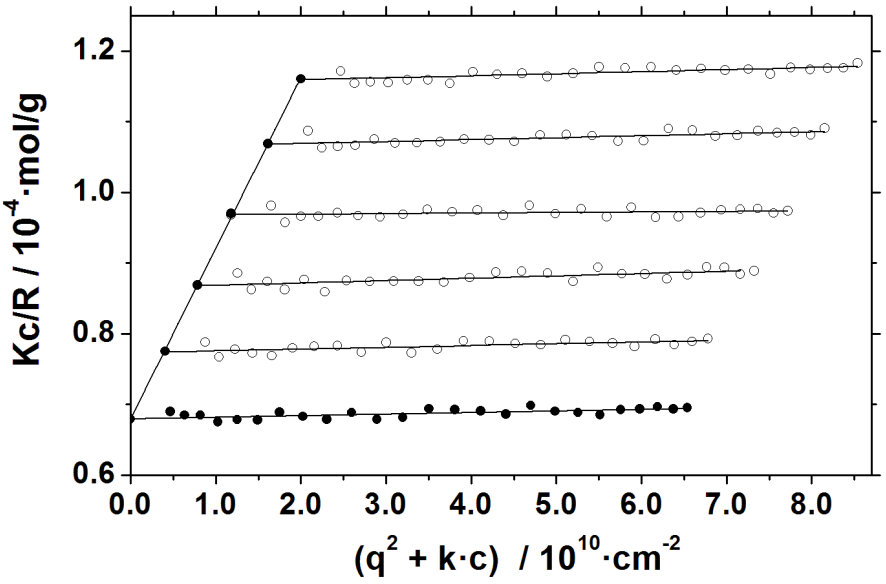

Figure 40: Zimm Plot of linear PLL in 0.1M NaBr, dn/dc = 0.1564 cm^3/g, λ = 632.8nm, T = 293.15K, (2g/L<c<10g/L), k = $2*10^{12}$ cm/g^2, M_w= 14.7 kg/mole, $\langle Rg^2 \rangle_z^{1/2}$<10nm, A_2=$2.4*10^{-3}$ $mole*cm^3/g^2$

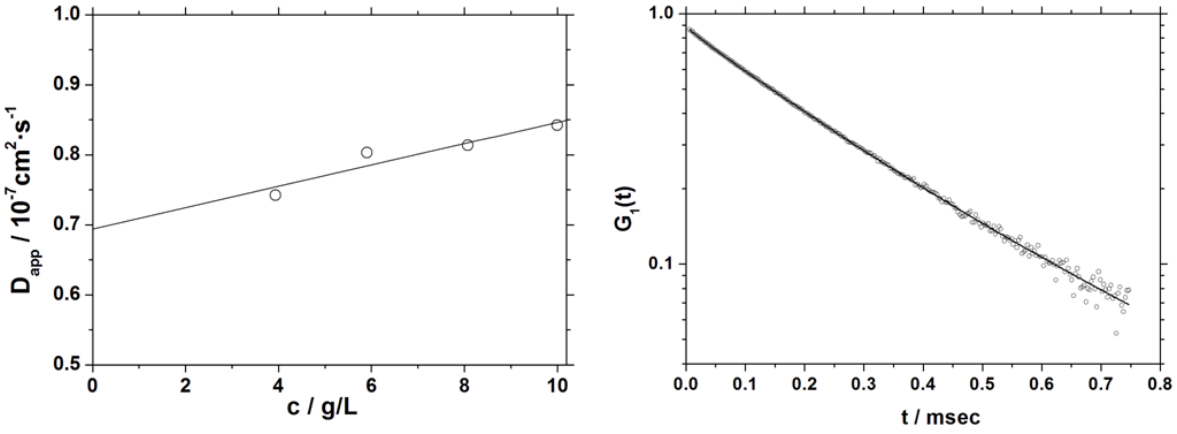

Figure 41: DLS of linear PLL; c = 10g/L in 0.1M HBr, GHP 0.2µm, θ = 30°, T = 293.15K; $\langle D \rangle_z$ = 6.94 * 10^{-7} cm2/s : $\langle 1/R_h \rangle_z^{-1}$ = 3.1nm, μ_2 = 0.1 (0.2nm fast mode subtracted with A_1 = 0.02)

Linear PLL and the PLL brush are labeled with the fluorescent dye AlexaFluor488. For the first experiments AlexaFluor488 Carboxylic Acid Succinimidyl Ester (NHS-Ester) is used. But this dye shows a huge quantum yield drop, which is assumed to occur due to dimerization of the reactive NHS ester. As the NHS ester is very instable to hydrolysis it is thought to form dimers via reaction of the amine at the benzyl ring of the dye with the unstable NHS ester (see structure of the AlexaFluor 488 dye in Table 1). Therefore, further labeling is performed with the more stable AlexaFluor488 Carboxylic Acid 2,3,5,6-Tetrafluorophenyl Ester, 5-isomer (TFP-Ester). TFP Esters are less susceptible to spontaneous hydrolysis during reaction and less side reactions occur, which also guarantees higher selectivity.

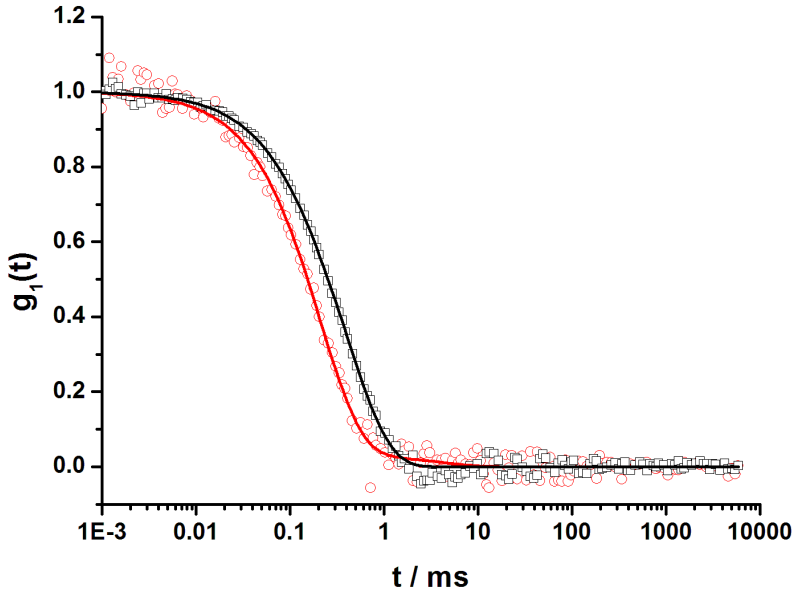

Figure 42: Autocorrelation function of PLL and PLL-AlexaFluor488 in 1x PBS, θ = 30°, T = 293.15K; ○ PLL, ▬ Fit PLL, □ PLL-AlexaFluor488, ▬ Fit PLL-AlexaFluro488

Comparison of the autocorrelation function of PLL and fluorescently labeled PLL at θ = 30° shows that the curve for PLL-AF488 is shifted to longer correlation times. The hydrodynamic radius after labeling marginally increases, which may be due to removal of smaller fractions of the polymer by fractionation during dialysis.

In order to determine the quantum yield drop, solutions of dye and dye-labeled PLL (all OD = 0.2) are measured with fluorescence spectroscopy and the area under the curve is compared. The pure AlexaFluor488 dye shows an integration of the peak area of 34 850 units at $\lambda_{excitation}$ = 495. AlexaFluor488 NHS Ester conjugated to PLL with the same UV absorption of 0.2 shows a peak area of 2540, which results in a quantum yield drop of a factor of ~13.7.

In order to avoid this high loss in quantum yield, PLL was labeled with the more stable AlexaFluor488 TFP Ester. In this measurement AlexaFluor488 reveals a peak area of 28 720 and PLL-AF488 (TFP Ester) a peak area of 19 885 which relates to a quantum yield drop of ~1.5 (Figure 43). Due to these results PLL is labeled with AlexaFluor488 TFP Ester for all further experiments.

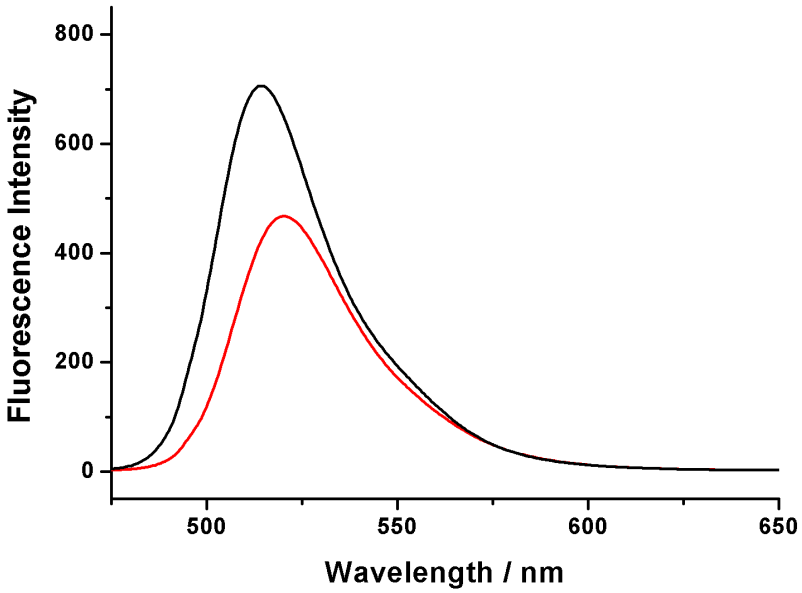

Figure 43: Fluorescence spectra of AlexaFluor488 and PLL-AlexaFluor488; AlexaFluor488, PLL-AlexaFluor488

The degree of labeling is determined with FCS. Free dye has a diffusion time of 23.3µs and 33.6 counts per molecule. PLL-AF488 (TFP Ester) has a diffusion time of 110.9µs and an R_h of ~2.4nm which is consistent with DLS measurements. Labeled PLL shows 35.7 counts per molecule and therefore the labeling efficiency is one dye per PLL chain.

The PLL brush (Lys 55-3-2) was synthesized by [redacted] in the group of [redacted]. It consists of poly-*L*-lysine grafted from a PMMA backbone. M_w of this brush is ~8*10^6 g/mole, its $\langle R_g^2 \rangle_z^{1/2}$ (in 0.5M NaCl) is 60.4nm and its $\langle \frac{1}{R_h} \rangle_z^{-1}$ is 44.8nm (in 0.5M NaCl). This gives a ρ-ratio of 1.35 which indicates coil structure[177].

The PLL brush is labeled with AlexaFluor488 NHS Ester and purified first with BioRad BioGel P30 column chromatography and then with Amicon Ultra Centrifugal Filter Units 10kDa. Purification of the PLL brush is difficult as the dye seems to adsorb to the polymer. After 20 filtration cycles with the Amicon Centrifugal Filter there is still a little bit of dye visible in UV spectra of the filtrate. Therefore, FCS measurement to determine the labeling efficiency is difficult as well. The results are not as accurate as for linear PLL. Approximately 50 dye molecules are conjugated to one brush with a hydrodynamic radius of 49nm in 1x PBS. This radius determined with FCS measurements accords with the R_h measured by DLS. The hydrodynamic radius determined with DLS in 1x PBS is 59.6nm before conjugation of the dye and 54.3nm after labeling (Figure 44). This shows that dye labeling does not dramatically affect the size of the brush.

Fluorescence spectroscopy of PLL brush-AlexaFluor488 exhibits a drop in the quantum yield of a factor of ~2.2 which is acceptable as most fluorescent dyes show a quantum yield drop after conjugation. Quantum yields may be lowered by dimer formation of dyes and/or reabsorption or energy migration at locally higher concentrations. Furthermore, halogen counterions like bromide or chloride located in the vicinity of excited dye molecules give reason for additional quenching possibilities.

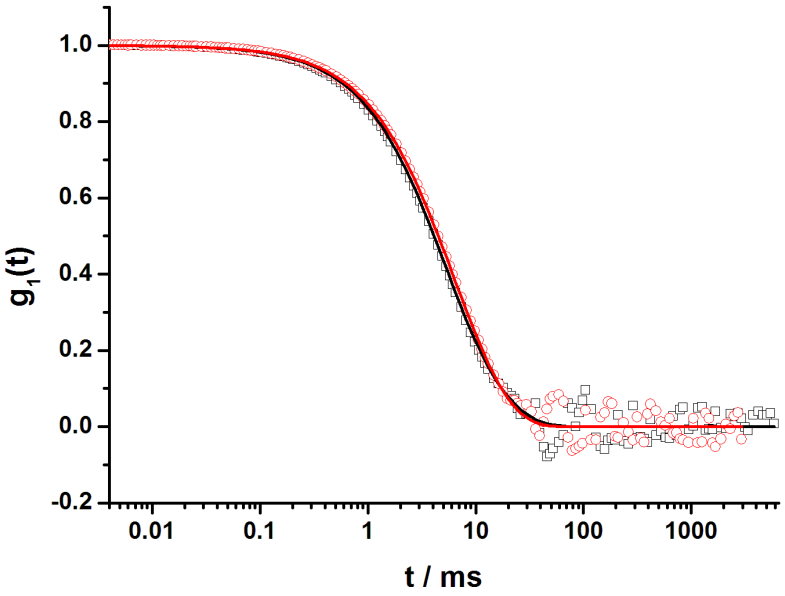

Figure 44: Autocorrelation function of PLL brush and PLL brush-AlexaFluor488 in 1x PBS, θ = 30°, T = 293.15K; ○ PLL brush, ▬ Fit PLL brush, □ PLL brush-AlexaFluor488, ▬ Fit PLL brush-AlexaFluro488

Toxicity of PLL and PLL brush was tested on HeLa and JAWS II cells in a MTT Assay for 24h. HeLa cells are used as these are the gold standard for all cell experiments and the cell line used most often. Toxicity is also investigated with JAWS II cells as this is an immortal dendritic cell line and therefore more relevant for the cell experiments performed in this thesis. The MTT assay is not performed with splenic DC as these are primary cells and cannot be cultured without the cells undergoing maturation which influences the survival rate of cells.

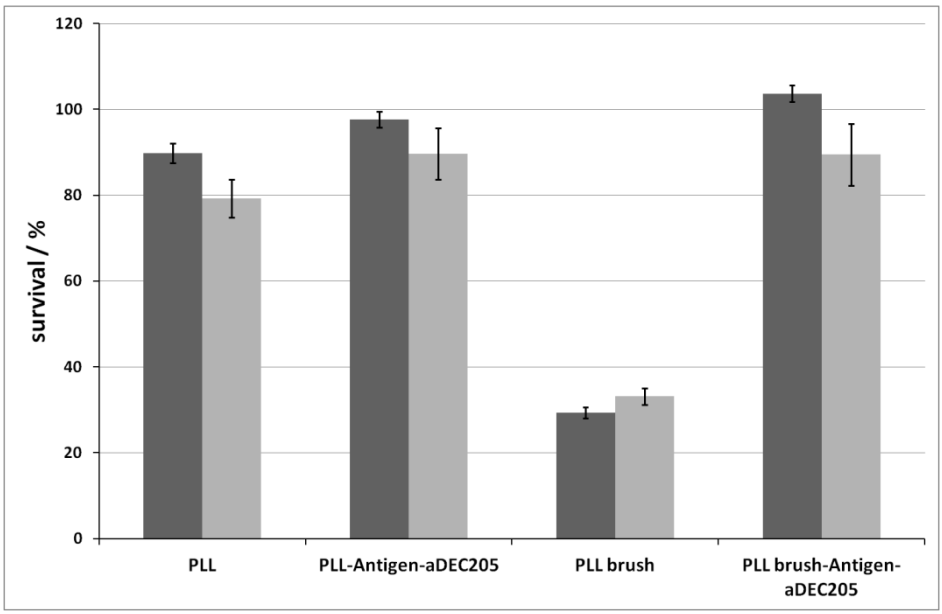

Figure 45: Toxicity of PLL, PLL brush and conjugates (c = $1*10^{-7}$ mole/L) on ■ HeLa and ■ JAWS II cells after incubation for 24h

In Figure 45 it can be seen that at a PLL concentration of $1*10^{-7}$ mole/L 89% of HeLa and 79% of JAWS II cells survive. For the PLL brush survival of cells decreases to 30% for HeLa and 33% for JAWS II, respectively. This higher toxicity of the PLL brush can be explained with the number of positive charges. The concentration is calculated to the number of chains and brushes, respectively. One PLL chain carries approximately 36 lysine residues with a M_n of 7.5kDa and a molar mass of the repeating unit of 209g/mole.

One PLL brush with a molecular weight of ~$8*10^6$ g/mole (Pn of the main chain ~690, Pn of the side chain ~55) contains ~37 000 lysine residues and thus ~1000 times more than linear PLL (M_n = 7500 g/mole, M_{WHE} = 209 g/mole, Pn = 36).

Due to the higher cationic charge density of the brush higher toxicity is expected on the one hand. On the other hand effective charge will be lower by one order of magnitude for the brush as a higher local charge density leads to lower dissociation and thus lower effective charge.

After conjugation of Antigen and aDEC205 to PLL and PLL brush toxicity decreases. This is caused by elimination and/or sterical shielding of positive charges. Modification with the crosslinkers Sulfo-SMCC and DIBO which react with the lysine residues of the polymer eliminates positive charges and aDEC205 sterically shields the charges. The PLL and PLL brush conjugates show nearly no toxicity at all in HeLa cells and survival of ~90% in JAWS II cells. This indicates that no cell death due to toxicity occurs during cell experiments with spleen and bmDC. For *in vivo* experiments further toxicity studies have to be performed. For example, PLL shows a high tendency for aggregation with human blood serum and therefore is not applicable in the body. PEGylation of PLL at a ratio of 20% diminishes the positive charges of PLL and PLL-PEG 20% does not aggregate in human blood serum[178]. So, PLL conjugates and their degradation products have to be tested for aggregation with biological media before they can be tested *in vivo*.

3.2.2. Internalization Studies of PLL into bone marrow-derived DC

The internalization of PLL into splenic DC is investigated using the SHIP technology and directly compared to PLL-aDEC205 conjugates in Chapter 3.3.1. PLL exhibits a binding specificity of 94.1% to immature DC, the PLL brush 99.2%.

The uptake of PLL into bone marrow derived DC is studied in collaboration with Ingrid Tubbe at the Department of Dermatology in Mainz. Different amounts of PLL are examined for uptake into bmDC. If $1*10^{12}$ PLL molecules are added to a well with $0.5*10^{6}$ cells, which equals $2*10^{6}$ PLL chains per cell, the uptake is ~50%. If $1*10^{13}$ PLL molecules per well are incubated, the uptake is ~99%. For $1.7*10^{6}$ PLL brushes per cell the uptake is ~74% (Figure 46).

These results show that uptake is concentration dependent and that with higher concentration of polymer the number of cells that take up polymer increases.

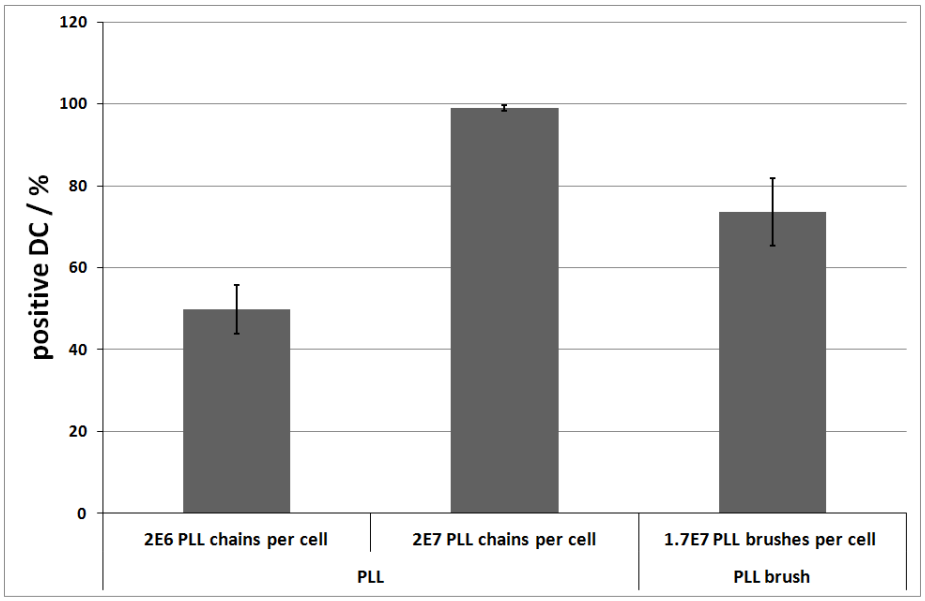

Figure 46: Uptake of PLL and PLL brush into bmDC after 4h incubation

Figure 47 shows the internalization of PLL in bmDC. In general, unspecific uptake of PLL is very high into cells due to the high cationic charge of the amine groups of lysine.

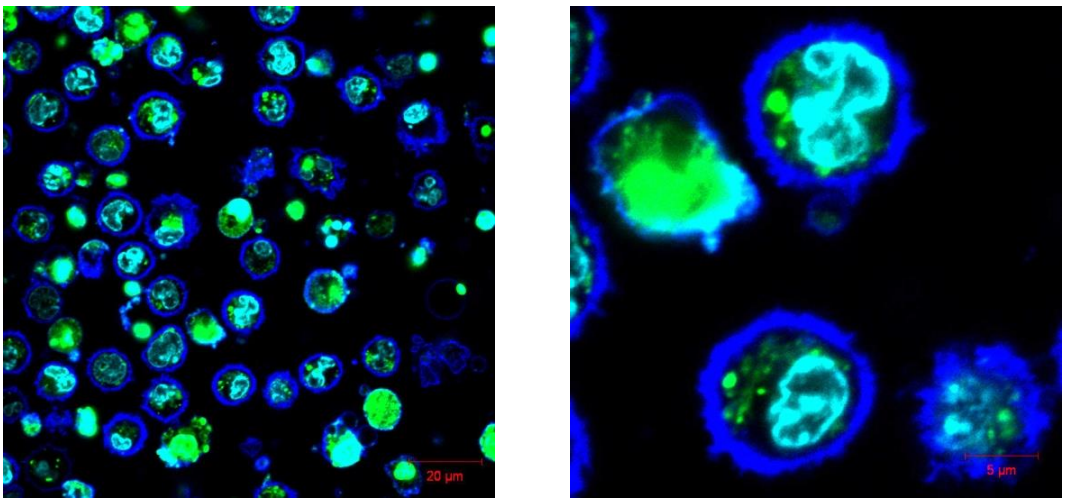

Figure 47: CLSM image of PLL in bmDC, 1xPBS, non-fixated, incubation time 4h, conc. $1*10^{12}$ particles per $5*10^5$ cells turquoise: Hoechst 33342 - Labeling of nucleus; blue: Cell Mask Orange – Labeling of cell membrane; green: PLL-AF488; red: aDEC205-AF647, scale bar: left: 20µm, right: 5µm

No colocalization of Mitotracker and PLL can be observed (Figure 48). Thus, PLL does not localize in mitochondria of bmDC. This is expected as literature proposes endosomal uptake for PLL, and therefore localization within endosome and lysosome[132], [133], [134].

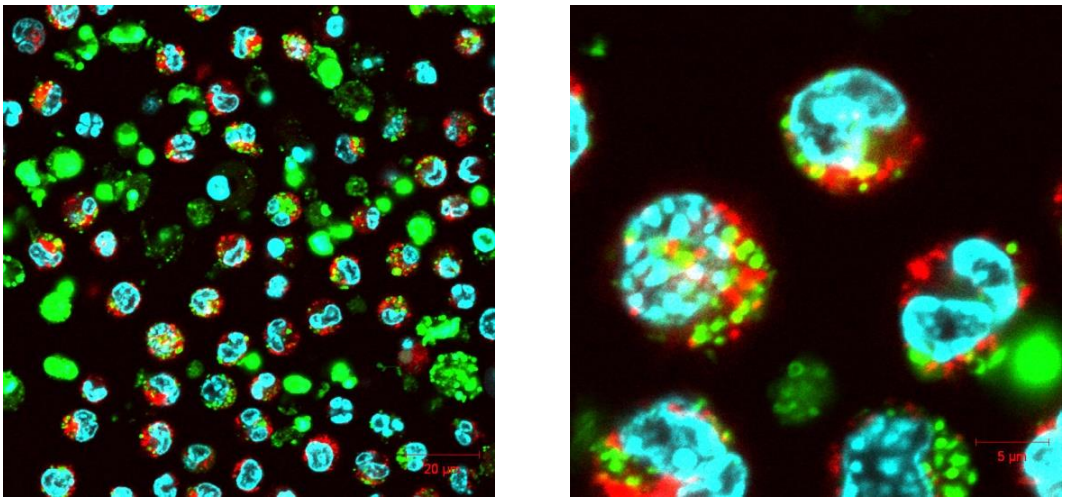

Figure 48: CLSM image of PLL in bmDC, 1xPBS, non-fixated, incubation time 4h, conc. $1*10^{12}$ particles per $5*10^5$ cells turquoise: Hoechst 33342 - Labeling of nucleus; red: Mitotracker – Labeling of mitochondria: PLL-AF488; red: aDEC205-AF647, scale bar: left: 20µm, right: 5µm

Summary of characterization and internalization of PLL and PLL brush

In summary, linear PLL exhibits a Mn of ~7500 g/mole and a hydrodynamic radius of 3nm. The PLL brush synthesized by Mike Sahl has a molecular weight of approximately $8*10^6$ g/mole and a hydrodynamic radius of ~50nm. Both polymers are labeled with AlexaFluor488 NHS Ester and the degree of labeling is determined with FCS to be one dye per PLL chain and ~50 dyes per PLL brush. The hydrodynamic radii do not change after dye labeling.

PLL at a concentration of $1*10^{-7}$ g/mole does not reveal high toxicity in HeLa or JAWS II cells, survival is between 80 and 90%. PLL brush at the same concentration demonstrates much higher toxicity, only ~30% of the cells survive. After conjugation of the bioactive components, toxicity dramatically decreases. In bone marrow derived DC both polymers reveal high unspecific and concentration dependent internalization which is due to the high cationic charge. PLL does not show colocalization in the mitochondria of DC and literature proposes localization within the lysosome which has to be investigated. Due to the high pH within the lysosome of dendritic cells normal lysosome trackers that are pH dependent cannot be used for localization studies.

The high unspecific uptake is a major drawback for the use of PLL or the PLL brush as carriers for targeted immunotherapy. Therefore, PLL has to be chemically modified to either reduce charges or to invert charges, for example by succinylation, in order to show no unspecific uptake.

3.3. Polymer Conjugates

In this section the synthesis and characterization of the polymer conjugates is discussed.

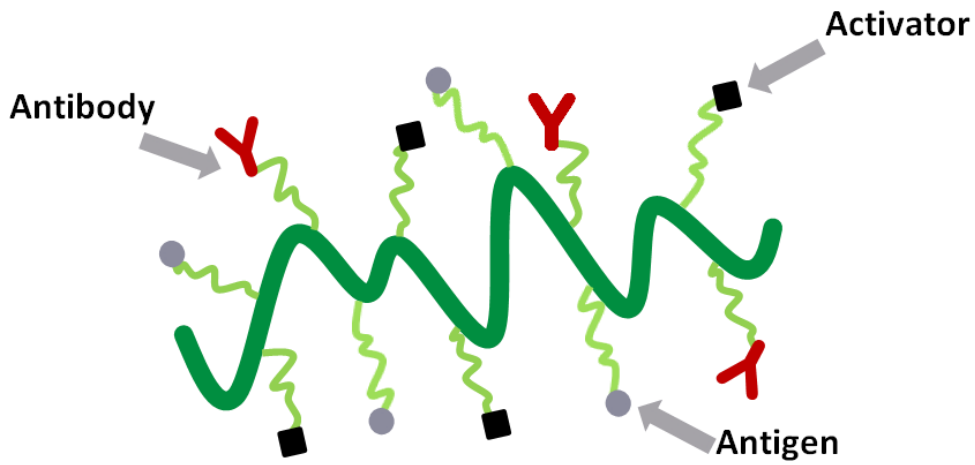

Figure 49: Scheme of PLL-Antigen-Activator-aDEC205 conjugate

First, antibody conjugation to PLL and PLL brush is investigated and internalization kinetics in splenic immature and mature DC is studied. Afterwards, Antigen and CpG are linked to the polymer and then the PLL-Antigen-CpG-aDEC205 conjugate is synthesized and characterized regarding the composition of the conjugate, the internalization and ability to stimulate T cell proliferation.

3.3.1. PLL-aDEC205 Conjugates

For conjugation of aDEC205 to PLL two different approaches are followed. The first approach to link the antibody via its glycosidyl residues to the lysine residues via Schiff Base formation directs the conjugation site away from the antigen binding site and therefore is thought to preserve biofunctionality of the antibody. The second way of conjugation is copper free click chemistry with two heterobifunctional crosslinkers. PLL is modified with dicyclobenzyl cyclooctylene (DIBO) at its lysine residues and aDEC205 is azide functionalized with NHS-PEG-azide. Click chemistry provides high conjugation efficiencies without side reactions. With these conjugates it is investigated if antibodies can mediate specific uptake into splenic dendritic cells.

Schiff Base formation of PLL with oxidized aDEC205 (Method 1)

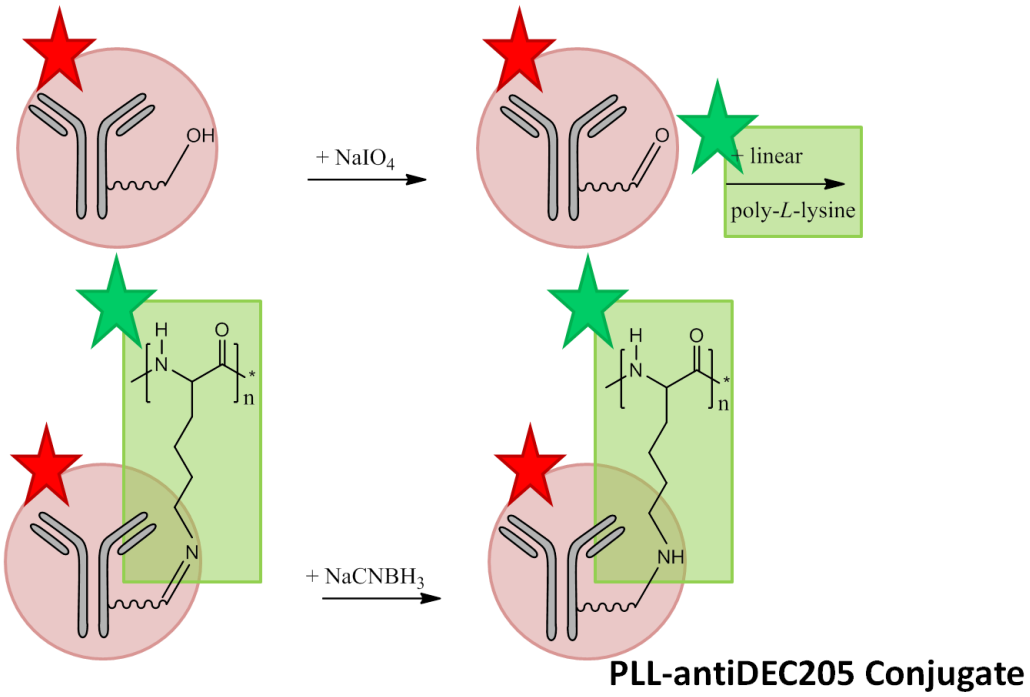

Figure 50: Scheme of aDEC205 conjugation to PLL via Method 1; ★: AlexaFluor647, ★: AlexaFluor488

aDEC205 is conjugated to PLL via oxidation of the glycosidyl residues in the Fc region (Fragment crystalizable) of the heavy chain of the IgG antibody. Aldehyde moieties are generated and to these the amine groups of the PLL are coupled via Schiff Base formation.

This instable bond is reduced with sodium cyano borohydride to form a stable secondary amine bond[94].

Conjugation at the glycosidyl residues is advantageous as the Fc region is far from the binding site of the antibody. Therefore stable conjugates without blocking of the binding site are yielded which keeps these conjugates biofunctional. Usually, lysine residues of the antibody are used to couple with crosslinkers, but as lysine is equally distributed over the whole IgG molecule, conjugation in the binding site cannot be eliminated.

Different molar ratios of PLL to antibody are tested: 10:1, 1:1, 1:10 (Table 7). These results show that for a ratio of 10:1 PLL to antibody after conjugation and purification with Sephadex G25 NAP 5 or additional Amicon Ultra Centrifugal Filter Units 50kDa or BioGel P-30 the ratio of PLL to antibody determined with UV is still 10:1. This indicates that free PLL can-

not be removed from the PLL-aDEC205 conjugate by size exclusion chromatography and the conjugation efficiency is one aDEC205 antibody per every 10^{th} PLL chain.

For a ratio of PLL to aDEC205 of 1:1 or 1:10 and purification with BioGel P-30 UV measurements give a conjugation efficiency of 0.52 and 0.44, respectively. This means that approximately every second PLL chain is labeled with one aDEC205. But it also indicates that aDEC205 got lost during conjugation or purification. It is expected that free PLL can be removed with this column as the size exclusion of 30kDa is above the molecular weight of PLL with M_n = 7.5 kDa. No separation should occur between PLL-aDEC205 and aDEC205 as both have a molecular weight way above the size exclusion limit. Both conjugate and free antibody should elute very fast at the same time without interacting with the column material. If interaction occurs between the column material and aDEC205 it is thought to be the same for free antibody and PLL-aDEC205. Therefore, the ratio of PLL to aDEC205 is expected to decrease for PLL and not for aDEC205. There is no explanation for the loss of antibody during purification with BioGel P-30.

Due to the very similar molecular weight, free aDEC205 (150kDa) cannot be separated from the PLL-aDEC205 conjugate (~160kDa) by size exclusion chromatography. Affinity chromatography is tested for separation of antibody and antibody conjugates, but free antibody and conjugate show the same binding affinity to the column and cannot be eluted separately.

Molar excess of PLL minimizes the probability of unreacted aDEC205. Free polymer should not interfere with internalization of the conjugate as it does not block the receptor that aDEC205 binds to, but unspecifically adsorbs to the cell membrane. Therefore for further conjugations excess of polymer is used.

Table 7: Summary of PLL-aDEC205 conjugates

PLL-aDEC205 Experiment	Ratio PLL: aDEC205	Purification	Conjugation Efficiency PLL: aDEC205	Uptake in bmDC	
				4h	24h
I	10:1	**1:** No purification	/	80,9	94,4
		2: Sephadex G25 NAP 5	/	89,1	97,2
		3: BioGel P-30	1: 0.11	87,4	96,8
II	1:1	BioGel P-30	1: 0.52	82,2	74,0
III	1:10	BioGel P-30	1: 0.44	12,3	21,0
IV	**1**: 10:1; reaction time: 2h	Sephadex G25 NAP 5	1: 0.10	88,4	72,0
	2: 10:1 reaction time: 7h		1: 0.10	87,6	72,0
V	10:1	Sephadex G25 NAP 5 + Amicon Ultra Centrifugal Filter Units 50kDa	1: 0.9	88,8	80,6
		Sephadex G25 NAP 5 + BioGel P-100	1: 0.9	F3: 84,7	F3: 56,2
				F4: 88,0	F4: 85,2

PLL-aDEC205 I is analyzed with SDS-PAGE (Figure 51). Reduced aDEC205 is applied in lane 1 and 2 and explained in Chapter 3.1.2. In lane 10 PLL is observed in the solvent front. PLL is thought not to migrate in the gel due to its high cationic charge. But obviously it is complexed with enough SDS to obtain a negative net charge and therefore migrates into the gel. But due to the high cationic charge of PLL and the unknown ratio of complexation with the anionic SDS the migration behavior for the conjugate cannot be predicted.

Lanes 3 to 8 show PLL-aDEC205 conjugate with different concentrations and different purification techniques. There is no difference visible between the unpurified sample (line 3 and 4) and the sample purified with BioGel P-30 (line 5 and 6) or Sephadex G25 NAP-5 (line 7 and 8).

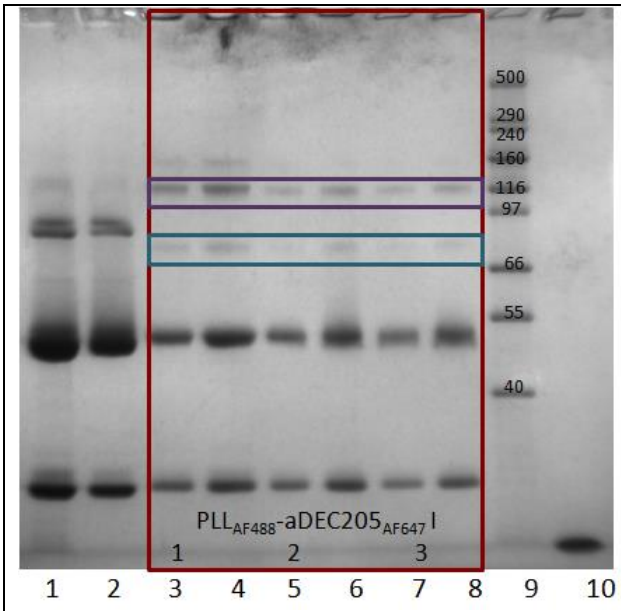

Lane	Sample
1	aDEC205 (10µg)
2	aDEC205 anotop (10µg)
3	PLL-aDEC205 I-1 (3µg)
4	PLL-aDEC205 I-1 (6µg)
5	PLL-aDEC205 I-2 (1.5µg)
6	PLL-aDEC205 I-2 (3µg)
7	PLL-aDEC205 I-3 (1.5µg)
8	PLL-aDEC205 I-3 (3µg)
9	Marker
10	PLL (50µg)

Figure 51: NUPAGE Tris Glycine Gel 4-12% of PLL-aDEC205 conjugate I; PLL-aDEC205 I-1: no purification; PLL-aDEC205 I-2: BioGel P-30; PLL-aDEC205 I-3: Sephadex G25 NAP-5

Two bands occur in the conjugate that are not observed for the pure antibody. A very slight band at ~70kDa might be due to conjugation of PLL to the heavy chain of the antibody (50kDa). The other band at ~ 120kDa might results from conjugation of the HL fragment (75kDa) to PLL. Due to the incomplete reduction of the antibody and the unpredictable migration of PLL, the bands probably do not occur at the correct corresponding molecular weight. If a polypeptide is unfolded incompletely due to incomplete reduction, it migrates faster in the gel which results in an apparently smaller molecular weight. But glycoproteins are not loaded with SDS the same amount as unglycosylated proteins and therefore they migrate slower which give apparently higher molecular weights[140]. As both cases apply to non-reduced aDEC205, no conclusions can be drawn for the molecular weight related to these bands. Together with the unknown PLL migration, no exact conclusion can be made from the SDS-PAGE.

Another problem with conjugation of the antibody and PLL are charge alteration effects[99]. Every modification of charges in the antibody or PLL molecule results in dramatic heteroge-

neity of the sample. Conjugation through lysine residues reduces the net positive charge of the antibody or PLL molecule by one for each attached linker if the linker is uncharged. This charge alteration leads to different migration behavior in the gel that is unpredictable due to the high heterogeneity.

The conjugates are tested with flow cytometry and confocal laser scanning microscopy in collaboration with [redacted] and [redacted] at the University Clinics in Mainz.
With flow cytometry the bmDC that are positive for both fluorescent dyes attached to PLL and aDEC205 are determined. In the dot plots bmDC are plotted with the APC (AlexaFluor647) channel on the y axis and the AlexaFluor488 channel on the x axis. For the control cells no fluorescence in neither of the channels is detected (Figure 52 a). If cells are incubated with aDEC205 or PLL alone, they show a shift of population in the APC or FITC channel, respectively (Figure 52 b and c). For cells incubated with the PLL-aDEC205 conjugate fluorescence is detected in both channels. The number of cells positive for both fluorescent dyes can be obtained from these results in the area of Q2 (Figure 52 d) and is illustrated in Figure 53.

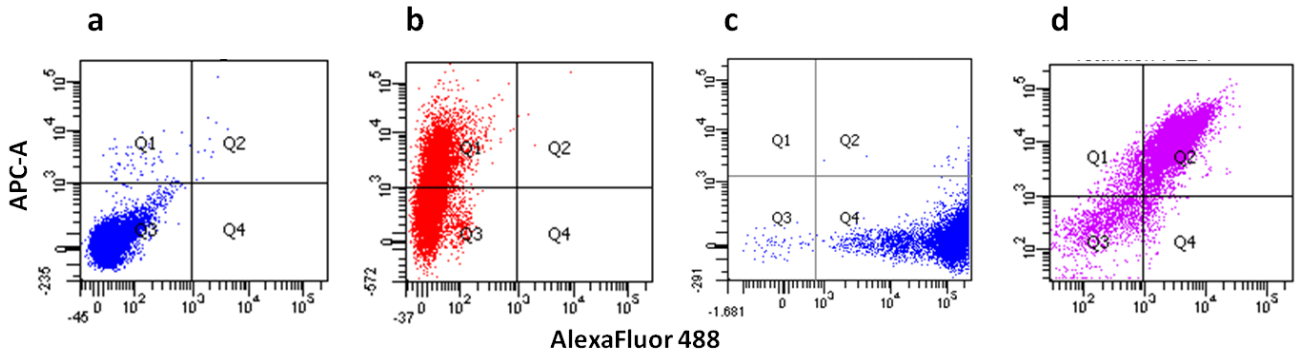

Figure 52: Dot plots of bmDC with APC-A for AlexaFluor647; a: control cells; b: aDEC205-AF647; c: PLL-AF488; d: PLL-aDEC205 I-1

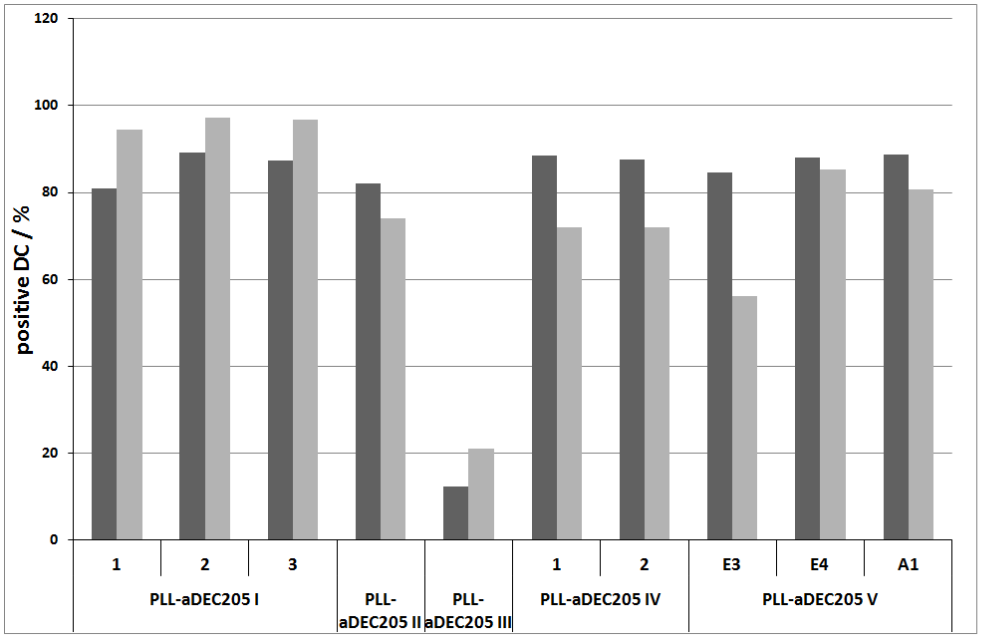

Figure 53: Internalization of PLL-aDEC205 conjugates into bmDC after ■ 4h and ■ 24h incubation

All PLL-aDEC205 conjugates show a very high internalization of around 80% into bmDC (Figure 53). As only ~22% of bmDC are CD8+ and can be targeted with aDEC205 (Figure 39), this indicates high unspecific uptake. This unspecific uptake is due to the high cationic charge of the lysine and is discussed in Chapter 3.2. In short, positively charged PLL adsorbs to the negatively charged cell membrane due to ionic interaction and is subsequently internalized by unspecific endocytosis. The only conjugate that shows low uptake (PLL-aDEC205 III) is reacted with a ratio of PLL to aDEC205 1:10. The low uptake can be due to higher sterical shielding of more antibodies bound to PLL. But CLSM images show no PLL which indicates lower conjugation efficiency.

Confocal laser scanning microscopy illustrates the localization of the conjugate within bmDC. These CLSM images show colocalization of both fluorescent dyes within the cell which suggests successful conjugation.

Figure 54 shows the localization of PLL-aDEC205 I in bmDC after 4h incubation. It can be seen that most of the dye is colocalized, but there are some spots of red and green that show no colocalization. This is the free antibody and free polymer that cannot be removed by size exclusion chromatography. If conjugation is not successful, no colocalization occurs, which is demonstrated in the control experiment (Figure 78).

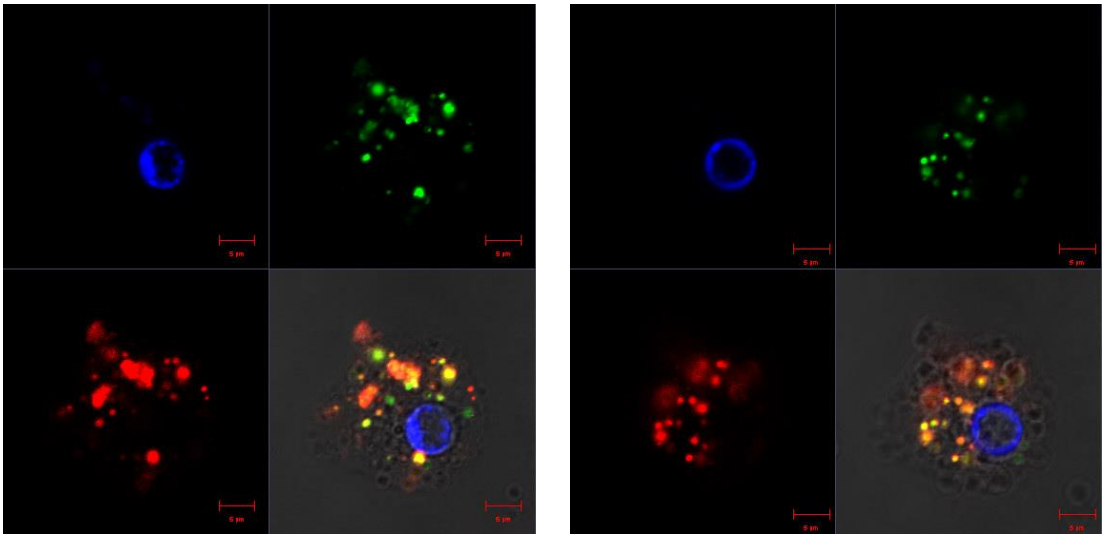

Figure 54: CLSM image of PLL-aDEC205 I-1 in bmDC, 1xPBS, non-fixated, incubation time 4h, conc. $1*10^{12}$ particles per $5*10^{5}$ DC; blue: Hoechst 33342 - Labeling of nucleus; green: PLL-AF488; red: aDEC205-AF647, scale bar: 5µm

In Figure 55 and Figure 56 the internalization of PLL-aDEC205 IV-2 is shown. Flow cytometry exhibits the same pattern as obtained for conjugate I (Figure 52).

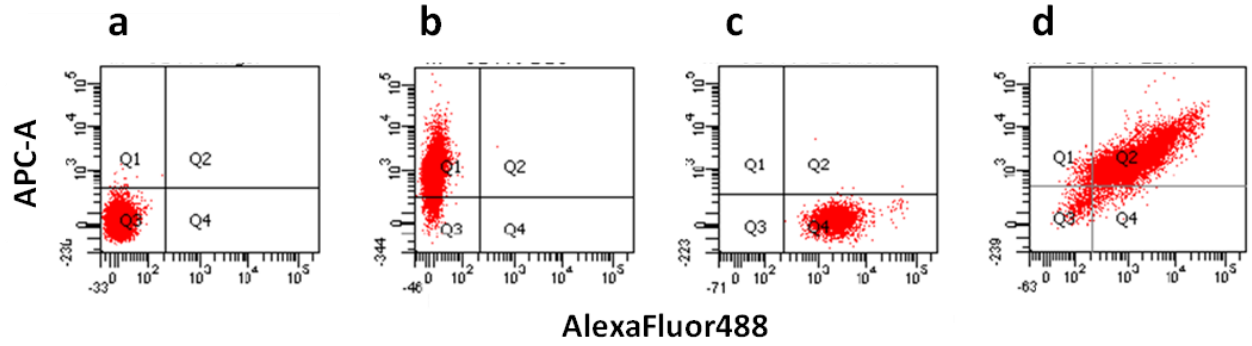

Figure 55: Dot plots of bmDC; a: control cells; b: aDEC205-AF647; c: PLL-AF488; d: PLL-aDEC205 IV-1; d: PLL-aDEC205 IV-2

Additionally, the cell membrane is stained with Cell Mask Orange which proves that the conjugate is within the cell and not only on the cell surface (Figure 56). The cells look dendritic and healthy and most of them reveal internalization and colocalization of the conjugate.

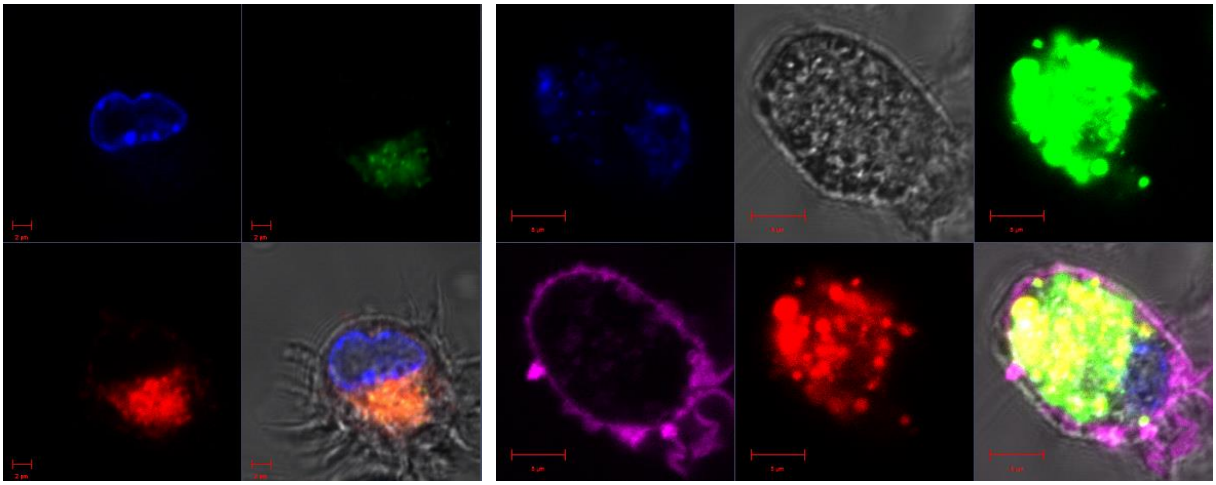

Figure 56: CLSM image of PLL-aDEC205 IV-2 (reaction time: 7h) in bmDC, 1xPBS, non-fixated, incubation time 4h, conc. $1*10^{12}$ particles per $5*10^{5}$ DC; blue: Hoechst 33342 - Labeling of nucleus; violet: Cell Mask Orange - Labeling of cell membrane; green: PLL-AF488; red: aDEC205-AF647, scale bar: 5µm

Click Reaction of PLL-DIBO with aDEC205-PEG-azide (Method 2)

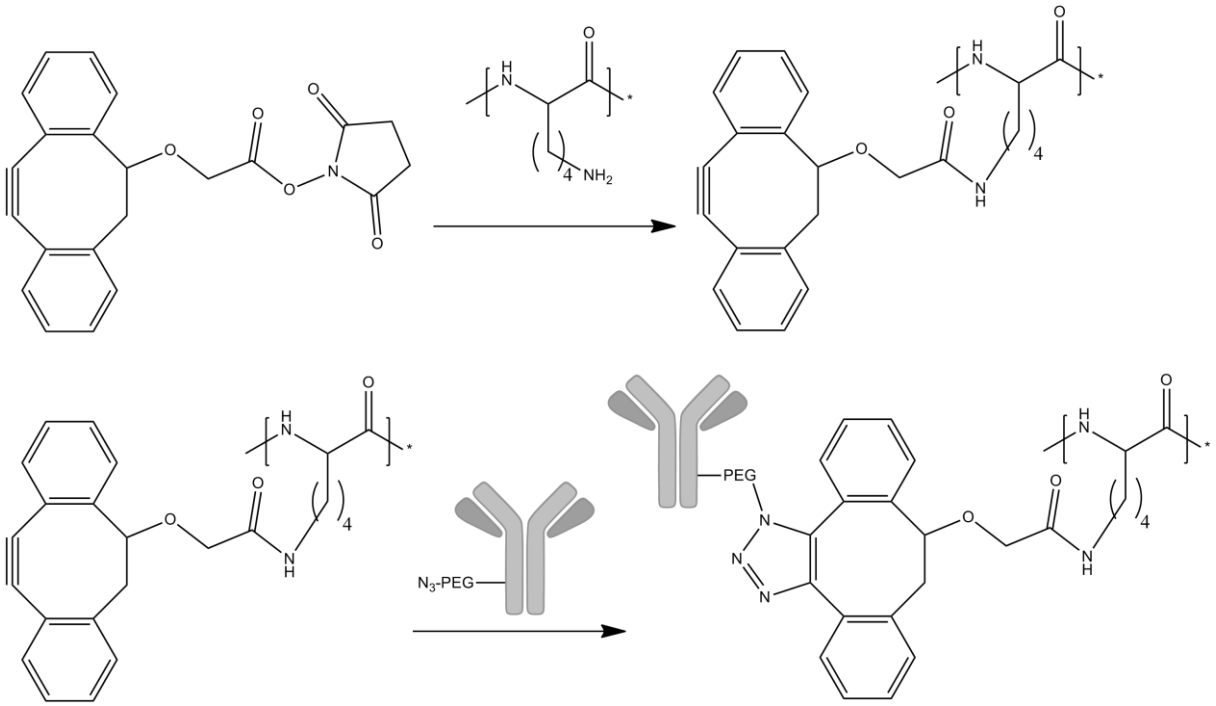

Figure 57: Scheme of aDEC205 conjugation to PLL via Method 2

In order to study the internalization of linear PLL, the PLL brush and their antibody conjugates into splenic dendritic cells PLL-SHIP and PLL_B-SHIP conjugates are prepared. Therefore PLL and PLL_B is functionalized with an excess of Click-IT® Succinimidyl Ester DIBO Alkyne and

in the second step SHIP-AlexaFluor 647-azide clicks with the alkyne group and forms a stable triazole. The ratio of SHIP to polymer is determined with UV measurements (Nanodrop) as the ratio of the absorbance of PLL-AF488 at 495 nm and the absorbance of SHIP-AF 647 at 650 nm.

The labeling efficiency for PLL is very poor, the ratio of PLL to SHIP is only ~ 1: 0.01. For some samples precipitation is observed that may be caused by interaction of the positively charged PLL with the negatively charged DNA. Aggregate formation may lower the conjugation efficiency. The ratio of the PLL brush to SHIP is ~ 1: 8.

The AlexaFluor555-labeled antibody was functionalized with PEG_{2000}-NHS-azide and reacted with PLL-DIBO at the same time SHIP-azide was conjugated to PLL. The conjugation efficiency of PLL to antibody is ~ 1: 0.1. The conjugation efficiency for PLL_B-SHIP-aDEC205 is 1: 8: 4. (calculated for ~50 dyes per brush)

This very low labeling efficiency for the PLL conjugates might be based on ionic interactions between the positively charged PLL and the negatively charged oligonucleotide. For some samples precipitation is observed which drastically lowers the reaction efficiency.

As the SHIP sensor is only the instrument to determine internalization, the term SHIP is left out in the designation of the conjugates.

The binding specificity was determined as the percentage of binding to spleen DC for 30 min at 4°C for aDEC205, PLL and conjugates of PLL with aDEC205, CD11c and a control IgG that does not bind to CD8+ DC.

Table 8: Binding specificity of PLL and PLL-antibody conjugates to immature and mature CD8+ DC

	aDEC205	**PLL**	**PLL-aDEC205**	**PLL-CD11c**	**PLL-cIgG**	**PLL brush**	**PLL brush-aDEC205**
iDC	81.4	94.1	92.6	100	95.7	99.2	97.8
mDC	36.3	95.1	94.3	98.8	98.7	/	/

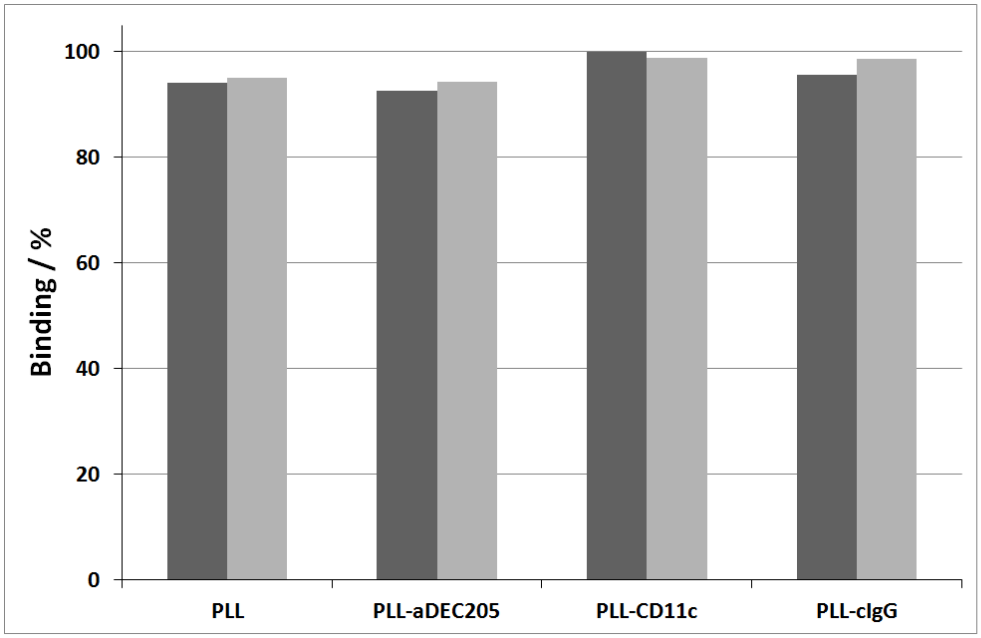

Figure 58: Binding specificity of PLL and PLL-antibody conjugates to ■ immature and ■ mature CD8+ DC

Figure 58 and Table 8 exhibit the high binding of PLL and PLL brush to dendritic cells. 94.1% of the immature dendritic cells have bound PLL to the cell surface and even 99.1% bound PLL brush. For the PLL brush conjugation of aDEC205 reduces binding marginally to 97.8%. By conjugation of aDEC205 to PLL binding is decreased to 92.6%. But conjugation of CD11c and control IgG enhances binding compared to PLL alone, to 100% and 95.7%, respectively. The binding specificities of PLL, PLL brush and conjugates show negligible differences between immature and mature dendritic cells. In general, conjugation of an antibody does not alter the binding specificity to immature or mature DC.
Due to the small amount of sample this experiment could not be performed in triplicates to obtain statistics.

Figure 59 compares the internalization of the conjugates into immature and mature CD8+ DC. In immature DC aDEC205 is internalized faster and to a higher amount (76.5%) than all PLL conjugates.

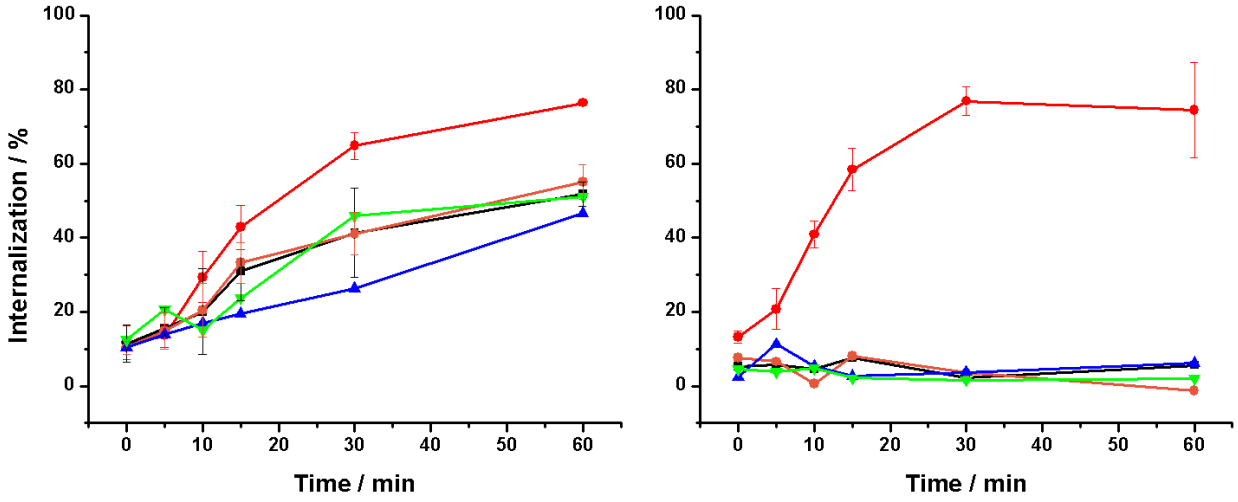

Figure 59: Internalization of PLL and targeted PLL into CD8+ iDC (left) and mDC (right); ● aDEC205, ■ PLL, ● PLL-aDEC205, ▲ PLL-CD11c, ▼ PLL-cIgG

There is only a marginal difference in the internalization kinetics of PLL and PLL-antibody conjugates. The amount of material internalized into immature DC after 60 min incubation is 51.8% for PLL and 55.1% for PLL-aDEC205. PLL-SHIP-CD11c is taken up a little slower and less than PLL-DEC205 (46.6%), while PLL-cIgG is internalized a little faster, but to the same amount after 60 min (51.2%). It is unknown whether conjugation of aDEC205 to PLL should enhance uptake due to efficient specific receptor-mediated endocytosis via the antibody or if the sterical shielding of the positively charged PLL by the antibody diminishes unspecific uptake of PLL. It is definitely not expected to observe the same internalization kinetics for PLL and PLL-aDEC205. One reason might be the very low conjugation efficiency. If only every 10^{th} PLL chain has one aDEC205 antibody attached, 90% of the PLL chains remain untargeted and therefore have the same internalization kinetic as PLL.

In mature DC the uptake of DEC205 is still high (as described in Chapter 3.1). PLL and the PLL antibody conjugates are not internalized into mature DC. This is not surprising for PLL as it is known in literature that DC shut down the unspecific internalization with maturation[73]. But dendritic cells in the mature state still capture, process and present antigens internalized by endocytotic receptors, e.g. DEC205. Therefore aDEC205-targeted PLL should still be taken up by mature dendritic cells as this conjugate is thought to enter the cell via receptor-mediated endocytosis of the DEC205 receptor. The control antibody conjugate is expected not to be internalized as it does not target any DC surface receptors.

The fact that PLL-aDEC205 is not internalized by mature DC can have several reasons. First it might be that the antibody is not bound to PLL. But this reason can be excluded as there are many indications of successful conjugation. It seems very unlikely as CSLM images show perfect colocalization of aDEC205 and PLL within the cell, while in the control experiment with unconjugated components nearly no colocalization is observed (see Chapter 3.3.3).

Furthermore it might be that the antibody lost its biofunctionality due to conjugation to PLL. This is not very likely as aDEC205 is modified via its lysine residues for both the aDEC-SHIP conjugate and for the PLL-SHIP-aDEC205 conjugate. The difference between the two conjugation strategies is that for the aDEC205-SHIP conjugate unlabeled aDEC205 is functionalized with DIBO succinimidyl ester to form the alkyne component of the click reaction which is then reacted with SHIP-azide. For the PLL-SHIP-aDEC205 conjugate aDEC205 was labeled with AlexaFluor555 succinimidyl ester first and then functionalized with PEG-NHS-azide in order to click with DIBO-functionalized PLL. Maybe those two reaction steps via the lysine residues affected the functionality of the antigen binding site of aDEC205 or PEG hindered the binding site sterically. This might lead to reduced binding between antibody and receptor. But most modifications of aDEC205 are done via lysine residues and targeting can still be achieved[37].

Another reason might be the high unspecific binding of PLL. This binding results from a non-specific ionic interaction between the positively charged polymer and the negatively charged cell surface. Anionically charged cell surface components, such as heparin sulfate, proteoglycans and integrins are responsible for the cellular binding of polyplexes or cationic peptides[128], [129], [130], [131]. The uptake of polyplexes occurs through endocytosis, but the pathways are very diverse. In general, PLL and PEI complexes are thought to enter the cell through clathrin-mediated endocytosis, but there is also evidence that the existence of caveolae is involved in the uptake of cationic polymer-DNA complexes and the class of protein transduction domains (PTDs), such as the cationically charged TAT peptide[132], [133], [134]. The uptake of cationic polymers is thought to be receptor-independent and therefore unspecific. This is an explanation of the inhibited internalization of PLL into mature DC. If the PLL-aDEC205 conjugate immediately binds unspecifically to the cell surface via ionic interactions, there might be no chance for antibody-receptor binding and therefore no specific receptor-mediated endocytosis[169].

The internalization of PLL brush and PLL brush-aDEC205 is only studied in immature dendritic cells (Figure 60) and not in multiplicates due to insufficient amount of sample. The PLL brush shows relatively high uptake at t=0, but this might be an error which cannot be excluded when the experiment is only performed once. Otherwise the same trend as for linear PLL is observed. aDEC205 is internalized more and faster than PLL brush and PLL brush-aDEC205. The kinetics of PLL brush and antibody conjugate look similar, but the PLL brush is offset about 10%. This offset might be an error in this particular data set or the decreased uptake after aDEC205 conjugation might be due to diminished unspecific uptake of the brush due to sterical shielding of the positive charges by the antibody.

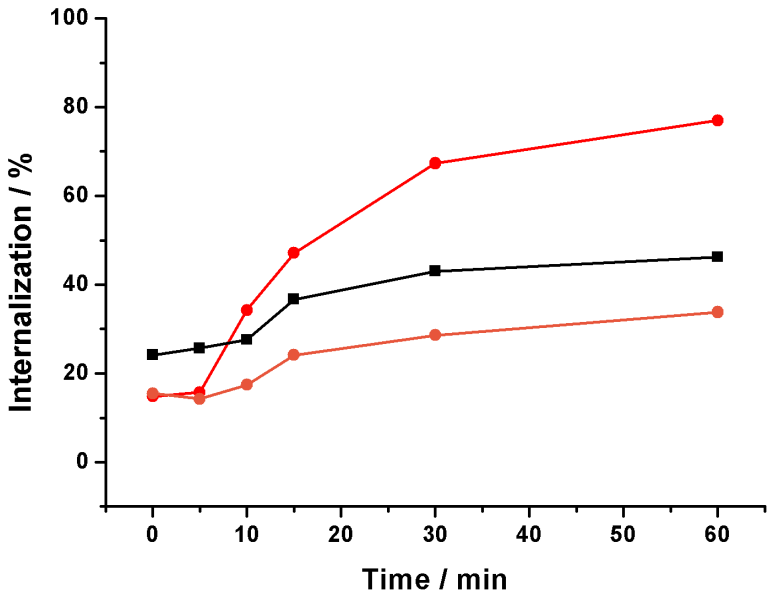

Figure 60: Internalization of PLL brush into immature CD8+ DC; ● aDEC205, ■ PLL brush, ● PLL brush-aDEC205

Summary of synthesis and characterization of PLL-aDEC205 conjugates

Conjugation of aDEC205 to PLL via Schiff base formation and subsequent reduction (reductive amination) is successful. Flow cytometry shows very high unspecific uptake of the conjugate which is caused by the unspecific uptake of cationically charged PLL. In CLSM images colocalization of both components is observed which indicates conjugation, as the control experiments show no colocalization.

Molar excess of PLL over aDEC205 is considered to be the best approach, as it gives the best signal for PLL in CLSM images and minimizes the probability of free antibody. Unreacted PLL or aDEC205 cannot be removed by size exclusion chromatography or other purification methods like affinity chromatography. But as PLL should not intervene with receptor-mediated endocytosis it is neglected.

Conjugation of PLL or PLL brush, respectively, and aDEC205 via click chemistry is successful and the internalization into splenic immature and mature DC is studied.

PLL shows a high unspecific binding to splenic immature and mature DC and unspecific uptake into immature DC due to the ionic interaction of the cationically charged polymer and the negatively charged cell surface. Targeting PLL to the DEC205 receptor on the surface of DC by conjugation with aDEC205 is not possible. There is no difference in the internalization kinetics of PLL and PLL-aDEC205 in immature DC, both are taken up to ~50% while aDEC205 shows high internalization of 76.5%.

In mature DC unconjugated aDEC205 is still internalized to 74.5%. There is no internalization at all for PLL and PLL conjugates into mature DC. As mature DC shut down unspecific uptake like macropinocytosis this means that PLL and PLL conjugates are only internalized via these unspecific ways and no receptor-mediated endocytosis of the PLL-aDEC205 conjugate occurs.

These problems can be approached by diminishing the positive charges of the carrier, e.g. via succinylation, acetylation or PEGylation, and the conjugation efficiency of antibody to polymer has to be enhanced in order to promote receptor-mediated endocytosis.

3.3.2. PLL-Antigen

Antigen and CpG are conjugated to PLL via the heterobifunctional crosslinker Sulfo-SMCC.

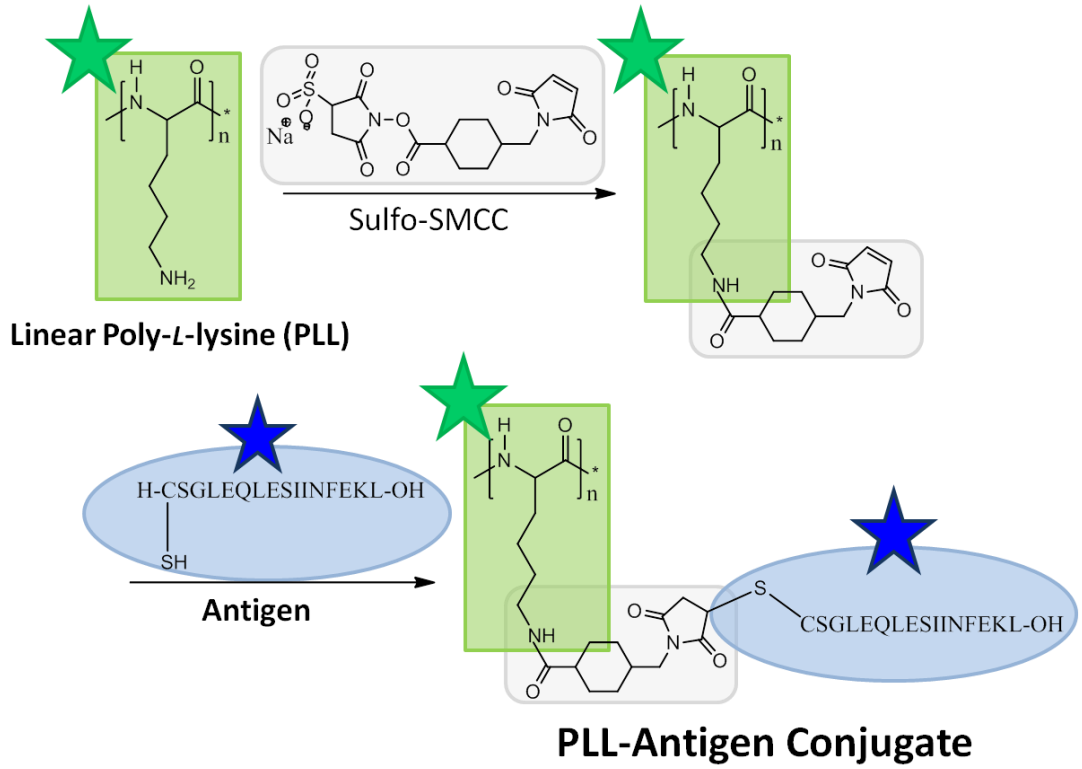

Figure 61: Scheme of antigen conjugation to PLL; ★: AlexaFluor488, ★: AlexaFluor546

In order to conjugate antigen or CpG to PLL, PLL-AF488 is reacted with the water soluble crosslinker Sulfo-SMCC. CpG is thiol-modified at its 3' end and Antigen-AF546 is reduced at its terminal cysteine residue to obtain a free thiol. The 3' end has to be used for conjugation as a single-stranded free 5' end of the ODN without end modification is assumed to be important for interaction of the ODN with the Toll-like receptor[65]. After purification, thiol-containing Antigen and CpG are simultaneously reacted with PLL-maleimide to form a stable thioether bond.

In literature, peptide-CpG conjugates are reported to have enhanced stability to degradation and show enhanced uptake and higher binding strength[124]. 15-17mer oligonucleotides conjugated to poly-*L*-lysine provide 50fold better protection against infection by vesicular stomatitis virus *in vitro* than unconjugated oligonucleotides. The proposed internalization mechanism for the conjugates is absorptive endocytosis[123].

Conjugation reactions with varying ratios of PLL to Antigen are performed (Table 9). CpG is present in experiments III, IV, VI, X and XIII. For the first two experiments, Antigen is reduced with DTT, but it is difficult to remove all excess of DTT with Sephadex G25 NAP5. Remaining DTT can react with maleimides and thus reduce conjugation efficiency of PLL and Antigen. For all further reductions TCEP is used as it does not react with maleimides and therefore does not have to be removed prior to conjugation.

In some experiments turbidity and/or precipitation is observed, especially in samples where CpG is present. In my diploma thesis, aggregate formation of PLL with Sulfo-SMCC was studied and it was shown that conjugation of PLL with the hydrophobic linker always resulted in aggregates of hydrodynamic radii between 40 and 70nm depending on the degree of functionalization. In this thesis these results are veryfied as DLS measurements of PLL-SMCC also exhibited a R_h of 71nm (Figure 64). It was also found that all other heterobifunctional linkers investigated in my diploma thesis exhibited aggregate formation to some extent. Thus, it is assumed that it is impractical to avoid aggregates when conjugating PLL with linkers. Therefore, in this thesis conjugation is pragmatically performed with PLL-SMCC aggregates and lower reaction efficiencies are accepted.

Table 9: Summary of PLL-Antigen conjugations

PLL-Antigen Experiment		**Ratio PLL: Antigen**	**Ratio PLL: CpG**	**Reduction of Antigen/ CpG**	**Labeling Efficiency PLL: Antigen: CpG**
I	120123	1:17	No	DTT	1 : 0.8
II	120305	1:17	No	DTT	??
III	120416	1:30	1: 35.8	TCEP	??
IV	120416	1:15	1:15	TCEP	??
V	120522	1:6	No	TCEP	1 : 2.6
VI	**120522**	**1:6**	**1:6**	**TCEP**	**1 : 2.5 : 7***
VII	**120529**	**1:12**	**No**	**TCEP**	**1 : 2**
VIII	**120611**	**1:2.3**	**No**	**TCEP**	**1 : 1.4**
IX	**120611**	**1:2.3**	**No**	**TCEP**	**1 : 2.2**
X	120917	1:10	1:10	TCEP	1 : 8.8

XI	120917	1:10	No	TCEP	1 : 8.6
XII	121105	1:10	No	TCEP	1 : 4.3
XIII	121105	1:10	1:1	TCEP	1 : 4.1

(*determined with CE)

Determining the ratio of PLL to Antigen is difficult and experimental uncertain. The UV/Vis spectra of PLL-AF488 and Antigen-AF546 overlay to a certain amount at the absorption maximum of AlexaFluro488 at a wavelength of 495nm. Hence, the amount of PLL might be overestimated. This is exemplary shown for PLL-Antigen VII in Figure 62.

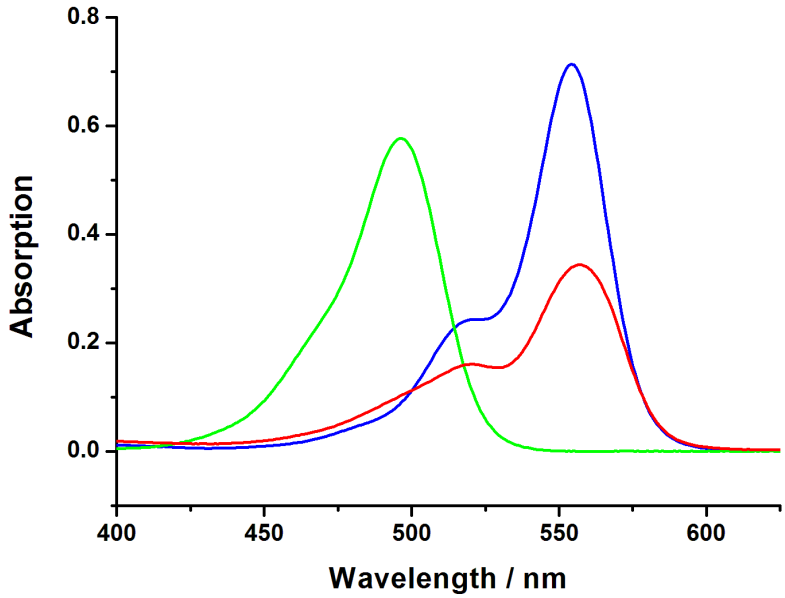

Figure 62: UV/Vis spectra of PLL-Antigen; Antigen-AF546, PLL-AF488, PLL-Antigen

As CpG is not fluorescently labeled, conjugation efficiency of PLL and CpG cannot be determined with UV/Vis measurements. Different other methods are tried to analyze the amount of CpG bound to PLL, but all exhibit large experimental uncertainties.

Capillary electrophoresis of the unpurified conjugate is measured with 25mM sodium phosphate pH 7.4 as eluent and fused silica capillaries coated with polyimide (length 45cm) at 30kV for 40min and CpG is detected at λ = 260nm. A calibration curve of CpG is used to determine the amount of free CpG in the reaction mixture. For experiment VI the amount of CpG bound to PLL is calculated is seven CpG to one PLL chain. The problem with capillary electrophoresis for this system is that the conjugate has to be measured salt free, but with-

out salt PLL and CpG aggregate which is observed with FCS. Another factor is that PLL also absorbs to a certain amount at λ = 260nm which leads to an overestimation of free CpG and underestimation of bound CpG. But in this experiment the number of bound CpG calculated (ratio 1:7) is already higher than the amount of CpG added to PLL (ratio 1:6). Due to all these errors in the measurement and analysis, CE is not used to determine the ratio of PLL to CpG.

Polyacrylamide gel electrophoresis is performed with the unpurified reaction mixture to determine free CpG. With free CpG a calibration for the band intensities at certain concentrations is tried to establish, but the intensities of the bands do not give reproducible results. Free CpG is observed in the gel, but the amount cannot be calculated.

Gel electrophoresis of the PLL-Antigen conjugate (Figure 63) shows that conjugation between PLL and Antigen is successful. Antigen and PLL alone run with the solvent front, Antigen because of its small molecular weight of 1.8kDa and PLL due to its molecular weight of 7.5kDa and its high cationic charge. The conjugate shows a different migration behavior and broad bands with intensity maxima at approximately 15kDa, 30kDa and at the top of the gel in the pocket.

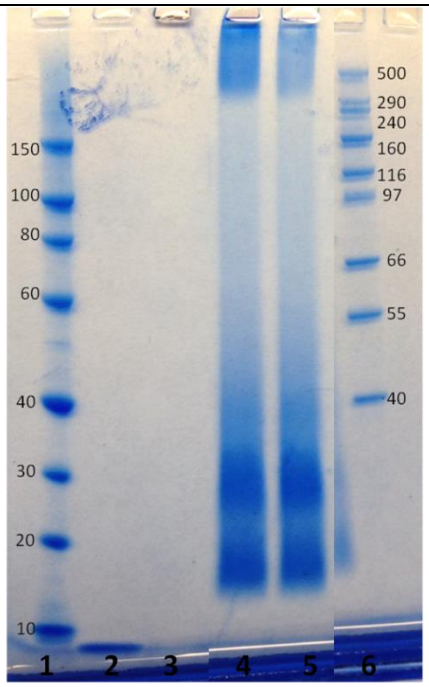

Lane	Sample
1	RotiMark 10-150kDa
2	Antigen-AF546
3	PLL-AF488
4	PLL-Antigen I F1
5	PLL-Antigen I F2
6	HiMark HMW Protein Marker

Figure 63: NUPAGE Tris Glycine Gel 4-12% of PLL-Antigen conjugate I

The broad bands and the smear across the whole gel are probably caused by the broad distribution of PLL-Antigen conjugates and indicate successful conjugation. In the mixture there

is unconjugated PLL, one Antigen conjugated to PLL and several Antigens linked to one PLL chain which give the broad distribution. Additionally, charge alteration effects contribute to a high heterogeneity of the sample as every PLL molecule reacts with a different amount of crosslinker and subsequently with a different amount of antigen and thus yields a different net charge[99].

In order to determine the aggregation behavior of the conjugates during in vitro experiments, samples are analyzed with dynamic light scattering in the cell media (RPMI + 5% FCS) by [redacted], group of [redacted]. RPMI + 5% FCS exhibits a hydrodynamic radius of 8.25nm (Figure 64, left). PLL-SMCC has a hydrodynamic radius of 71nm in 1x PBS and shows no further aggregation in RPMI + 5% FCS at a concentration the internalization experiments are performed ($1*10^{12}$ PLL chains in 200µL).

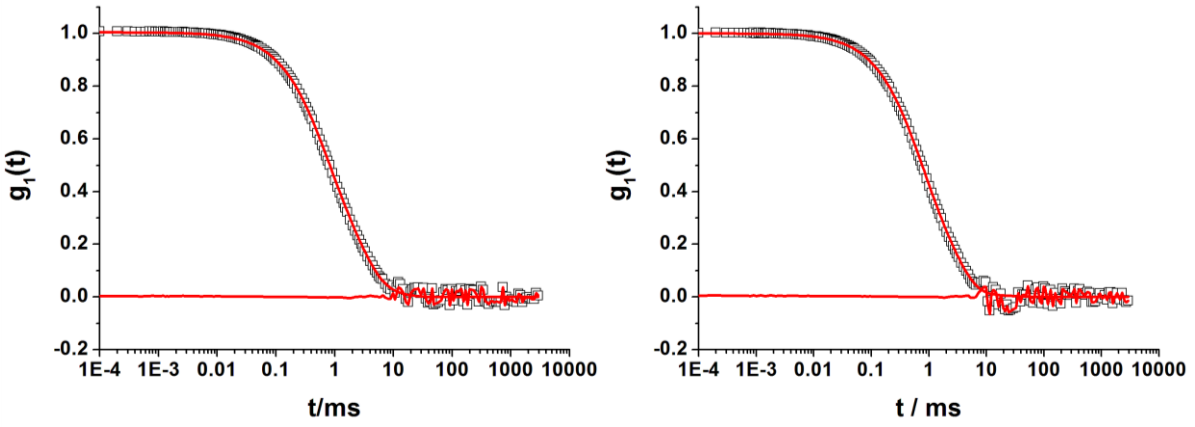

Figure 64: left: DLS of PLL-SMCC in RPMI + 5% FCS, θ = 30°, T = 293.15K, □ PLL-SMCC, ▬ force fit; right: DLS of PLL-Antigen-CpG X in RPMI + 5% FCS, θ = 30°, T = 293.15K, □ PLL-Antigen-CpG, ▬ force fit

PLL-Antigen-CpG X has a hydrodynamic radius of 131nm in RPMI + 5% FCS and shows no further aggregate formation. The force fit is sufficient to fit the autocorrelation function of the mixture of serum and conjugate and no additional fit parameter for larger particles is needed. The correlation function of PLL-Antigen II is depicted in Figure 72 in Chapter 3.3.3. and described in comparison to PLL-Antigen-aDEC205.

With flow cytometry the uptake of PLL-Antigen into bmDC is studied. Not all experiments produced reasonable data, therefore only the successful flow experiments are depicted in

Figure 65. As Antigen does not influence the uptake of the conjugate, different experiments with different conjugation ratios can be compared.

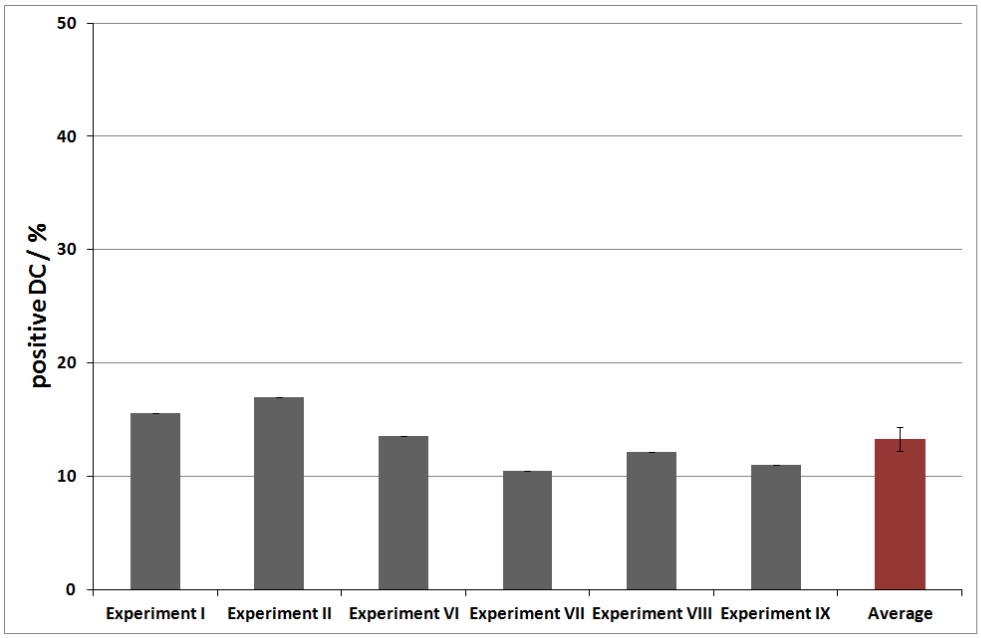

Figure 65: Uptake of different PLL-Antigen conjugates into bmDC after 4h incubation time

Antigen alone shows no internalization into bmDC (~0.6%). Average uptake of PLL-Antigen conjugate is 13.3%. This number shows that conjugation of Antigen to PLL is successful as otherwise cells are not positive for Antigen-AF546. Additionally, conjugation of Antigen to the lysine residues of PLL via Sulfo-SMCC greatly reduces the positive charges of the polymer and therefore diminish cell uptake compared to unconjugated polymer.

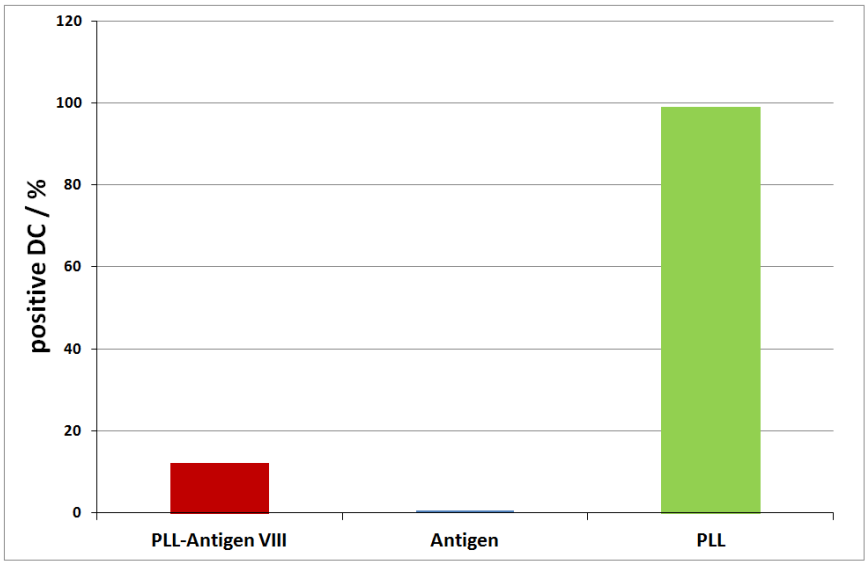

Figure 66: Comparison of internalization into bmDC for PLL, Antigen and PLL-Antigen VIII

Confocal laser scanning microscopy images illustrate the localization of the conjugate within bmDC and colocalization of the fluorescent dyes within the cell (Figure 67). This colocalization does not occur for the control experiments (Figure 78) and therefore suggests successful conjugation.

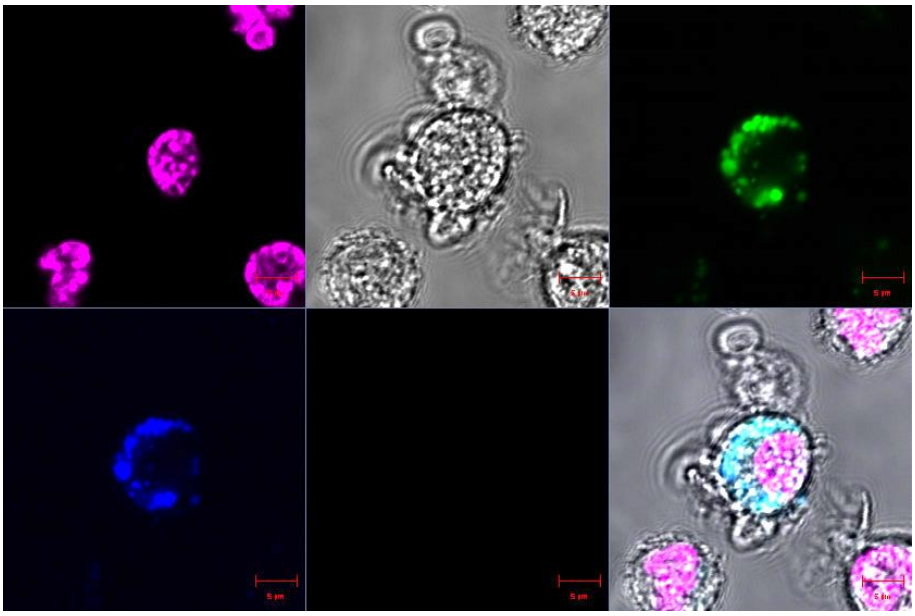

Figure 67: CLSM image of PLL-Antigen VII in bmDC, 1xPBS, non-fixated, incubation time 4h, conc. $1*10^{12}$ particles per $5*10^{5}$ DC; violet: Hoechst 33342 - Labeling of nucleus; green: PLL-AF488; blue: Antigen-AF546, scale bar: 5µm

Summary of synthesis and characterization of PLL-Antigen

In summary, conjugation of Antigen to PLL is successful and proven by gel electrophoresis, flow cytometry and CLSM. Determination of the degree of labeling with UV/Vis-Spectroscopy is difficult and no reproducible conjugation efficiencies are obtained. It is not possible to detect the amount of CpG bound to PLL as CpG is not fluorescently labeled and agarose gel electrophoresis and capillary electrophoresis do not provide reasonable results.
Flow cytometry measurements show uptake of Antigen conjugated to PLL while Antigen alone is not internalized. CLSM images reveal colocalization of both fluorescent dyes attached to PLL and Antigen, respectively. PLL-Antigen-CpG conjugate exhibits a hydrodynamic radius of 131nm in RPMI + 5% FCS and shows no further aggregation with serum proteins.

3.3.3. PLL-Antigen-aDEC205 conjugates

In order to synthesize PLL-Antigen-aDEC205 conjugates, Antigen is reacted to PLL first and afterwards the aDEC205 antibody is conjugated to the PLL-Antigen conjugate. The reasons for this order are the sterical hindrance of the aDEC205 antibody and furthermore the possible side reactions of conjugating the antigen to lysine residues of aDEC205 if the antibody is conjugated to PLL first.

Two different strategies are followed to conjugate aDEC205 to PLL-Antigen: Schiff base formation and DIBO click reaction (explained in Chapter 3.3.1.).

Schiff Base formation of PLL with oxidized aDEC205 (Method 1)

For synthesis of PLL-Antigen-aDEC205 conjugates PLL-Antigen conjugates, described in the previous Chapter 3.3.2., are reacted with oxidized antibody under reductive amination (see Chapter 3.3.1.). All conjugations are summarized in Table 10.

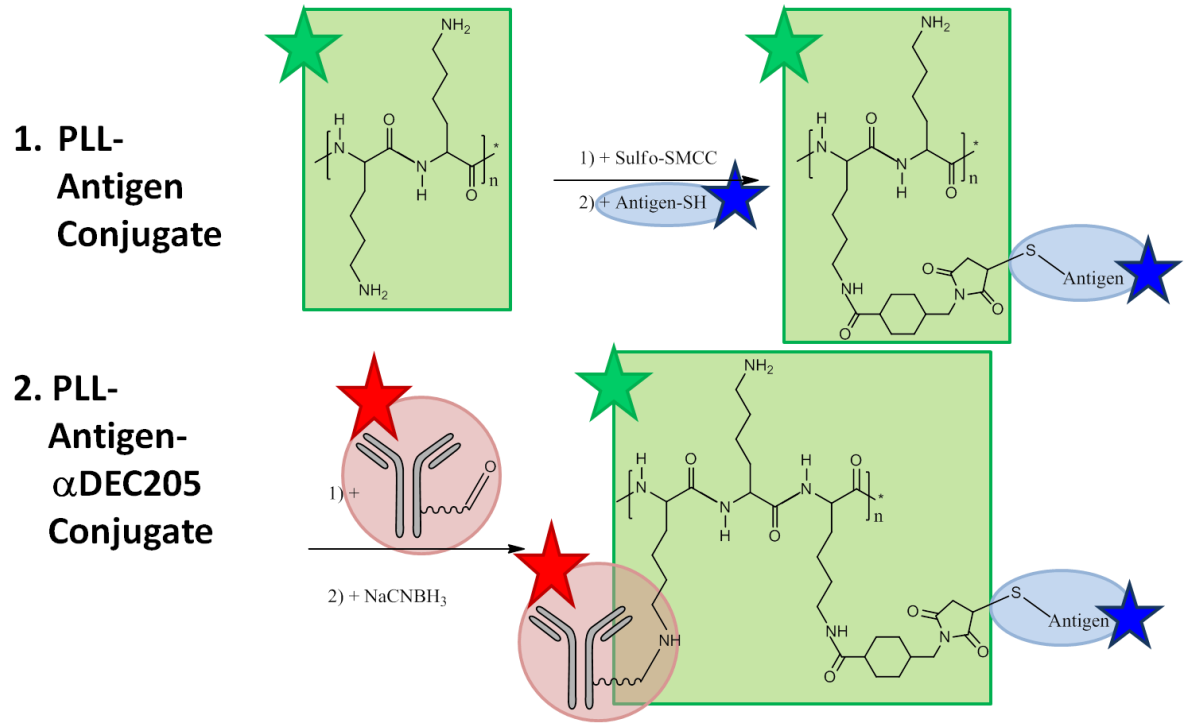

Figure 68: Reaction scheme for the PLL-Antigen-aDEC205 conjugate, Method 1 via Schiff base reaction; ★: AlexaFluor488, ★: AlexaFluor546, ★: AlexaFluor647

Table 10: Summary of PLL-Antigen-aDEC205 conjugations

PLL-Antigen-aDEC205		**Ratio PLL: aDEC205**	**CpG**	**Conjugation Efficiency PLL: Antigen: aDEC205**
I	120125	10:1	No	1 : 0.8 : 0.4
II	120305	10:1	No	??
III	120416	1:1	1: 35.8	??
IV	120416	1:1	1:15	??
V	120530	1:2	No	?? : 0.7 : 1
VI	**120530**	**1:2**	**1:6**	**1 : 6.2 : 4.1**
VII	**120530**	**1:2**	**No**	**1 : 3.1 : 1**
VIII	**120611**	**5:1**	**No**	**1 : 2.1 : 0.4**
IX	**120611**	**5:1**	**No**	**1 : 2.2 : 0.5**
X	120917	10:1	1:10	1 : 5.9 : 0.4
XI	120917	10:1	No	1 : 1.2 : 0.8
XII	121105	1:5	No	1 : 4.3 : 0
XIII	121105	1:5	1:1	1 : 2.4 : 0.2

CpG is conjugated to PLL in experiments III, IV, VI, X and XIII, but as described in Chapter 3.3.2. the amount of CpG in the conjugate cannot be determined.

Conjugation efficiency of Antigen and aDEC205 to PLL is determined with UV/Vis measurements and exemplary shown for PLL-Antigen-aDEC205 VII in Figure 69. As free aDEC205 cannot be removed from the PLL-Antigen-aDEC205 conjugate, the amount of aDEC205 is overestimated. But as excess of 10:1 of PLL-Antigen over aDEC205 is used it is assumed that most of the antibody reacted with PLL-Antigen and nearly no free antibody is left in the reaction mixture.

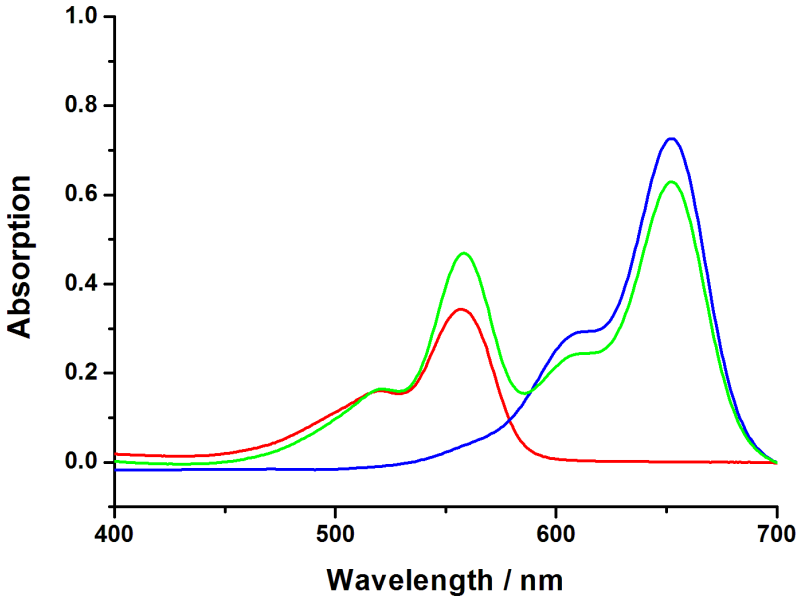

Figure 69: UV/Vis spectra of PLL-Antigen-aDEC205 VII; aDEC205, PLL-Antigen, PLL-Antigen-aDEC205

Conjugates are characterized with SDS-PAGE, flow cytometry and CLSM. In SDS PAGE (Figure 70), PLL-Antigen-aDEC205 shows a different migration behavior from PLL-Antigen and PLL-SMCC (Figure 71, lane 6).

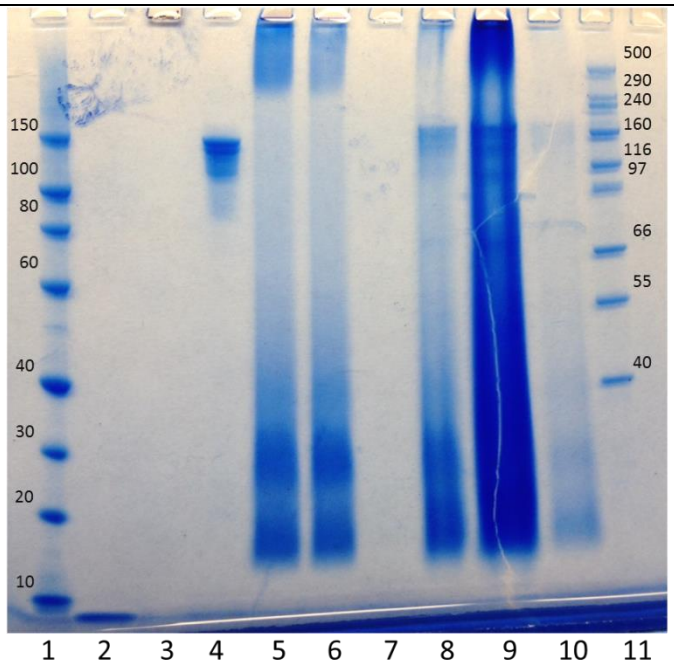

Lane	Sample
1	RotiMark 10-150kDa
2	Antigen-AF546
3	PLL-AF488
4	aDEC205-AF647
5	PLL-Antigen I F1
6	PLL-Antigen I F2
7	PLL-Antigen-aDEC205 I F1
8	PLL-Antigen-aDEC205 I F2
9	PLL-Antigen-aDEC205 I F3
10	PLL-Antigen-aDEC205 I F4
11	Hi Mark Protein Marker

Figure 70: NUPAGE Tris Glycine Gel 4-12%, non reducing, of PLL-Antigen-aDEC205 conjugate I; F1-4: different fractions after purification with Sephadex G25 NAP-5

Another band at approximately 150kDa appears which can be related to aDEC205 or aDEC205 conjugate as the gel is run under non-reducing conditions and the disulfide bonds within the IgG molecule should be intact. In addition, the smear across the gel increases which can be observed in lane 9.

In Figure 71, aDEC205 and oxidized aDEC205 is shown in lane 2 and 3. Oxidized antibody does not show the same band broadening as unreduced antibody. This may be due to difference in concentration and different complexation with SDS.

In lane 4 and 5 Antigen and reduced Antigen is depicted. Reduced Antigen shows a stronger band probably because of a higher concentration that cannot be determined with UV/Vis spectroscopy as free dye cannot be removed from Antigen-dye conjugate and therefore no Antigen concentration can be calculated from the absorption at the maxima of the dye. SMCC-modified PLL (lane 6) shows a band between 10 and 20kDa that is not visible for unmodified PLL (Figure 51, lane 10). This might be due to the different mass to charge ratio as positive charges are eliminated during linker conjugation. PLL-aDEC205 exhibits a band at ~150kDa which is related to the IgG molecule or PLL-aDEC205 conjugate. PLL-Antigen smears across the gel with intensity maxima at ~15kDa and below the pocket at the top of the gel. PLL-Antigen-aDEC205 depicts the bands seen for PLL-aDEC205 at ~150kDa and for PLL-Antigen. No increased smearing across the gel can be observed which might be due to lower concentration.Therefore for this conjugate the gel is no proof of conjugation as no new band or increased smear occurs. Again, charge alteration effects and the consequential heterogeneity in the sample make it difficult to interpret gel images.

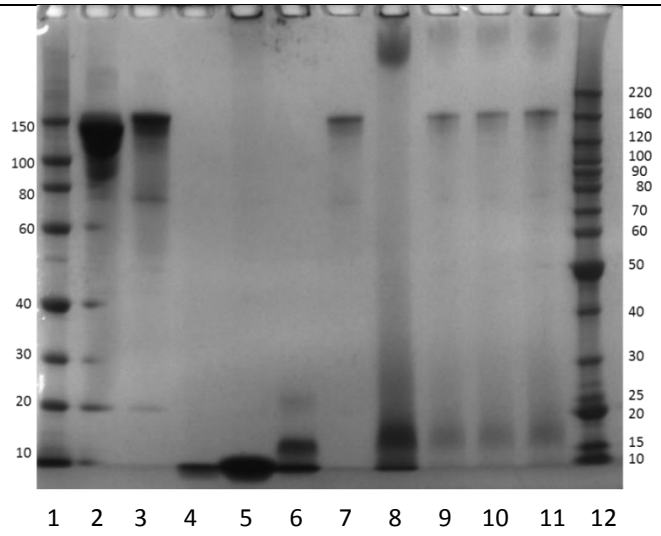

Lane	Sample
1	RotiMark 10-150kDa
2	aDEC205-AF647
3	aDEC205-AF647-ox.
4	Antigen-AF546
5	Antigen-AF546 + DTT
6	PLL-SMCC
7	PLL-aDEC205
8	PLL-Antigen II
9	PLL-Antigen-aDEC205 II
10	PLL-Antigen-aDEC205 II
11	PLL-Antigen-aDEC205 II
12	Bench Mark Protein Ladder

Figure 71: NUPAGE Tris Glycine Gel 4-12%, non reducing, of PLL-Antigen-aDEC205 conjugate II

Dynamic light scattering experiments are performed in 1x PBS with PLL-Antigen II and PLL-Antigen-aDEC205 II (Figure 72). The PLL-Antigen sample has to be fitted with a biexponential fit in order to obtain a smooth residuum and the hydrodynamic radii are summarized in Table 11. PLL-Antigen exhibits two modes with R_h 2.2nm and 53.3nm, which is approximately the R_h of PLL and the larger R_h probably correlates to the conjugate and aggregates. This indicates that, next to the conjugate, free PLL (R_{h1}) and aggregates (R_{h3}) reside in the solution. These probably hydrophobic aggregates can occur due to the high degree of functionalization of PLL with hydrophobic linker. The antigen is also slightly hydrophobic due to the leucine and phenylalanine residues.

In Figure 72 it can be observed that after conjugation of the aDEC205 antibody the autocorrelation function becomes clearly bimodal, which may be due to the large amount of free antibody in solution. The slow mode of the PLL-Antigen-aDEC205 sample has to be fitted with a bioexponential fit, subtracted and the other mode is then also fitted with a biexponential fit. These two fits of the two modes yield hydrodynamic radii of 5.9nm and 121nm. The correlation function of the faster mode, after subtraction of the slower mode, equals the correlation function of aDEC205 and also the hydrodynamic radius of 5nm implies that

this mode correlates to free antibody. The antibody alone already is a little bit polydisperse and has to be fitted biexponential, therefore, this mode is also fitted with a biexponential fit. Additionally, in gel electrophoresis (Figure 71) free antibody is observed. On the other hand at a ratio of PLL to antibody of 10:1, no free antibody with this amplitude should be detectable; the amount of antibody would be much too high. This indicates that this mode may not be free antibody or that the concentration ratios are different from what is assumed. The concentration of PLL may have changed due to filtration loss of larger aggregates. A GHP200nm filter is used for these experiments, thus, it may be possible that aggregates with R_h larger than 100nm remain in the filter and are filtered out of the solution. Elimination of larger aggregates influences the concentration ratio of PLL to aDEC205 and therefore, free antibody can be observed. Due to the very low amount of sample no control experiments with other filters can be conducted and preparing larger scales to obtain more sample volume is too expensive.

The analysis of the other mode with R_h 121nm contains a large imprecision and the hydrodynamic radius has to be declared with an error of approximately 20%, so the R_h is 121 ± 24nm. This indicates, that next to the conjugation reaction that yields a PLL-Antigen-aDEC205 conjugate, aggregate formation occurs to obtain aggregates with $R_h = 121 \pm 24$nm. The graphs of the angular dependency can be found in the appendix.

Hence, the details are not pursued as the results are not of major importance for the biological part of this thesis and CLSM images that show colocalization of aDEC205 and PLL prove that at least a certain fraction of the antibody is conjugated to the polymer.

Table 11: Hydrodynamic radii for PLL-Antigen and PLL-Antigen-aDEC205 in 1xPBS

Conjugate	**R_{h1} / nm**	**R_{h2} / nm**
PLL-Antigen	2.2	53.3
PLL-Antigen-aDEC205	5.9	121 ± 24

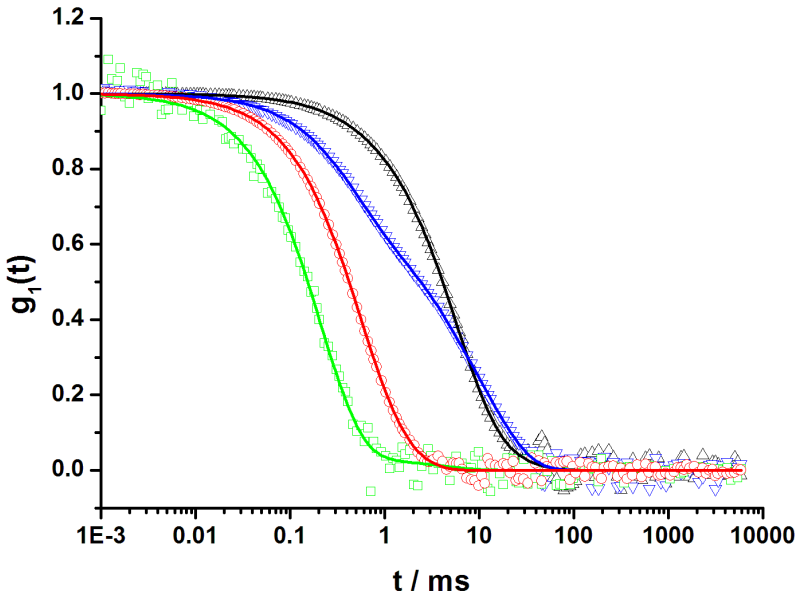

Figure 72: Autocorrelation function of □ PLL-AF488, ○ aDEC205, Δ PLL-Antigen II and ∇ PLL-Antigen-aDEC205 II, θ = 30°, T = 293.15K in 1xPBS

Dynamic light scattering measurements in RPMI + 5% FCS are accomplished by [redacted], group of [redacted]. Oxidized aDEC205-AF647 has a hydrodynamic radius of 11nm in 1x PBS which is larger than unoxidized aDEC205 that has a R_h = 5nm. In RPMI + 5% FCS aDEC205 can be perfectly fitted with a force fit without additional aggregate function. PLL-Antigen-CpG-aDEC205 X shows a R_h = 169nm in 1x PBS. Positively charged PLL can aggregate with the negatively charged oligonucleotide to form interionic complexes that can precipitate. This can lead to a high apparent R_h for conjugate X. In RPMI + 5% FCS no further aggregate formation can be observed (Figure 73).

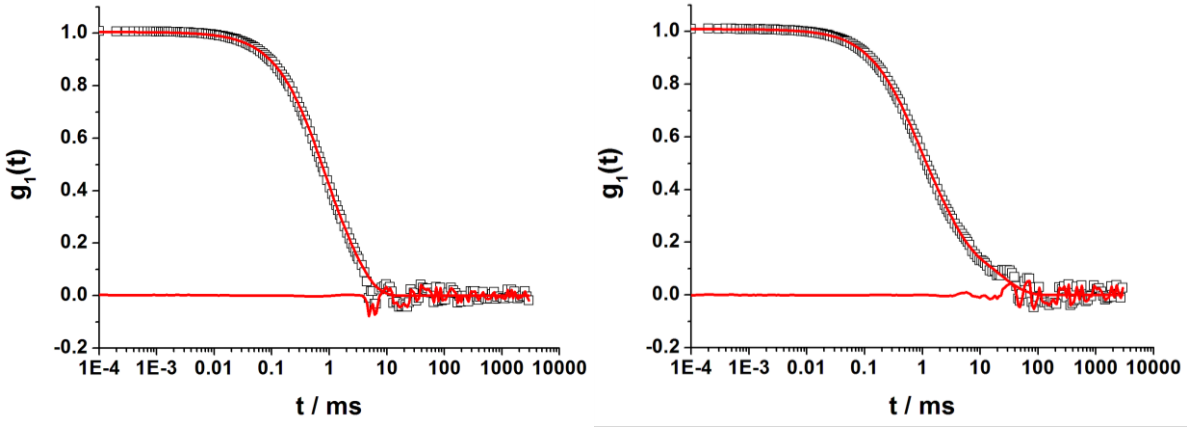

Figure 73: left: DLS of aDEC205-ox in RPMI + 5% FCS, θ = 30°, T = 20°C; right: DLS of PLL-Antigen-CpG-aDEC205 X in RPMI + 5% FCS, θ = 30°, T = 293.15K; left: □ aDEC205-ox, ▬ force fit and residuum; right: □ PLL-Antigen-CpG-aDEC205, ▬ force fit and residuum

PLL-Antigen-DEC205 XI only has a R_h of 7.7 nm in 1x PBS. This might be due to free antibody (R_h = 5nm) that accounts for a smaller apparent hydrodynamic radius.

Dynamic light scattering measurements in human serum are performed by [redacted], group of [redacted].

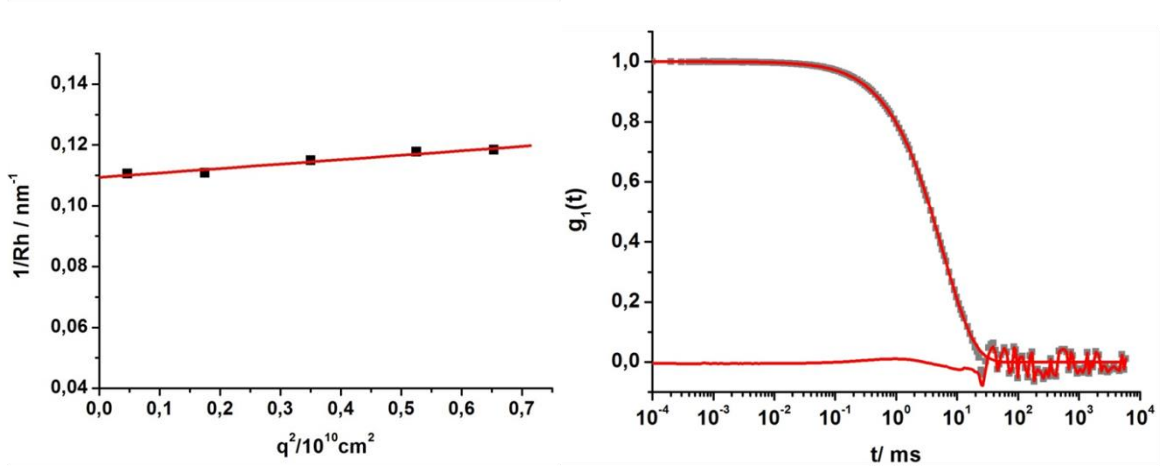

Figure 74: left: Angular dependency of the reciprocal hydrodynamic radius of PLL-Antigen-aDEC205 VII in 1x PBS; R_h = 9nm; right: autocorrelation function of PLL-Antigen-aDEC205 in human serum, θ = 30°, T = 293.15K, ■ DLS of PLL-Antigen-aDEC205 in human serum, ▬ Force fit and residuum

DLS in 1x PBS buffer with physiological salt content exhibits a hydrodynamic radius of PLL-Antigen-aDEC205 VII of $\langle\frac{1}{R_h}\rangle_z^{-1}$ = 9nm. DLS in human serum shows no further aggregate formation which can be seen in the smooth force fit as no additional function to fit aggregates is needed in the multicomponent analysis (Figure 74).

PLL-Antigen-aDEC205 conjugates are analyzed with flow cytometry and exemplarily depicted for PLL-Antigen-aDEC205 I in Figure 75. With the forward– side scatter plot it is gated over living cells (population 1 (P1): % parent= 47.3%). This is a normal value as even cells without conjugate exhibit P1 to be ~50%.

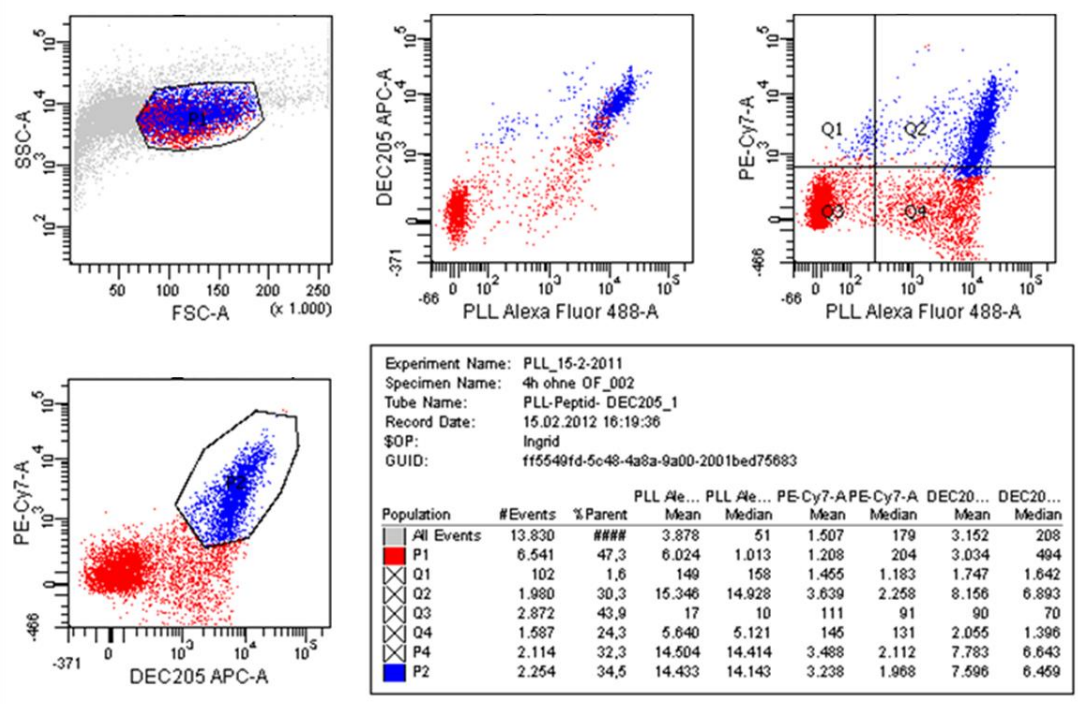

Population	#Events	%Parent	PLL Ale... Mean	PLL Ale... Median	PE-Cy7-A Mean	PE-Cy7-A Median	DEC20... Mean	DEC20... Median
All Events	13.830	####	3.878	51	1.507	179	3.152	208
P1	6.541	47,3	6.024	1.013	1.208	204	3.034	494
Q1	102	1,6	149	158	1.455	1.183	1.747	1.642
Q2	1.980	30,3	15.346	14.928	3.639	2.258	8.156	6.893
Q3	2.872	43,9	17	10	111	91	90	70
Q4	1.587	24,3	5.640	5.121	146	131	2.055	1.396
P4	2.114	32,3	14.504	14.414	3.488	2.112	7.783	6.643
P2	2.254	34,5	14.433	14.143	3.238	1.968	7.596	6.459

Figure 75: Gating strategy for PLL-Antigen-aDEC205 I

In the histogram the APC channel (aDEC205-AF647) is plotted versus the AlexaFluor488 channel (PLL-AF488) and the cells positive for aDEC205 and PLL are depicted in blue in the upper right corner of the plot. The next histogram shows the PE-Cy7 channel (Antigen-AF546) plotted versus the PLL channel. Again, cells positive for Antigen and PLL reside in Q2 (30.3%). The last histogram plots the PE-Cy7 channel (Antigen-AF546) versus the APC channel (aDEC205-AF647) and the positive cells are shown in blue with the population P2 to be 34.5%. This blue population is also illustrated in the other histograms as blue and one can observe that this population is positive in all plots. Therefore, 34.5% of the cells took up all three fluorescent dyes attached to the components. As this number stays constant in all histograms this indicates uptake of conjugate and not of the single components. Free PLL and free aDEC205 can also be observed in the FACS plots (free PLL in Q4).

This flow analysis is done for all PLL-Antigen and PLL-Antigen-aDEC205 experiments and illustrated in Figure 76. This graph shows that in general, uptake of PLL-Antigen-aDEC205 is marginally enhanced in comparison to PLL-Antigen. On the one hand, the results in Chapter 3.3.1 prove that there is no specific uptake into splenic dendritic cells and there is no reason to believe that this is different for bone marrow derived dendritic cells. On the other hand, the

results in Chapter 3.3.1 are obtained with conjugates synthesized via Click Chemistry which requires modification of the lysine residues of aDEC205 with NHS-PEG-azide. This conjugation chemistry might affect binding of antibody and receptor as it might occur in the binding site of the antibody. The conjugation in this chapter is performed site-specifically via the glycosidyl resiued of the antibody and therefore, biofunctionality is preserved. But biofunctionality is not very likely to be the reason as aDEC205-SHIP is also synthesized with click chemistry and still shows binding to the receptor as explained in Chapter 3.2.1.

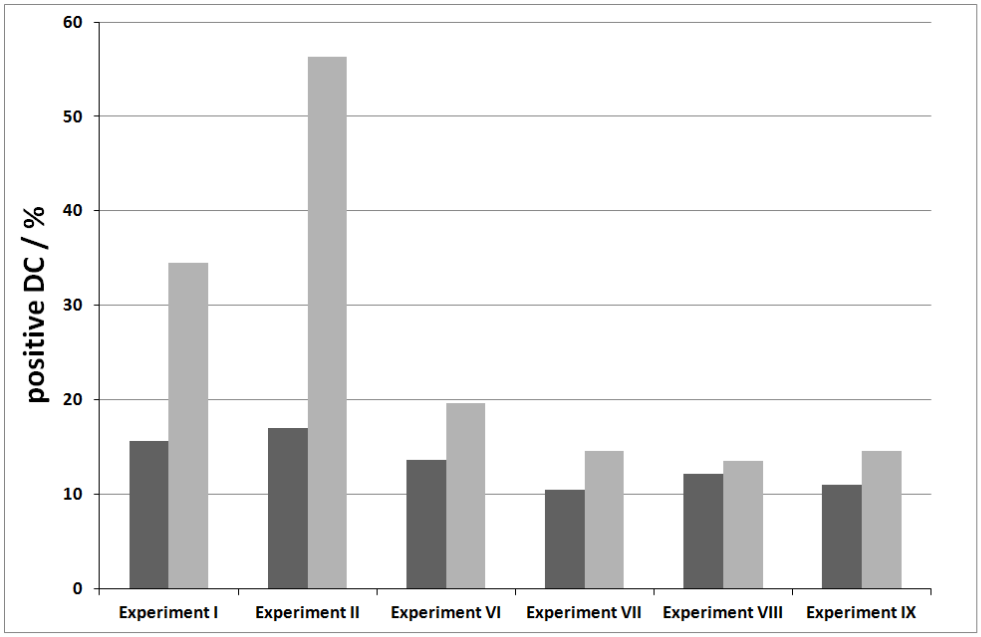

Figure 76: Flow analysis of PLL-Antigen and PLL-Antigen-aDEC205 experiments in bmDC: ■ PLL-Antigen and ■ PLL-Antigen-aDEC205

In detail, experiment 1 shows a 21% higher uptake into bmDC after aDEC205 conjugation. In experiment 2 uptake increases at 39%, but as no ratio of components and no concentration is retrieved for this experiment, this difference in uptake is probably caused by a difference in concentration. The other experiments show only a marginally increased uptake of 1-6%, which is still in the regime of the measurement error.

The conjugates are also analyzed with CLSM in collaboration with Steffen Lorenz, FZI Mainz. CLSM images show perfect colocalization of all components within nearly all bmDC (Figure 77). As for the control experiment no superposition of the components is observed (Figure

78), this colocalization is a strong indication for successful conjugation. In these CLSM images nuclei are depicted in turquoise, PLL in green, Antigen in blue and aDEC205 in red.

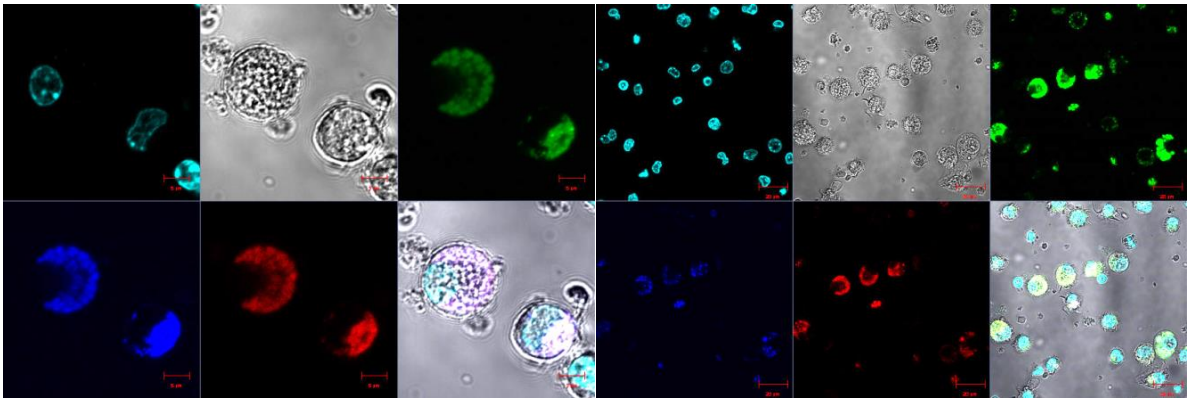

Figure 77: CLSM image of PLL-Antigen-aDEC205 conjugate in living murine bmDC, 1xPBS, non-fixated, incubation time 4h, conc. $1*10^{13}$ particles per $5*10^{5}$ cells; turquoise: Hoechst 33342 - Labeling of nucleus; green: PLL-AF488; blue: Antigen-AF546; red: aDEC205-AF647, scale bar: 5µm

For the control experiment cells are incubated with unconjugated PLL-AF488, Antigen-AF546 and aDEC205-AF647 (Figure 78). As these cells do not show colocalization and look completely different from the cells incubated with conjugate, this is strong evidence that conjugation is successful.

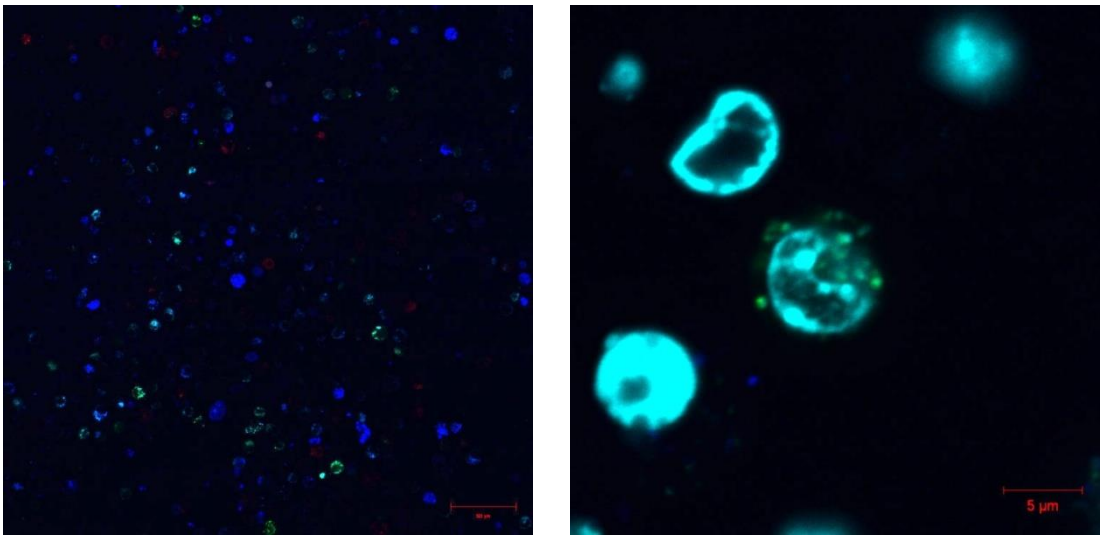

Figure 78: CSLM image of mixture of unconjugated PLL, aDEC205 and Antigen in living bmDC in PBS buffer, non-fixated, incubation time 4h, conc. $1*10^{13}$ particles per $5*10^{5}$ cells, turquoise: nucleus - Hoechst 33342, green: PLL-AF488, blue: Antigen-AF546, red: aDEC205-AF647, scale bar: left: 20µm, right: 5µm

The T cell proliferation assay with bone marrow-derived DC is performed by [redacted] in the group of [redacted] at the Department of Dermatology, University Clinics Mainz.

The ^{3}H-thymidine incorporation assay is used to determine the extent of cell division in response to a stimulus. In this case, proliferation of T cells stimulated by Antigen-loaded DC is analyzed. Thus, DC are incubated with conjugates, washed and then cultured together with T cells and ^{3}H-thymidine, which is a radioactive labeled nucleoside and a precursor of thymine found in DNA. After activation of T cells by Antigen-presentation on the surface of dendritic cells, proliferating T cells replicate their chromosomal DNA and incorporate ^{3}H-thymidine into new strands. The extent of proliferation can be determined by measuring radioactivity in DNA with a scintillation beta-counter in counts per minute (cpm). By comparing the relative counts to a control sample the extent of cell division can be calculated.

Figure 79 shows that, if no Antigen is included in the conjugate, no T cell proliferation occurs. PLL (green curve) and PLL-aDEC205 (black curve) show no 3H-thymidine incorporation and therefore no T cell proliferation. PLL-Antigen (grey curve) and PLL-Antigen-aDEC205 (pink curve) both exhibit activation of T cells. The extent of proliferation is higher for the targeted conjugate than for the untargeted. This might indicate that efficiency of the conjugate is higher if targeted to DCs and internalized by receptor-mediated endocytosis. Soluble Antigen still exhibits the highest potential to activate T cells. The reason might be that the short OVA-derived SIINFEKL peptide can charge DC directly without being internalized, while longer peptides have to be internalized, processed and loaded onto MHC class I complexes within dendritic cells in order to be presented on the cell surface and specifically address CD8+ T cells[107], [106].

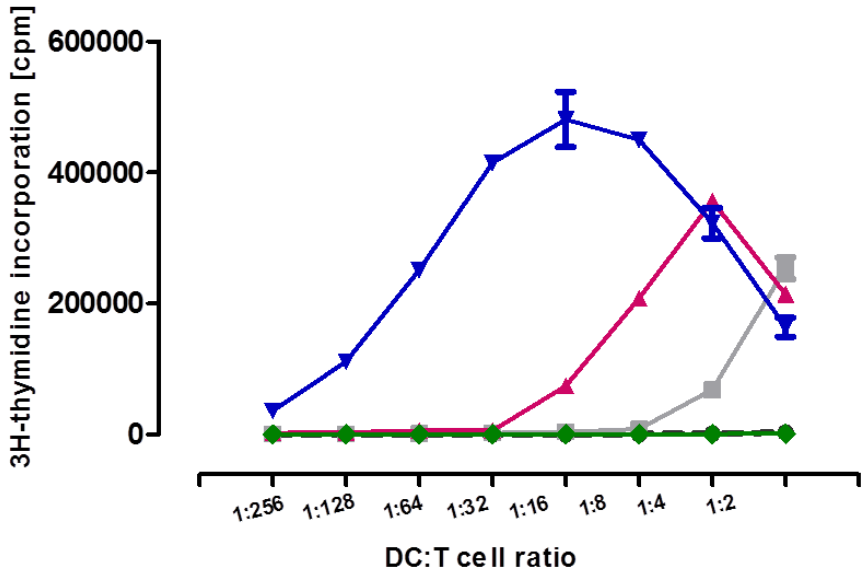

Figure 79: T cell proliferation Assay of PLL conjugates with bmDC, ● PLL-aDEC205, ■ PLL-Antigen, ▲ PLL-Antigen-aDEC205, ▼ soluble SIINFEKL, ♦ PLL

For this conjugate IV no ratio of PLL to Antigen and aDEC205 could be determined and therefore the concentration of Antigen is unknown. Hence, no quantitative conclusion can be drawn and no comparison of the conjugates with soluble antigen can be made. Qualitatively, this experiment states that Antigen is still able to induce T cell proliferation after conjugation to PLL, i.e. Antigen retains bioactivity, and that Antigen is needed for T cells to proliferate as the PLL and PLL-aDEC205 control do not exhibit cell division.

Click reaction of aDEC205-PEG-azide with PLL-DIBO (Method 2)

Conjugates via Click reaction are synthesized at the University of Melbourne in the group of Dr. Angus Johnston. Thus, Antigen and CpG are conjugated to PLL first via the heterobifunctional linker Sulfo-SMCC as described for Method 1 and afterwards the conjugates are functionalized with DIBO and reacted with aDEC205-PEG-azide (reaction scheme see Figure 57). Conjugation efficiency are determined with UV/Vis spectroscopy and summarized in Table 12.

Table 12: Summary of PLL-Antigen-aDEC205 conjugates synthesized with Click chemistry

	Ratio PLL : Antigen : aDEC205	
	Experiment 1	Experiment 2
PLL-Ag-CpG	1: 0.3: 0	1: 0.33: 0
PLL-Ag-CpG-aDEC205	1: 0.5: 0.03	1: 0.61: 0.25
PLL-Ag-aDEC205	1: 0.56: 0.09	1: 0.20: 0.30
PLL-CpG-aDEC205	1: 0: 0.03	1: 0: 0.20

The different experiments are performed in different conjugation order. For experiment 1, Sulfo-SMCC and DIBO are added to PLL, reacted for 2h on ice and purified with Zeba 7k columns. Then, reduced Antigen and CpG are conjugated to maleimide-functionalized PLL and afterwards aDEC205-PEG-azide is added to the reaction mixture. Conjugates are purified with Zeba 40k column. In experiment 2, PLL is incubated with Sulfo-SMCC, purified and reacted with reduced Antigen and CpG. Afterwards, PLL-Antigen/ PLL-Antigen-CpG is modified with DIBO, conjugated to aDEC205-PEG-azide and purified with Zeba 40k column.

The conjugation efficiencies show that method 2 yields better ratios of PLL to aDEC205. An explanation may be that DIBO aggregates with PLL which siginficantly decreases reaction efficiencies. If PLL is reacted with Sulfo-SMCC and DIBO hydrophobic aggregates can form due to the hydrophobicity of both crosslinkers. If PLL-SMCC is reacted with Antigen first, before DIBO is added, the slightly more hydrophilic Antigen decreases hydrophobicity of the conjugate and therefore less aggregate formation occurs, which increases conjugation efficiency of aDEC205 to PLL-Antigen.

Hence, the following characterization with CLSM and antigen cross presentation assay is performed with conjugates that have a higher conjugation efficiency.

Internalization of these conjugates into immature and mature dendritic cells is studied with confocal laser scanning microscopy. Colocalization is observed for all components which indicates successful conjugation (Figure 80). The image on the left hand side depicts immature dendritic cells. It can be observed that most of the conjugate is located on the cell surface, but there is also some internalization into the cell. With mature DC (right hand side) the conjugate is only attached to the cell surface and no uptake is visible. This result is concordant with the internalization studies in Chapter 3.3.1. There it is shown that PLL-aDEC205 conju-

gates are not internalized into mature splenic DC as during maturation dendritic cells shut down unspecific uptake and aDEC205 cannot induce receptor-mediated uptake of the conjugate.

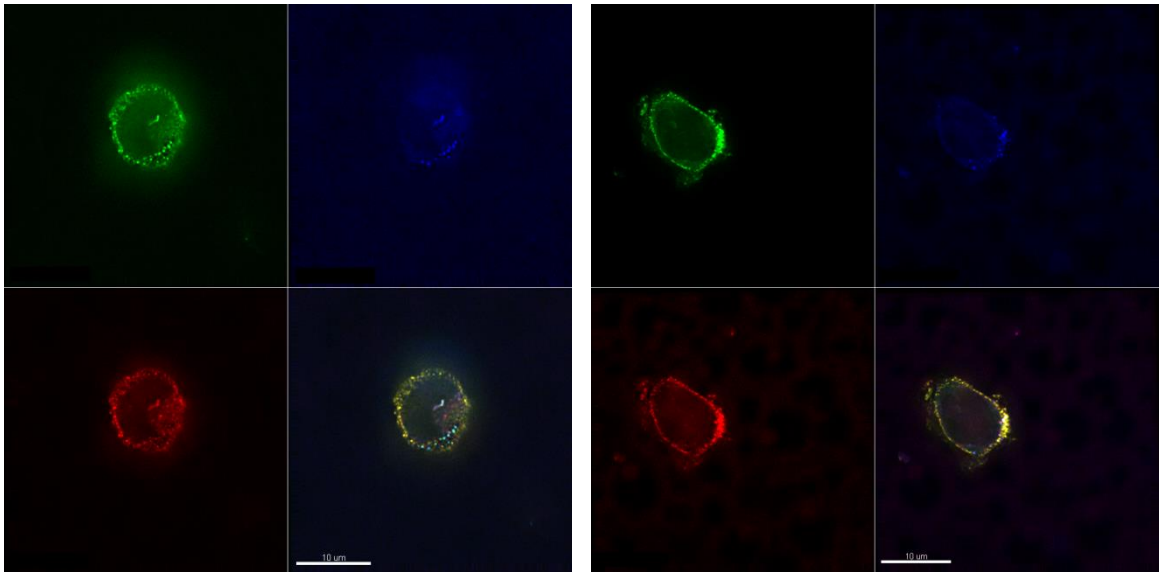

Figure 80: CLSM image of PLL-Antigen-aDEC205 into immature (left) and mature (right) spleen dendritic cells; incubation 1h; green: PLL-AF488, blue: Antigen-AF546, red: aDEC205-AF647; scale bar: 10µm

Again, control experiments with unconjugated components in spleen immature (Figure 81) and mature DC (Figure 82) show no colocalization of the single components within cells.

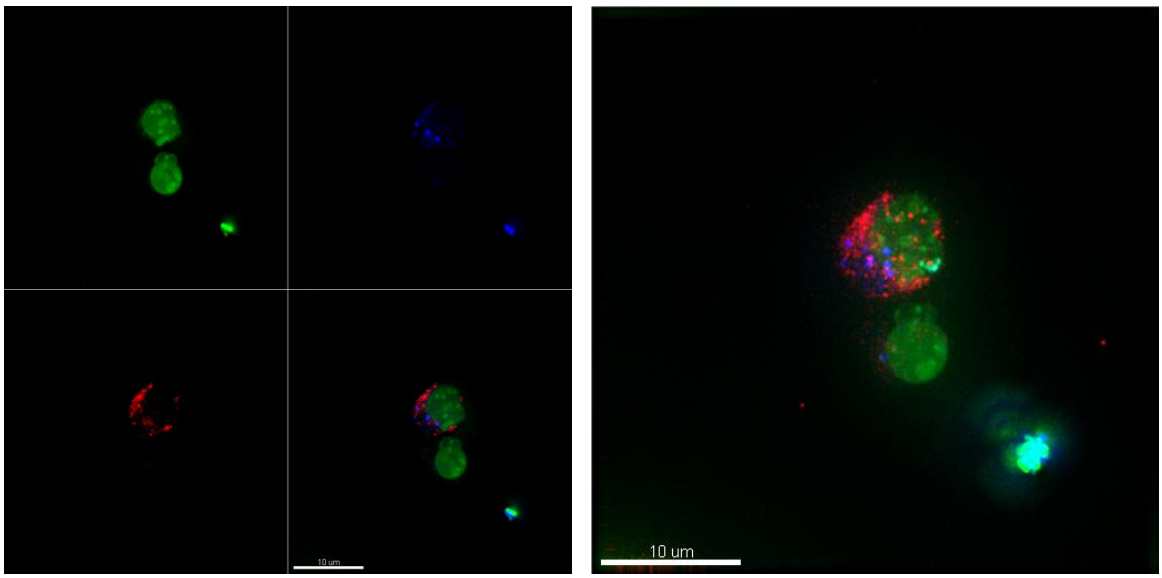

Figure 81: CSLM image of mixture of unconjugated PLL, aDEC205 and Antigen in splenic immature DC in PBS buffer, incubation time 1h, green: PLL-AF488, blue: Antigen-AF546, red: aDEC205-AF647, scale bar: 10µm, right: maximum intensity projection

In the control experiment, PLL is internalized unspecifically into immature dendritic cells (Figure 81) while there is no uptake into mature DC (Figure 82). aDEC205 is still internalized to a high amount into mature DC.

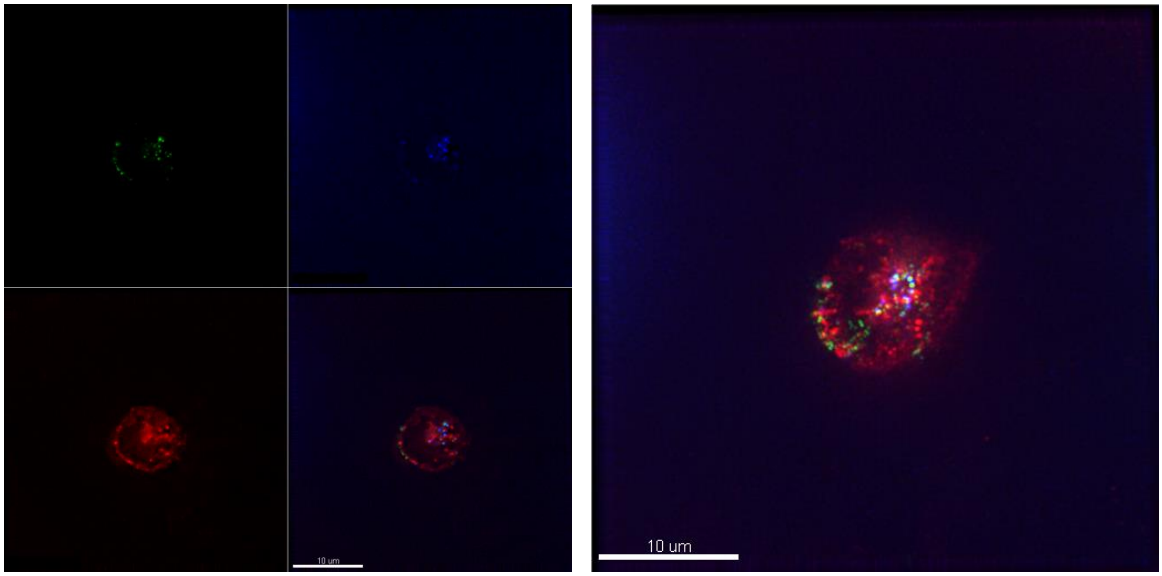

Figure 82: CSLM image of mixture of unconjugated PLL, aDEC205 and Antigen in splenic mature DC in PBS buffer, incubation time 1h, green: PLL-AF488, blue: Antigen-AF546, red: aDEC205-AF647, scale bar: 10µm, right: maximum intensity projection

Antigen Cross Presentation Assays are performed in the laboratory of [redacted] in collaboration with [redacted] and [redacted]. For this assay dendritic cells are isolated from murine spleens and incubated with different concentrations of the samples for 45min at 37°C and 10% CO_2 ($1.5*10^4$ cell per well). OT-I T cells are isolated from murine lymph nodes, stained with purple proliferation dye and checked for purity (>90%). $5*10^4$ OT-I CD8+ T cells per well are cocultured with the Antigen-loaded DC for 72h at 37°C, 10% CO_2. Afterwards, cells are stained with CD8-APC and Vα2-PE for flow cytometry analysis to determine Vα2+ CD8+ T cells (Figure 83, b). Vα2-PE stains T cell receptor (TCR) alpha chain Vα2, which is the specific alpha chain that in combination with TCR beta chain Vβ5 recognizes MHC molecule H-2Kb loaded with SIINFEKL peptide. The OT-I T cells express these chains as transgenes.

Just before the measurement cells are stained with propidiom iodide (Figure 83, c) and 25µL of diluted beads (Sphero Blank calibration particles) are added to be able to normalize the counts (Figure 83, a). By collecting a certain number of beads, in this case 10 000, the num-

ber of cells analyzed is normalized to the beads and thus, a quantitative analysis can be performed.

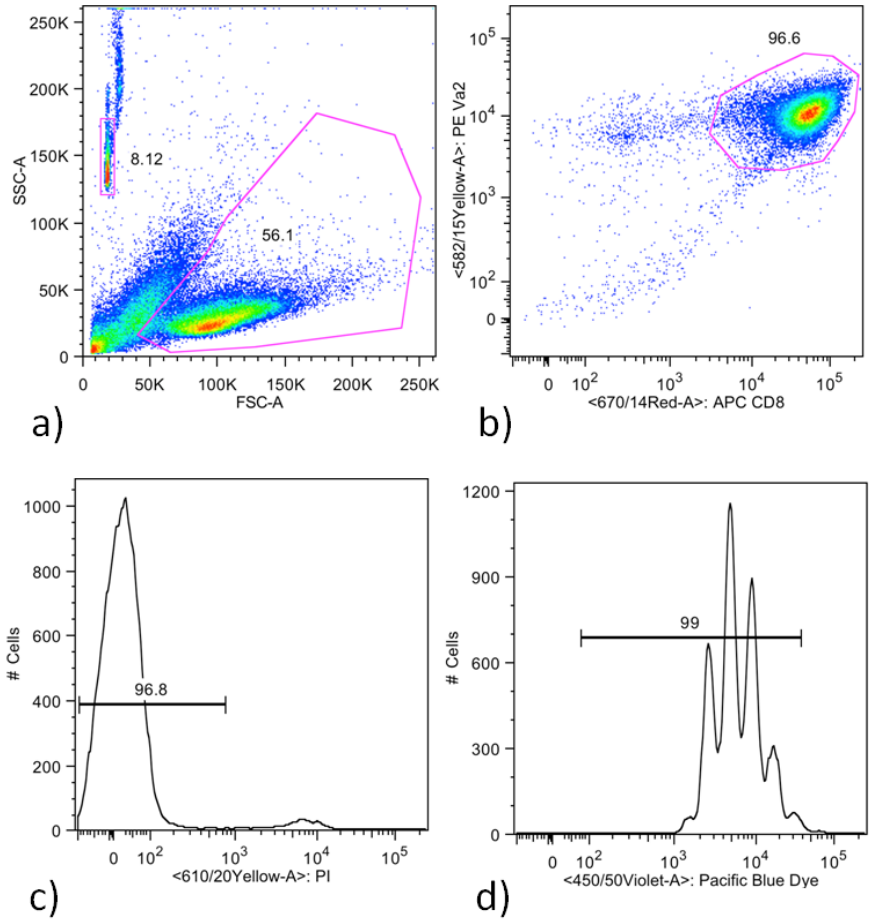

Figure 83: Gating strategy for the antigen cross presentation assay; a) Forward and side scatter dot plot, gating for beads and live cells (56.1%); b) gating for Vα2+ CD8+ T cells (96.6%); c) staining with propidium iodide for cell viability; d) distribution of the violet pacific blue proliferation dye

This assay does not measure radioactivity, but the purple proliferation dye allows to detect the number of cell divisions. CellTrace™ Violet can easily diffuse into cells where intracellular esterases cleve the dye to obtain a highly fluorescent compound. This fluorescent dye covalently binds to intracellular amines and when cells divide it is equally distributed to daughter cells. Thus, violet peaks that represent successive generations of cells can be observed with flow cytometry (Figure 84). This is representatively shown for SIINFEKL as a control (a) and PLL-Antigen-aDEC205 (b). These histograms already show that no proliferation occurs at the lowest Antigen concentration (top curve in dark orange). With increasing Antigen concentration the number of cell division increases until every T cell divided at least

once which can be seen in the blue curve where the original peak is gone. At a certain number of cell division cycles the number of T cells decreases again due to cell death.

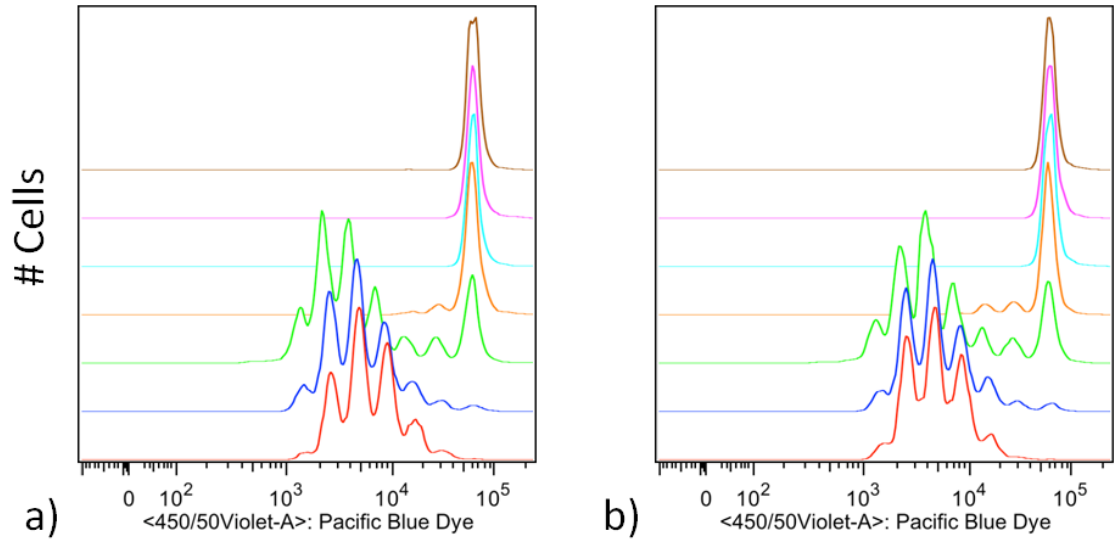

Figure 84: Distribution of the violet pacific blue proliferation dye for the lowest concentration (top) to the highest concentration of Antigen (bottom); a) SIINFEKL and b) PLL-Antigen-aDEC205 conjugate

Figure 85 shows the normalized proliferation of OT-I T cells after coculture with DC versus the concentration of Antigen, that splenic iDC are incubated with. PLL-CpG-aDEC205 conjugate is not illustrated in this graph as it shows no T cell proliferation due to no Antigen content and serves as a negative control. All conjugates that contain Antigen show proliferation of T cells. Soluble SIINFEKL shows the highest amount of proliferation and induces T cell activation at the lowest concentration. Antigen is the Antigen-AF546 that is used for all conjugations. This sample shows a weird behavior as its normalized proliferation is much lower than for all other samples. This might be due to the amount of DMSO still present in the sample, as Antigen-AF546 is not purified after dye labeling. DMSO is known to be toxic and leads to increased permeability of the cell membrane, especially at higher concentrations (>1%) and higher temperatures.

All PLL conjugates show a similar curve progression. Normalized proliferation increases with Antigen concentration until it reaches a maximum. The decrease at higher concentrations is caused by a too high proliferation rate that produces too many cells in the well so that space and medium is not sufficient enough for that many cells and therefore leads to cells death.

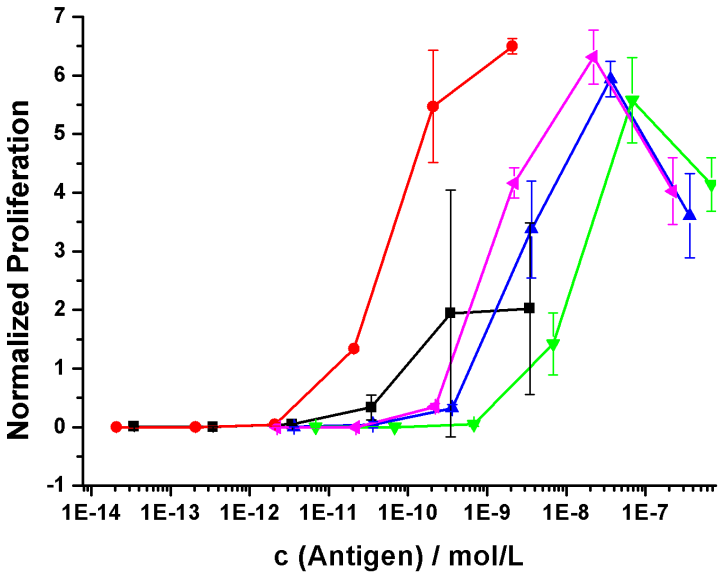

Figure 85: Antigen Presentation Assay with splenic iDC, incubated with PLL conjugates, and OT-I CD8+ T cells; ■ Antigen, ● SIINFEKL, ▲ PLL-Antigen-CpG, ▼ PLL-Antigen-CpG-aDEC205, ◀ PLL-Antigen-aDEC205

PLL-Antigen-aDEC205 induces proliferation at the lowest Antigen concentration, PLL-Antigen-CpG at a little bit higher concentration and the curve for PLL-Antigen-CpG-aDEC205 is not as steep as for the other conjugates. There is no trend visible for the ability to induce proliferation between targeted and untargeted conjugates. This is not surprising as there is no trend as well in internalization of the conjugates and all conjugates are taken up unspecifically.

In conclusion, all Antigen-containing conjugates are able to induce T cell profiferation. Immature dendritic cells are able to internalize the conjugates, process the Antigen and cross-present SIINFEKL on MHC class I to CD8+ T cells. No significant difference in the ability to induce T cell proliferation between the conjugates is observed. But as the results in Chapter 3.3.1. state that there is no receptor-mediated endocytosis, uptake of the conjugates is unspecific and targeting the conjugate with aDEC205 to CD8+ DC does not alter its internalization. Therefore, it is not surprising that no difference in the ability to induce T cell proliferation is observed for targeted and untargeted conjugate. Soluble SIINFEKL again induces T cell proliferation at the lowest concentration, which might be due to the fact that short OVA-derived SIINFEKL peptide can charge DC directly without the need for internalization and intracellular processing[107], [106].

3.3.4. PLL brush conjugates

Conjugation chemistry studied for linear PLL is now transferred to the polylysine brush. The PLL brush is thought to exhibit better properties for drug delivery as it has a prolonged circulation time in the body and different internalization behavior due to its more rigid elongated shape.
For conjugation of Antigen, CpG and aDEC205 to the PLL brush, the same reaction mechanism is performed as described in Chapter 3.3.3. for linear PLL.

Schiff Base formation of PLL brush with oxidized aDEC205 (Method 1)

The conjugation efficiency of Antigen and aDEC205 to PLL brush is determined with UV/Vis spectroscopy and summarized in Table 13. Conjugation efficiencies are higher for conjugates without CpG which might be due to aggregation of the negatively charged ODN with the cationic PLL brush.

Table 13: Summary of PLL brush conjugates synthesized with Method 1

	Ratio PLL brush: Antigen: aDEC205
PLL brush-Ag-aDEC205	1: 10.7: 9.0
PLL brush-Ag-CpG-aDEC205	1: 4.4: 2.4

Flow cytometry measurements do not give reasonable results for PLL brush conjugates in bmDC. PLL brush alone exhibits high unspecific uptake of 95.2 $\pm$ 1.2%.For the PLL brush-Antigen or PLL brush-Antigen-CpG conjugate no uptake of Antigen is detected, only polymer is internalized. The targeted conjugates show internalization of 91.6 $\pm$ 0.8% for PLL brush-Antigen-aDEC205 and 90.8 $\pm$ 5.2% for PLL brush-Antigen-CpG-aDEC205.

CLSM images show internalization of the PLL brush conjugates and colocalization within bmDC which proves successful conjugation. Figure 86 a shows PLL brush-Antigen-aDEC205 and Figure 86 b PLL brush-Antigen-CpG-aDEC205 conjugate.

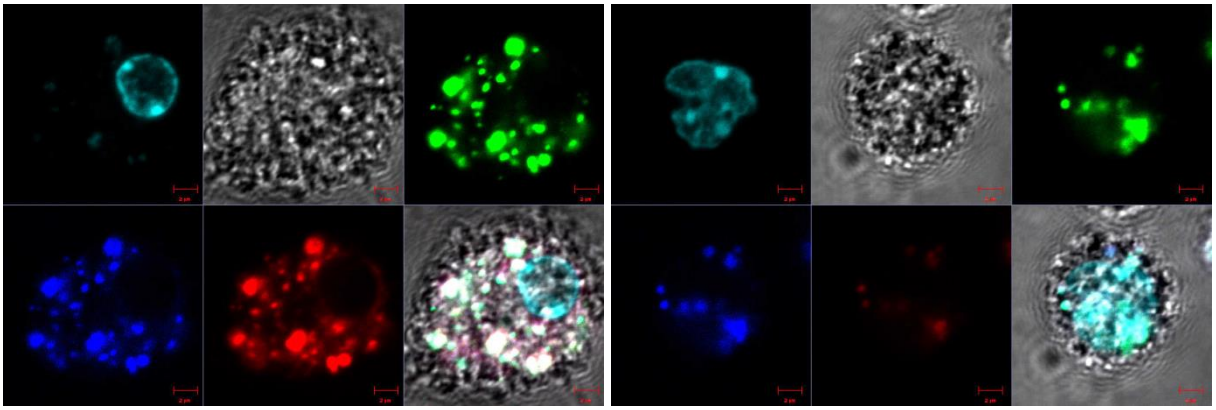

Figure 86: CLSM image of a: PLL brush -Antigen-aDEC205 conjugate and b: PLL brush-Antigen-CpG-aDEC205 conjugate in living murine bmDC, 1xPBS, non-fixated, incubation time 4h, conc. $1*10^{12}$ particles; turquoise: Hoechst 33342 - Labeling of nucleus; green: PLL-AF488; blue: Antigen-AF546; red: aDEC205-AF647, scale bar: 5µm

Click reaction of aDEC205-PEG-azide with PLL brush-DIBO (Method 2)

Polymer brush conjugates are also prepared using click chemistry, as described for PLL in Method 2, and studied in splenic immature DC.

The conjugation efficiency of Antigen and aDEC205 to PLL brush is determined with UV/Vis spectroscopy and summarized in Table 14. It is observed that again the conjugation efficiency is much higher if no CpG is present in the reaction mixture. This may be caused by aggregate formation of the highly positively charged PLL brush with the negatively charged oligonucleotide.

Table 14: Summary of PLL brush conjugates synthesized with Method 2

	Ratio PLL brush: Antigen: aDEC205
PLL brush-Ag-CpG	1: 44.8: 0
PLL brush-Ag-CpG-aDEC205	1: 33.9: 15.6
PLL brush-Ag-aDEC205	1: 119.5: 189.0
PLL brush-CpG-aDEC205	1: 0: 17.5

CLSM images again exhibit colocalization in CD8+ DC (Figure 87 and Figure 88) which proves successful conjugation.

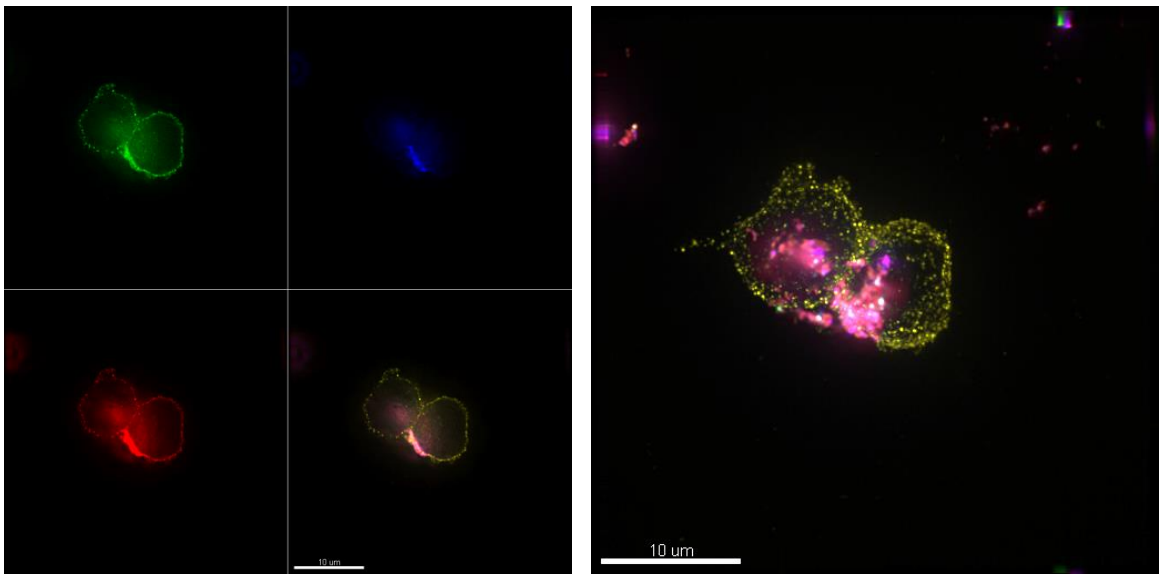

Figure 87: CLSM image of PLL brush-Antigen-CpG-aDEC205 conjugate in murine splenic DC, 1xPBS, fixated, incubation time 4h, conc. $1*10^{12}$ particles; yellow (image a): CD8-PE phenotyping stain for CD8+ DC; green: PLL-AF488; blue: Antigen-AF546; red: aDEC205-AF647, scale bar: 10µm, right: maximum intensity projection, scale bar: 10µm

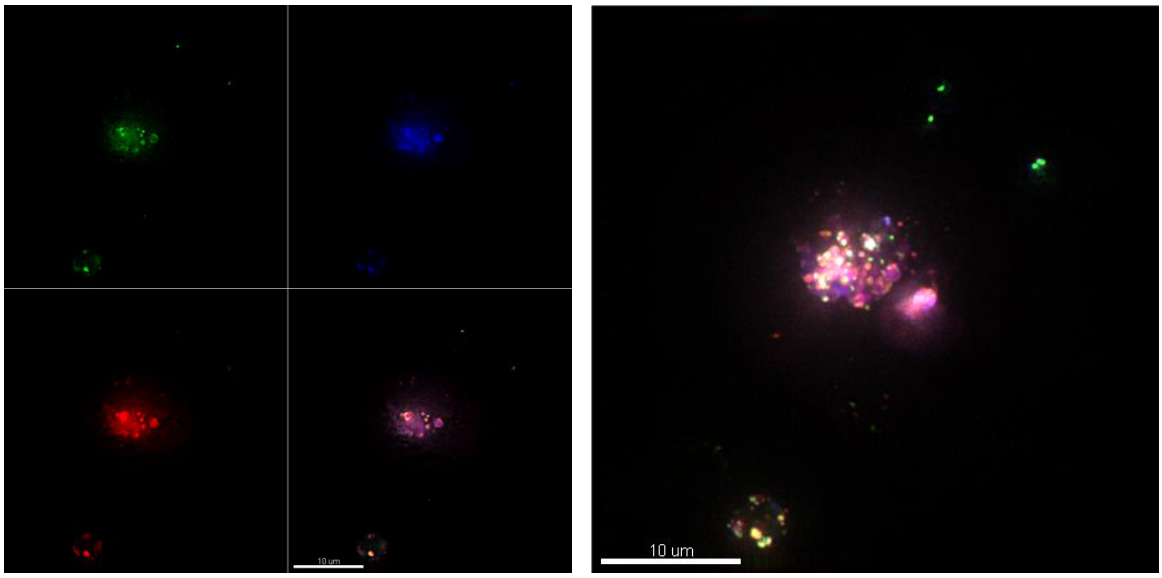

Figure 88: CLSM image of PLL brush-Antigen-CpG-aDEC205 conjugate in murine splenic DC, 1xPBS, fixated, incubation time 4h, conc. $1*10^{12}$ particles; green: PLL-AF488; blue: Antigen-AF546; red: aDEC205-AF647, scale bar: 10µm, right: maximum intensity projection, scale bar: 10µm

The Antigen cross presentation assay is performed as described for linear PLL and the results depicted in Figure 89. The curves show similar behavior to those of conjugates with linear PLL. T cell proliferation occurs in the same Antigen concentration range of $1*10^{-9}$ mole/L to $1*10^{-7}$ mole/L. For the brush conjugates saturation is not reached, so the curves do not drop in the concentration ranged tested. Again, no difference between the targeted and the un-

targeted conjugate occurs due to the high unspecific uptake of the brush. And also SIINFEKL shows the best capability to induce T cell proliferation due to the extracellular binding to MHC class II complexes.

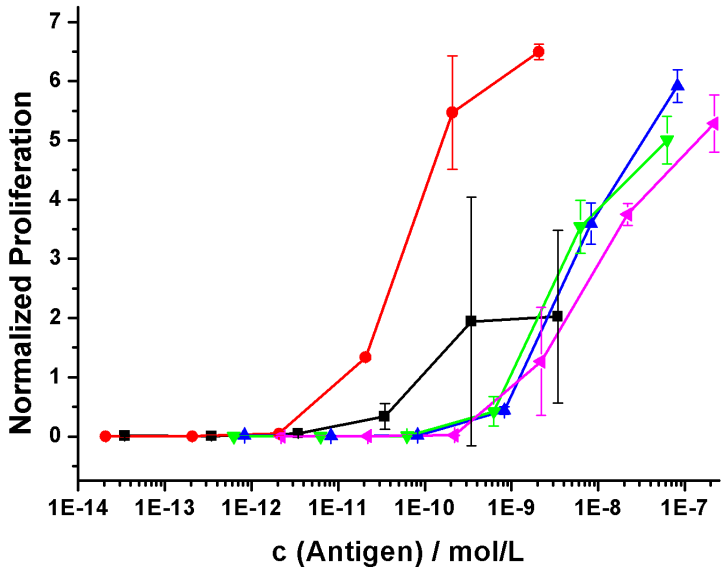

Figure 89: Antigen Presentation Assay with splenic iDC, incubated with PLL brush conjugates, and OT-I CD8+ T cells; ■ Antigen, ● SIINFEKL, ▲ PLL brush-Antigen-CpG, ▼ PLL brush-Antigen-CpG-aDEC205, ◀ PLL brush-Antigen-aDEC205

Summary of synthesis and characterization of PLL- and PLL brush-Antigen-aDEC205

In summary, synthesis of the whole three-component conjugate is accomplished via the two conjugation methods.

UV/Vis spectroscopy, gel electrophoresis and flow cytometry are used to analyze the conjugate and to prove conjugation via Schiff base formation. In general, conjugation of aDEC205 enhances internalization into bmDC as exemplarily shown for conjugate I in Figure 90 that shows particularly high internalization. For all other experiments the difference in internalization is only small.

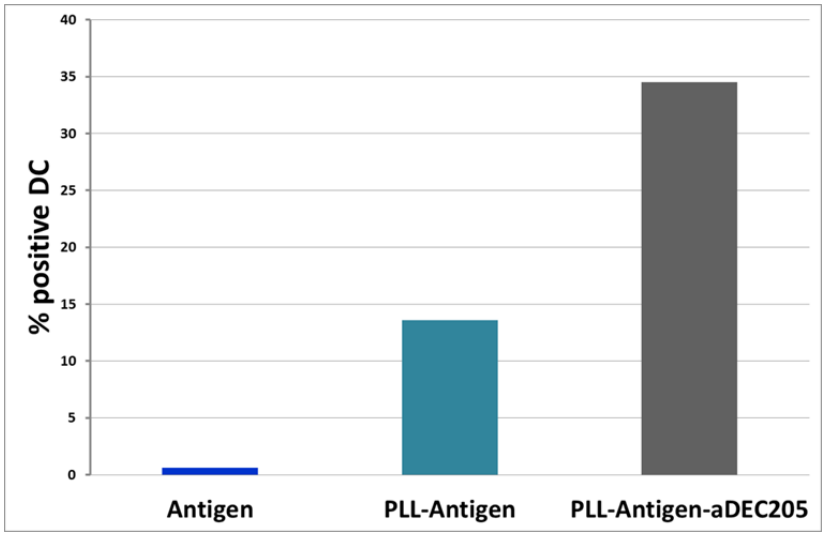

Figure 90: Comparison of internalization of Antigen, PLL-Antigen and PLL-Antigen-aDEC205 in bmDC

Colocalization of all components is observed in bmDC with CLSM and DLS reveals that no aggregate formation occurs in RPMI + 5% FCS. The antigen presentation assay shows T cell proliferation for all conjugates that contain Antigen. This proves that the conjugate is taken up and processed within DC and the Antigen is still able to activate T cells.

Conjugation via Click chemistry also results in conjugates that show colocalization of all components within splenic dendritic cells. Antigen cross presentation assays are performed and show that with escalating Antigen concentration proliferation of OT-I T cells increases.

The PLL brush conjugate exhibits higher conjugation ratios as linear PLL and also show colocalization within DC and T cell proliferation induced by Antigen-containing conjugates.

In general, the problem with the PLL-Antigen-aDEC205 and PLL brush conjugates, respectively, is the variable conjugation efficiency. Too many factors play a role during conjugation, so that no definite control over the system can be achieved. The varying conjugates obtained are characterized and show the same trend for incubation and T cell proliferation, but no reproducibility in composition is obtained.

3.4. Transfer to other polymeric carriers

PLL turned out to be not the most suitable carrier for targeted delivery as it readily enters all cell types unspecifically and no targeting with the aDEC205 antibody could be achieved. Therefore, other approaches to either reduce the positive charges of PLL or transfer the conjugation chemistry to different polymeric systems are investigated.

3.4.1. Succinylation of linear poly-*L*-lysine

In order to reduce the highly cationic charge of PLL, the lysine residues of PLL are reacted with succinimidyl ester to obtain negative charges. These reactions are performed with varying degrees of succinylation by Sabine Gietzen, group of Prof. Dr. Manfred Schmidt, and the degree of succinylation is determined with nuclear magnetic resonance spectroscopy, elementary analysis and 2,4,6-Trinitrobenzene sulfonic acid (TNBSA) assay to determine the number of amine groups.

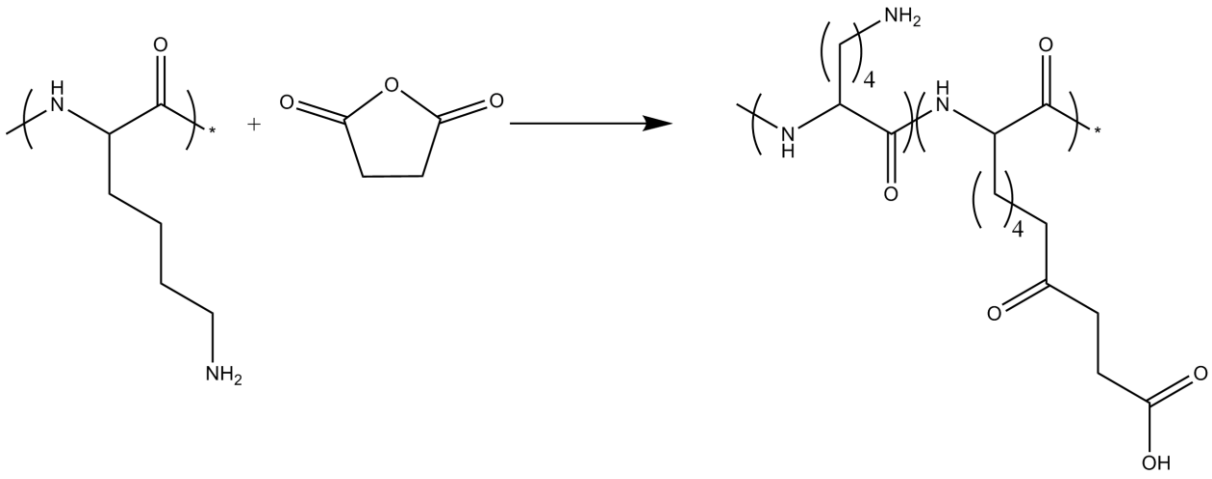

Figure 91: Scheme for succinylation of PLL

Succinylated PLL is subsequently labeled with AlexaFluor488 and analyzed with flow cytometry and CLSM. Flow cytometry exhibits high binding for 37% succ PLL and 49% succ PLL, but nearly no binding for 60% succ PLL and 70% succ PLL (Table 15 and Figure 92). This demonstrates that as soon as the polymer obtains a negative net charge it does not bind to the negatively charged cell surface anymore but the negative charges repel each other.

Table 15: Flow cytometry analysis of internalization of PLL and succinylated PLL

Polymer	PLL	37% succ PLL	49% succ PLL	60% succ PLL	70% succ PLL
Pos DC / %	99.80±0.05	91.95±1.23	77.10±3.25	2.50±0.10	2.35±0.18

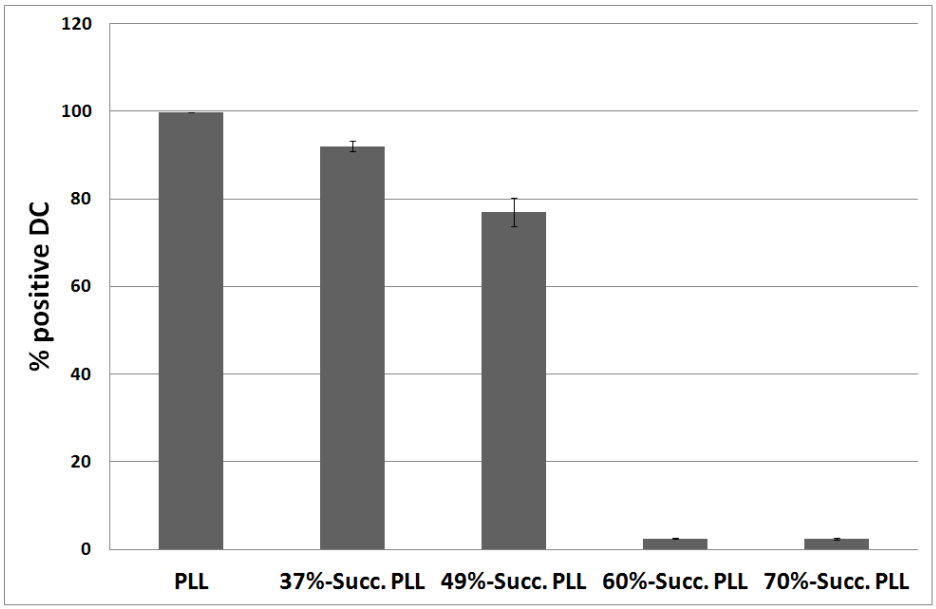

Figure 92: Internalization of PLL and succinylated PLL into bmDC

With CLSM no internalization into bmDC is observed for the 60% and 70% succinylated PLL. This indicates that unspecific uptake of PLL can be inhibited by reduction of the positive charges and generation of negative charges via succinylation.

Due to these findings, succinylation of PLL seems to be a promising approach to obtain a polymer that can be specifically targeted to dendritic cells by conjugation of the aDEC205 antibody. This strategy will be pursued by Sabine Gietzen in her PhD thesis.

3.4.2. Heparin-Protamine Nanoparticles

A completely different system investigated is heparin/protamine nanoparticles. Heparin and protamine are both natural polymers that are FDA approved and find application in clinical practice. Heparin is a polysaccharide (variable esterified glycosaminoglycanes), consisting of alternating D-glucosamine and a uronic acid (D-glucuronic acid or L-iduronic acid) with a molecular weight between 4000 and 40 000 g/mole. Heparin has a high negative charge that enables it to bind to antithrombine III which results in its coagulation-inhibiting quality and is therefore used as an anticoagulant. The molecular weight of the repeating unit is 281 g/mole and every repeating unit has average 1.43 negative charges. Protamine has a molecular weight of ~ 4250 g/mole and 21 positive charges.

Mori et al. describe the formation of heparin/protamine complexes with different dilutions and a volume ratio of 7:3 for heparin and protamine resulting in particles between 85 and 110nm. These particles are stable and show no aggregate formation. Conjugation of the cytokine FGF-2 results in protection of the molecule against degradation[179].

Thus, heparin/protamine nanoparticles (H/P NPs) are synthesized with a volume ratio of 7:3 of heparin (0.3g/L) and protamine (0.5g/L) which results in a ratio of 1.4 negative to positive charges. These heparin/protamine complexes therefore have a negative excess charge. Additionally, protamine is modified with PEG and also tested regarding its complex formation ability. Different approaches for the formation of H/P NPs are compared in Table 16 and Figure 93. Heparin is filled into the cuvette and protamine is added drop wise. In experiment 3 protamine and PEG-protamine are added alternating to the heparin solution, while for experiment 4 and 5 protamine and PEG-protamine are mixed at a ratio of 1:1 and 2:1, respectively, and then added to the heparin solution. Nanoparticles with hydrodynamic radii between 34 and 104nm are obtained, depending on the amount of PEG-protamine and the mixing technique. Heparin/protamine NPs have an R_h of 104nm while heparin/PEG-protamine NPs exhibit an R_h of 38nm. The smallest nanoparticles with 34nm are obtained when protamine and PEG-protamine is mixed at a ratio of 1:1 and a ratio of 2:1 yields NPs with R_h = 48nm. These results indicate that the size of H/P NPs is adjustable by varying the ratio of protamine to PEG-protamine.

Table 16: Different approaches for the formation of heparin-protamine nanoparticles

Experiment	Nanoparticle	Ratio heparin : protamine	R_h / nm
1	Heparin/protamine	7 : 3	104
2	Heparin/PEG-protamine	7 : 3	38
3	Heparin/protamine/PEG-protamine	7 : 1.5 : 1.5	93
4	Heparin/protamine/PEG-protamine	7 : 3 (mixture protamine/PEG-protamine 1:1)	34
5	Heparin/protamine/PEG-protamine	7 : 3 (mixture protamine/PEG-protamine 2:1)	48

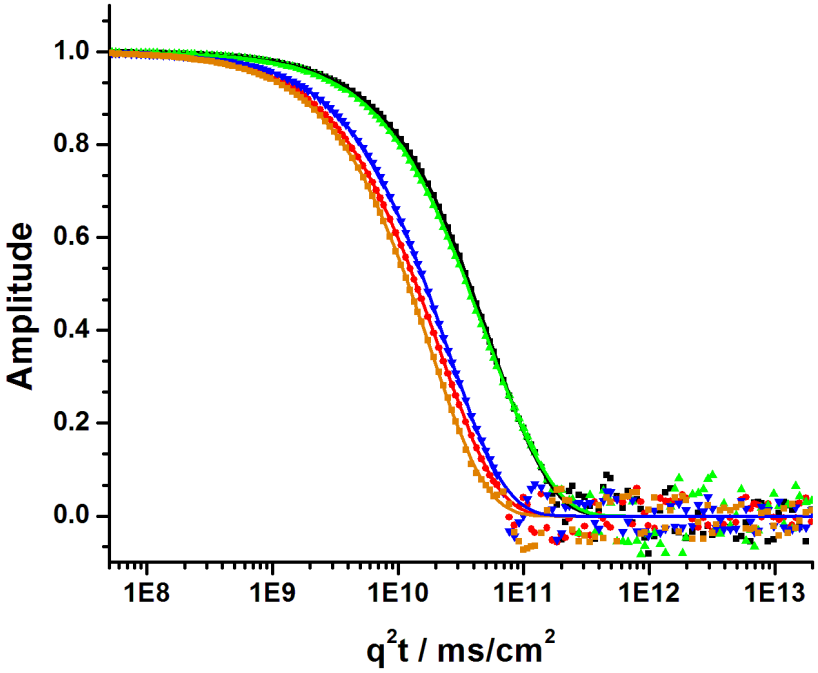

Figure 93: DLS of heparin/protamine nanoparticles in 1x PBS, θ = 30°, T = 20°C; ■: Experiment 1, ●: Experiment 2, ▲: Experiment 3, ■: Experiment 4, ▼: Experiment 5

These nanoparticles are stable at physiological salt concentration (1xPBS buffer, 0.15M NaCl) but collapse at 2M sodium chloride. Therefore, these particles are tried to crosslink with adipic acid dihydrazide. Heparin is oxidized with sodium nitrite and functionalized with an excess of adipic acid dihydrazide. Unreacted dihydrazide is removed by gel filtration and heparin-hydrazide is mixed with oxidized heparin and in different cuvettes reacted for 2h, 16h and 24h at RT and 40°C. The cuvettes are measured before and after addition of sodium chloride to a final concentration of 2M. Before salt addition the particles exhibited hydrody-

namic radii between 118 and 147nm after 2h incubation at RT, 196nm after 16h incubation at RT and ~300nm after 16 and 24h incubation at 40°C. After addition of salt the particles collapse and the single components can be detected next to aggregates. These findings indicate that the crosslinking reaction between heparin-hydrazide and oxidized heparin is not successful.

So far, the H/P NPs had a final charge ratio -/+ of 1.43 which means the particles are negatively charged. But the charge ratio where the drop hits the solution is -/+ = 0.62, as heparin has 1.42 negative charges per 281g/mole and a concentration of 0.3g/L and protamine has 21 positive charges per 4250g/mole and a concentration of 0.5g/L. Therefore, particles with equal charge concentrations at the local area where the drop hits the surface are produced by reducing the concentration of protamine to 0.3g/L.

The NP size increases with addition of protamine to a solution until it reaches a critical concentration at a molar fraction of negative charges of 0.4 where the particles start to aggregate (Figure 94). It is not possible to reach the miscibility gap by adding heparin to protamine as aggregates form immediately. The same trend is visible if protamine at a concentration of 0.3g/L (blue) or 0.1g/L (red) is added to 0.3g/L heparin.

These results show that the hydrodynamic radius stays constant up until a charge ratio -/+ of ~0.4, which means that the complexes always have to be negatively charged.

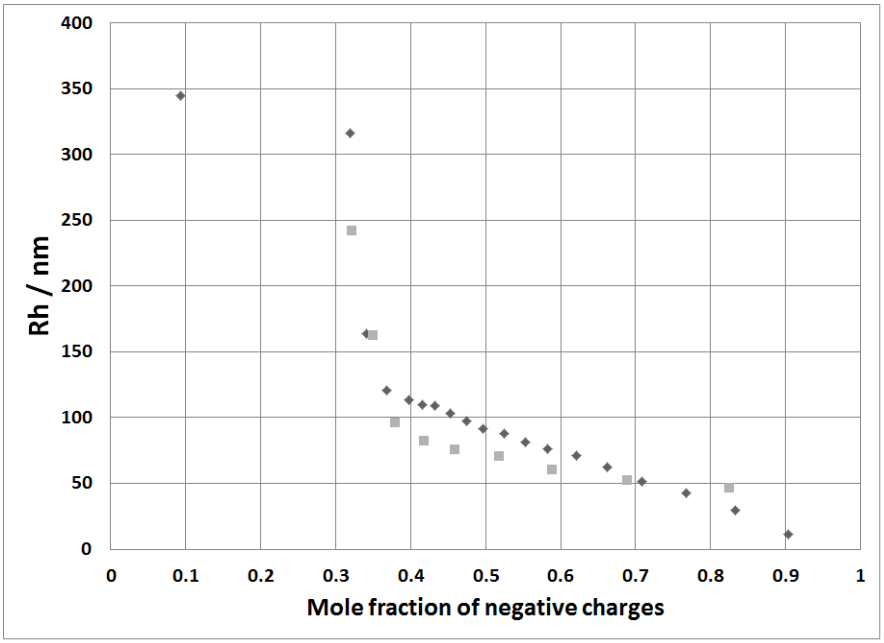

Figure 94: Hydrodynamic radius with mole fraction of negative charges for heparin/protamine nanoparticles; blue: concentrated, red: diluted

Before heparin and protamine are mixed to form complexes, they can be conjugated with biocomponents. Thus, different conjugation strategies seem reasonable.

Antibodies can be conjugated to protamine through modification of the N terminus of protamine with Sulfo-LC-SPDP via the amine-reactive NHS ester. The other end of the spacer is terminated in the pyridyl disulfide group that reacts with free thiols to form a reversible disulfide bond. Thus, SPDP-modified protamine can react with the thiols in the hinge region of a reduced antibody or with thiol-modified antigen and/or CpG. The pyridyl disulfide can also be reduced to obtain a free thiol group that can react with maleimide-functionalized antibodies.

Another strategy is conjugation of the antibody to heparin. This can be achieved by oxidation of heparin and the glycosidyl residues of the antibody and conjugation via a dihydrazide linker[180], e.g. adipic acid dihydrazide.

No results are obtained for these conjugation reactions so far. Problems with this system are the difficult characterization of oxidized heparin and the amount of heparin- or protamine-antibody conjugate that has to be synthesized as a huge amount of sample is needed to form heparin-protamine complexes. Furthermore, it is not known how conjugation might affect the complex formation.

4. Summary and Outlook

In this thesis, the synthesis and characterization of polymer conjugates for application in cancer immunotherapy were investigated.

Two different polymeric carriers were studied, linear poly-*L*-lysine (PLL) and a polylysine brush (PLL brush). To convey biological function, three biologically active components were conjugated to these polymers: an antiDEC205-antibody for specific targeting of CD8+ dendritic cells; an OVA-specific model Antigen with the core peptide sequence SIINFEKL which initiates a specific immune response against cancer cells presenting this antigen; and an immune-activating TLR9 ligand (CpG1826).

First, the binding affinity and internalization kinetics of different antibodies to immature and mature CD8+ DC was investigated to determine if aDEC205 is the most suitable antibody to target CD8+ DC. CD8+ DC are able to cross-present exogenous antigen and induce a CD8+ CTL immune response and therefore are the prime target for vaccine therapies.

To perform the experiments with DC of different maturation states, i.e. immature and mature DC, different maturation stimuli for DC were investigated, CpG, LPS, poly I:C and overnight culture. As all yielded the same aDEC205 internalization kinetics, overnight culture was chosen to induce maturation of DC for all further experiments with mature DC.

To investigate the internalization kinetics, antibodies were labeled with the SHIP internalization sensor via copper free click chemistry at a SHIP to antibody ratio of ~1:1. This sensor enabled the differentiation between material internalized and bound to the cell surface. The antibodies investigated were aDEC205, CD11c, MHC class II, Clec12a and Clec9a. CD11c integrin is known to be a universal DC marker and was found to be highly expressed on immature splenic DC. aDEC205 and Clec12a showed high binding specificity for CD8+ DC while their receptors were not expressed on CD8- DC. MHC class II and Clec9a exhibited lower binding, but were still selective for CD8+ DC. In mature DC there was no difference in the expression of the CD11c receptor compared to immature DC and there was a slight increase in the expression of DEC205 on CD8+ DC. aDEC205 and Clec12a showed no capping, while CD11c and MHC class II exhibited a loss of fluorescence intensity with time which indicated that the antibody-receptor complex was pulled from the cell surface rather than being inter-

nalized. With the SHIP internalization techniques the results of MHC class II and CD11c antibody could be corrected for capping which avoided overestimation of internalization.

aDEC205 showed the fastest and highest uptake into CD8+ immature and mature DC. Clec12a also exhibited similar kinetics, only a little lower. MHC class II and CD11c showed medium internalization into CD8+ iDC and decreased uptake into mDC. These results revealed that mDC internalize via receptor-mediated endocytosis and aDEC205 was the most suitable antibody for targeting CD8+ iDC and mDC.

Characterization of aDEC205 with DLS resulted in an R_h of 5nm and no aggregation in 1x PBS at 20°C and 37°C or with PLL. Gel electrophoresis confirmed a molecular weight of 150kDa and showed reduction of disulfide bonds to obtain single chain fragments. Labeling of the lysine residues of aDEC205 with AlexaFluor647 NHS ester resulted in a degree of labeling of three dyes per antibody molecule, determined by UV/Vis spectroscopy and FCS. Fluorescence spectroscopy revealed no drop in quantum yield. With aDEC205-AF647, approximately 22% of bone marrow-derived DC could be labeled and thus identified as CD8+ DC.

The polymers were surveyed for their application as carriers for immunotherapy. Light scattering experiments with linear PLL determined the M_w to be 14700 g/mole and R_h 3.1nm. Labeling the lysine residues with AlexaFluor 488 TFP ester yielded one dye per polymer chain and a quantum yield drop of a factor of 1.5 with no change in R_h. The PLL brush with a molecular weight of approximately $8*10^6$ g/mole was labeled with AlexaFluor488 NHS ester to obtain approximately 50 dyes per brush with a quantum yield drop of a factor of two and no change in R_h. PLL showed no significant toxicity in HeLa or JAWS II cells, while for the PLL brush only one third of the cells survive. However, after conjugation of aDEC205 and/or Antigen toxicity was dramatically decreased and limited toxicity was observed for all samples.

The components conjugated to the polymeric carrier were an OVA-derived tumor-associated antigen for the specificity of the immune response and an activating TLR9 ligand CpG for enhancement of CTL immunity. Antigen and CpG were conjugated to maleimide-functionalized PLL and PLL brush via free thiol groups and the labeling efficiency of PLL / PLL brush-Antigen was determined with UV/Vis spectroscopy. Conjugation of Antigen to the polymer was proven by SDS PAGE, flow cytometry and colocalization in bmDC determined by CLSM. FACS exhibited diminished uptake compared to free PLL due to the reduction of positive charges. Antigen alone was not internalized, but conjugated to the carrier antigen inter-

nalization was increased. The PLL conjugates showed hydrodynamic radii of ~70nm, but no further aggregation in cell medium.

In order to target the conjugate to cross-presenting CD8+ DC, aDEC205 was used as a targeting moiety. Conjugation of aDEC205 to the polymer was conducted via two ways, Schiff base formation and subsequent reduction to yield a stable secondary amine as a "zero-length crosslinker" or via copper free click chemistry with DIBO-modified PLL and PEG-azide functionalized aDEC205. Purification of the conjugates was difficult as there is only a marginal difference in the size and molecular weight. Flow cytometry and CLSM demonstrated successful conjugation as for the conjugates colocalization was observed in bmDC while the control experiments with unconjugated components exhibited no colocalization inside DC. SHIP experiments showed high binding of PLL and PLL-antibody conjugates with aDEC205, CD11c and a control IgG to immature and mature CD8+ DC. Internalization occurred into immature DC, however, mature DC only internalized free aDEC205, not the PLL-antibody conjugates which indicated that these conjugates were only internalized via unspecific uptake and no receptor-mediated uptake could be imparted by conjugation of the aDEC205 antibody.

In order to obtain the complete conjugate, Antigen and CpG were conjugated first, before the antibody was reacted in order to preserve antibody reactivity. The labeling efficiency of PLL/ PLL brush-Antigen-aDEC205 was determined with UV/Vis spectroscopy and conjugation was proven by SDS PAGE. Colocalization within DC was observed with CLSM while no colocalization occurred for unconjugated components. Flow cytometry showed marginally enhanced uptake for the targeted conjugate compared to PLL-Antigen. DLS revealed formation of small aggregates for the PLL conjugates, probably due to the hydrophobic linker and ionic interactions between PLL and CpG, but no further aggregation occurred in cell medium or human serum. Antigen cross-presentation assays exhibited proliferation of OT-I T cells for all conjugates containing Antigen, while conjugates without Antigen served as a negative control and showed no T cell proliferation. There was no difference in T cell proliferation for the targeted and untargeted conjugate.

In summary, these results constituted a promising foundation for further research in the field of polymeric carriers for cancer immunotherapy. aDEC205 was confirmed to be the

most suitable antibody for targeting immature and mature CD8+ DC as its internalization is faster than all other antibodies. The synthesis of hybrid materials consisting of antigen, adjuvant and aDEC205 antibody conjugated to a polymeric carrier was demonstrated and their bioactivity shown in antigen presentation assays as antigen-containing conjugates showed T cell proliferation. The conjugates bound to both iDC and mDC, but only internalized into iDC – this shows that the interaction of PLL dominates over the antibody and that the antibody is sterically shielded or inactive. No specific internalization of the conjugates via receptor-mediated endocytosis could be achieved by conjugation of the targeting antibody. The reason may be that the antibody is sterically shielded by the polymer or that the antibody loses its bioactivity during the conjugation reaction. Hence, it is a major challenge for future research to conjugate the antibody to a polymeric carrier in a way that antibody-mediated targeting and specific internalization can be achieved.

Another major drawback for application as a carrier for targeted therapy is the high unspecific uptake of the polymers into all cells due to their high cationic charge. Preliminary results showed that diminishing positive charges by succinylation of PLL inhibits unspecific uptake and therefore succinylated PLL is further investigated in another PhD thesis. Additionally the conjugation chemistry can be transferred to other polymers such as poly(oxazoline) brushes or zwitterionic poly-ε-methacryloly-*L*-lysine. These systems are expected to exhibit no unspecific uptake and no aggregation in human serum and therefore seem to be promising carriers for application in cancer immunotherapy.

5. Experimental Part

5.1. Labeling Protocols

5.1.1. Labeling of Antibodies with fluorescent dyes

Labeling instructions for AlexaFluor dyes

AlexaFluor647 Protein Labeling Kit (Cat# A20173):

To 0.5mL aDEC205 (2mg/mL in 1xPBS) 100µL 1M sodium bicarbonate solution are added to raise the pH of the reaction solution. This is necessary as succinimidyl ester react most efficiently at alkaline conditions between pH 7.5 and 8.5. The alkaline antibody solution is transferred into the vial with reactive dye and incubated at RT for 1h in the dark agitating. The reaction mixture is purified with a BioRad BioGel P-30 column and 1xPBS as eluent. Two fractions can be observed, the first one being the antibody-dye conjugate which runs a lot faster than free dye due to the high molecular weight of the antibody.

AlexaFluor647 Carboxylic Acid Succinimidyl Ester (Cat# A20006):

Labeling is performed as described above. With 1mg dye dissolved in 0.5mL DMSO 36.5mg aDEC205 is labeled and purification is accomplished with BioRad BioGel P-100.

The degree of labeling (DOL) is determined with UV/Vis spectroscopy and Fluorescence correlation spectroscopy (FCS) to be ~3 dyes per antibody molecule.

UV/Vis spectroscopy:

$$Protein\ concentration\ (M) = \frac{[A_{280} - (A_{650} * 0.03)] * dilution\ factor}{203\ 000}$$

Where 0.03 = correction factor for the contribution of the dye to the absorption at 280nm, and 203 000 = ε of the IgG antibody at a wavelength of 280nm

$$mole\ dye\ per\ mole\ protein = \frac{A_{650} * dilution\ factor}{239\ 000 * protein\ conc.\ (M)}$$

With 239 000 = ε of AlexaFluor 647 at a wavelength of 650 nm.

Representative example for the calculation:

Table 17: Calculation for degree of labeling

Sample	Dilution factor	A_{650}	A_{280}	Protein conc. / M	# dyes per Ab
aDEC205-AF647	30	0.39	0.12	$1.56*10^{-5}$	3.14

Fluorescence correlation spectroscopy:

Representative calculation

- AlexaFluor 647: Diffusion time = 350µs, counts per molecule = 7.3
- aDEC205-AF647: Diffusion time = 370µs, counts per molecule = 28.4

  ➔ (28.4/7.3) = 3.89 dyes per antibody molecule

Labeling of antibodies with AlexaFluor succinimidyl ester

Incubate 50µL of antibody (~5g/L) with 10µL of AlexaFluor succinimidyl ester (10g/L) for 2h on ice. Purify with Zeba 7k Column. Labeling efficiency is determined with Nanodrop to be ~1.5.

5.1.2. Labeling of Polymers with AlexaFluor 488 fluorescent dyes

The polymer is dissolved in 1xPBS overnight. 100µL 1M sodium bicarbonate pro mL reaction volume is added to raise the pH as TFP ester react most efficiently at slightly alkaline pH. The PLL solution is transferred into the vial with reactive dye and incubated at RT for 1h in the dark agitating. The reaction mixture is purified with a BioRad BioGel P-30 column and 1xPBS as eluent.

The degree of labeling is determined with FCS.

Representative calculation

- AlexaFluor 488: Diffusion time = 22.6µs, counts per molecule = 6.2
- PLL-AF488: Diffusion time = 112.1µs, counts per molecule = 8.5

  ➔ (8.5/6.2) = 1.37 dyes per polymer chain

Table 18: Labeling conditions for PLL with AlexaFluor488

	$m_{polymer}$ / mg	$n_{polymer}$ / mole	dye	m_{dye} / mg	n_{dye} / mole	Purification	Degree of Labeling
PLL	4	$5.0*10^{-7}$	AF488 NHS (643.41)	1.8	$2.80*10^{-6}$	BioGel P30	1
PLL	4.5	$6.0*10^{-7}$	AF488 TFP (884.91)	1	$1.13*10^{-6}$	BioGel P30	1
PLL brush	19	$2.4*10^{-9}$	AF488 NHS (643.41)	1	$1.55*10^{-6}$	BioGel P30, Amicon 10k	50
Succ-PLL	1	$1.3*10^{-7}$	AF488 TFP (884.91)	0.25	$2.83*10^{-7}$	BioGel P30	1-2
Poly(ε-methacryloyl-*L*-lysine)	31	$5.4*10^{-8}$	AF488 NHS (643.41)	1.3	$2.0*10^{-6}$	Amicon Ultra Centrifugal Filter Units 3k	15

5.1.3. Labeling of Antigen with AlexaFluor 546 NHS Ester

To 0.5mL antigen (2mg/mL in 1xPBS) 100µL 1M sodium bicarbonate solution are added to raise the pH of the reaction solution. This is necessary as succinimidyl ester react most efficiently at alkaline conditions between pH 7.5 and 8.5. The alkaline antigen solution is transferred into the vial with reactive dye and incubated at RT for 1h in the dark agitating. The reaction mixture is purified with a BioRad BioGel P-30 column and 1xPBS as eluent. Only a single band is observed, free dye cannot be removed from the conjugate. This is expected as AlexaFluor546 has a molecular weight of ~1.1kDa and antigen ~1.8kDa. Therefore the differ-

ence between the molecular weight of the free dye and of the antigen-dye conjugate is not sufficient to separate those via size exclusion chromatography. Further separation or analytical techniques like analytical ultracentrifugation yielded no results to determine the degree of labeling or to separate. Therefore, due to the molar ratio that is used for labeling the labeling efficiency is assumed to be one dye per peptide molecule.

5.2. Conjugation Protocols

5.2.1. Conjugation of Antibodies with SHIP Internalization Sensor

Functionalization of antibody with DIBO

Prepare all samples on ice. Add 20µL of DIBO (1g/L in DMSO) to antibody solution (~5g/L). Incubate samples in the fridge for 2h.

Prepare Zeba Spin Desalting columns 7k by centrifuging at 1500g for 1 min with soft slow-down to remove preserving agent. Wash column once with PBS buffer.

Fill samples up to 100µL and load to the middle of the column. Spin columns for 2 min at 1500g to remove excess of crosslinker.

Labeling with SHIP sensor

Add 10µL of azide-functionalized DNA [FIPCy5 (5’ Cy5-TCAGTTCAGGACCCTCGGCT-N3 3’)] labeled with AlexaFluor647 to DIBO-labeled antibody and incubate in the fridge overnight.

Prepare Zeba Spin Desalting Columns 40k, fill samples up to 100µL and centrifuge to remove unconjugated DNA. Nearly no color remains in the columns.

Measurement of labeling efficiency

Nanodrop 1000, Program ND-100 V3.8.1, Proteins and Labeling

Clean the instrument with water. Initialize the instrument with water and measure a blank sample of water. Measure PBS buffer as blank sample, then measure the samples. The ratio of the absorbance at a wavelength of 647 over that at 280 is calculated and gives the labeling efficiency of 1.2 to 1.4 depending on the antibody.

5.2.2. Conjugation of polymer with SHIP Internalization Sensor

PLL-SHIP Conjugates

Incubate 100µL of PLL-AF488 with 20µL DIBO (1g/L in DMSO) for 2h on ice. Remove excess of DIBO with Zeba 7k column.

At the same time incubate 50µL of DEC205-AF555, CD11c-AF555 and cIgG-AF555 with 10µL PEG_{2000}-NHS-azide (10g/L in DMSO) for 2h on ice and purify with Zeba 7k column.

React

50µL PLL-DIBO + 10µL DNA-azide and

50µL PLL-DIBO + 10µL DNA-azide + 20µL DEC-azide and

50µL PLL-DIBO + 10µL DNA-azide + 20µL cIgG-azide and

50µL PLL-DIBO + 10µL DNA-azide + 30µL CD11c-azide.

Incubate in fridge overnight. Purify antibody sample with Zeba 40k column, other sample cannot be purified due to the very similar molecular weight of PLL and DNA.

PLL brush-SHIP Conjugates

Incubate 85µL of PLL brush-AF488 with 15µL DIBO (1g/L in DMSO) for 2h on ice. Remove excess of DIBO with Zeba 7k column.

React

50µL PLLb-DIBO + 10µL DNA-azide and

50µL PLLb-DIBO + 10µL DNA-azide + 20µL DEC205-AF555-azide.

Incubate samples for 4h at 4°C and purify with Zeba 40k column.

Table 19: UV/Vis spectroscopy absorption for PLL brush-SHIP conjugates

Sample	**A_{495}**	**A_{555}**	**A_{650}**	**comments**
PLL-SHIP	0,855		0,031	Aggregation of SHIP with PLL?!
PLL-SHIP-DEC205	0,319	0,045	0,009	
PLLb-SHIP	0,892		0,502	
PLLb-SHIP-DEC205	0,549	0,093	0,262	

5.2.3. Conjugation of PLL with aDEC205 (PLL-aDEC205)

Schiff Base formation of PLL with oxidized aDEC205 (Method 1)

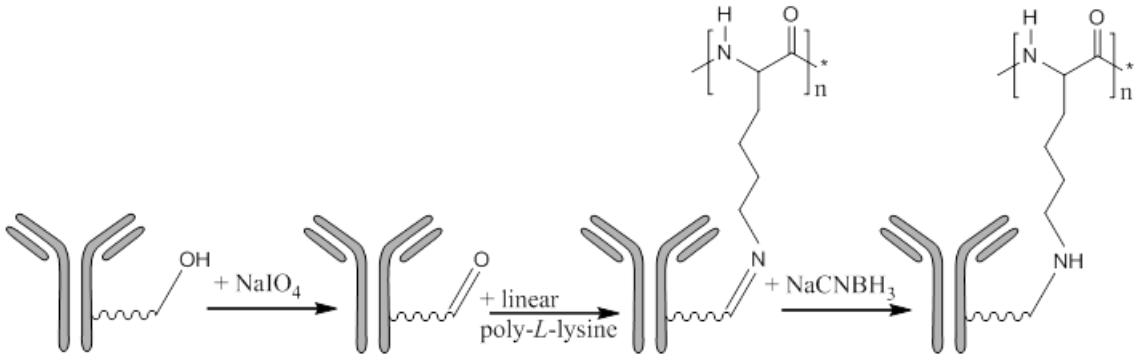

Figure 95: Reaction scheme of conjugation of PLL with aDEC205 via Schiff Base formation

Oxidation of aDEC205

Oxidation of fluorescence labeled aDEC205 with sodium periodate provides aldehyde groups in the Fc region on the glycosidyl residues of the antibody.

Per mL of aDEC205 solution (1mg/mL in 1xPBS) 100µL sodium periodate solution (21.4mg/mL in H_2O; 0.1M) are added and incubated for 20 min at RT in the dark. The final concentration of sodium periodate in the reaction mixture is 10mM. Excess of sodium periodate is removed with a Sephadex G25 NAP 5 column with sodium bicarbonate buffer at pH 9.6. The oxidized antibody is immediately reacted with amine-containing probes.

Reaction of oxidized aDEC205 with PLL

Oxidized aDEC205-AF647 is conjugated to PLL-AF488 in 0.2M sodium bicarbonate buffer at pH 9.6. The reaction mixture is incubated for 2h until 7h at RT in the dark and subsequently reduced with sodium cyanoborohydride (13mg/40µL, 5M) to a final concentration of 50mM.

The different experiments performed are summarized in Chapter 3.3.1, Table 7.

Different purification strategies are performed: BioRad BioGel P-30 and P-100, Sephadex G25 NAP5, Amicon Ultra Centrifugal Filter 50kDa after manufacturer instructions.

Click Reaction of PLL-DIBO with aDEC205-PEG-azide (Method 2)

PLL is reacted with DIBO-NHS and purified with Zeba 7k. aDEC205 is incubated with NHS-PEG_{2000}-azide and purified with Zeba 7k. PLL-DIBO and aDEC205-PEG_{2000}-azide are incubated for 2h at RT and purified with Zeba 40k (see also page 158 and page 161).

5.2.4. Conjugation of PLL with Antigen (PLL-Antigen)

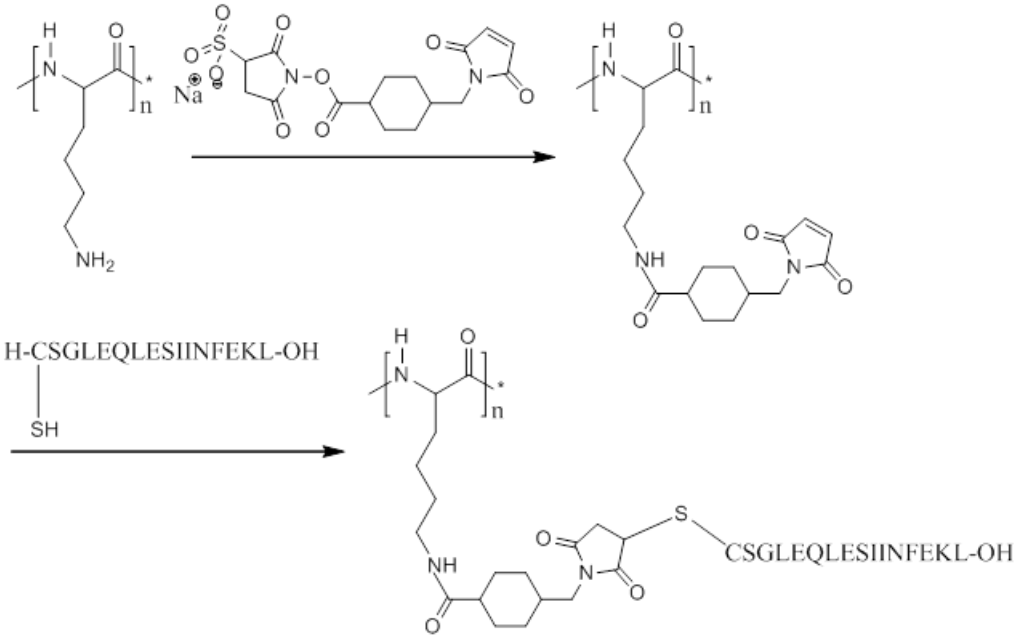

Figure 96: Reaction scheme of PLL with Antigen

Functionalization of PLL-AF488 with Sulfo-SMCC:

PLL-AF488 is functionalized with Sulfo-SMCC at a ratio of ~4 repeating units per linker, which means 25% of all repeating units are targeted to be maleimide-functionalized. PLL is dissolved in 1xPBS and Sulfo-SMCC in H_2O (salt reduces solubility) is added to the solution. After 30min incubation at RT unreacted crosslinker is removed with a Sephadex G25 NAP5 column.

Reduction of the fluorescence labeled antigen:

For the first two experiments, Antigen is reduced with DTT. But unremoved DTT can also react with maleimides and therefore reduce conjugation efficiency. Therefore, TCEP, which

does not react with maleimides and does not have to be removed completely, is used for all further reductions at a molar excess of 1:10.

Reaction of PLL with antigen:

Maleimide functionalized PLL is reacted for 6h at RT with antigen-SH to form stable thioether bonds.

The different PLL-Antigen experiments are summarized in Chapter 3.3.2, Table 9.

5.2.5. Reaction of PLL with aDEC205 and Antigen (PLL-Antigen-aDEC205)

Via Schiff Base formation (Method 1)

PLL-Ag is conjugated as described before and then purified with Sephadex G25 NAP5 to exchange PBS buffer to 0.2M sodium bicarbonate buffer pH 9.6. aDEC205 is oxidized with $NaIO_4$ and subsequently reacted with PLL-Ag as described previously for PLL.

Different purification methods are tested as BioRad BioGel P-30 and P-100, Sephadex G25 NAP-5, Amicon Ultra Centrifugal Filter Units 40kDa.

The different conjugation experiments are shown in Table 10 in Chapter 3.3.3.

Via DIBO click reaction (Method 2)

Approach 1:

React 400µL PLL-AF488 ($1.5x10^{-5}$ mole/L) with 10µL Sulfo-SMCC (10g/L), immediately take out 100µL, add another 5µL Sulfo-SMCC and to the other 300µL PLL add 60µL DIBO (1g/L) and incubate for 2h on ice. Purify both samples with Zeba 7k column.

Incubate 60µL SIINFEKL ($9.4x10^{-4}$ mole/L) with 10µL TCEP (10g/L) and 15µL CpG (10g/L) with 15µL TCEP (10g/L) for 2h on ice.

Tube 1: PLL-Ag: 100µL PLL + 20µL Ag

Tube 2: PLL-CpG: 100µL PLL + 5µL CpG

Tube 3: PLL-Ag-CpG: 100µL PLL + 20µL Ag + 5µL CpG

Tube 4: PLL-Ag-CpG: 100µL PLL (without DIBO) + 20µL Ag + 5µL CpG

Incubate on ice/ in fridge overnight, do not purify.

React 150µL DEC205-AlexaFluor647 + 25µL PEG_{2000}-NHS-azide (20g/L), incubate for 5h on ice, purify with Zeba 7k column.

Add 50µL DEC205-AF647-azide to tubes 1-3 and incubate for 4h at 4°C.

Table 20: UV/Vis spectroscopy absorption for PLL conjugates via Click Chemistry and approach 1

Conjugate	A at 495nm	A at 560nm	A at 650nm
PLL-Ag-CpG	0.51	0.231	0
PLL-Ag-CpG-DEC	0.26	0.188	0.065
PLL-Ag-DEC	0.332	0.284	0.302
PLL-CpG-DEC	0.392	0	0.112

Approach 2:

Incubate 200µL PLL-AF488 ($1.5x10^{-5}$ mole/L) with 5µL Sulfo-SMCC (10g/L) for 2h on ice. Purify with Zeba 7k column. Incubate 30µL SIINFEKL ($9.4x10^{-4}$ mole/L) with 5µL TCEP (10g/L) and 100µL CpG (1g/L) with 10µL TCEP (10g/L) for 2h at RT.

Tube 1: PLL-Ag: 50µL PLL + 10µL Ag

Tube 2: PLL-CpG: 50µL PLL + 60µL CpG

Tube 3: PLL-Ag-CpG: 100µL PLL + 20µL Ag + 40µL CpG

Incubate on ice/ in fridge overnight. Purification with Zeba columns is not possible because of the very similar molecular weight of PLL and PLL conjugate.

React samples with 10µL DIBO (only ½ of tube 3) and purify with Zeba 7k column.

Incubate 150µL DEC205-AF647 with 50µL PEG_{2000}-NHS-azide (10g/L in DMSO) and purify with Zeba 7k column. Add 50µL DEC205-AF647-azide to each DIBO-functionalized sample and incubate for 4h at 4°C.

Table 21: UV/Vis spectroscopy absorption for PLL conjugates via Click Chemistry and approach 2

Conjugate	A at 495nm	A at 560nm	A at 650nm
PLL-Ag-CpG	0.248	0.124 ($1.11x10^{-5}$mole/L)	
PLL-Ag-CpG-DEC	0.213	0.200 ($1.79x10^{-5}$mole/L)	0.522
PLL-Ag-DEC	0.112	0.034 ($3.04x10^{-7}$mole/L)	0.333
PLL-CpG-DEC	0.164	0.030 = 0	0.317

PLL conjugates with different control antibodies

Incubate 250µL PLL-AF488 ($1.5x10^{-5}$ mole/L) with 7µL Sulfo-SMCC (10g/L) and 50µL DIBO (1g/L) for 2h on ice and purify with Zeba 7k column.

Incubate 40µL Antigen ($9.4x10^{-4}$ mole/L) with 7µL TCEP (10g/L) and 20µL CpG (10g/L) with 20µL TCEP (10g/L) for 2h on ice, purify with Zeba 7k column.

Incubate 150µL PLL-Linker with 47µL Antigen and 40µL CpG for 2h on ice, purify with Zeba 7k column

Incubate each 50µL DEC205 and 100µL CD11c or cIgG with 9µL PEG_{2000}-NHS-azide (20g/L) for 2h on ice, purify with Zeba 7k column.

React 50µL PLL-Ag-CpG with 25µL DEC205 or 100µL CD11c/ cIgG on ice overnight and purify with Zeba 40k column

PLL-Ag- CpG-DEC/ PLL-Ag- CpG-CD11c/ PLL-Ag- CpG-cIgG

5.2.6. PLL brush Conjugates

Via Schiff Base formation (Method 1)

PLL brush conjugates are synthesized analogous to PLL conjugates described in Chapter 3.3.3.

Table 22: Conjugation reactions for PLL brush conjugates via Schiff base formation

	Mass / mg	**Mole**	**concentration**	**solvent**
PLL brush(AF488)	2	$2.5*10^{-10}$	10 mg/mL	1x PBS, pH 7.2
Sulfo-SMCC (MW= 436.37)	1.25	$2.7*10^{-6}$	25 mg/mL	H_2O
Antigen (AF546), red. mit TCEP	1	$5.5*10^{-4}$	2 mg/mL	1xPBS, pH 7.2
aDEC205	0.8	$5.3*10^{-9}$	1.6 mg/mL	Sodium bicarbo-nate buffer, pH 8.5

Via DIBO Click Chemistry (Method 2)

Incubate 100µL PLL brush-AF488 with 8µL Sulfo-SMCC (10g/L) for 2h on ice. Purify with Zeba 7k column.

Incubate 30µL SIINFEKL ($9.4x10^{-4}$ mole/L) with 5µL TCEP (10g/L) and 100µL CpG (1g/L) with 10µL TCEP (10g/L) for 2h at RT.

Tube 1: PLL brush-Ag: 25µL PLL brush + 10µL Ag

Tube 2: PLL brush-CpG: 25µL PLL brush+ 60µL CpG

Tube 3: PLL brush-Ag-CpG: 50µL PLL brush+ 20µL Ag + 40µL CpG

Incubate at 4°C overnight, do not purify.

React samples (only ½ of tube 3) with 10µL DIBO (1g/L in DMSO) and purify with Zeba 7k column. Incubate 150µL DEC205-AF647 with 50µL PEG_{2000}-NHS-azide (10g/L) and purify with Zeba 7k column. Add 50µL DEC205-AF647-azide to each tube and incubate for 4h at 4°C.

Table 23: UV/Vis spectroscopy absorption for PLL brush conjugates via Click Chemistry

Conjugate	A at 505nm	A at 560nm	A at 650nm
PLL_B-Ag-CpG	0,28	0,385 ($3,44*10^{-5}$mole/L)	
PLL_B-Ag-CpG-DEC	0,149	0,155 ($1,38*10^{-5}$mole/L)	0,457
PLL_B-Ag-DEC	0,0,15	0,055 ($0,5*10^{-6}$mole/L)	0,557
PLL_B-CpG-DEC	0,107	0	0,368

5.3. Heparin-Protamine Nanoparticles

5.3.1. PEGylation of Protamine

Protamine is PEGylated as reported by Chang *et al*.[181].

A freshly prepared solution of 750mg PEG NHS ester in 10mL 1xPBS is added to 500mg protamine dissolved in 10mL 1xPBS. To the slightly dull solution additional 10mL 1xPBS are added to obtain a clear yellowish solution. The solution is stirred overnight at RT and subsequently dialyzed against Milli-Q-water to remove salt before freeze-drying.

Separation of unreacted PEG is tried via anion exchange (AG1-X8), but protamine and PEG elute simultaneously so that no separation can be obtained.

Table 24: Reaction conditions for PEGylation of protamine

	Mass /g	MW / g/mole	mole	Equivalent	Concentration	Solvent
Protamine	0.5	4250	$1.2*10^{-4}$	0.8	100 g/L	1x PBS
PEG-NHS-Ester	0.75	5000	$1.5*10^{-4}$	1	75 g/L	1x PBS

5.3.2. Oxidation of Heparin

Heparin is oxidized with sodium nitrite as reported by Liang *et al.*[182].

510mg Heparin are dissolved in 150mL Milli-Q-water and cooled to 0°C in an ice bath. 10mg $NaNO_2$ are added to the solution and the pH is adjusted to 2-3 with HCl. The reaction mixture is stirred for 30 min at 0°C and then terminated by adjusting the pH to 7 with NaOH. The solution is dialyzed against Milli-Q-water (MWCO 1kDa) before freeze drying.

The amount of aldehydes generated by oxidation is determined by complexation with Purpald and UV/Vis measurements[183].

5.3.3. Reaction of oxidized Heparin with Adipic acid dihydrazide

10mg of oxidized heparin are dissolved in 2mL 0.05M sodium acetate buffer and 5mg adipic acid dihydrazide in 0.5mL buffer are added and agitated for 2h at RT. The reaction mixture is purified via Sephadex G25 NAP 5 with 0.3M sodium acetate buffer.

Conjugation of dihydrazide is proven with GPC (Figure 97).

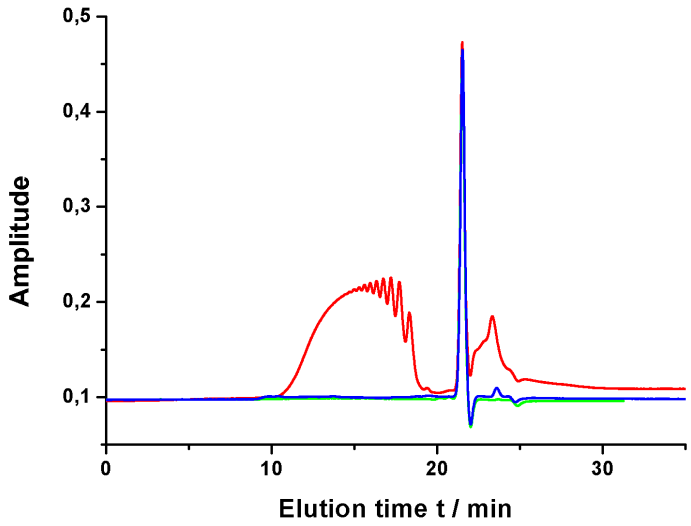

Figure 97: GPC of heparin, oxidized heparin and heparin-dihydrazide with Tosoh SW2000+SW3000 columns, running buffer 0.1M ammonium acetate pH = 7, flow 0.7 mL/min, detection at a wavelength of 234nm

Heparin-dihydrazide can either be mixed with oxidized heparin (c = 0.3g/L) at a ratio of 1:1 and then adding protamine to obtain crosslinked nanoparticles, or reacted with oxidized antibody to yield heparin antibody conjugates.

5.4. Protocols for Isolation of Dendritic Cells

5.4.1. Isolation of Dendritic Cells from Murine Spleen

This protocol for isolation of dendritic cells from murine spleen is developed in the laboratory of [redacted] at the Department of Microbiology and Immunology at the University of Melbourne.

The protocol is optimized for 8 organs, scale up or down proportionately.
Procedure:

- Take 10mL 1.077 nycodenz/4 spleens. Thaw on ice, mix. (for the density gradient)
- Take 1mL DNA/Collagenase/ 8 spleens. Thaw on ice, mix.
- Take 10mL aliquot of Fetal Calf Serum (FCS). Thaw at room temperature or in water bath. Make FCS 10% EDTA.
- Take antibody cocktail for conventional DCs (red dot):
    - CD3-ε (KT3-1.1) (T cells)
    - CD45R (RA36B2)
    - CD90 (T24/31.7) (T cells)
    - Ly6G & Ly6C (RB68C5) (Macrophages, Neutrophiles, …)
    - erythroid (TER119) (red blood cells)

1. Euthanize C57Bl/6 mice and harvest spleens by placing mice on the right side. Store in RPMI 2% FCS.
2. Pour spleens and media into a petri dish. Take each spleen into the clean half and remove pancreas, fat and connective tissue.
3. Cut the spleens with scissors until a paste forms, then cut an extra five minutes!
4. Transfer to a tube then top up to 6mL with RPMI 2% FCS.
5. Add 1mL DNase/ collagenase (volume: 7mL) (DNA/collagenase help to digest fibrous spleen.)
6. Use transfer pipette to resuspend periodically at room temperature for 20 minutes. NOTE: After digestion with DNase/ collagenase, approximately 1% of solution is DCs.

7. Add 600µL 0.1M EDTA at room temperature. (EDTA is a chelating agent that binds to calcium and prevents joining of cadherins between cells, preventing clumping of cells grown in liquid suspension.)
8. At room temperature for 5 minutes, use transfer pipette to resuspend periodically.
9. Filter through a metal sieve and wash sieve with RPMI 2% FCS.
10. Transfer into a 50mL falcon tube with RPMI 2% FCS to approximately 30mL.
11. Create a FCS/ 10% 0.1M EDTA underlay in falcon tube with a glass pipette.
12. Spin for 7 minutes, 1700rpm at 4°C.

Next the sample is enriched for DCs by creating a density gradient that will select "light" cells.

13. Aspirate supernatant and resuspend pellet in 5mL Nycodenz (mixed well before use) (10mL for 8 spleens)
14. Create density gradient in 'density gradient tube' (polypropylene tube), place 5mL of Nycodenz in a 14mL density gradient tube.
15. With a glass transfer pipette add Nycodenz- cell suspension in circular motions on side of tube wall to prevent disruption of gradient. Next add overlay of FCS/ 10% 0.1M EDTA to approximately 12mL using same technique.
16. Spin for 10 minutes, 3100rpm, 4°C with a slow brake as to not interfere with the gradient. Approximately 20% of cells are now DCs.
17. In a 50mL falcon tube, add 30mL EDTA/BSS (buffered saline solution) + 2% FCS. Take interphase from density gradient down to 3mL, add to EDTA/BSS + 2% FCS. Make up to a known volume by spinning down and resuspend in a known volume. Remove sample to count cells using a hemocytometer. Use 90µL Trypan blue (1:4 solution, to stain dead cells) and 10µL of sample (spin!)

    To calculate the number of cells:

    - (cell count (30 – 300) x 10^4 x stain dilution factor) x volume of sample (mL)
18. Spin collected cells for 7 minutes, 1700rpm at 4°C and remove supernatant.
19. Resuspend in 10µL Ab cocktail/10^6 cells and incubate for 30 minutes at 4°C (stains cells we don't want)
20. Wash Ab-labeled cells to remove excess antibody by adding EDTA/BSS + 2% FCS up to 10mL.

21. Spin cells for 7 minutes, 1700rpm at 4°C
22. Resuspend pellet in 500µL EDTA/BSS + 2% FCS
23. Prepare anti-rat IgG magnetic beads for negative enrichment in a polypropylene tube (magnetic beads with antiFc receptor: captures ab-labeled cells). Require 1mL of beads per 500µL of antibody cocktail (= 10 beads per cell). Wash beads in EDTA/BSS + 2% FCS (fill to the top of the tube). To do this, place tube with beads on the magnet for >30 seconds, remove media with a transfer pipette, then remove tube and resuspend beads in EDTA/BSS + 2% FCS. Repeat 3 times.
24. Transfer 500µL cells to tube of pre-washed magnetic beads.
25. Rotate on the roller for 20 minutes at 4°C in EDTA/BSS + 2% FCS.
26. Place tube in magnet for 2 minutes, transfer non magnetic fraction using a glass pipette into a new tube. If desired, repeat step to ensure removal of all magnetic bead-bound cells.
27. Spin down for 7min, 1700rpm at 4°C, resuspend cells in a known volume of medium (3-4mL), count cells, estimated purity is 50-90%. The protocol is optimized for 8 spleens so purity can decrease if fewer than 8 spleens are used.

Approximately $5x10^6$ DC per spleen can be isolated.

5.4.2. Isolation of Dendritic Cells from Murine Bone Marrow

Isolation of dendritic cells from murine bone marrow is performed in collaboration with [redacted] in the group of [redacted] at the Department of Dermatology at the University Clinics in Mainz.

1. Euthanize C57Bl/6 mice and harvest femora. Isolate femora, remove flesh and tendons from the bone and separate femur and tibia. Store bones in complete medium, sterilize in 70% ethanol for 60 seconds and then store again in a new well with fresh complete medium. With a disinfected forceps hold the femur and cut of the end of the bone.
2. After isolation of the femora wash out the bone marrow with a fitted cannula (0,6x25 mm, B.Braun) into clean petri dishes.

3. Pipette up and down to obtain single cell suspensions. Count cells and centrifuge 7min at 1400g.
4. Resuspend cells in DC medium (GM-CSF containing R5-Medium) to a final concentration of $4*10^6$ cells /mL and distribute in a 24 well plate with 1mL per well.
5. Add 3 mL DC medium per well and incubate at 37°C and 5% CO_2.
6. After 48h add another 3mL DC medium per well.
7. At day 6 harvest the supernatant and gently wash the plate once with prewarmed PBS to wash out the bone marrow derived DC.
8. Centrifuge cells and resuspend in media for further use.

Approximately 40-60$*10^6$ DC per mouse can be isolated and retrieved at day 6.

5.4.3. Synthesis of aDEC205 with Hybridoma Technology

aDEC205 is produced with hybridoma technology in the laboratory of [redacted] at the department of dermatology at the University clinics in Mainz.

Antibody Synthesis

The hybridoma cell line HB290 (American Type Culture Collection, Manassas, VI, USA) secretes the monoclonal anti-DEC205-antibody (mNLDC-145) for the murine receptor DEC205 on the cell surface of dendritic cells. Furthermore a control IgG2a was synthesized (GL-117).

1. Keep a back up culture in RPMI + 5% FCS in a 24 well plate and incubate at 37°C and 5% CO_2.
2. Incubate hybridoma cells at 37°C and 5% CO_2 in RPMI1640 with 5% FCS, 2 mM glutamine, 10 mM HEPES, 1 mM sodium pyruvat und penicillin/streptamycin 150cm^3 culture flasks (seed stock, strain).
3. Split cells every 3-5 days and renew medium.
4. Harvest cells from stock, leave 1mL in the flask for a new stock. Refill the flask with RPMI + 5% FCS and incubate as described for the seed stock.

5. Put medium from flask in a tube and centrifuge 10 min at 300g and discard the supernatant. Redissolve the pellet in RPMI + 2% FCS and transfer to a flask (production culture). Incubate at 37°C and 5% CO_2.
6. Harvest cells after 3 days. Transfer cells into a tube and centrifuge 15min at 1000g. Resuspend in 1x PBS. Take 1mL and test for antibody concentration. Freeze the supernatant at -20°C until purification.

Antibody Purification

Precipitation of the Antibody

1. Precipitate antibody-hybridoma supernatant in 50% ammonium sulfate and 45% ammonium sulfate at 4°C. While stirring the solution add ammonium sulfate and let a yellowish precipitate form overnight.
2. Ultracentrifuge the precipitate at 1000g for 30min at 4°C.
3. Take the supernatant for analysis with ELISA and resuspend the pellet in 0.1M $NaHCO_3$/50% ammonium sulfate pH 8.3 and spin down at 1000g for 30 min at 4°C.
4. Again take the supernatant for ELISA and resuspend the pellet in max. 15mL 1x PBS and ultracentrifuge at 1000g for 30 min at 4°C. The antibody is now in the supernatant.

Purification with Protein G Column

1. Ultracentrifuge the antibody in PBS at 1000g for 30 min at 4°C and afterwards filtrate with a 0.45µm filter to avoid blocking of the column.
2. Degas buffer and avoid bubbles in the setup when the column is connected to the equipment.
3. Adjust the flow rate to 1mL/min and equilibrate the column with 20mL 1x PBS, afterwards with 15mL glycine buffer and then again with 20mL PBS.
4. Apply the antibody solution to the column at a lower flow rate, the column turns slightly pink and the first peak is detected with the pen recorder on the paper. Take a sample of the flow through for ELISA
5. Use PBS as a running buffer, the column turns colorless again until the baseline is reached.

6. Then use glycine buffer to elute the antibody bound to the column. Collect the eluate and neutralize with TRIS-HCl (34µL/ mL eluate).
7. Precipitate the eluate with 50% ammonium sulfate overnight.

Desalting of the Antibody

1. Centrifuge the precipitated antibody at 1000g for 30 min at 4°C and discard the supernatant.
2. Resuspend the pellet in 2.5mL PBS and purify over a PD10 column.
3. Filtrate the antibody with a 0.45µm filter for sterilization.

ELISA testing obtains a concentration of 3µg/mL in a total volume of 3mL. So the obtained amount antibody is 9µg which is way too little for conjugation experiments.
Therefore, the monoclonal antibody (NLDC145) for further conjugation experiments is purchased from BioXCell (Product: DEC205/HB290, Antigen: Mouse dendritic cell, Isotype: Rat IgG2a, Cat. # BE00105). The antibody was produced by stirred tank fermentation with hybridoma-serum free medium with 1% FCS, L-glutamine, glucose, penicillin and streptomycin. The supernatant was purified with protein G column in 1x PBS. SDS PAGE gives a purity > 95% according to the manufacturer and the final concentration was determined by absorption at 280nm to be 7mg/mL. This commercially available antibody is used for all experiments in this thesis.

5.5. Characterization

5.5.1. Flow Cytometry

Internalization into bmDC

Isolate cells from bone marrow and culture $3*10^6$ cells in 4mL DC medium (day 0). On day 4 add 3mL DC medium + GM-CSF (4ng/mL). Harvest DC on day 6 and control purity with FACS (~85%).

Place $0.5*10^6$ cells in 200µL per well in a 96 well plate and add $1*10^{12}$ particles per well. Harvest DC after 4h incubation at 37°C, 5% CO_2 and measure FACS (phenotyping with CD11c-APC, if particles only labeled with AlexaFluor488). For CLSM images, nuclei are labeled with Hoechst 33342, 1:10 000 (stock: 10mg/mL) for 1h on Rotamax at RT, wash cells and place in 1xPBS, transfer cells into chamber-slide and store at 4°C overnight. Repeat this procedure after 24h incubation and measure cells with CLSM on the same day. Prepare duplicates or triplicates if possible.

For aDEC205 additional incubation times are prepared: 30 min on ice and 30 min at 37°C.

SHIP Internalization Protocol

For each well/ time point $2.5x10^5$ cells in 250µL are used. Each sample gives 6 time points, therefore prepare $1.5x10^6$ cells in 1.5mL DC medium with the appropriate amount of sample (~2µL) in one polypropylene tube. The polypropylene tube minimizes binding of DC to the inner tube wall.

Incubate for 30 min on ice first and wash twice with PBS/EDTA. Take out 250µL for the t=0 sample. Then start the incubation at 37°C with 10%CO_2 and take out 250µL at every time point (t= 5, 10, 15, 30, 60 min) and put sample into 96-well plate on ice.

By doing the incubation at 4°C the antibodies will bind specifically to their cell surface receptor and unbound conjugate is washed away. If untargeted polymer is used the polymer will bind unspecifically to the cell surface due to ionic interaction. Internalization, specific for the antibody-receptor complex or unspecific for polymers, starts when incubating at 37°C.

After incubation the samples are prepared for phenotyping. Cells are centrifuged for 2 min, 1700rpm/670g at 4°C and the pellet is resuspended in 50µL of the phenotyping antibody solution. Stain the control cells with the single phenotyping antibody (CD11c, CD8, DEC205 and mix -> single stain controls) and all cells incubated with sample with a mix of the CD11c and CD8 phenotyping antibodies (Master mix). Cells are incubated with the phenotyping solution for 30 min on ice and afterwards washed twice with PBS/EDTA and then resuspended in 200µL PBS/EDTA.

Split samples into 2 wells with 100µL each and to one well add 2µL Quencher (150mM, 1:30 diluted)

[FIPCy5 (5' Cy5-TCAGTTCAGGACCCTCGGCT-N3 3'), QPC (5' AGCCGAGGGTCCTGAACTGA-BHQ2 3')]. Flow cytometry measurements were performed on all samples.

If the samples are labeled with AlexaFluor488 and AlexaFluor555 the brilliant violet phenotyping stains have to be used as otherwise the spectra of FITC and AF488 or PE and AF555 overlay.

Table 25: Phenotyping antibodies for SHIP internalization experiments

Phenotyping	**Stain**	**Dilution**
CD11c	FITC	1:300
	Brilliant Violet 621	1:50
CD8	PE	1:400
	Brilliant Violet 405	1:50

Table 26: Samples for SHIP Internalization experiment with different antibodies

Sample	aDEC205	CD11c	M5/114	10B4	5P1
µL sample/ $6x10^5$ cells	1.2	1.2	1.2	1.2	1.2

Table 27: Samples for SHIP internalization experiments with PLL conjugates

Sample	PLL	PLL-aDEC205	PLL-CD11c	PLL-cIgG	PLL brush	PLL brush-aDEC205
µL sample/ $6x10^5$ cells	4/ 7.5	11/ 20	30	30	4	6.5

5.5.2. Imaging of Conjugates

Clathrin and Caveolin Staining of DC

(STORM Protocol – Sample Preparation; 2b. Immunofluorescence Protocol B – Clathrin)

Incubate cells with sample as described in Antibody Internalization Protocol. Wash 2x with PBS.

In order to fix dendritic cells, remove medium and resuspend pellet in 1mL 3% TFA. Incubate cells for 30 min on ice, spin at 4°C, 300g for 5 min and wash 2x with PBS. Cells can be stored at 4°C overnight.

Spin cells (4°C, 300g, 5 min) and block cells in 200µL blocking buffer for 90 min at RT, rocking. Blocking buffer: 3% BSA + 0.1% Triton X-100

Resuspend the pellet in 100µL blocking buffer and divide into 2 tubes with 50µL each. Add 50µL of a 1:100 dilution of primary antibodies in blocking buffer to each tube and incubate 60 min at RT, rocking.

Tube 1: Clathrin (D3C6 XP(tm) Rabbit mAb, Cell Signaling Technology #47965)

Tube 2: Caveolin-1 (D46G3 XP(tm) Rabbit mAb, Cell Signaling Technology #32675)

Aspirate blocking buffer and wash 3 times with 200µL washing buffer for 15 min per wash at RT, rocking. Washing buffer: 0.2% BSA + 0.05% Triton X-100 in PBS

Add 50µL of a 1:200 dilution of secondary antibody (Alexa488-labeled) in blocking buffer and incubate for 30 min at RT, rocking. Remove blocking buffer and wash 3 times with 200µL washing buffer for 10 min per wash at RT, rocking, and finally resuspend cells in 200µL PBS. Cells are now ready for microscopy.

LAMP-1 Staining of DC with Conjugate

Reagents:

Phosphate-Buffered Saline (PBS), 1X

Bovine Serum Albumin

Triton X-100

Fixation solution: 3% paraformaldehyde (PFA)

Blocking buffer: 3% BSA + 0.2% Triton X-100 in PBS

Washing buffer: 0.2% BSA + 0.05% Triton X-100 in PBS

Equipment:

Coverglass: 8-well Labtek II

Protocol:

Plate cells to 50-60% confluency (or suitable amount for cell type) on chambered cover glass and incubate overnight. Gently wash with 500µl PBS once. Fix with 200µl of 3% PFA for 10 minutes at room temperature. Wash 3 times with 400µl PBS. At this stage the sample can be stored overnight at 4°C once it is fixed.

Block cells in 200µl blocking buffer for 120 minutes at room temperature. Add 150µl primary antibody dilutions in blocking buffer and incubate for 60 minutes at room temperature.

Primary Antibody: Dilute mLamp1 (LYC6) 1:200 in blocking buffer.

Aspirate and wash 3 times with 200µl washing buffer for 10 minutes per wash at room temperature. Add 150µl labeled secondary antibody dilutions in blocking buffer, protected from light, and incubate for 30 minutes at room temperature. Secondary Antibody: Dilute Brilliant Violet 421 donkey anti-rabbit (Biolegend 406410) 1:200 in blocking buffer. Aspirate and wash 3 times with 200µl washing buffer for 10 minutes per wash at room temperature.

Wash with 500µl PBS once.

Image in PBS first, may add an antifade agent if required (check if it is suitable for the fluorophores used).

Notes:

Prepare buffers fresh.

Take care to wash gently, as harsh washing can remove cells from the cover slip.

Primary antibodies are usually diluted in the range of 100:1 to 1000:1. Check the manufacturers guidelines and you may need to aliquot your antibody to determine the best concentration for immunofluorescence. A low dilution factor increases the likelihood of non-specific staining and doesn’t necessarily result in increased signal.

Suitable antifade agents are SlowFade Gold (Invitrogen #S36936) or Vectashield (Vector Labs H-1000).

Multiple antibodies can be used together, as long as they come from different host species (but plan carefully to minimize cross-reactivity).

Non-antibody stains can be used at different points (e.g. Wheat Germ Agglutinin to AlexaFluor conjugates can be added to live cells just before fixing to stain the plasma membrane, DAPI or Hoechst to stain nucleic acids can be added after antibody staining).

Imaging of Conjugates

Incubation of DC with conjugate for imaging

Table 28: Amount of conjugate for imaging

Sample	PLL-Ag-CpG	PLL-Ag-CpG-DEC	PLL-Ag-DEC	PLL-CpG-DEC	PLL_B-Ag-CpG	PLL_B-Ag-CpG-DEC	PLL_B-Ag-DEC	PLL_B-CpG-DEC
µL sample/ $2*10^5$ cells	6.54	7.60	14.48	9.88	4.80	9.20	8.96	12.40

Preparation of chamber slides

Coat wells with 30µL αMHCII Ab N22 (10mg/mL) and incubate for 2h on ice, remove liquid, wash 2x with PBS, wash 1x with KDS-RPMI+2%FCS and remove liquid just before adding the cells.

Preparation of cells

8 tubes with $2*10^5$ cells per well in 200µL KDS-RPMI + 2% FCS, add amount of conjugate, incubate 30 min on ice, wash 3x with KDS-RPMI+2%FCS, resuspend in 300µL KDS-RPMI+2%FCS, take 150µL and put sample in prepared chamber slides on ice, incubate the other 150µL at 37°C with 10%CO_2 for 1h, put in chamber slide.

Adhere 30 min at 37°C, wash 1x with PBS, fix with 150µL PFA 3% for 15min at RT, wash 3x with PBS and store samples at 4°C.

5.5.3. MTT Assay

Reagents:

MTT sigma M-2128, dissolved in PBS to 5mg/ml

Filter sterilized and aliquoted in 5ml tubes, stored at -20°C

Stable at 4°C for 2 weeks

1M HCl: 44.6ml of conc. HCl (11.2M) into 455.4ml H2O

Acidified isopropanol: 20ml 1M HCl to 480ml isopropanol

Protocol:

Cells grown in 100µl media in 96-well plates overnight.

(JAWS, Passage 32, 10,000 cells per well in JAWS complete medium; HeLa, Passage 11, 10,000 cells per well in DMEM + 10% FBS – too many cells, next time use less)

Add amount of sample, which can be found in Table 29, directly to the cells and incubate for 24h at 37°C and 10% CO_2.

Remove the supernatant and add 200µl of media containing 0.5mg/ml MTT (diluted 10 times from stock solution) into each well. Incubate at 37C for 3-4h. Carefully remove the supernatant. Add 100-150µl acidified isopropanol per well, depending on how much purple precipitation. Solve the precipitation well. Read OD at 570nm with plate reader.

Ascent Software, Mode: continues, Type: single, Filter: 560 nm

Place plate without lid, START, Copy results to Excel sheet

Table 29: Samples for MTT Assay

Sample	**µL**	**µL**	**µL**	**µL**
PLL	5,5	2,75	1,37	**0,55**
PLL-Linker	5	2,5	**1**	0,5
PLLb	2,5	**1**	0,5	0,25
PLL-Ag-CpG-DEC	3,8	1,9	0,76	**0,38**
PLLb-Ag-CpG-DEC	0,45	0,22	0,09	**0,045**
DEC	1,12	**0,56**	0,28	0,14
SIINFEKL	1,1	0,11	**0,011**	0,0011
CpG	0,6	0,06	**0,006**	0,0006

5.5.4. Antigen Presentation Assay

The antigen cross presentation assay (described in Chapter 3.3.3. and 3.3.4.) is performed in the laboratory of [redacted] in collaboration with [redacted].

Prepare DC:

1. For CD8+ DC:
    a. Isolate dendritic cells as per Dendritic Cell Isolation SOP
    b. Wash dendritic cells 2 times EDTA/BSS 2% FCS at 1700rmp, 7 mins, 4^{o}C
    c. Antibody stain dendritic cells (CD11c N418 and CD8 YTS169.4/53-6.7) for 30 minutes on the ice in the dark
    d. Wash away excess antibodies 2 times EDTA/BSS 2% FCS at 1700rmp, 7 mins, 4^{o}C
    e. Stain with Propidium Iodide
    f. Sort, collecting only CD11c+CD8+ cells
    g. Recount cells post sort
2. Titrate conjugates and antigen across a 96 well plate at the desired concentrations with a final volume/well of 100µL

Titrating SIINFEKL and plating DC:

- Dilute the peptide: 1mg/mL stock
    a. First 1:100 (5µL SIINFEKL into 495µL DC media)
    b. Then 1:500 (5µL [a] into 2495µL DC media)
- Place 111µL of [b] into the first well, serially dilute 11µL into 100µL DC media across the plate (leave the last well without peptide as a negative control)
- Once SIINFEKL is titrated across the wells, the final volume is 100µL/well
- Add 100µL of DC at a concentration of 1.5x10^{4} DC/100µL/well (this is where CpG may also be added if desired at 2µL CpG/mL media).

3. Plate 100µL of 1.5x10^{4} cells/100µL of CD8+ DC/well of a 96 well U-bottom plate to each well containing antigen/ conjugate.
4. Place 96 well plate at 37^{o}C, 10% CO_2 for 45 minutes, pulsing the DC with antigen.
5. Spin plate 1700rmp, 2 mins, 4^{o}C
6. Wash 3 times with RPMI 2%FCS at 1700rmp, 2 mins, 4^{o}C, each time removing 180µL from the 200µL resuspension volume with a pipette, careful not to disturb

the loose, sometimes invisible, pellet. Do not flick the plate as this will disrupt the loose pellet and will result in the DCs being removed and lost.

Prepare CD8+ T cells:

1. Harvest lymph node (LN) from desired mouse.
2. Push LN through a 40µm sieve with RPMI + 2% FCS
3. Spin cells 1700rmp, 7 mins, 4^{o}C.
4. Resuspend cells in a known volume and count cells.
5. Spin cells at 1700rmp, 7 mins, 4^{o}C.
6. Resuspend in 10µL/1x10^{6} cells of the CD8 antibody cocktail (M1/70, F4/80, Ter119, RB6-8C5, M5/114, GK1.5), allowing for negative selection of cells.
7. Incubate on ice for 30 minutes in the dark.
8. Quench reaction with 10mL BSS + 2% FCS and spin cells at 1700rmp, 7 mins, 4^{o}C.
9. Resuspend antibody-labeled cells in 500µL HANKS BSS 2% FCS.
10. Place on BioMag IgG magnetic beads:
    a. BioMag IgG magnetic beads are at a concentration of 10^{8} beads/mL and are to be used at 20µL/1x10^{6} cells, i.e. 2 times the volume of antibody cocktail used.
    b. BioMag IgG beads are to be prewashed in 5mL polystyrene tubes 3 times in HANKS BSS 2% FCS on the magnet to remove azide in the original bead solution.
    c. No more than 2mL of beads are to be washed per tube to ensure total removal of azide.
11. Place tubes on the roller at 4^{o}C for 20 minutes.
12. Fill tubes with HANKS BSS 2% FCS approximately 2cm from the top.
13. Place the tubes on the magnet and wait for the beads to stick to the sides of the tubes.
14. Collect the supernatant containing CD8+ T cells.
15. Spin 1700rmp, 7 mins, 4^{o}C.
16. Resuspend in a known volume and count cells.
17. Stain cells with purple proliferation dye as per manufacturer's instructions.

- Spin cells, resuspend in 20mL prewarmed 0.1% BSA/PBS, add 20µL purple dye and stain for 20 min at 37°C in the dark, quench with RPMI + 2% FCS for 5 min on ice

18. Wash cells 1 times RPMI 2% FCS at 1700rmp, 7 mins, 4°C.
19. Resuspend cells in 2mL RPMI + 2% FCS and recount cells.
20. Spin at 1700rmp, 7 mins, 4°C.
21. Resuspend cells in DC media + 1:500 GM-CSF to a concentration of $5x10^4$ CD8+ T cells/200µL.
    a. NOTE: DC media is 440mL of KDS RPMI, 50mL of DC-FCS, 910uL of 1000x 2-Me (beta-mercaptaethanol), 5mL of PenStrep and 5mL Glutamine (L-Glutamax)
22. Perform a FACS purity stain to ensure the majority of cells are antigen specific CD8+ T cells. For OTI T cells stain for CD8 in 53-6.7 (APC) and Vα2 in B20.1 (PE). Aim for ≥ 90% purity. The purity determined by FACS is ~88% OTI and the OTI stained successfully with the purple dye. The number of OTIs is $(11.2*10^6)x0.88 = 9.856x10^6$ OTIs.
23. The amount of OTIs needed for the AP is 9 samples x 6 titrations x 3 (triplicate) = 162 wells, with 50000 cells per well = $8.1x10^6$ cells.

<u>Coculture CD8+ T cells with DC</u>

1. After the final wash of DC, remove 180uL of the supernatant.
2. Place $5x10^4$ CD8+ T cells/200µL/well.
3. Incubate at 37°C, 10% CO_2 for 72 hours.
4. Stain cells 30 min on ice in the dark with CD8 in 53-6.7 (APC) and Vα2 in B20.1 (PE) in a 1:200 dilution.
5. Wash cells 3 times with FACS buffer, remove supernatant and resuspend cells in 120µL propidium iodide solution (1mg/mL, 1:1000 in FACS buffer).
6. Add 25µL of 1:10 diluted beads (Sphero Blank Calibration particles 6.0 – 6.4µm, BD Bioscience, Cat: 556296).
7. Analyse results by FACS.

6. Appendix

6.1. Additional Data

6.1.1. Further results of PLL-aDEC205 conjugates via Method 1:

PLL-aDEC205 II:

Conjugation ratio PLL: aDEC205 was 1: 1, purification with BioGel P30.

CLSM images show that labeling was not successful, probably due to the low amount of PLL.

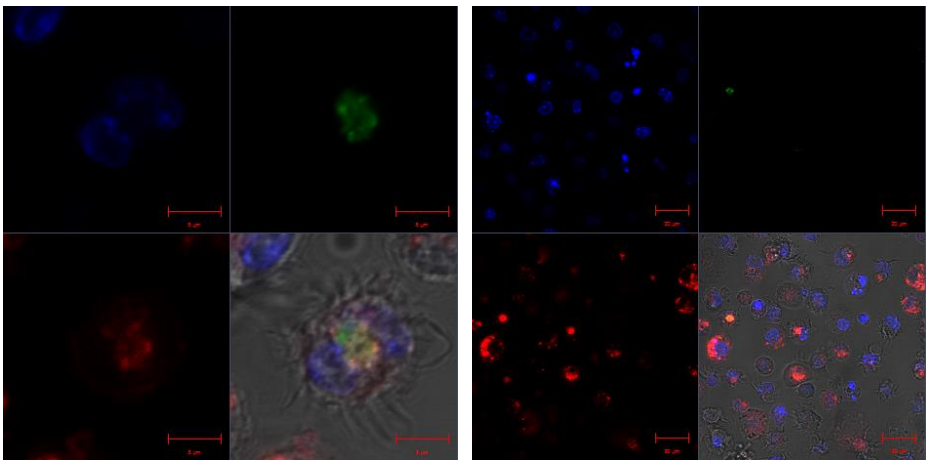

Figure 98: CLSM image of PLL-aDEC205 II in bmDC, incubation time 4h, conc. 25pmole; blue: Hoechst 33342 - Labeling of nucleus; green: PLL-AF488; red: aDEC205-AF647, scale bar: left: 5µm, right: 10µm

PLL-aDEC205 III:

Conjugation ratio PLL: aDEC205 was 1: 10, purification with BioGel P30.

CLSM images show that labeling was not successful, probably due to the low amount of PLL.

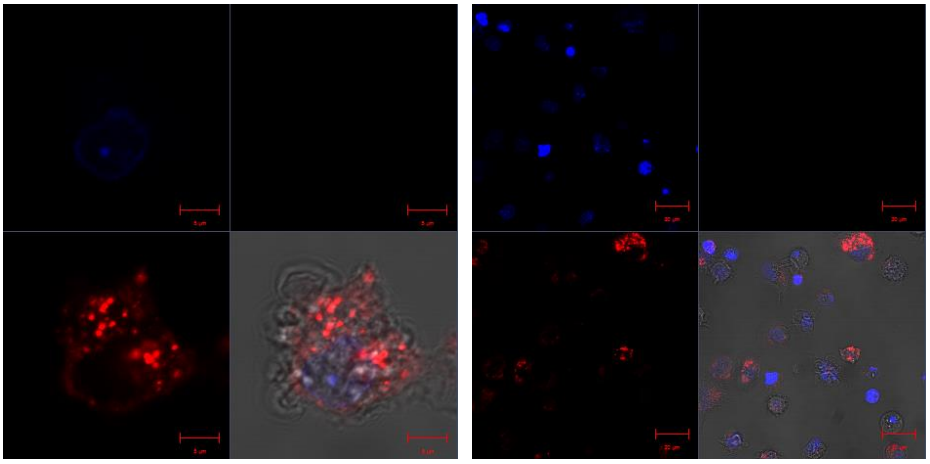

Figure 99: CLSM image of PLL-aDEC205 III in bmDC, incubation time 4h, conc. 25pmole; blue: Hoechst 33342 - Labeling of nucleus; green: PLL-AF488; red: aDEC205-AF647, scale bar: left: 5µm, right: 10µm

PLL-aDEC205 IV

Conjugation ratio PLL: aDEC205 was 10: 1, purification with Sephadex G25 NAP-5.

PLL-aDEC205 IV-1: conjugation for 2h

PLL-aDEC205 IV-2: conjugation for 7h

CLSM images show no difference of uptake after different reaction times

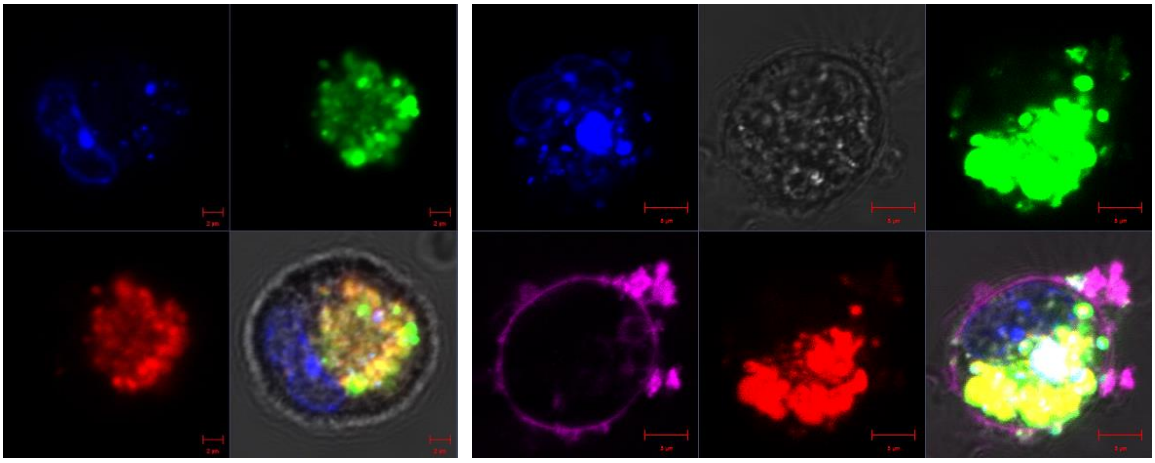

Figure 100: CLSM image of PLL-aDEC205 IV-1 (reaction time: 2h) in bmDC, incubation time 4h, conc. 25pmole; blue: Hoechst 33342 - Labeling of nucleus; violet: Cell Mask Orange - Labeling of cell membrane; green: PLL-AF488; red: aDEC205-AF647, scale bar: 5µm

PLL-aDEC205 V

Conjugation ratio PLL: aDEC205 was 1: 1, purification with Sephadex G25 NAP-5 and subsequently with Amicon Ultra Centrifugal Filter Units 50kDa (2a) or BioGel P100 (2b).

The different purification strategies yielded no difference in uptake observed with FACS or CLSM.

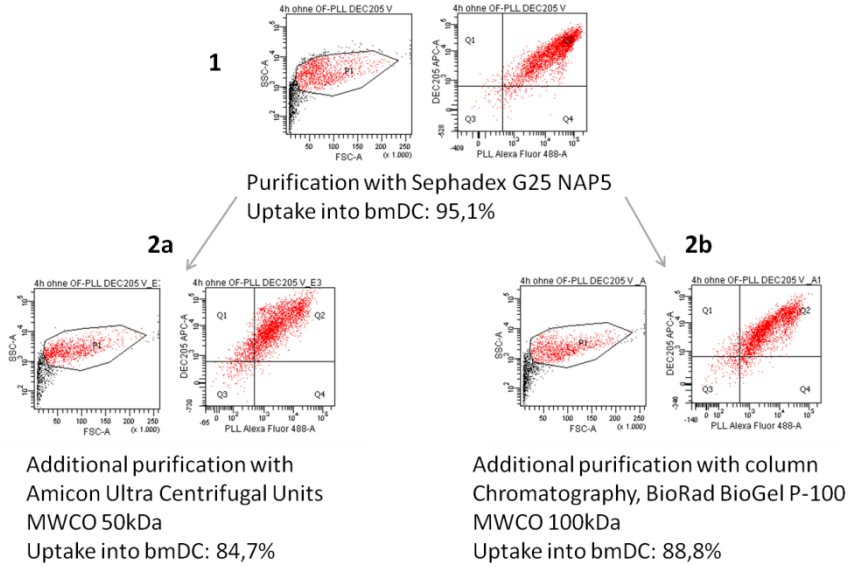

Figure 101: Dot plots of PLL-aDEC205 V in bmDC

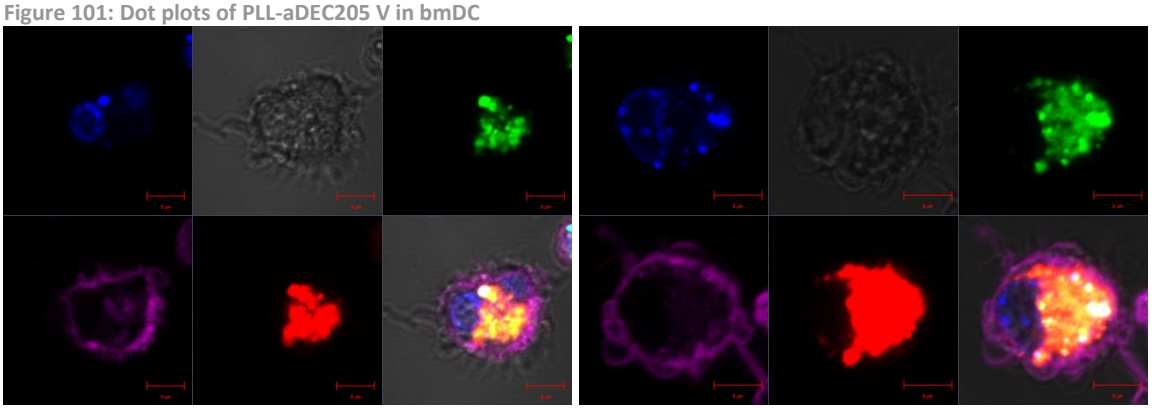

Figure 102: CLSM image of PLL-aDEC205 V-1 and 2a in bmDC; left: PLL-aDEC205 V-1: purification with Sephadex G5 NAP5; right: PLL-aDEC205 V-2a: purification with Sephadex G25 NAP 5 and Amicon Ultra Centrifugal Filter Units MWCO 50kDa; incubation time 4h, $1*10^{12}$ particles; violet: Hoechst 33342 - Labeling of nucleus; blue: Cell Mask Orange, labeling of cell membrane; green: PLL-AF488; red: aDEC205-AF647, scale bar: 5µm

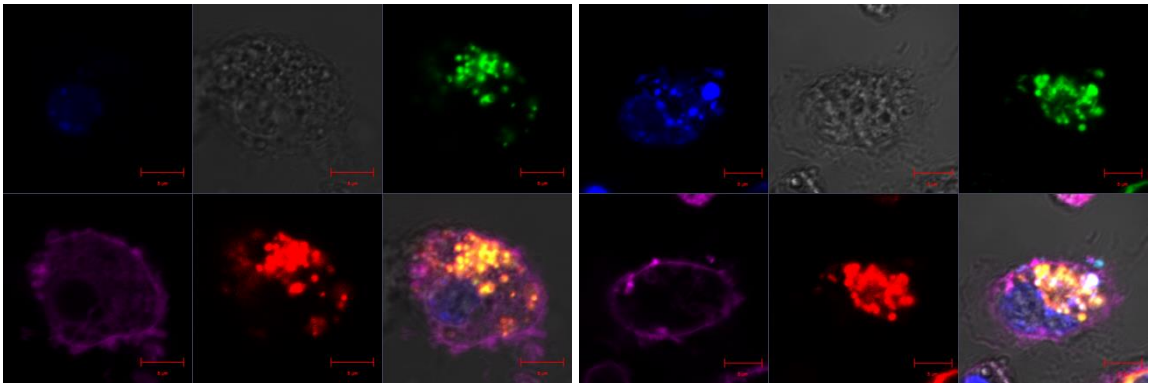

Figure 103: CLSM image of PLL-aDEC205 V-2b, purification with Sephadex G25 NAP 5 and BioRad BioGel P-100; Fraction 3 (left) and Fraction 4 (right) in bmDC; incubation time 4h, $1*10^{12}$ particles;; violet: Hoechst 33342 - Labeling of nucleus; blue: Cell Mask Orange, labeling of cell membrane; green: PLL-AF488; red: aDEC205-AF647, scale bar: 5µm

6.1.2. DLS Analysis of PLL-Antigen and PLL-Antigen-aDEC205

PLL-Antigen II

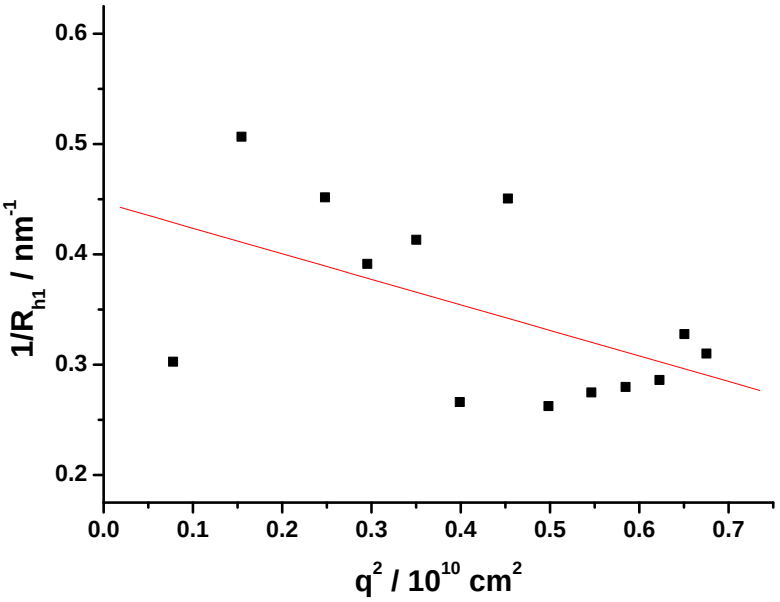

Figure 104: Angular dependency of the reciprocal hydrodynamic radius of PLL-Antigen II in 1x PBS; R_{h1} = 2.2nm

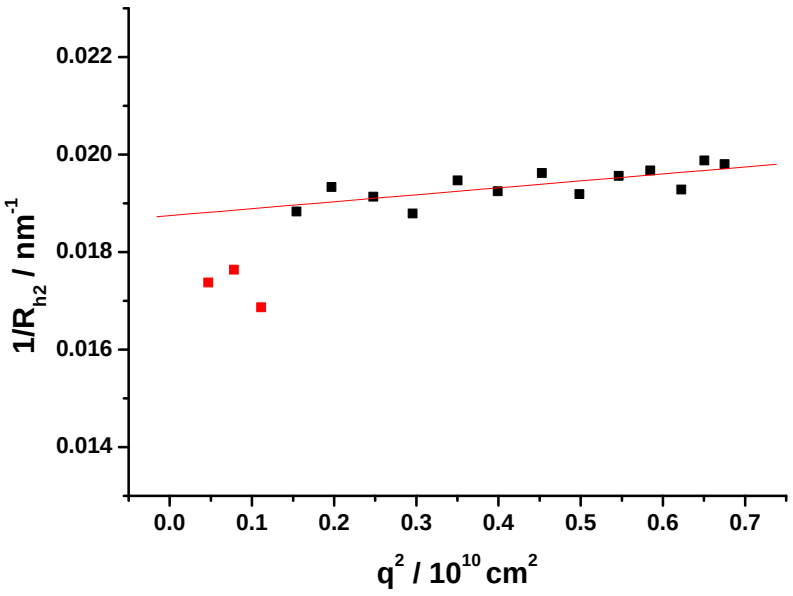

Figure 105: Angular dependency of the reciprocal hydrodynamic radius of PLL-Antigen II in 1x PBS; R_{h2} = 53.3nm

PLL-Antigen-aDEC205 II

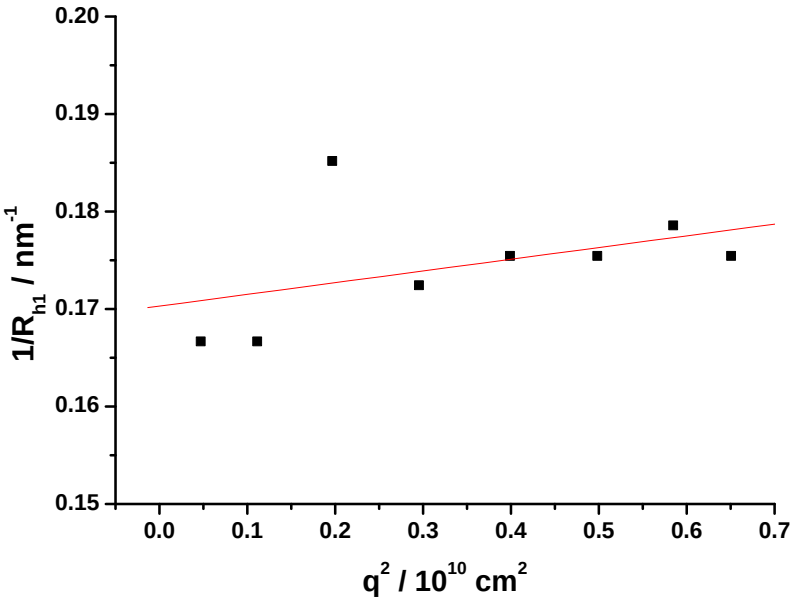

Figure 106: Angular dependency of the reciprocal hydrodynamic radius of PLL-Antigen-aDEC205 II in 1x PBS; R_{h1} = 5.9nm

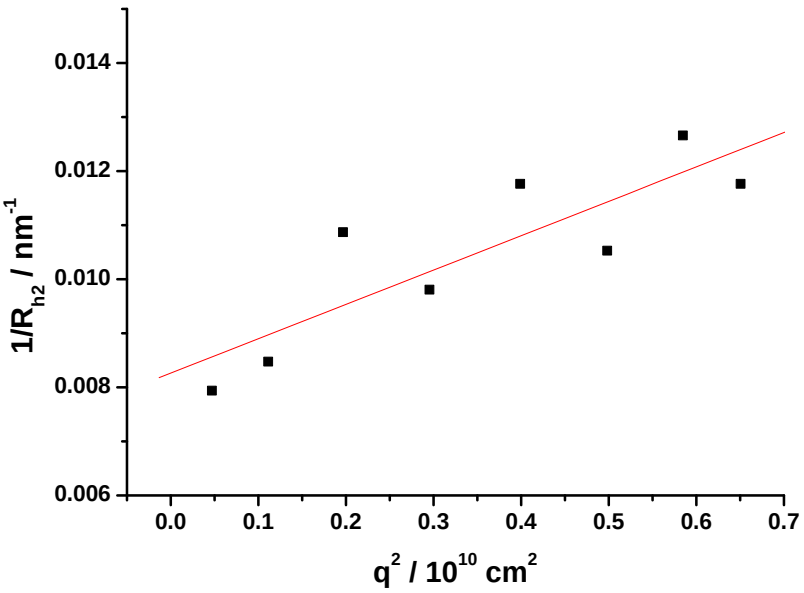

Figure 107: Angular dependency of the reciprocal hydrodynamic radius of PLL-Antigen-aDEC205 II in 1x PBS; R_{h2} = 121±24nm

6.2. Materials and Equipment

6.2.1. Chemicals and Reagents

Reagent	Company	Cat #	Application
PLL	Sigma Aldrich	P7890	Conjugation
aDEC205 (DEC205/HB290, rat αmouse IgG2a)	BioXCell	BE00105	Conjugation
Antigen (CSGLEQLESIINFEKL)	BACHEM	4062191	Conjugation
AlexaFluor®647 Protein Labeling Kit	Invitrogen	A20173	Fluorescence Labeling
AlexaFluor®647 Carboxylic Acid Succinimidyl Ester	Invitrogen	A20006	Fluorescence Labeling
AlexaFluor®488 Protein Labeling Kit	Invitrogen	A10235	Fluorescence Labeling
Alexa Fluor®488 Carboxylic Acid, Succinimidyl Ester	Invitrogen	A20000	Fluorescence Labeling
Alexa Fluor®488 Carboxylic Acid,5-TFP Ester	Invitrogen	A30005	Fluorescence Labeling
Sulfo-SMCC	Pierce	22322	Crosslinker
DIBO Click-IT® Succinimidyl Ester DIBO Alkyne	Invitrogen	C-10414	Crosslinker
sodium periodate	Sigma Aldrich	311448	Oxidation
sodium cyanoborohydride	Sigma Aldrich	156159	Reduction
DTT	Sigma Aldrich	43815	Reduction
TCEP	Sigma Aldrich	75259	Reduction
DPBS buffer, no calcium/magnesium	Invitrogen	14190136	Buffer
RPMI 1640 Medium	Invitrogen	11875-093	DC Medium
DMSO	Sigma Aldrich	41648	Solvent
BioGel P30	BioRad	150-4150	Purification
BioGel P100	BioRad	150-4174	Purification
Sephadex G25 NAP 5	GE Healthcare	17-0853-02	Purification
Sephadex G25 NaAP 25	GE Healthcare	17-0852-02	Purification
Amicon Ultra Centrifugal Filter Units 3kDa	Millipore	UCF 800324	Purification
Amicon Ultra Centrifugal Filter Units 10kDa	Millipore	UCF 801024	Purification
Zeba Columns 7kDa	Invitrogen	89882	Purification
Zeba Columns 40kDa	Invitrogen	87766	Purification
NuPAGE® Novex® 4-12% Bis-Tris gels	Invitrogen	NP0322Box	Characterization
NUPAGE® SDS MOPS running buffer	Invitrogen	NP0001	Characterization
NuPAGE® LDS sample buffer	Invitrogen	NP0007	Characterization
NuPAGE® reducing agent	Invitrogen	NP0004	Characterization
SimplyBlue™ SafeStain	Invitrogen	LC6060	Characterization
IgG from mouse serum (025K7580)	Sigma Aldrich	I5381	Control Ab, conjugation
D3C6 XP^{Tm} Rabbit mAb	Cell Signaling Technology	47965	Clathrin Stain, prim. Ab
D46G3 XP^{Tm} Rabbit mAb	Cell Signaling Technology	32675	Caveolin Stain, prim. Ab
LAMP-1 H-228 (rabbit polyclonal IgG)	Santa Cruz	SC-5570	LAMP-1 Stain, prim. Ab
Brilliant Violet 421 Goat anti-rat IgG	Biolegend	405414	Staining, sec. Ab
Brilliant Violet 421 Donkey anti-rabbit	Biolegend	406410	Staining, sec. Ab
AlexaFluor 488 Goat anti-rabbit IgG (H+L)	Invitrogen	A-11008	Staining, sec. Ab
Cell MaskTM Orange Plasma membrane Stain	Invitrogen	C10045	Cell Membrane Staining
Hoechst 33342 Trihydrochloride Trihydrate	Invitrogen	H3570	Nucleus Staining (Chromatin)

6.2.2. Equipment

Gel electrophoresis

The SDS-PAGE was performed in an XCell Surelock Mini-Cell (Invitrogen) using precast pore gradient NuPAGE® Novex® 4-12% Bis-Tris gels with a large resolution range from 25 to 500kDa. The gels were run in a 1x NUPAGE® SDS MOPS running buffer and the conditions were chosen according to the standard procedure by Invitrogen. Usually the gel were run at constant voltage of U=200V for 30-40min. The samples (c_{final}=0.1-0.3µg/µl) were diluted with 2.5µl NuPAGE® LDS sample buffer and Milli-Q water to a final volume of 10 µl and NuPAGE® reducing agent was added if the gel is run under reducing conditions. The gels were stained with SimplyBlue™ SafeStain. All components are purchased from Invitrogen/ Life Technologies

Flow Cytometry

Flow cytometry measurements for the antibody internalization studies (Chapter 3.1) and the PLL internalization studies (Chapter 3.2) were performed at the LSR Fortessa (BD Bioscience) at the Department of Microbiology and Immunology at the University of Melbourne. The LSR Fortessa uses lasers that can excite at a wavelength of 488nm, 561nm, 633nm and 405nm and detect fluorescence with 16 fluroescence detectors. The instrument is operated with the DiVa Digital software and the data was analyzed with FlowJo.

For all other flow cytometry measurements the LSR II flow cytometer (BD Bioscience) at the Department of Dermatology at the University Clinics in Mainz was used. It contains laser with an excitation laser line at 488nm, 633nm, 355nm and 405 nm.

Light Scattering

The dynamic light scattering measurements were performed with multi angle light scattering setup. The instrument exhibits the following specifications: Goniometer SP-125 with ALV/SO-SIPD, Single Photon Detector (fibre optic cable), ALV-5000/EPP/60X multitau realtime digital correlator (ALV, Langen), and an Argon ion laser (SpectraPhysics Stabilite 2060-4S, wavelength 514.5 nm, power 500 mW).

Static light scattering is performed at an instrument equipped with a He-Ne laser (λ=632.8nm, 25mW, JDS Uniphase 1145p-3083), a goniometer SP-86#060 (ALV9) with an ALV/Hugh QEAPD Avalanche photodiode and an ALV-3000 digital correlator (ALV, Langen).
The measurements were performed at 20°C at scattering angles from 30° to 150°. The solutions were filtered with different filters, for example a GHP filter (0.2µm, d=13mm, Pall) and an Anotop filter (0.02µm, d=13mm, Whatman) into dust-free Suprasil cuvettes (20mm diameter or 10mm diameter, Hellma, Mülheim, Germany). The data is analyzed with the program HDRC (programmed by Oliver Nirschl, group of Prof. Dr. M. Schmidt).

UV/Vis Spectroscopy

UV/Vis spectra were recorded using a Cary 100Bio UV/Vis Spectrophotometer (Varian, Inc). Spectra were monitored from 200 to 700nm at a scanning speed of 100nm/min.

Fluorescence Spectroscopy

Fluorescence spectra were recorded using a Jasco FP-6500 (ETC-273) Spectrometer (Serial No. C065260822) equipped with the software Fluorometer FP-6500 JASCO-SpectraManager, Spectrum Measurement. Always the same instrument setting was used: λ_{ex} = 495nm, λ_{em} = 519nm, band $width_{ex/em}$ = 3nm, response = 2sec, sensitivity: low, measurement range: 475-700nm, data pitch: 0.5nm, scanning speed: 100nm/min.

Fluorescence Correlation Spectroscopy (FCS)

The experiments were performed on a commercial setup combining an inverted microscope IX70, a FluoView300 confocal laser scanning unit (both Olympus) and a FCS unit (PicoQuant) consisting of a single-photon avalanche diode (τ-SPAD) and the time-correlated single-photon counting card TimeHarp 200. Excitation was done by an argon-ion laser at λ = 488 nm (8 mW, CVI Melles Griot) and the fluorescence signal was detected after filtering with a LP488R Raman Edge long-pass filer. A water immersion objective Olympus UPLSAPO 60XW was used for the measurements.

Nanodrop

For UV/Vis measurements at the Department of Chemical and Biomolecular Engineering the Nanodrop 1000 instrument with the Program ND-100 V3.8.1 and the setup Proteins and Labeling was used. The instrument was cleaned and initialized with water and then a blank sample of water was measured. Then, PBS buffer was measured as a blank sample and then the sample was recorded.

CLSM

Confocal Laser Scanning Microscopy was performed at the Core Facility of the FZI Mainz in collaboration with [redacted]. The setup includes a Zeiss Confocal LSM510-UV equipped with the following laser:

Argon-UV: UV (351nm, 364nm) – Hoechst, DAPI

Argon Laser: (458nm, 488nm) – FITC, AlexaFluor488

Helium-Neon Laser (543nm) – AlexaFluor546

Helium-Neon Laser (633nm) – Cy5, AlexaFluor647

The image analysis was performed using the Zeiss Zen-2009 software (Carl Zeiss Microimaging GmbH, Jena, Germany).

GPC Measurements

GPC measurements were performed using Tosoh G2500PW and G3000PW with 1x PBS as eluent. The column material is hydroxylated polymethacrylate with a defined pore size of 200 Å. For detection a UV detector (Waters 486 at λ = 280nm) and a RI detector (Hitachi L-2490) were used. In the sample loop 20µL were injected and the constant flow rate was 0.7 mL/min (pump: Hitachi L-2130). All measurements were performed at 25°C (Hitachi L-2350).

6.3. List of Abbreviations

A_2	2nd Virial coefficient
Ab	Antibody
AF	AlexaFluor
APC	Antigen presenting cell, (rarely also: Allophycocyanine)
B cell	bursal or bone marrow-derived cell
bmDC	bone marrow-derived dendritic cell
BV	Brilliant violet
c	concentration
C	Cytosine
CD	Cluster of differentiation; Antigens detected by monoclonal antibodies
cDC	conventional dendritic cell
$CD4^+$ T cell	T cell that carries the CD4 receptor
$CD8^+$ T cell	T cell that carries the CD8 receptor
C_H	Constant region of the heavy chain of an IgG
CLSM	Confocal laser scanning microscopy
CPG-DNA	2‘-Deoxy(cytidine phosphate guanosine)-DNA
CTL	cytotoxic T lymphocyte
Cy	Cyanine
DC	dendritic cell
DEC205	receptor for aDEC205 antibody
DIBO	Dicyclobenzyl cyclooctylene NHS ester
DLS	Dynamic light scattering
DM1	mertansine
DMF	Dimethylformamide
DMSO	Dimethylsulfoxide
DNA	Deoxyribonucleic acid
DN DC	Double negative DC (CD4 and CD8 negative)
DTT	Dithiothreitol
EPR-Effect	Enhanced permeability and retention effect
FACS	Fluorescence associated cell sorting; flow cytometry
Fc	Fragment crystallizable
FCS	Fluorescence correlation spectroscopy
FDA	US Food and Drug Administration
FIP	Fluorescence internalization probe
FITC	Fluoresceinisothiocyanate
FSC	Forward scatter
G	Guanosine
GM-CSF	Granulocyte macrophage colony stimulating factor
GMP	Good manufacturing practice
GPC	Gelpermeation chromatography
HBV	Hepatitis B virus
HER-2	Human epidermal growth factor receptor number 2
HPMA	N-(2-hydroxypropyl)methacrylamide
HPV	Human papilloma virus

IFN	Interferon
IgG	Immunoglobulin
IL	Interleukin
IRAP	Insulin-regulated aminopeptidase
kDa	kilo Dalton
LPS	Lipopolysaccharide
LS	Light scattering
mAb	Monoclonal antibody
MEA	Mercapto ethylamine
MeOH	Methanol
MHC	Major histocompatibility complex
M_l	lower molecular weight
MMAE	monomethyl auristratin E
MR	Mannose receptor
M_u	upper molecular weight
MW	molecular weight
NCA	N-carboxy anhydride
NHS	N-Hydroxysuccinimide, Carboxylic Acid Succinimidyl Ester
NK cell	Natural killer cell
NMR	nuclear magnetic resonance spectroscopy
NP	Nanoparticle
OD	Optical density
ODN	Oligodeoxynucleotide
OVA	Ovalbumin
PAMP	Pathogen-associated molecular pattern
PAP	Prostatic acid phosphatase
PBS	Phosphate buffered saline
PE	R-Phycoerythrin
PEG	Poly(ethylene glycol)
PEO	Poly(ethylene oxide)
PLGA	poly(lactid-co-glycolic acid)
PLL	Poly-*L*-lysine (7500 g/mole)
PLL_B	polylysine brush ($8*10^6$ g/mole)
PO	Phosphodiester deoxyribose backbone for ODN
PPS	Poly(propylene sulfide)
PRR	Pathogen recognition receptor
PT	Phenotype
PTO	Phosphothioate deoxyribose backbone for ODN
QP_C	Quenching probe
R_g	Radius of gyration
R_h	Hydrodynamic radius
RI	Refractive index
RNA	Ribonucleic acid
RT	Room temperature
SDS	Sodiumdodecylsulfate
SEC	Size exclusion chromatography
SHIP	Specific hybridization internalization probe

SLS	Static light scattering
SPDP	N-succinimidyl-3-(2-pyridyldithio)propionate
SSC	Side scatter
Sulfo-SMCC	Sulfosuccinimidyl-4-(N-maleimidomethyl)cyclohexane-1-carboxylate
T cell	thymus-derived cell
TAA	Tumor associated antigen
TAP	Transporter associated with antigen processing
TBE	Tris-Borat-EDTA
TCEP	Tris(2-carboxethyl)phosphine
TCR	T cell receptor
TFH	T follicular helper cell
T_H	T helper cell
TLR	Toll-like receptor
T_{reg}	regulatory T cell
UV/Vis	Ultraviolet/Visible
V	Volume
V_H	Variable region of the heavy chain of an IgG
V_L	Variable region of the light chain of an IgG

6.4. Bibliography

[1] W. M. Yokoyama, *Nature* **2002**, *419*, 679–680.
[2] V. Groh, J. Wu, C. Yee, T. Spies, *Nature* **2002**, *419*, 734–738.
[3] G. P. Dunn, L. J. Old, R. D. Schreiber, *Annu. Rev. Immunol.* **2004**, *22*, 329–360.
[4] G. P. Dunn, A. T. Bruce, H. Ikeda, L. J. Old, R. D. Schreiber, *Nat Immunol* **2002**, *3*, 991–998.
[5] S. Sakaguchi, T. Yamaguchi, T. Nomura, M. Ono, *Cell* **2008**, *133*, 775–787.
[6] K. Mahnke, S. Ring, T. S. Johnson, S. Schallenberg, K. Schönfeld, V. Storn, T. Bedke, A. H. Enk, *Eur. J. Immunol.* **2007**, *37*, 2117–2126.
[7] M. Dean, T. Fojo, S. Bates, *Nat Rev Cancer* **2005**, *5*, 275–284.
[8] J. J. Moon, B. Huang, D. J. Irvine, *Adv. Mater.* **2012**, *24*, 3724–3746.
[9] "Types of immunotherapy", http://www.cancer.org/treatment/treatmentsandsideeffects/treatmenttypes/immunotherapy/immunotherapy-types.
[10] A. M. Scott, J. D. Wolchok, L. J. Old, *Nat Rev Cancer* **2012**, *12*, 278–287.
[11] S. Dawood, K. Broglio, F. J. Esteva, N. K. Ibrahim, S.-W. Kau, R. Islam, K. D. Aldape, T.-K. Yu, G. N. Hortobagyi, A. M. Gonzalez-Angulo, *Annals of Oncology* **2008**, *19*, 1242–1248.
[12] H. Joensuu, P.-L. Kellokumpu-Lehtinen, P. Bono, T. Alanko, V. Kataja, R. Asola, T. Utriainen, R. Kokko, A. Hemminki, M. Tarkkanen et al., *N Engl J Med* **2006**, *354*, 809–820.
[13] S. Dawood, K. Broglio, Y. Gong, W.-T. Yang, M. Cristofanilli, S.-W. Kau, F. Meric-Bernstam, T. A. Buchholz, G. N. Hortobagyi, A. M. Gonzalez-Angulo, *Cancer* **2008**, *112*, 1905–1911.
[14] M. Marty, *Journal of Clinical Oncology* **2005**, *23*, 4265–4274.
[15] R. Marcus, A. Hagenbeek, *European Journal of Haematology* **2007**, *78*, 5–14.
[16] R. C. Kane, A. T. Farrell, H. Saber, S. Tang, G. Williams, J. M. Jee, C. Liang, B. Booth, N. Chidambaram, D. Morse et al., *Clinical Cancer Research* **2006**, *12*, 7271–7278.
[17] B. Escudier, T. Eisen, W. M. Stadler, C. Szczylik, S. Oudard, M. Siebels, S. Negrier, C. Chevreau, E. Solska, A. A. Desai et al., *N Engl J Med* **2007**, *356*, 125–134.
[18] A. X. Zhu, N. S. Holalkere, A. Muzikansky, K. Horgan, D. V. Sahani, *The Oncologist* **2008**, *13*, 120–125.
[19] N. Lassau, S. Koscielny, L. Chami, M. Chebil, B. Benatsou, A. Roche, M. Ducreux, D. Malka, V. Boige, *Radiology* **2010**, *258*, 291–300.
[20] C. Vaklavas, A. Forero-Torres, *Therapeutic Advances in Hematology* **2012**, *3*, 209–225.
[21] A. M. Bradley, M. Devine, D. DeRemer, *American Journal of Health-System Pharmacy* **2013**, *70*, 589–597.
[22] P. M. LoRusso, D. Weiss, E. Guardino, S. Girish, M. X. Sliwkowski, *Clinical Cancer Research* **2011**, *17*, 6437–6447.
[23] T. Witzig, *Drugs Today* **2004**, *40*, 111.
[24] F. Morschhauser, J. Radford, A. van Hoof, B. Botto, A. Z. S. Rohatiner, G. Salles, P. Soubeyran, H. Tilly, A. Bischof-Delaloye, W. L. J. van Putten et al., *Journal of Clinical Oncology* **2013**, *31*, 1977–1983.
[25] T. T. Hansel, H. Kropshofer, T. Singer, J. A. Mitchell, A. J. T. George, *Nat Rev Drug Discov* **2010**, *9*, 325–338.

[26] P. A. Farazi, R. A. DePinho, *Nat Rev Cancer* **2006**, *6*, 674–687.
[27] M. H. Einstein, M. Baron, M. J. Levin, A. Chatterjee, R. P. Edwards, F. Zepp, I. Carletti, F. J. Dessy, A. F. Trofa, A. Schuind et al., *Human Vaccines* **2009**, *5*, 705–719.
[28] P. W. Kantoff, C. S. Higano, N. D. Shore, E. R. Berger, E. J. Small, D. F. Penson, C. H. Redfern, A. C. Ferrari, R. Dreicer, R. B. Sims et al., *N Engl J Med* **2010**, *363*, 411–422.
[29] G. Dranoff, E. M. Jaffee, A. Lazenby, P. Golumbek, H. I. Levitsky, K. Brose, V. Jackson, H. Hamada, D. M. Pardoll, R. C. Mulligan, *Proceedings of the National Academy of Sciences* **1993**, *90*, 3539–3543.
[30] F. K. Stevenson, C. Ottensmeier, P. Johnson, D. Zhu, S. L. Buchan, K. J. McCann, J. S. Roddick, A. T. King, F. McNicholl, N. Savelyeva et al., *Proceedings of the National Academy of Sciences* **2004**, *101*, 14646–14652.
[31] R. Maas, H. J. Dullens, W. Otter, *Cancer Immunol Immunother* **1993**, *36*, 141-148.
[32] E. K. Waller, *The Oncologist* **2007**, *12*, 22–26.
[33] M. Dierendonck, S. de Koker, C. Vervaet, J. P. Remon, B. G. de Geest, *Drug Delivery Research in Europe* **2012**, *161*, 592–599.
[34] M. E. Davis, Z. Chen, D. M. Shin, *Nat Rev Drug Discov* **2008**, *7*, 771–782.
[35] D. Peer, J. M. Karp, S. Hong, O. C. Farokhzad, R. Margalit, R. Langer, *Nature Nanotech* **2007**, *2*, 751–760.
[36] F. Greco, M. J. Vicent, *Polymer Therapeutics: Clinical Applications and Challenges for Development* **2009**, *61*, 1203–1213.
[37] M. Kreutz, B. Giquel, Q. Hu, R. Abuknesha, S. Uematsu, S. Akira, F. O. Nestle, S. S. Diebold, S. Kovats, *PLoS ONE* **2012**, *7*, e40208.
[38] M. E. Fox, F. C. Szoka, J. M. J. Fréchet, *Acc. Chem. Res.* **2009**, *42*, 1141–1151.
[39] M. A. Dobrovolskaia, S. E. McNeil, *Nature Nanotech* **2007**, *2*, 469–478.
[40] I. Bajaj, R. Singhal, *Bioresource Technology* **2011**, *102*, 5551–5561.
[41] G. Pasut, F. M. Veronese, *Advanced Drug Delivery Reviews* **2009**, *61*, 1177–1188.
[42] R. Duncan, *Advanced Drug Delivery Reviews* **2009**, *61*, 1131–1148.
[43] H. Maeda, *Special issue dedicated to Dr. Eric Tomlinson, Advanced Drug Delivery Reviews, A Selection of the Most Highly Cited Articles, 1991-1998* **2001**, *46*, 169–185.
[44] M. Look, A. Bandyopadhyay, J. S. Blum, T. M. Fahmy, *Nanotechnology Solutions for Infectious Diseases in Developing Nations* **2010**, *62*, 378–393.
[45] S. T. Reddy, M. A. Swartz, J. A. Hubbell, *Trends in Immunology* **2006**, *27*, 573–579.
[46] C. L. van Broekhoven, C. R. Parish, C. Demangel, et al., *Cancer Research* **2004**, *64*, 4357–4365.
[47] Y. J. Kwon, E. James, N. Shastri, J. M. J. Fréchet, *Proceedings of the National Academy of Sciences* **2005**, *102*, 18264–18268.
[48] A. Rehor, J. A. Hubbell, N. Tirelli, *Langmuir* **2005**, *21*, 411–417.
[49] S. T. Reddy, A. Rehor, H. G. Schmoekel, J. A. Hubbell, M. A. Swartz, *Journal of Controlled Release* **2006**, *112*, 26–34.
[50] A. Bandyopadhyay, R. L. Fine, S. Demento, L. K. Bockenstedt, T. M. Fahmy, *Biomaterials* **2011**, *32*, 3094–3105.
[51] A. C. Shirali, M. Look, W. Du, E. Kassis, H. W. Stout-Delgado, T. M. Fahmy, D. R. Goldstein, *American Journal of Transplantation* **2011**, *11*, 2582–2592.
[52] J. Park, W. Gao, R. Whiston, T. B. Strom, S. Metcalfe, T. M. Fahmy, *Mol. Pharmaceutics* **2011**, *8*, 143–152.
[53] L. J. Cruz, P. J. Tacken, F. Bonetto, S. I. Buschow, H. J. Croes, M. Wijers, I. J. de Vries, C. G. Figdor, *Mol. Pharmaceutics* **2011**, *8*, 520–531.

[54] S. A. Rosenberg, J. C. Yang, N. P. Restifo, *Nat Med* **2004**, *10*, 909–915.
[55] L. Fong, E. G. Engleman, *Annu. Rev. Immunol.* **2000**, *18*, 245–273.
[56] K. Palucka, J. Banchereau, *Nat Rev Cancer* **2012**, *12*, 265–277.
[57] L. C. Bonifaz, D. P. Bonnyay, A. Charalambous, D. I. Darguste, S. Fujii, H. Soares, M. K. Brimnes, B. Moltedo, T. M. Moran, R. M. Steinman, *Journal of Experimental Medicine* **2004**, *199*, 815–824.
[58] I. Caminschi, M. H. Lahoud, K. Shortman, *Eur. J. Immunol.* **2009**, *39*, 931–938.
[59] D. Sancho, O. P. Joffre, A. M. Keller, N. C. Rogers, D. Martínez, P. Hernanz-Falcón, I. Rosewell, C. R. e. Sousa, *Nature* **2009**, *458*, 899–903.
[60] M. H. Lahoud, A. I. Proietto, F. Ahmet, S. Kitsoulis, L. Eidsmo, L. Wu, P. Sathe, S. Pietersz, H.-W. Chang, I. D. Walker et al., *The Journal of Immunology* **2009**, *182*, 7587–7594.
[61] R. Duncan, *Anti-Cancer Drugs* **1992**, *3*, 175–210.
[62] W. Shen, H. Ryser, *Proceedings of the National Academy of Sciences* **1981**, *78*, 7589–7593.
[63] A. Pezzutto, T. Ulrichs, G.-R. Burmester, *Taschenatlas der Immunologie*. *Grundlagen, Labor, Klinik*, Thieme, Stuttgart, **2007**.
[64] R. Medzhitov, C. A. Janeway, JR., *Cell* **1997**, *91*, 295–298.
[65] K. Heeg, A. Dalpke, M. Peter, S. Zimmermann, *International Journal of Medical Microbiology* **2008**, *298*, 33–38.
[66] K. Hoebe, E. Janssen, B. Beutler, *Nat Immunol* **2004**, *5*, 971–974.
[67] G. Dranoff, *Nat Rev Cancer* **2004**, *4*, 11–22.
[68] C. Mauri, A. Bosma, *Annu. Rev. Immunol.* **2012**, *30*, 221–241.
[69] T. W. LeBien, T. F. Tedder, *Blood* **2008**, *112*, 1570–1580.
[70] R. M. Steinman, M. C. Nussenzweig, *Immunol Rev* **1980**, *53*, 127–147.
[71] R. M. Steinman, K. Inaba, S. Turley, P. Pierre, I. Mellman, *Human Immunology* **1999**, *60*, 562–567.
[72] R. M. Steinman, *Annu. Rev. Immunol.* **2012**, *30*, 1–22.
[73] C. D. Platt, J. K. Ma, C. Chalouni, M. Ebersold, H. Bou-Reslan, R. A. D. Carano, I. Mellman, L. Delamarre, *Proceedings of the National Academy of Sciences* **2010**, *107*, 4287–4292.
[74] I. Caminschi, E. Maraskovsky, W. R. Heath, *Front. Immun.* **2012**, *3*.
[75] D. Vremec, J. Pooley, H. Hochrein, L. Wu, K. Shortman, *The Journal of Immunology* **2000**, *164*, 2978–2986.
[76] A. Savina, A. Peres, I. Cebrian, N. Carmo, C. Moita, N. Hacohen, L. F. Moita, S. Amigorena, *Immunity* **2009**, *30*, 544–555.
[77] E. Segura, M. Durand, S. Amigorena, *Journal of Experimental Medicine* **2013**, *210*, 1035–1047.
[78] E. Segura, J. A. Villadangos, *Traffic* **2011**, *12*, 1677–1685.
[79] K. Mahnke, M. Guo, S. Lee, H. Sepulveda, S. L. Swain, M. Nussenzweig, R. M. Steinman, *The Journal of Cell Biology* **2000**, *151*, 673–684.
[80] E. S. Trombetta, I. Mellman, *Annu. Rev. Immunol.* **2005**, *23*, 975–1028.
[81] D. Hawiger, K. Inaba, Y. Dorsett, M. Guo, K. Mahnke, M. Rivera, J. V. Ravetch, R. M. Steinman, M. C. Nussenzweig, *Journal of Experimental Medicine* **2001**, *194*, 769–780.
[82] K. Mahnke, Y. Quian, J. Knop, A. H. Enk, *Blood* **2003**, *101*, 4862–4869.
[83] K. Mahnke, Y. Qian, S. Fondel, J. Brueck, C. Becker, A. H. Enk, *Cancer Research* **2005**, *65*, 7007–7012.

[84] M. V. Dhodapkar, *Blood* **2002**, *100*, 174–177.
[85] H. Jonuleit, A. Giesecke-Tuettenberg, T. Tüting, B. Thurner-Schuler, T. B. Stuge, L. Paragnik, A. Kandemir, P. P. Lee, G. Schuler, J. Knop et al., *Int. J. Cancer* **2001**, *93*, 243–251.
[86] K. Garrigan, P. Moroni-Rawson, C. McMurray, I. Hermans, N. Abernethy, J. Watson, F. Ronchese, *Blood* **1996**, *88*, 3508–3512.
[87] L. Bar-On, S. Jung, *Immunological Reviews* **2010**, *234*, 76–89.
[88] J. K. H. Tan, H. C. O'Neill, "Concise Review: Dendritic Cell Development in the Context of the Spleen Microenvironment", **2007**.
[89] M. H. Lahoud, F. Ahmet, J.-G. Zhang, S. Meuter, A. N. Policheni, S. Kitsoulis, C.-N. Lee, M. O'Keeffe, L. C. Sullivan, A. G. Brooks et al., *Proceedings of the National Academy of Sciences* **2012**, *109*, 16270–16275.
[90] M. Kato, T. K. Neil, D. B. Fearnley, A. D. McLellan, S. Vuckovic, D. N. Hart, *International Immunology* **2000**, *12*, 1511–1519.
[91] J. L. Goldstein, R. G. W. Anderson, M. S. Brown, *Nature* **1979**, *279*, 679–685.
[92] D. J. O'Shannessy, R. H. Quarles, *Journal of Immunological Methods* **1987**, *99*, 153–161.
[93] L. J. Harris, S. B. Larson, K. W. Hasel, A. McPherson, *Biochemistry* **1997**, *36*, 1581–1597.
[94] G. T. Hermanson, *Bioconjugate techniques*, Elsevier Acad. Press, Amsterdam, **2008**.
[95] L. Bonifaz, D. Bonnyay, K. Mahnke, M. Rivera, M. C. Nussenzweig, R. M. Steinman, *Journal of Experimental Medicine* **2002**, *196*, 1627–1638.
[96] D. L. Costantini, K. Bateman, K. McLarty, K. A. Vallis, R. M. Reilly, *Journal of Nuclear Medicine* **2008**, *49*, 1498–1505.
[97] M. M. C. Sun, K. S. Beam, C. G. Cerveny, K. J. Hamblett, R. S. Blackmore, M. Y. Torgov, F. G. M. Handley, N. C. Ihle, P. D. Senter, S. C. Alley, *Bioconjugate Chem.* **2005**, *16*, 1282–1290.
[98] C. A. C. Wolfe, D. S. Hage, *Analytical Biochemistry* **1995**, *231*, 123–130.
[99] N. J. Boylan, W. Zhou, R. J. Proos, T. J. Tolbert, J. L. Wolfe, J. S. Laurence, *Bioconjugate Chem* **2013**, *24*, 1008–1016.
[100] A. Wakankar, Y. Chen, Y. Gokarn, F. S. Jacobson, *mAbs* **2011**, *3*, 161–172.
[101] A. O. Kamphorst, P. Guermonprez, D. Dudziak, M. C. Nussenzweig, *The Journal of Immunology* **2010**, *185*, 3426–3435.
[102] S. Burgdorf, A. Kautz, V. Bohnert, P. A. Knolle, C. Kurts, *Science* **2007**, *316*, 612–616.
[103] N. Zietara, M. Lyszkiewicz, J. Puchalka, G. Pei, M. G. Gutierrez, S. Lienenklaus, E. Hobeika, M. Reth, V. A. P. Martins dos Santos, A. Krueger et al., *Proceedings of the National Academy of Sciences* **2013**, *110*, 2282–2287.
[104] S. A. Rosenberg, R. M. Sherry, K. E. Morton, W. J. Scharfman, J. C. Yang, S. L. Topalian, R. E. Royal, U. Kammula, N. P. Restifo, M. S. Hughes et al., *The Journal of Immunology* **2005**, *175*, 6169–6176.
[105] D. E. Speiser, D. Liénard, N. Rufer, V. Rubio-Godoy, D. Rimoldi, F. Lejeune, A. M. Krieg, J.-C. Cerottini, P. Romero, *J. Clin. Invest.* **2005**, *115*, 739–746.
[106] S. H. van der Burg, M. S. Bijker, M. J. P. Welters, R. Offringa, C. J. M. Melief, *Human Cancer Vaccines* **2006**, *58*, 916–930.
[107] R. J. Binder, *Proceedings of the National Academy of Sciences* **2004**, *101*, 6128–6133.
[108] S. Gnjatic, D. Atanackovic, M. Matsuo, E. Jäger, S. Y. Lee, D. Valmori, Y.-T. Chen, G. Ritter, A. Knuth, L. J. Old, *The Journal of Immunology* **2003**, *170*, 1191–1196.

[109] G. B. Lipford, M. Bauer, C. Blank, R. Reiter, H. Wagner, K. Heeg, *Eur. J. Immunol.* **1997**, *27*, 2340–2344.
[110] T. Maurer, A. Heit, H. Hochrein, F. Ampenberger, M. O'Keeffe, S. Bauer, G. B. Lipford, R. M. Vabulas, H. Wagner, *Eur. J. Immunol.* **2002**, *32*, 2356–2364.
[111] T. Sparwasser, R. M. Vabulas, B. Villmow, G. B. Lipford, H. Wagner, *Eur. J. Immunol.* **2000**, *30*, 3591–3597.
[112] S. Akira, H. Hemmi, *Immunology Letters* **2003**, *85*, 85–95.
[113] A. M. Krieg, A.-K. Yi, S. Matson, T. J. Waldschmidt, G. A. Bishop, R. Teasdale, G. A. Koretzky, D. M. Klinman, *Nature* **1995**, *374*, 546–549.
[114] Z. K. Ballas, A. M. Krieg, T. Warren, W. Rasmussen, H. L. Davis, M. Waldschmidt, G. J. Weiner, *The Journal of Immunology* **2001**, *167*, 4878–4886.
[115] L. Beloeil, M. Tomkowiak, G. Angelov, T. Walzer, P. Dubois, J. Marvel, *The Journal of Immunology* **2003**, *171*, 2995–3002.
[116] G. J. Weiner, H.-M. Liu, J. E. Wooldridge, C. E. Dahle, A. M. Krieg, *Proceedings of the National Academy of Sciences* **1997**, *94*, 10833–10837.
[117] B. Jahrsdörfer, G. J. Weiner, *Update Cancer Therapy* **2008**, *3*, 27–32.
[118] W. Schmidt, M. Buschle, W. Zauner, H. Kirlappos, K. Mechtler, B. Trska, M. L. Birnstiel, *Proceedings of the National Academy of Sciences* **1997**, *94*, 3262–3267.
[119] Z. Kadlecova, L. Baldi, D. Hacker, F. M. Wurm, H.-A. Klok, *Biomacromolecules* **2012**, *13*, 3127–3137.
[120] L. J. Arnold, A. Dagan, J. Gutheil, N. O. Kaplan, *Proceedings of the National Academy of Sciences* **1979**, *76*, 3246–3250.
[121] S. E. Kornguth, M. A. Stahmann, *Cancer Res* **1961**, *21*, 907-.
[122] W. Zauner, M. Ogris, E. Wagner, *Advanced Drug Delivery Reviews* **1998**, *30*, 97–113.
[123] L. J. B. M. D. C. L. B. Degols G, *Antisense research and development 2:4 1992 pg 293-301* **1992**, *2*, 293–301.
[124] Y. Singh, P. Murat, E. Defrancq, *Chem. Soc. Rev.* **2010**, *39*, 2054.
[125] V. S. Trubetskoy, V. P. Torchilin, S. J. Kennel, L. Huang, *Bioconjugate Chem.* **1992**, *3*, 323–327.
[126] J. H. Park, S. Lee, J.-H. Kim, K. Park, K. Kim, I. C. Kwon, *Progress in Polymer Science* **2008**, *33*, 113–137.
[127] Z. Zhou, Y. Shen, J. Tang, M. Fan, E. A. van Kirk, W. J. Murdoch, M. Radosz, *Adv. Funct. Mater.* **2009**, *19*, 3580–3589.
[128] J. P. Behr, B. Demeneix, J. P. Loeffler, J. Perez-Mutul, *Proceedings of the National Academy of Sciences* **1989**, *86*, 6982–6986.
[129] F. Labat-Moleur, A. M. Steffan, C. Brisson, H. Perron, O. Feugeas, P. Furstenberger, F. Oberling, E. Brambilla, J. P. Behr, *Gene Ther* **1996**, *3*, 1010–1017.
[130] M. Tyagi, M. Rusnat, M. Presta, *Journal of Biological Chemistry* **2000**, *276*, 3254–3261.
[131] J. P. Richard, K. Melikov, H. Brooks, P. Prevot, B. Lebleu, L. V. Chernomordik, *Journal of Biological Chemistry* **2005**, *280*, 15300–15306.
[132] A. Ferrari, V. Pellegrini, C. Arcangeli, A. Fittipaldi, M. Giacca, F. Beltram, *Mol Ther* **2003**, *8*, 284–294.
[133] A. Fittipaldi, A. Ferrari, M. Zoppé, C. Arcangeli, V. Pellegrini, Beltram F., M. Giacca, *Journal of Biological Chemistry* **2003**, *278*, 34141–34149.
[134] J. REJMAN, A. BRAGONZI, M. CONESE, *Molecular Therapy* **2005**, *12*, 468–474.
[135] J. Cheng, T. J. Deming, *Top Curr Chem* **2011**, *310*, 1–26.

[136] G. Odian, *Principles of Polymerization (Fourth Edition)*, Wiley-Interscience, S.l, **2004**.
[137] J. A. Champion, S. Mitragotri, *Pharm Res* **2009**, *26*, 244-249.
[138] Y. Geng, P. Dalhaimer, S. Cai, R. Tsai, M. Tewari, T. Minko, D. E. Discher, *Nature Nanotech* **2007**, *2*, 249–255.
[139] S. Cai, K. Vijayan, D. Cheng, E. Lima, D. Discher, *Pharm Res* **2007**, *24*, 2099-2109.
[140] F. Lottspeich, J. W. Engels, *Bioanalytik*, Spektrum Akad. Verl, München, **2006**.
[141] J. Krieger, K. Tóth, J. Langowski, "Absorption and Fluorescence Spectroscopy, Fluorescence Correlation Spectroscopy. Practical Course Biophysics", can be found under http://www.dkfz.de/Macromol/teaching/files/fcs_practical.pdf.
[142] J. R. Lakowicz, *Principles of Fluorescence Spectroscopy*, Springer-Verlag, s.l, **2010**.
[143] E. L. Elson, D. Magde, *Biopolymers* **1974**, *13*, 1–27.
[144] "Fluoreszenz-Korrelations-Spektroskopie (FCS). Praktikum der Physik für Fortgeschrittene an der Universität Ulm, Abteilung Biophysik", http://wwwex.physik.uni-ulm.de/lehre/fortgeschrittenenpraktikum/fp/FCS.pdf, **2006**.
[145] K. Bacia, S. A. Kim, P. Schwille, *Nat Meth* **2006**, *3*, 83–89.
[146] E. Haustein, P. Schwille, *Annu. Rev. Biophys. Biomol. Struct.* **2007**, *36*, 151–169.
[147] "Olympus FluoView Resource Center: Introduction to Confocal Microscopy", can be found under http://www.olympusconfocal.com/theory/confocalintro.html.
[148] A. L. Givan.
[149] "Flow cytometry - Wikipedia, the free encyclopedia", can be found under http://en.wikipedia.org/w/index.php?oldid=557243848, **2013**.
[150] F. C. C. F. Boston University, "Flow cytometer setup", can be found under http://www.bu.edu/flow-cytometry/, **2013**.
[151] C. Matthes, *2006*.
[152] H. Liu, A. P. R. Johnston, *Angew. Chem. Int. Ed.* **2013**, *52*, 5744–5748.
[153] S. Mori, H. G. Barth, *Size exclusion chromatography*, Springer, Berlin u. a, **1999**.
[154] D. M. Meunier, "Molecular Weight Determinations. Handbook of Instrumental Techniques for Analytical Chemistry", can be found under http://www.prenhall.com/settle/chapters/ch46.pdf, **1997**.
[155] A. E. Barron, H. W. Blanch, *Separation & Purification Reviews* **1995**, *24*, 1–118.
[156] B. G. Johansson, *Scandinavian Journal of Clinical & Laboratory Investigation* **1972**, *29*, 7–19.
[157] S.-H. Chiou, S.-H. Wu, *Analytica Chimica Acta* **1999**, *383*, 47–60.
[158] M. Muthukumar, *Electrophoresis* **1996**, *17*, 1167–1172.
[159] S.-H. Chiou, S.-H. Wu, *Analytica Chimica Acta* **1999**, *383*, 47–60.
[160] M. Schmidt, *Simultaneous Static and Dynamic Light Scattering: Application to Polymer Structure Analysis*. *Dynamic Light Scattering, The Method and Some Application*, Clarendon Press, Oxford, **1993**.
[161] W. Schärtl, *Light scattering from polymer solutions and nanoparticle dispersions*, Springer, Berlin, Heidelberg, **op. 2010**.
[162] F. Kühn, *Synthese, Charakterisierung und Bildungskinetik von DNA-Interpolyelektrolyt-Komplexen*. *Diplomarbeit*, **2007**.
[163] W. Schärtl, *Light Scattering from Polymer Solutions and Nanoparticle Dispersions*, Springer-Verlag, **2007**.
[164] W. Burchard, W. Richtering in *Progress in Colloid & Polymer Science* (Eds.: M. Pietralla, W. Pechhold), Steinkopff, **1989**.
[165] O. P. Joffre, E. Segura, A. Savina, S. Amigorena, *Nat Rev Immunol* **2012**, *12*, 557–569.

[166] C. Lamaze, S. L. Schmid, *Current Opinion in Cell Biology* **1995**, *7*, 573–580.
[167] R. M. Steinman, *Immunity* **2008**, *29*, 319–324.
[168] R. Maldonado-Lopez, T. de Smedt, P. Michel, J. Godfroid, B. Pajak, C. Heirman, K. Thielemans, O. Leo, J. Urbain, M. Moser, *Journal of Experimental Medicine* **1999**, *189*, 587–592.
[169] I. A. Khalil, K. Kogure, H. Akita, H. Harashima, *Pharmacological Reviews* **2006**, *58*, 32–45.
[170] S. D. Conner, S. L. Schmid, *Nature* **2003**, *422*, 37–44.
[171] J. Harris, D. Werling, J. C. Hope, G. Taylor, C. J. Howard, *Trends in Immunology* **2002**, *23*, 158–164.
[172] J. Rejman, V. Oberle, I. S. Zuhorn, D. Hoekstra, *Biochem. J.* **2004**, *377*, 159.
[173] W. Jiang, W. J. Swiggard, C. Heufler, M. Peng, A. Mirza, R. M. Steinman, M. C. Nussenzweig, *Nature* **1995**, *375*, 151–155.
[174] M. A. West, *Science* **2004**, *305*, 1153–1157.
[175] W. S. Garrett, L.-M. Chen, R. Kroschewski, M. Ebersold, S. Turley, S. Trombetta, J. E. Galán, I. Mellman, *Cell* **2000**, *102*, 325–334.
[176] K. Kafi, D. J. Betting, R. E. Yamada, M. Bacica, K. K. Steward, J. M. Timmerman, *Molecular Immunology* **2009**, *46*, 448–456.
[177] Mike Sahl, *Dissertation*, Johannes Gutenberg-Universität Mainz, Mainz, **2011**.
[178] K. Rausch, A. Reuter, K. Fischer, M. Schmidt, *Biomacromolecules* **2010**, *11*, 2836–2839.
[179] Y. Mori, S. Nakamura, S. Kishimoto, M. Kawakami, S. Suzuki, T. Matsui, M. Ishihara, *International Journal of Nanomedicine* **2010**, *5*, 147–155.
[180] U. Heimgartner, B. Kozulić, K. Mosbach, *Biochem. J.* **1990**, *267*, 585–591.
[181] L.-C. Chang, H.-F. Lee, M.-J. Chung, V. C. Yang, *Bioconjugate Chem.* **2005**, *16*, 147–155.
[182] J. F. Liang, Y. T. Li, M. E. Connell, V. C. Yang, *AAPS PharmSci* **2000**, *2*, 59–67.
[183] R. H. Reiner, H.-G. Batz, *Makromol. Chem.* **1981**, *182*, 1641–1648.
[184] D. I. Gabrilovich, S. Nagaraj, *Nature* **2009**, 9, 162-174.